Legionella pneumophila and the Host Endoplasmic Reticulum: How a Single Bacterial Protein Catalyzes a Novel Multi-Step Ubiquitination Pathway to Manipulate Tubular ER

A thesis submitted by

Kristin M. Kotewicz

in partial fulfillment of the requirements for the degree of

Doctor of Philosophy [PhD]

in

Molecular Microbiology

Tufts University

Sackler School of Graduate Biomedical Sciences

February 2018

Advisor: Ralph Isberg, Ph.D.

Abstract

Intracellular pathogens manipulate host organelles to support replication within cells. In the case of *Legionella pneumophila*, the bacterium translocates proteins that establish an endoplasmic reticulum (ER)-associated replication compartment. Using high-resolution electron microscopy and fluorescence microscopy we show that the bacterial Sde proteins target host reticulon 4 (Rtn4) to control tubular ER dynamics, resulting in tubule rearrangements as well as structural alterations to Rtn4 proximal to the *Legionella pneumophila* containing vacuole (LCV). We utilized both *in vitro* recombinant protein systems and *L. pneumophila* infection models to characterize the Sde proteins and were able to identify the molecular mechanism promoting these ER rearrangements. Sde ubiquitin (Ub) ligation to Rtn4, which occurs almost immediately after bacterial uptake, is dependent on two sequential enzymatic activities expressed from a single Sde polypeptide: an ADP-ribosyltransferase (ART) and a nucleotidase/phosphohydrolase (NP). The ADP-ribosylated moiety of ubiquitin is a substrate for the nucleotidase/phosphohydrolase, resulting in either transfer of ubiquitin to Rtn4, or phosphoribosylation of ubiquitin in the absence of a ubiquitination target. These enzymatic activities collaborate to promote ubiquitin ligation through a phosphodiester bond, rather than the classic isopeptide ubiquitin linkage and specifically target Rtn4 and a subset of Rabs, including Rab33b and Rab1[396].

These enzymatic activities are essential for robust intracellular replication and ER association in amoeba, but not macrophages. We show Sde targeting of LCV associated polyUb conjugates with ADP-ribosylate or phosphoribosylate modifications protect these products from host disassembly and are required for intracellular replication in amoeba.

We also identified a third enzymatic domain in Sde proteins, a K63-polyubiquitin specific deubiquitinase (DUB) that limits LCV polyUb within the first 30 minutes of infection that fuels Sde Ub ligase function by generation of a free monoubiquitin substrate pool, while also preventing lysosomal targeting ubiquitin signals (K63) from accumulating on the *Legionella* vacuole membrane. This work demonstrates that Sde mediated ubiquitination transforms peripheral ER tubules associated with the LCV through a novel molecular mechanism, where a single bacterial protein catalyzes a multistep biochemical pathway to control ubiquitination via both ubiquitin conjugation and deconjugation.

Table of Contents

List of Tables

List of Figures

List of Copyrighted Materials (as they appear)

1. Goyal U, Blackstone C. Untangling the web: Mechanisms underlying ER network formation. *Biochimica et biophysica acta*. 2013;1833(11):2492-2498.
2. Phillips MJ, Voeltz GK. Structure and function of ER membrane contact sites with other organelles. *Nature reviews Molecular cell biology*. 2016;17(2):69-82.
3. Shibata Y, Shemesh T, Prinz WA, Palazzo AF, Kozlov MM, Rapoport TA. Mechanisms determining the morphology of the peripheral ER. *Cell.* 2010;143(5):774-788.
4. Yang YS, Strittmatter SM. The reticulons: a family of proteins with diverse functions. *Genome Biology.* 2007;8(12):234.
5. Kempf A, and Schwab ME. Nogo-A Represses Anatomical and Synaptic Plasticity in the Central Nervous System. *Physiology*. 2013;28:151-163.
6. Lin Y, Machner MP. Exploitation of the host cell ubiquitin machinery by microbial effector proteins. *Journal of Cell Science*. 2017;130:1985-1996.
7. Boya P, Reggiori F, Codogno P. Emerging regulation and functions of autophagy. *Nat. Cell Biol.* 2013;5(7):713-20.
8. Lamb CA, Yoshimori T, Tooze SA. The autophagosome: origins unknown, biogenesis complex. *Nat. Rev. Mol. Cell Biol.* 2013;14:759–774.
9. Wang Y, Li Y, Wei F, Duan Y. Optical Imaging Paves the Way for Autophagy Research. *Trends Biotechnol.* 2017. Epub ahead of publication.
10. Balducci E, Bonucci A, Picchianti M, Pogni R, Talluri E. Structural and Functional Consequences Induced by Post-Translational Modifications in α-Defensins. *International Journal of Peptides*. 2011;594723.
11. Yamamoto Y, Yamamoto H. Controlling the receptor for advanced glycation end-products to conquer diabetic vascular complications. *Journal of Diabetes* Investigation. 2012;3(2):107-114.
12. Allombert J, Fuche F, Michard C, Doublet P. Molecular mimicry and original biochemical strategies for the biogenesis of a *Legionella pneumophila* replicative niche in phagocytic cells. *Microbes Infect.*, 2013;15 (14-15): 981-988.
13. So EC, Mattheis C, Tate EW, Frankel G, Schroeder GN. Creating a customized intracellular niche : subversion of host cell signaling by *Legionella* type IV secretion system effectors. *Can. J. Microbiol*. 2015; 61(9):617-35. doi: 10.1139/cjm-2015-0166.
14. Boyle KB, Randow F. The role of ‘ eat-me ’ signals and autophagy cargo receptors in innate immunity. *Curr. Opin. Microbiol.* 2013;16(3):339-48.
15. Levine B, Mizushima N, Virgin H. Autophagy in immunity and inflammation. *Nature*. 2011;469:1–5.
16. Jeong KC, Sexton JA,Vogel JP. Spatiotemporal Regulation of a *Legionella pneumophila* T4SS Substrate by the Metaeffector SidJ. *PLoS Pathog.* 2015; 16(3):339-48.
17. Haenssler E, Ramabhadran V, Murphy CS, Heidtman MI, Isberg RR. *Infect Immun.* 2015 Sep; 83(9):3479-89. Epub 2015 Jun 22.
18. Kotewicz KM, Ramabhadran V, Sjoblom N, Vogel JP, Haenssler E, Zhang M, Behringer J, Scheck RA, Isberg RR. *Cell Host Microbe*. 2017 Feb 8; 21(2):169-181. Epub 2016 Dec 29.

Abbreviations

ADP-ribose – Adenosine Diphosphate Ribose
ADH – ADP-ribosyl hydrolase
AGE – Advanced glycation end products
A/J – Inbreed mouse strain (Jackson Laboratories)
a.k.a – Also Known As
ALS – Amyotrophic Lateral Sclerosis
APEX2 – Engineered ascorbate peroxidase (electron microscopy tag)
ART – ADP-Ribosylating Toxin
Atg – Autophagy genes
ATP – Adenosine triphosphate
AMP – Adenosine monophosphate
BACE – Beta-secretase 1
BFA – Brefeldin A
BMDM – Bone Marrow Derived Macrophages
Calcoco2 – Calcium Binding And Coiled-Coil Domain 2
CRAC – Calcium release-activated channels
DALIS – Dendritic cell aggresome-like structures
DFCP1 – Double FYVE Containing Protein 1
DSS - Disuccinimidyl suberate crosslinker
DUB – Deubiquitinase/Deubiquitinating enzyme
E1 – Ubiquitin activating enzyme
E2 – Ubiquitin conjugating enzyme
E3 – Ubiquitin ligase
EE – Early endosome
ELISA – enzyme-linked immunosorbent assay
EM – Electron microscopy
ε-NAD – Etheno Nicotinamide Adenine Dinucleotide
ER – Endoplasmic Reticulum
ERES – ER exit sites
ERGIC – ER-Golgi intermediate compartment
FRAP – Fluorescence recovery after photobleaching
GAP – GTPase-activating proteins
GDI – Guanosine nucleotide dissociation inhibitor
GEF – Guanine nucleotide exchange factors
GFP – Green Fluorescent Protein
GTPase – guanosine triphosphate (GTP) hydrolase
GST – Glutathione S transferase
HA - Human influenza **h**em**a**gglutinin (AA 98-106, epitope tag)
HECT – homologous to the E6AP carboxyl terminus domain family
HPI – Hours post infection
HEK – Human Embryonic Kidney
HMW – High Molecular Weight
IDTS – Icm/Dot translocated substrates
IP – Immunoprecipitation

IPTG – Isopropyl β-D-1-thiogalactopyranoside
KO – Knockout
LC3 - Microtubule-associated protein 1A/1B-light chain 3
LC3-I – cytosolic immature form of LC3
LC3-II - phosphatidylethanolamine conjugated LC3 (recruited to autophagosomal membranes)
LC-MS/MS – Liquid chromatography tandem mass spectrometry
LCV – *Legionella* containing vacuole
LE – Late Endosome
LINC – linker of nucleoskeleton and cytoskeleton complex
L.p. – Legionella pneumophila
MAMs – Mitochondria-ER Associated Membranes
mART – Mono-ADP-Ribosylating Toxin / Mono-ADP-ribosyltransferase
MOI – Multiplicity Of Infection
MPI – Minutes post infection
NDP52 - Nuclear Domain 10 Protein 52
NE – Nuclear envelope
NEL – Novel E3 Ligase
NgbR – Nogo-B receptor
NgR – Nogo-66 receptor
Nogo – Neurite outgrowth inhibitor, Rtn4
NP – Nucleotidase/Phosphohydrolase
ONM/INM – Outer/Inner nuclear membrane
OPTN – Optenurin
PAS – Preautophagosomal site/Phagopore assembly site
PBS – Phosphate Buffered Saline
PBST – Phosphate Buffered Saline with 0.1% Tween-20
PCR – Polymerase Chain Reaction
PDE - Phosphodiesterase
PE – Phosphoethanolamine
PolyUb - Polyubiquitin
PTM – Post translational modifications
PV – parasitophorous vacuole
R – Arginine residue
REEP - Receptor expression enhancing proteins
RER – Rough Endoplasmic Reticulum
RHD – Reticulon Homology Domain
Rtn - Reticulon
SCF complex – Skp, Cullin, F-box containing complex
SDS-PAGE - Sodium dodecyl sulfate polyacrylamide gel electrophoresis
Sde – SidE family subset including only SdeC, SdeB, and SdeA
SidE – Substrate of Icm/Dot system paralogues group E
SOCE – Store-operated calcium entry
SNARE – Soluble NSF Attachment Protein Receptor
STX17 – Syntaxin 17
SUN – Sad1 and UNC-84 homology domain

T4SS – Type IV Secretion System
TBS – Tris Buffered Saline
TBST – Tris Buffered Saline with 0.1% Tween-20
TLR – Toll-like receptor
UPR – Unfolded protein response
Ub – Ubiquitin
WT – Wild Type

Chapter 1:

Introduction

This chapter contains excerpts that have previously been published in (reprinted with permission of publisher):

Haenssler E, Ramabhadran V, Murphy CS, Heidtman MI, Isberg RR.
Infect Immun. 2015 Sep; 83(9):3479-89. Epub 2015 Jun 22.

Kotewicz KM, Ramabhadran V, Sjoblom N, Vogel JP, Haenssler E, Zhang M, Behringer J, Scheck RA, Isberg RR. Cell Host Microbe. 2017 Feb 8; 21(2):169-181. Epub 2016 Dec 29.

Other figures/captions from this chapter have been reprinted here with permission of publisher (Listed in Copyrighted Material Section, above)

1.1. Endoplasmic Reticulum: Form and Function

The endoplasmic reticulum (ER) is a large, contiguous, membrane-enclosed organelle that is involved in a wide array of critical cell functions[141,164]. These roles include, but are not limited to protein synthesis, modification, folding, translocation, secretion, and its quality control through the unfolded protein response (UPR), as well as serving in lipid manufacturing, hormone production, and regulating Ca^{2+} homeostasis[120,289,305,445,522]. To provide all these distinct functions across the vast intracellular expanses of the cell, the ER has differentiated into distinctive structural and functional domains. Furthermore, the ER serves as a mesh network of connections to the plasma membrane and other organelles, offering contact points with mitochondria, Golgi, endosomes, lipid droplets, and peroxisomes[44,120,140,302]. Structurally, the ER can be segregated into several broad sub-regions, each of which is responsible for a unique set of cellular functions. These divergent ER subdomains can be broadly assigned to: 1) the dynamic peripheral ER tubules, also known as smooth ER; 2) the flattened sacs known as cisternae or rough ER sheets; 3) and the nuclear envelope ((NE) Figure 1.1). All of these separate subdomains are interconnected through a contiguous luminal space (Figure 1.1)[54,77,121,289,308,458]. Recent high-resolution studies of the ER reveal that these classifications are an oversimplification of the breadth of ER structures that form within a cell[141,393,538]. For instance, architecture that was formerly described as peripheral sheets were revealed instead to be composed of cross-linked ER tubules, termed ER matrices[349]. The unearthing of these novel ER structures hidden within the archetypal classifications of the past raises the possibility that there may be many additional ER structures and novel complementary functions that have yet to be discovered.

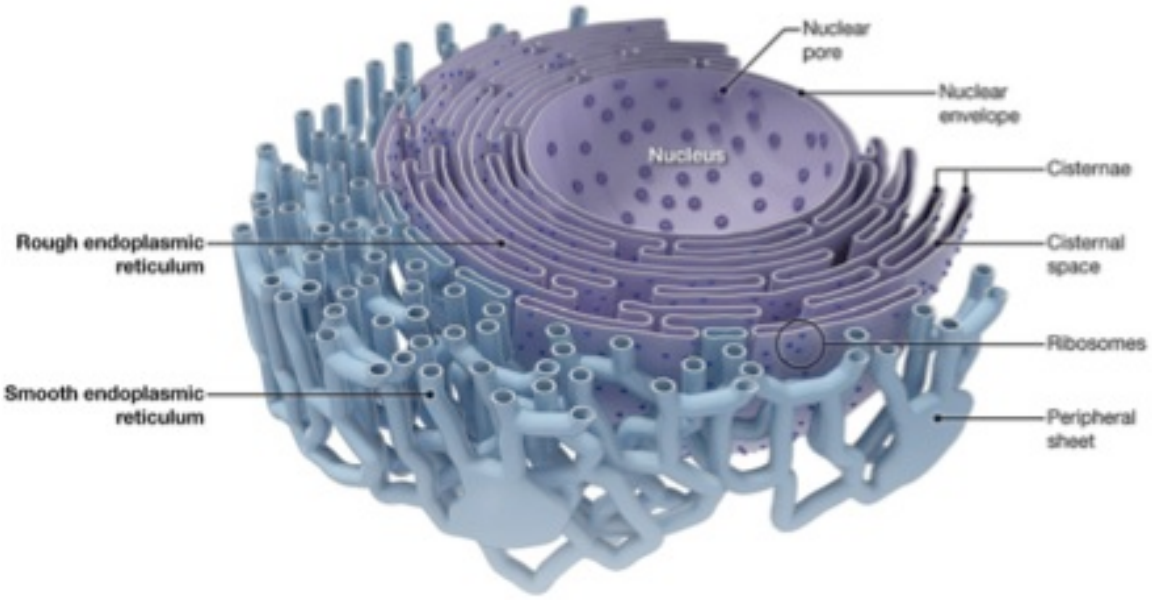

Figure 1.1. ER structure and subdomains.
Schematic diagram depicting the ER network with different structural features and morphologies segregating ER subdomains, while remaining physically connected through a continuous lumen. Reprint with permission from Goyal and Blackstone[164].

1.1.1. Smooth ER tubules.

The first ER subdomain mentioned, the smooth ER tubules, is composed of membrane encapsulated high curvature cylinders (cross section view) formed by a phospholipid bilayers with a membrane width of ~4nm, which generates an ER lumen diameter of ~50nm in mammalian cells[99,277]. These tubules are highly dynamic, continually forming, retracting, and interconnecting, primarily at 3-way junctions to generate a polygonal network extending throughout the entire cytoplasm, out to the plasma membrane[142,161,167,501,531,541] (Figure 1.2.A,B). This tubule network is commonly referred to as smooth ER due to the visible lack of ribosomes studding the membrane observed in early electron microscopy (EM) studies[458]. This vast system of highly curved membranes on ER tubules results in ER regions with a high surface-to-lumen volume ratio, making this subdomain's architecture well suited for its role in lipid synthesis,

protein transport and trafficking, as well as offering a branching network to facilitate organelle contact points regardless of their localization within a cell[54,289,538].

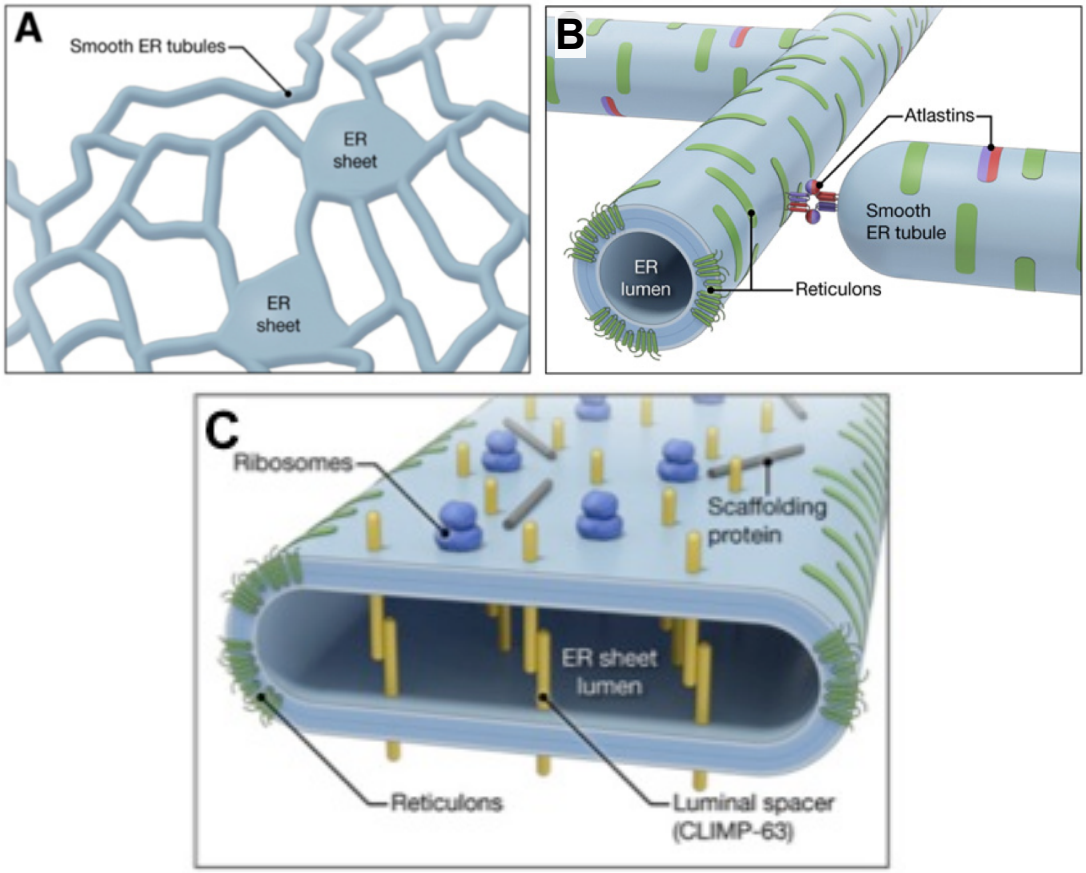

Figure 1.2. Mechanisms and players shaping ER tubules and sheets.
(A) Schematic diagram showing interconnected smooth ER tubules and peripheral sheets. **(B)** Membrane curvature inducing reticulons and atlastins that are GTPases mediating ER membrane fusion on ER tubules, with a schematic depiction of atlastin-dependent tubule fusion. **(C)** ER proteins involved in the generation and stabilization of ER sheets, including Climp-63, polyribosomes, and scaffolding proteins, like p180 and kinectin. Adapted from Goyal and Blackstone, 2013 to show select panels[164].

Cell types enriched in ER tubules are often associated with these specific tubular ER functions. For instance, cells with extensive tubular networks include those specializing in lipid synthesis, such as adrenal cortex cells, which are responsible for heavy levels of steroid production. An additional example of cells relying on ER tubule structure and function are muscle cells. These specialized cells heavily rely on calcium

signaling to rapidly respond to cues to produce muscle contractions through a specialized smooth ER called the sarcoplasmic reticulum[68,69,221,308,422]. The recognizable increase in tubular ER within these cells demonstrates the tight link between structure and function and the importance of ER subdomain specialization. The physical properties and specialization of function observed in ER subdomains is fueled by compartmentalization of specific structural protein families[392,457,538]. The networks of elongated cylinders that compose the tubular ER network are heavily enriched in structural ER membrane proteins, such as Dp1/Yop1p, Lunapark/Lnp1p, and the reticulon family[76,121,122,527]. A small fraction of these tubular ER proteins localize to ER sheets or NE, this fraction is primarily limited to areas of high curvature at the edge of cisternae or nuclear pore regions (Figure 1.2.C). For the most part, these tubular ER membrane shaping proteins are excluded from the flat surfaces of ER cisternae and define the tubular network from the PM to the nuclear envelope[352,459,506,520] (Figure 1.3.A).

Reticulons and Dp1/Yop1p are integral ER membrane proteins that contain a conserved membrane spanning structure that has been implicated in membrane deformation to generate curvature and stabilization of curved membrane surfaces, but the details of how these proteins function remains ambiguous. The structural similarities between Dp1/Yop1p and reticulons, particularly in regards to their topology relative to the phospholipid bilayer, provides clues to the mechanisms promoting tubular ER formation. Although these protein families are unrelated in sequence, they share a common structural feature of ~200 amino acids that includes two hydrophobic segments believed to adopt hairpin-like topology in ER membranes, which sandwich a cytosolic or luminal facing loop. This topology along with the ability to form homo- and hetero-

oligomers are critical for their role in promoting tubular ER structure and controlling diffusion rates through the membrane. Shibata *et al* demonstrated that Rtn1 and Yop1p diffused slowly through the membrane as a result of their homo- and hetero-oligomerization, with slow diffusion demonstrated by fluorescent recovery after photobleaching (FRAP) relative to another control resident ER protein, Sec63[459]. Furthermore, the researchers found that overexpression of reticulons and Yop1p/Dp1 limits protein mobility within the membrane. Upon ATP depletion, Rtn1p and Yop1p diffusion ceased entirely, yet this depletion had no effect on Sec63 mobility. The ATP depletion study results suggest that the decoupling of reticulon or Yop1p/Dp1 oligomers requires an energetic process utilizing ATP[459]. This postulate was further substantiated by cellular phenotypes resulting from an oligomerization-defective Rtn1p mutant. This mutant enhanced membrane mobility independently of cellular ATP levels and the mutant was unable to reconstitute tubular ER morphology in a reticulon/Yop1p triple knockout (*Δrtn1 Δrtn2 Δyop1*)[459]. Taken together, the evidence suggests reticulons and Dp1/Yop1p readily oligomerize into higher order complexes that limits protein movement migration within the ER and promotes membrane curvature for ER tubule production.

1.1.2. ER—Organelle contact points.

Another critically important region of tubular ER are ERES, or ER exit sites, which are highly specialized regions of the tubular ER that act as a critical junction in the secretory pathway and serve to connect the ER with other organelles, specifically the Golgi[48,192,275,359]. The high-curvature architecture is crucial for proper ERES localization and cargo movement in *Saccharomyces cerevisiae*[359]. Membrane-associated structural

proteins and stabilizing proteins, like Reticulon 1, localize to ERES and are involved in membrane deformation, which is particularly important for cargo trafficking. At these sites, ER-to-Golgi (COPII/COPI) transport vesicles form and bud from the ERES to enable protein export of soluble and membrane/lipid cargo[60,215,532]. These sites have also been shown to supply some of the core autophagosomal components and possibly donate membrane to the assembling autophagic compartment, further linking the ER structure to critical catabolic processes necessary for cellular homeostasis [141,165,178,437,481].

The tubular ER network provides a continual series of contact points with nearly every organelle in the cell (Figure 1.3.A). These intimate associations are critical for organelle structure, signaling, lipid synthesis, lipid exchange, and more. One of the ER contact sites that has been subjected to intense study is the mitochondria-ER contact point. These sites, often referred to as mitochondria-ER associated membranes (MAMs) represent the fraction of ER where there is direct association between the cytoplasmic face of ER tubules and the mitochondrial outer membrane[53,187,305,404]. The close association between the opposing membrane faces generate a structure in which protein interactions across organelles enable tethering of the organelles, while simultaneously maintaining independent membrane integrity[95,404,411,424]. High-resolution EM visualization of these regions revealed the presence of electron dense structures extending between the two organelles, suggesting a physical proteinaceous bridge that tethers the organelles[95,187].

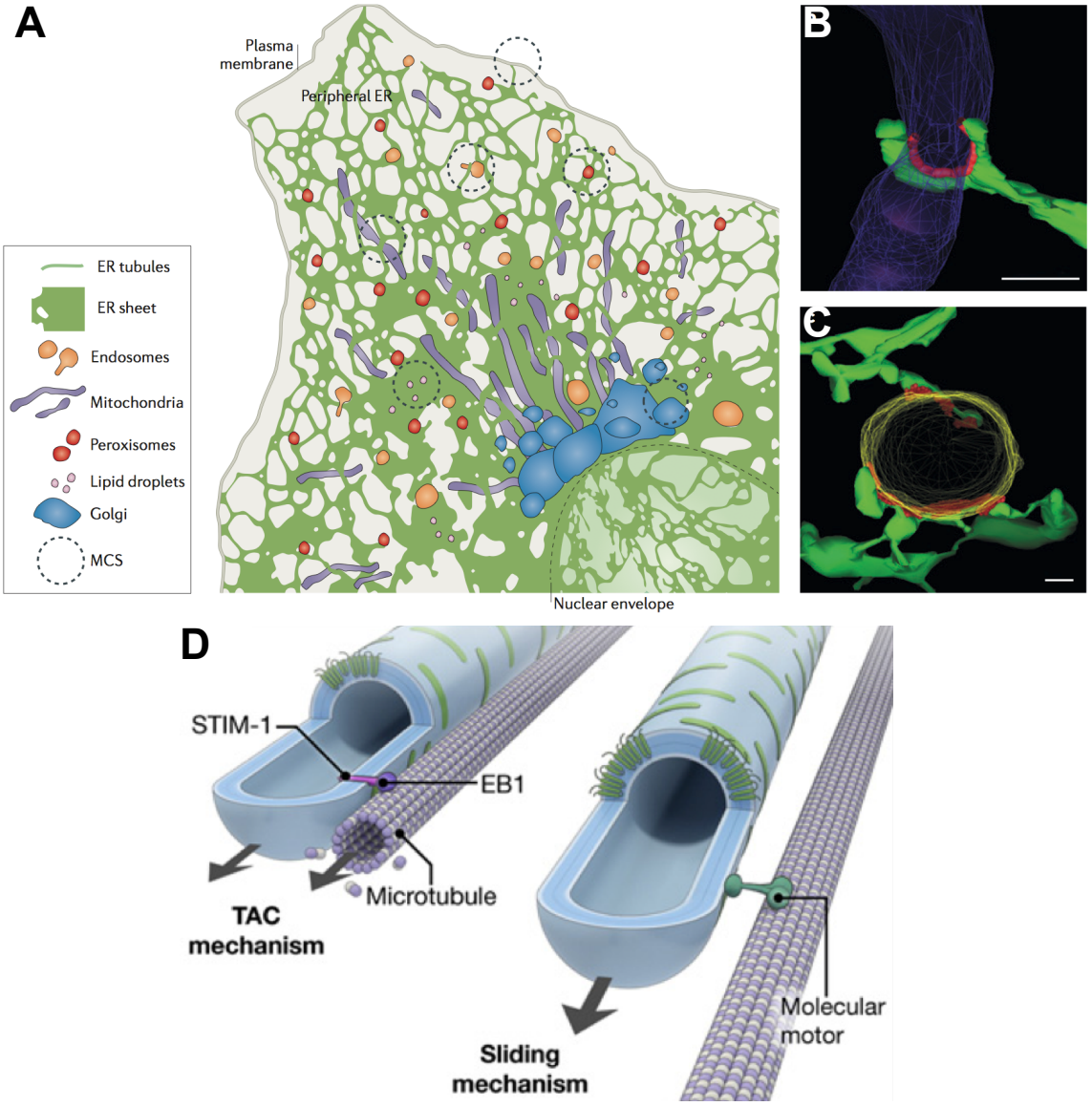

Figure 1.3. ER interconnections with other cellular organelles and structures. **(A)** The nuclear envelope (dashed line, bottom right) extends out into the peripheral ER, which spreads into the cytosol as a network of sheets and tubules (green). The peripheral ER forms membrane contact sites (MCSs) with the plasma membrane, mitochondria, endosomes, peroxisomes, lipid droplets and the Golgi. **(B,C)** Electron tomography exposes three-dimensional structure of MCSs (red) with ER tubules (green) and mitochondria (purple) in yeast (**B**)[140] or ER tubules with an endosome (yellow-orange) in an animal cell (**C**)[139]. Scale bars 200 nm. **(D)** ER tubule interaction with cytoskeletal components facilitating, ER movement and extension by sliding or tip attachment complex (TAC) mechanism movement using molecular motors to travel along stable, acetylated microtubule tracks and polymerizing microtubules, respectively. Green membrane proteins represent reticulons; molecular motors include myosin V and kinesin-1. EB1, microtubule +TIP protein end binding 1; STIM-1, stromal interaction molecule 1; TAC, tip attachment complex mechanism. Reproduced with permission from Phillips and Voeltz, 2016 **(A-C)** [378] and Goyal and Blackstone, 2013 **(D)** [378].

The physiological functions and membrane integrity of the mitochondria necessitates a continuous supply of lipids making their interaction with the ER essential for lipid recycling. MAMs are also proposed to be fundamental in lipid flipping between apposed membranes during the biosynthesis of phospholipids and phosphatidylcholine[5,201,259,313]. Consistent with MAMs association with lipid production and transport, these ER regions are heavily enriched in lipid biosynthesis enzymes when compared against the bulk of the ER[313,429,485,513,518,547]. Experimental evidence also indicates MAMs designate the sites of mitochondrial fission. The Voeltz group used electron microscopy and tomography to generate three-dimensional structures of ER–mitochondria contacts. In these studies, the authors followed the mitochondrial fission process and found the mitochondrial constriction sites were associated with ER tubules wrapping around the mitochondrial membrane, much like a lasso (Figure 1.3.B)[120,140,305]. The tubular ER at these contact sites is hypothesized to play an early role constricting the mitochondria and ultimately provide a scaffold for the division machinery[120,140,424].

In mammalian cells, the ER-mitochondrial contact sites have been found to serve as a major calcium-signaling hub, where the controlled exchange of calcium from the ER to the mitochondria regulates apoptosis and is important for mitochondrial functions. Calcium release from the ER to the mitochondria serves several specific purposes including 1) production of a localized area of highly concentrated Ca^{2+} for mitochondrial membrane proteins that require Ca^{2+}, but the proteins do not have a K_d high enough to bind calcium at cytoplasmic concentrations, 2) maintaining mitochondrial morphology, mobility, and fission through a repertoire of calcium regulated proteins 3) and activation of apoptosis through localized Ca^{2+} flux promoting the mitochondrial permeability

transition pore to open resulting in cytochrome *c* release and proliferation of the caspase cascade[31,53,175,253,412,424]. Furthermore, ER-localized MAM has been described as preferred locale for autophagic initiation. After induction of autophagy, MAM-proximal ER membranes produce an ER-derived cup structure that serves to coordinate autophagopore development into a mature autophagosome as well as function to assemble early autophagic machinery[210,498,512].

Another cellular structure that interacts with the ER is the plasma membrane (PM). ER-PM contact sites serve as sites for phosphatidylinositol (PI) metabolism[32,155,479,480], phosphoinositide signaling[94,479,561], maintenance of reticular ER morphology [67,561], non-vesicular transfer of sterols[32,285], and regulation of Ca^{2+} levels in both the ER and PM[2,58,155,477,480]. The close association of these organelles was revealed in EM studies of budding yeast, in which 20%– 45% of the cytoplasmic face of the PM was within tethering distance of the ER[379,538]. Levels of the signaling molecule phosphatidylinositol 4-phosphate (PI4P) are also regulated at ER-PM contact sites through sterol and phosphoinositol phosphate exchange proteins, like the Osh family (oxysterol-binding homology protein family) and integral ER VAP proteins[155,479,561]. As with MAM sites, ER-PM interaction sites serve as a calcium-signaling hubs, where depleted ER stores are replenished by extracellular sources through the formation of PM Ca^{2+} channels[154,420,468,480]. The ER-localized stromal interaction molecule (STIM1/2) proteins serve as ER calcium sensors and upon Ca^{2+} depletion, Ca^{2+} is transferred from the PM through a process known as store-operated calcium entry (SOCE), which sustains prolonged Ca^{2+} transfer and refills internal stock piles [67]. Under low Ca^{2+} conditions, the STIM proteins oligomerize at the ER-PM contact sites and then interact with plasma

membrane localized store-operated ORAI Ca^{2+} channels to form a Ca^{2+}-released-activated-Ca^{2+} influx (CRAC) channel, enabling Ca^{2+} transfer from the PM to the ER[292,420,468]. The coupling of STIM proteins with ORAI1 channels fundamentally relies on the structural ER proteins such as the reticulons. In the absence of Reticulon 4, a loss of ER tubulation and a redistribution of STIM1 to ER sheets was observed, which presumably limits STIM-ORAI interactions [239]. These Rtn4-KO (knockout) cells are unable to sustain elevated cytoplasmic Ca^{2+} levels via SOCE, resulting in cells that were more resistant to apoptosis resulting from Ca^{2+} overload[239].

The ER and Golgi form a number of membrane contacts to regulate the transfer of secreted proteins and lipids between the two organelles. These ER-Golgi interaction sites facilitate COPII-mediated anterograde trafficking, COPI-mediated retrograde transit, and non-vesicular lipid transfer between apposed membranes. Electron tomography studies on ER interactions with organelles demonstrated the extensive contact regions between endosomes and ER tubules within animal cells (Figure 1.3.C). ER-endosome contact sites are proposed to function in lipid and sterol exchange, as sustained interaction between early endosomes and the ER has been observed with live confocal fluorescence microscopy[120,142,237]. Late endosomes (LE) have also been observed in association with the ER, which was remarkably regulated by LE cholesterol levels, with increased cholesterol concentration promoting ER-LE association[415]. Peroxisomes are also closely associated with the ER as much of the donor material, both membrane proteins and lipids, is derived from the ER[302,303]. Peroxisome formation relies on transfer of ER-derived material through both vesicular and non-vesicular transfer mechanisms. Intriguingly, live cell imaging of ER budding in a cell-free *in vitro* assay revealed vesicles rich in

peroxisome-associated membrane proteins that would fuse with other ER-derived vesicles producing new peroxisome-like compartments[6,560]. The observation that peroxisomes were ER-derived demonstrated the ER's fascinating capacity to generate morphologically and functionally divergent organelles[120]. With this meshwork of tubules serving as the contact points to many of the aforementioned cellular organelles, it is not surprising that tubular ER would represents the most dynamic ER subdomain. The ER needs to be able to promptly adapt to the shifting needs of a stressed or stimulated cell. This is driven by microtubule and myosin networks, that produce movements like tubule extension, retraction, branching, and forming intersections with ER structures[49,142,500,531] (Figure 1.3.D.).

1.1.3. Rough ER sheets and the nuclear envelope.

In contrast to the dynamic ER tubules, both the rough ER sheets and NE form more persistent structures, adopting a consistently organized form. The NE is composed of two large flat membrane bilayers separated by a perinuclear space of ~40-50nM that separates the outer and inner nuclear membranes (ONM/INM) [195,524] (Figure 1.4.Top panel). These bilayers remain connected through nuclear pores and the linker of nucleoskeleton and cytoskeleton (LINC) complex, which maintains a constant distance between the inner and outer membranes (Figure 1.4. Bottom panels)[195,400]. This structural complex maintains the NE overall architecture through the SUN complex (Sad1 and UNC-84), which is present within the inner nuclear membrane, interacting with KASH (klarsicht, ANC-1, and syne-1/nesprin homology) domain proteins of the ONM nuclear membrane (Figure 1.4. Bottom left panel). These protein-protein interactions result in a

protein bridge spanning across both NE membranes to maintain space and structure[63,328,366,406,472].

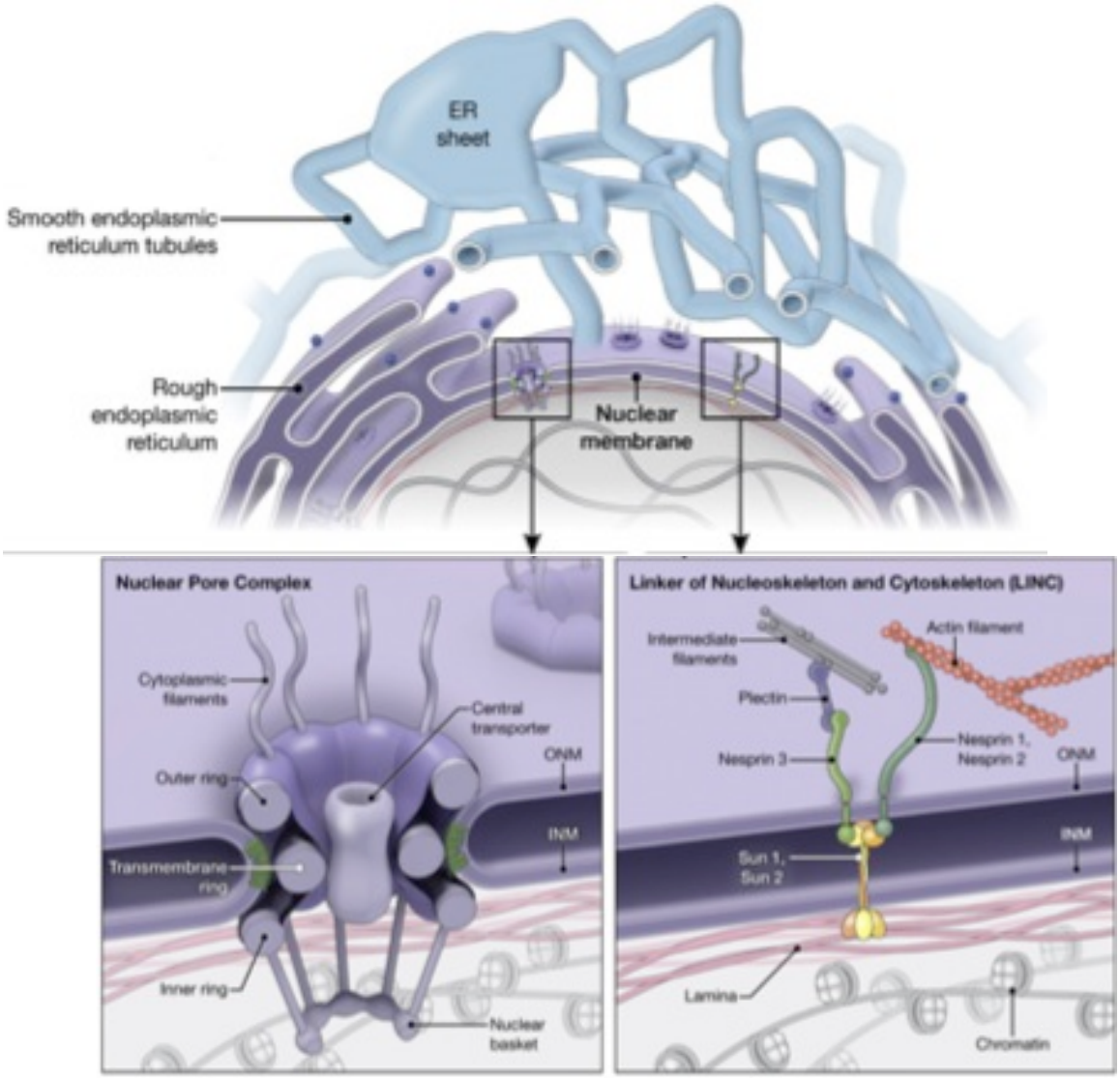

Figure 1.4. Maintaining rough ER sheets and the nuclear envelope structure. **(Top)** Schematic diagram showing the continuous lumen between the nuclear envelope and the ER network. **(Bottom)** Enlargements of the boxed areas outlined in **(A)**, showing the structure of the nuclear pore complex with ER-membrane sculpting reticulons (green) **(Bottom left)** and LINC complex **(Bottom right)**. Blue circles on rough ER represent ribosomes, INM, inner nuclear membrane; ONM, outer nuclear membrane. Reproduced with permission from Goyal and Blackstone, 2013[164].

The LINC complex also serves as a NE connection to the nuclear lamina and to the cytoplasmic cytoskeleton[406,474,526]. The expansive flat regions of the NE are further supported through interactions with the nuclear lamina and chromatin (Figure 1.4. Bottom right panel)[195,289,524]. Interestingly, although structural proteins like DP1/REEP/Yop1 and reticulon families are predominantly excluded from flat faces of the cisternae except at their sharply curved edges, nuclear pore formation requires these proteins (Figure 1.2.C, 1.4. Bottom left panel) [101,400]. It was proposed that these predominantly ER tubule localized proteins are required at nuclear pores to generate the necessary membrane curvature and aide in stabilizing these regions[101,499,551].

The ONM of the NE extends out into the cytoplasm as a tubular network and a large system of flat cisternal-stacked sheets, which are often closely associated with the NE in the perinuclear area. The sheets often adopt a 'pancake pile' arrangement, where the sheets are organized in parallel stacks connected by twisted membrane surfaces to maximize packing efficiency (Figure 1.4. Top panel). These properties are important for this particular ER subdomain's critical role in protein production and folding. Further evidence of the relationship between ER morphology prevalence and function can be observed in pervasiveness of rough ER in professional secretory cells, like plasma cells and pancreatic cells in which protein secretion is the predominate function[457]. These ER sheets are coated with polyribosomes, which give the ER subdomain the moniker rough ER. Ribosomes are clearly observed studding the highly organized membrane stacks in EM images[392,458,519]. Other than polyribosomes, ER sheets are heavily enriched in translocon proteins like Sec61, which facilitate protein transport across membranes. Both translocon complexes and polyribosomes are proposed to help stabilize and maintain ER

sheets. Further support for these conclusions come from studies using puromycin treatment to displace ribosomes from cisternae, which ultimately resulted in increased tubule formation[141,393].

These observations along with studies in *S. cerevisiae* lead to a model where relative ratio of phospholipids and curvature-stabilizing proteins determines the relative abundance of tubules and sheets[502]. If more ER tubule curvature-stabilizing proteins are present, then more tubules are generated, but inversely if ER sheet proteins predominate, then the protein ratio favors sheet formation. Proteins favoring sheet formation over ER tubules include coiled-coil proteins kinectin, p180, Climp-63 (cytoskeleton linking membrane protein formerly p63), and human TMEM170A (Figure 1.5.B)[84,289,519]. These proteins are integral membrane proteins that localize to the rough ER, but are excluded from the NE membrane with the exception of TMEM170A, which is present in both locations. The importance of this structural membrane protein ratio was further demonstrated by experiments in which knockdown of p180 led to an increase in ER tubules, whereas knockdown of Dp1/Yop1p and the reticulons lead to an increase of ER sheets. Knockdown of many of the aforementioned rough ER proteins or overexpression of ER tubule proteins such as reticulons results in sheet depletion and an increase in tubules (Figure 1.5.A)[289,458]. Interestingly, Climp63 depletion does not affect the ratio of ER structures, but overexpression results in an intense increase in sheets and a reduction in tubules (Figure 1.5.B), suggesting that these proteins function in opposition to the reticulon/Dp1/Yop1 families. Simultaneous overexpression of a sheet-promoting ER protein, Climp-63, and a ER tubule protein, Reticulon 4, normalizes the tubule to sheet ratio (Figure 1.5.C). These studies support the model in which ER subdomain structure

and prevalence within a cell results from the localization and ratio of structural ER tubule or sheet-associated proteins.

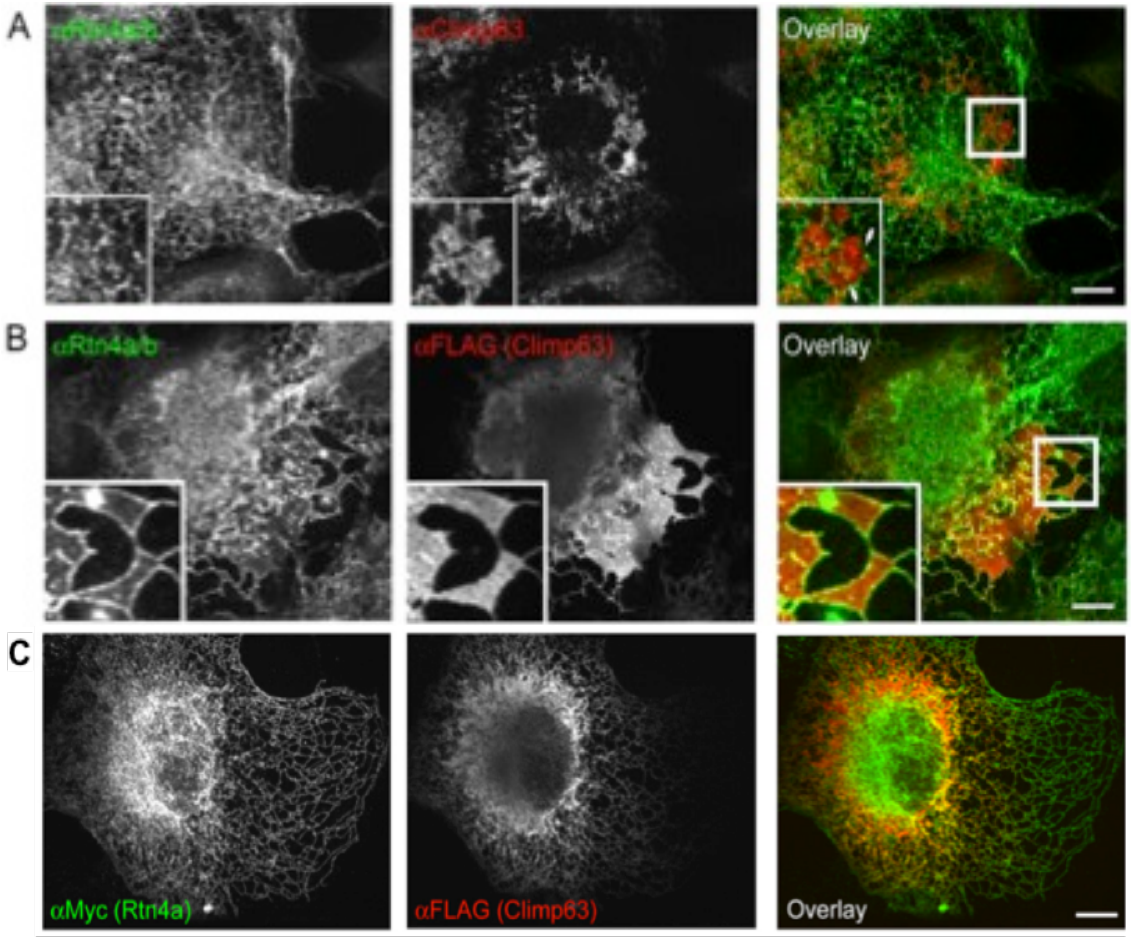

Figure 1.5. Ratio of structural ER tubule proteins relative to ER sheet shaping proteins determines prevalence each type of ER structure.[457]
(A) The localization of endogenous Rtn4a/b (green) is compared with that of Climp63 (red) using indirect immunofluorescence with specific antibodies in COS7 cells. The insets show enlargements of the boxed region. Arrows point to reticulons lining the sheets. The far-right panel shows merged images. Scale bar, 10 mm. **(B)** As in (A) but with cells overexpressing FLAG-Climp63. **(C)** Myc-Rtn4a and FLAG-Climp63 were both highly expressed in COS7 cells. The far-right panel shows a merged image. Note that the ER morphology is almost normal. Reproduced with permission from Shibata *et al*, 2010[457].

1.1.4. Reticulon family

Reticulons (Rtn) are an ancient family of membrane-associated proteins present throughout all eukaryotic cells. This family of proteins is evolutionarily conserved from yeast to humans[551], with four subfamilies in mammalian cells[549]. Reticulon subfamilies each have multiple spliced forms, yielding multiple isoforms for each group. Complicating matters is that Rtn subfamilies, even isoforms within the same subfamily, display highly divergent levels of protein expression dependent on cell types and origin. Although there are a wide assortment of reticulon isoforms that can be produced by any one cell, each isoform maintains the conserved reticulon homology domain (RHD) structural feature at its C-terminus, suggesting the array of reticulons have evolved species-and cell-type-specific roles (Figure 1.6.A)[441]. As such, reticulons have been shown to play a role in membrane trafficking, cytoskeletal rearrangement, endoplasmic reticulum curvature, apoptosis, viral restriction, autophagy, adhesion, ER-phagy, and regulation of migration of endothelial and vascular cells[75,103,108,166,169,416,439,545,551,568]. To adapt to these many functions, reticulons are found in various topological conformations (Figure 1.6.B)[551]. Reticulons share a conserved common carboxy-terminal domain known as the reticulon homology domain (RHD) consisting of two hydrophobic transmembrane domains bordering a 60-70 hydrophilic amino acid loop[57,268,353]. Although the structure of these transmembrane domains is the subject of debate, it is believed that the transmembrane domains adopt hairpin like turns within the membrane, as indicated by a 30-35 amino acid hydrophobic transmembrane domain, relative to the traditional 20 amino acid membrane spanning helix (Figure 1.6.B). This structure places the bulk of the hydrophobic regions in the outer leaflet of the phospholipid bilayer

(Figure 1.6.B, structure #2, #3), thus driving membrane curvature through a wedging mechanism.

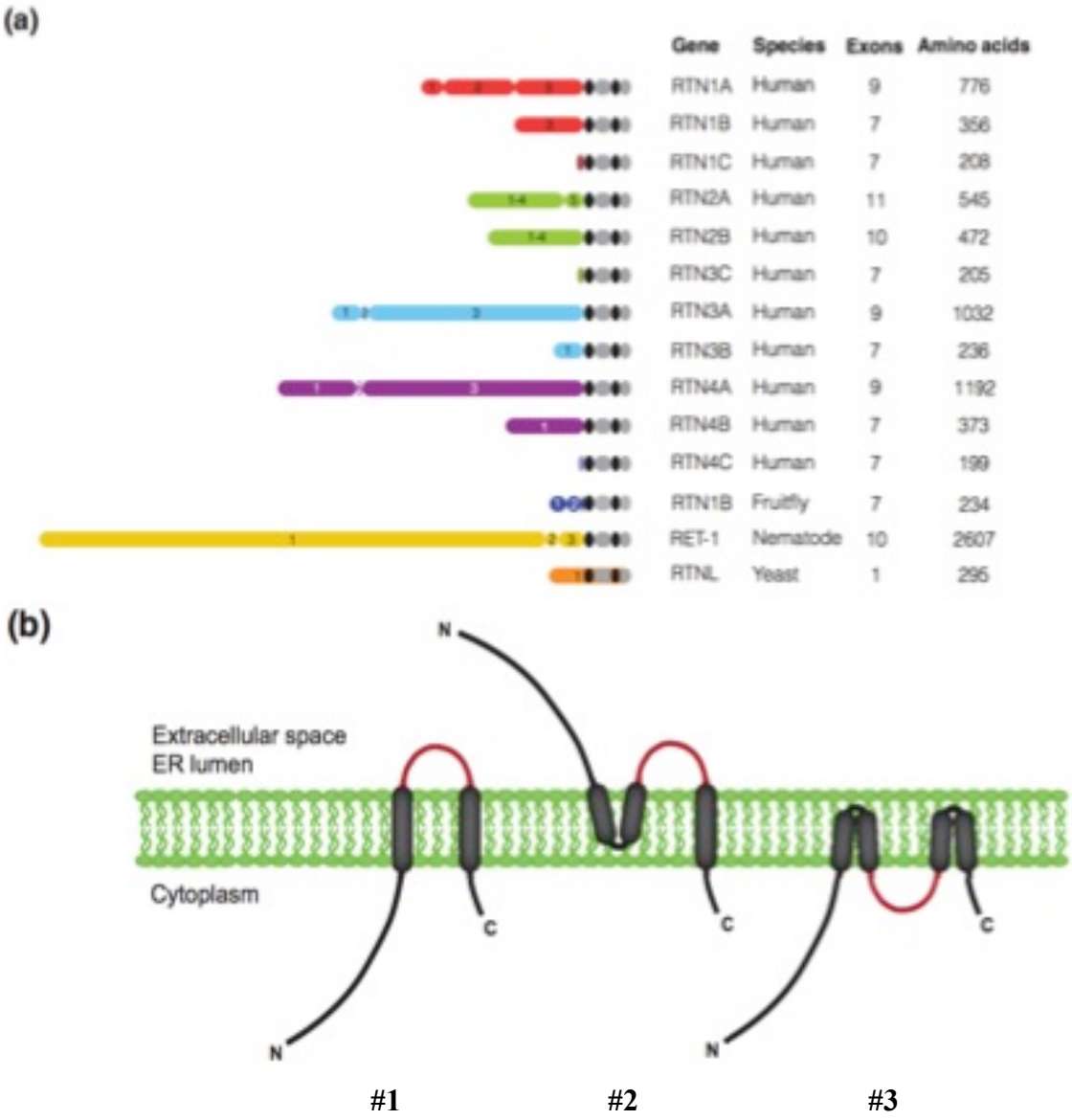

Figure 1.6. Reticulon family and membrane topology.
The structure and membrane topology of the reticulon family. **(a)** Structure of reticulons, aligned by C-terminus RHD (Reticulon homology domain), which consists of two membrane-anchored hydrophobic regions (black ovals) sandwiching a hydrophilic region (grey oval). Numbers indicate exons that encode designated protein segment. **(b)** Possible topologies of reticulon proteins within ER or plasma membranes. Although eight or more conformations are possible, the three depicted represent topologies supported by experimental evidence. Topologies are presumed to vary across cell types and differ depending on the type of membrane the reticulon is localized to. Reproduced with permission from Yang and Strittmatter, 2007[551].

Other proposed structures of the RHD have either the carboxy terminus transmembrane region or both transmembrane regions spanning the entire length of the bilayer, suggested through antibody access to reticulon domains experiments and predicted secondary structures (Figure 1.6.B, structures #1, #2)[190,268,499,551]. Contrary to the structurally conserved RHD, the amino termini of reticulons share little sequence homology and are highly divergent in size (Figure 1.6.A). Despite these differences, this family of proteins predominantly localizes to regions of high curvature in the ER, including the tubular ER, the curved edges of cisternae, and edges of NE pore sites (Figure 1.2.B,C; Figure 1.4. Bottom left panel; Figure 1.5.B). This localization to the ER is mediated by the RHD as reticulons do not contain an ER signal sequence and their localization only requires this conserved domain[80,439,551]. A fraction, typically less than >10%, of the reticulon population is detected at the plasma membrane with the amino termini present on the cell exterior according to antibody profiling[110]. This population of reticulons has been implicated in neurite outgrowth inhibition and chemotaxis[134,315,443,499].

Reticulon protein-interactions are important to their function throughout the cell, but also reflect the vast array of cellular processes that the protein family functions in. One of the most clinically important reticulon interactors is BACE1, the δ-secretase that cleaves amyloid precursor protein (APP) into β-amyloid peptide (Aβ). This enzyme is intimately involved in the development of Alzheimer's disease and Rtn1, Rtn2, Rtn3 and Rtn4 were all found to co-immunoprecipitate with BACE1[189]. Studies in which Rtn3 was knocked down, Aβ peptide levels increased and conversely, when Rtn was overexpressed the levels of Aβ was substantially reduced[189,336,390]. Researchers discovered that Rtn3 and Rtn4 specifically utilize RHD structure to interact with BACE1 and inhibit Aβ

production[188,190,268,336]. Clinically, it was discovered that Rtn3 was down regulated in the frontal lobes of Alzheimer's patients through a subtractive hybridization screen. This suggests alterations to reticulon levels are in fact associated with this important pathology[555].

Another important group of reticulon interacting proteins are other reticulons[169,403,449,459,520]. Both homo- and hetero-oligomers of reticulons have been described in the literature[459,570]. The protein's ability to homo- or hetero-oligomerize with other Rtns is essential for preserving tubular ER morphology and maintaining fluid membrane trafficking. The role of oligomers in trafficking was demonstrated in the aforementioned FRAP studies, in which oligomerization deficient reticulon mutants resulted in immobilization within the membrane. Furthermore reticulon interaction with other cellular proteins is affected by their oligomerization status, with some interactions preferentially occurring with Rtn monomers versus Rtn oligomers, such as the interaction with BACE1 and Rtn3[188,190,268,336]. Although the reticulon field has struggled with the breadth of reticulon associated functions, the connection between this protein family and several debilitating, incurable, neurological diseases makes reticulons irresistible targets for continued research and experimentation with therapeutic avenues, particularly in neurology [134,549,551,555].

1.1.5. Reticulon 4

Reticulon 4 (Rtn4), also known as neurite outgrowth inhibitor (NOGO) or neuroendocrine-specific protein (NSP), is transcribed from a 75kb gene with 9 major exons. The gene encodes 10 known variants through differential splicing and promoter

usage. Nogo A, B, C, and D also commonly referred to as Rtn4-A, B, C, and D are the four most common isoforms, with at least one expressed in most mammalian cells (Figure 1.7.A)[499,551,559]. Nogo/Rtn4-A is the largest isoform and is primarily expressed in brain and spinal cord cells and has been well studied in neurobiology field due to its functionally established role as a neurite outgrowth inhibitor. Rtn4-B is ubiquitously expressed in cells, with the most prominent expression in endothelial, inflammatory, and vascular smooth muscle cells. Nogo-C is the smallest of the three predominant isoforms and is primarily expressed in neurons and skeletal muscle cells (Figure 1.7.A)[442,499,520,570]. Reticulon 4 isoforms generate ER curvature through their RHD containing two conserved hydrophobic hairpins inserted in the cytoplasmic leaflet of the lipid bilayer (Figure 1.7. Bottom panel)[570]. Homo- and hetero-reticulon oligomers are believed to establish arc-like scaffolds[570]. Nogo isoforms are predominantly ER localized (>95%), but many of the functions attributed to the Rtn4 family in published literature originates from the small portion of Nogo's that are expressed at the cell surface[499,520]. The topology of Reticulon 4 within the membrane also varies depending on cellular localization and cell type as with other reticulon family members (Figure 1.7.B). More recent research has begun to focus on the Rtn4 family's role within the peripheral tubular ER and its association with debilitating and incurable neurodegenerative disorders like ALS (amyotrophic lateral sclerosis), hereditary spastic paraplegia, and Alzheimer's disease[80,439,443,549].

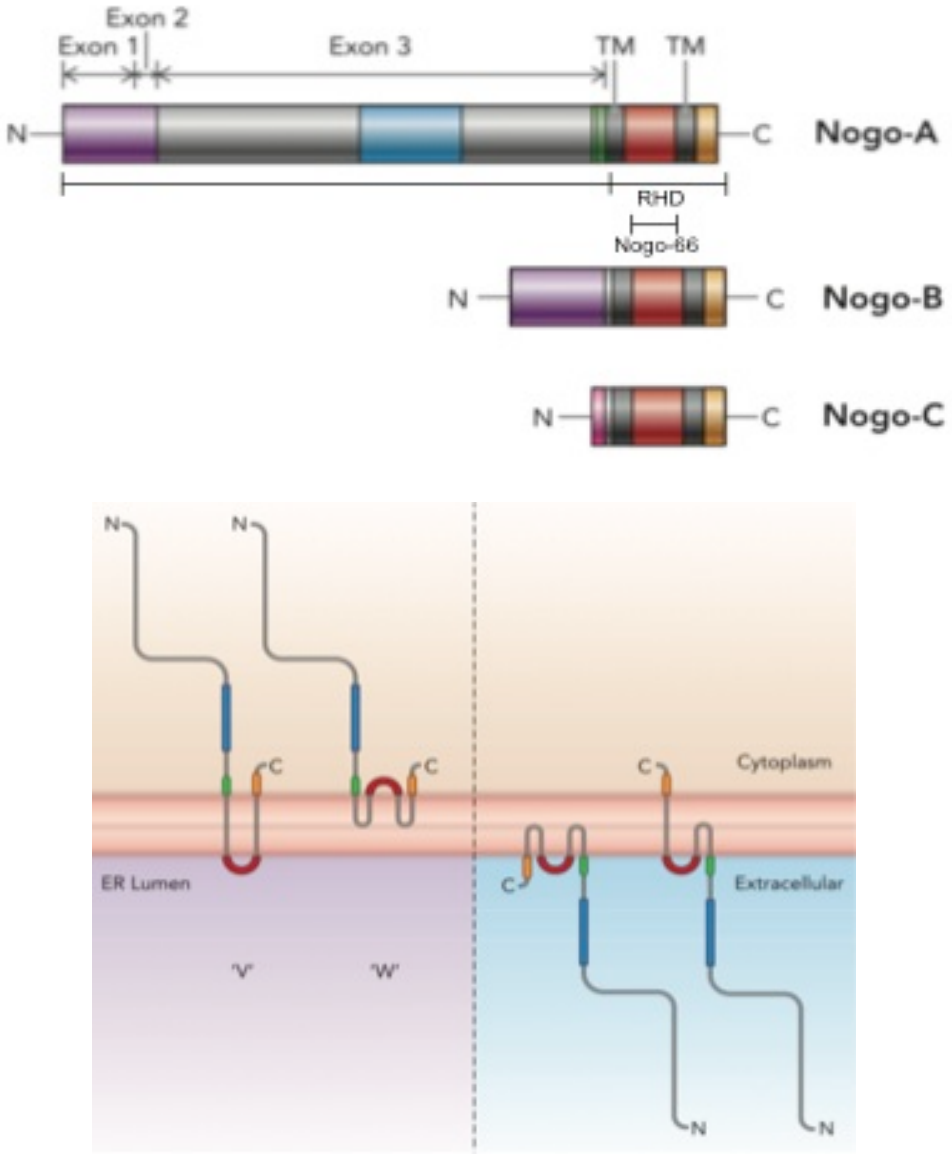

Figure 1.7. Protein structure and membrane topology of Rtn4/Nogo proteins. **(Top)** A graphic outline of the structure for Nogo/Rtn4 isoforms Nogo-A, Nogo-B, and Nogo-C. Several functional domains are indicated by colored sections. Nogo-A-Δ20 (blue) and Nogo-66 loop (red) are involved in neurite outgrowth inhibition and growth cone collapse. Nogo-A-24 (green) increases binding affinity of Nogo-66 to Nogo receptor 1 (NgR1) and Nogo-C39 (orange), which seems to enhance Nogo growth inhibitory properties relative to Nogo-66 alone. Nogo-66 is located between the transmembrane domains (TM) and found in all three isoforms. The Δ20 domain is encoded by parts of exon 3 and is specific to Nogo-A. **(Bottom)** Just as with other reticulons, multiple topologies have been proposed for Rtn4 within the ER (left) or the plasma membrane (right). Nogo-66 is present inside and outside of the ER lumen, suggesting the protein adopts a 'V' or 'W' configuration relative to the membrane. At the plasma membrane, both Nogo-A-Δ20 and Nogo-66 are extracellular. Reproduced with permission from Kempf and Schwab, 2013[246].

The wealth of Rtn4-interacting proteins reveals insights into the evolving list of Rtn4 functions. Rtn4 forms homo- and hetero-oligomers with other Rtns, particularly Rtn3 and Rtn4, and interacts with Atlastin-1, a GTPase involved in tethering and homotypic membrane fusion and the formation of 3-way junctions (Figure 1.2.B)[42,208,363,410,565]. Rtn4 also forms associations with the mitochondrial membrane associated anti-apoptotic factors Bcl-2 and Bcl-XL[493,525,568]. ADP-ribosylation factor-like protein 6-interacting protein 1 (Arl6IP1/ARMER) is another Rtn4 interactor that exhibits anti-apoptotic activity, likely by modulating caspase-9[300]. Rtn4 also interacts with the cytoskeletal protein alpha-tubulin and myelin basic protein[499]. An Rtn4b specific receptor, NogoB receptor (NgBR/NPC2-interacting protein), has also been discovered. This receptor interacts with the amino-terminal of Rtn4b and is important for cholesterol trafficking, as NgBR deficiency results in increased intracellular cholesterol and impaired sterol sensing[182,315]. Another Rtn4 receptor is the glycosylphosphatidylinositol (GPI)-linked cell-surface Nogo-66 receptor (NgR). This receptor relies on binding Nogo-66, a 66-aa loop within the RHD, to inhibit neuronal outgrowth upon receptor binding or cell receptor mediated cell adhesion and chemotaxis after NgR binding NogoB[52,137,315]. Other than Rtn4 localization to the ER, Rtn4 is further linked to the secretory system through interactions with several sorting nexins and synaptotagmin-16[419,536]. The wealth of Rtn4 interacting proteins across several key cell processes, along with the proteins functional and topological flexibility, indicate that there is likely still much to be uncovered by studying reticulons 4, particularly in ER biology and specific neurological pathologies.

1.2. Ubiquitination System

Post-translational modifications (PTMs) of proteins offer cells an opportunity to vastly increase the functional scope and utility of its proteome. These modifications offer a means of rapidly adapting cellular responses to quickly changing environments. Ubiquitination is the process of adding ubiquitin, a 76 amino acid polypeptide or ~8.5kDa protein, to a substrate protein through the formation of an isopeptide bond between the carboxy terminus of ubiquitin and a substrate protein often through a lysine residue[39,119,226,234,257,511]. This PTM was discovered in the 1970s and is found in all eukaryotic cells, but not bacteria or archea[247,431]. It represents one of the most important and ubiquitous PTMs in addition to phosphorylation. Ubiquitination of proteins is a reversible process that plays a crucial role in nearly all aspects of cellular biology, including regulation, signaling, and proteasomal degradation. Ubiquitin conjugation to a target protein can modulate target function and its ultimate fate within a cell[98,217,381,465]. Addition of this large protein modification to target proteins can serve to signal a protein for degradation by the proteasome, regulate enzymes, modulate protein trafficking and subcellular localization, or alter protein-protein interactions and signaling cascades[226,247,250,257,432,563]. The attachment of a single Ub moiety, termed monoubiquitination, or the production of Ub chains, either branched or linear in structure, termed polyubiquitination, provides clues to the modifications intent. For instance, polyubiquitination of proteins typically target the substrates for degradation, either through proteasomal or lysosomal systems[97,144,562], whereas monoubiquitination is involved in altering protein trafficking patterns[198,402], enlargement of COPII vesicles for large cargo transport [234], targeting proteins to the site of DNA repair[197,564], viral

budding[364,373,486], and also acting as a seeding event for the nucleation of protein aggregates in neuronal plaques present in neurodegenerative diseases, such as Parkinson's and Alzheimers[119].

This PTM is classically catalyzed by three enzymes: a ubiquitin-activating enzyme (E1s), which activates ubiquitin in an ATP-dependent step; ubiquitin-conjugating enzyme (E2s), which accepts activated ubiquitin from the E1; and ubiquitin ligase enzyme (E3s), which accepts ubiquitin from the E2 and transfers it to a specific substrate protein (Figure 1.8.A)[39,129,197,376,431,432]. There several diverse categories of E3 Ub ligases, the most variable and abundant class of Ub enzymes with several hundred being reported in humans[216]. These enzymes can be classified as either 1) HECT (homologous to the E6AP C-terminus) E3s that use a cysteine residue to directly accept charged Ub from an E2 prior to Ub ligation to a substrate, 2) RING (really interesting new gene)/U-box (RING/U-box) E3s, which act primarily as a Ub scaffold recruiting a Ub charged E2 and substrate to promote direct transfer from the E2 to the substrate, 3) F-box containing proteins, which function similar to RING ligases, 4) NEL (Novel E3 Ligase) E3 ligase, which is structurally divergent from other ligases, but functions similarly to HECT Ub conjugation, or finally 5) SidC, an *L. pneumophila* T4SS translocated proteins with a highly unconventional Ub ligase fold unlike any other described E3 (Figure 1.8.B)[106,183,206,216,389,432]. E3 enzymes are responsible for positioning substrates for ubiquitination and determining the Ub chain linkage. E3 RING ligases rely on the recruited E2 to dictate Ub linkage[106,183,377], whereas HECT E3s encode the Ub linkage preference through a C-terminal lobe in the E3[91,249].

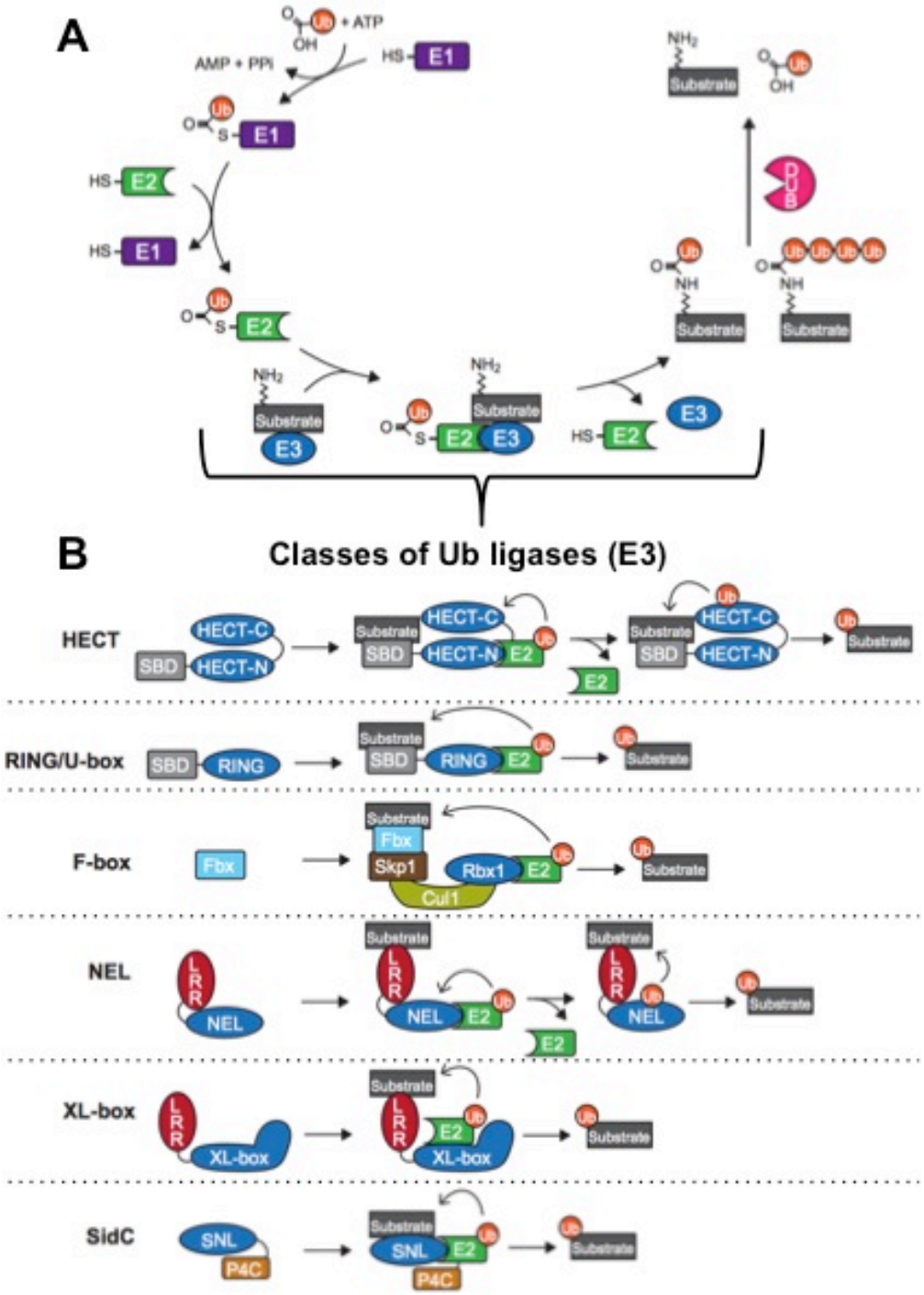

Figure 1.8. Ub conjugation/deconjugation system and classes of Ub ligases (E3s). **(A)** The reversible ubiquitination process relies on a series of enzymes. The ubiquitination cascade can be divided into three distinct steps, with a different class of enzyme catalyzing each step. Steps: 1) Ubiquitin-activating enzymes (E1, purple rectangle) utilize energy from ATP hydrolysis (to AMP and PPi) to form a covalent thioester linkage with the C-terminus of Ubiquitin (Ub, small orange circle). 2) Activated Ub is transferred to a cysteine residue on a Ub-conjugating enzyme (E2, green rectangle

with semi-circle cut out). 3) Lastly, an E2 complexes with a ubiquitin ligase (E3, blue oval) that coordinates covalent attachment of Ub or Ub chains to a substrate protein (grey box labeled substrate). Reversal of the substrate ubiquitination is catalyzed by proteases called deubiquitinase (DUB, pink 'Pac-man' shape) enzymes that deconjugate ubiquitin or ubiquitin chains from substrates. **(B)** There are several classes of E3 ligases that are differentiated by structure and mechanism used to coordinate Ub ligation with E2 enzymes. A schematic showing the Ub transfer from E2 to substrate protein for each E3 class is shown. For simplicity, the substrate protein is shown with only one Ub molecule attached. The **HECT**-type E3 ligase is composed of an N- and C-terminal lobe. Ubiquitin is transferred from the E2 to a cysteine residue in the C-lobe before its final attachment to the substrate protein, which is bound by the substrate-binding domain (SBD). **RING/U-box-type** E3 ligases do not form a stable intermediate with ubiquitin, rather they serve as a scaffold to arbitrate Ub transfer directly from an E2 to the substrate. **F-box** (Fbx) domain-containing proteins interact with the SCF complex (Skp1, Cul1, and the E3 ligase Rbx1) to bind a substrate protein and facilitate ubiquitin transfer. **NEL** E3 ligases, rely on a mechanism similar to HECT ligases. An N-terminal leucine-rich repeat (LRR) domain in NEL enzymes enables substrate binding and a transient Ub intermediate forms with a cysteine in the NEL domain prior to transfer to the bound substrate. **XL-box**-containing E3 ligases are similar to RING/U-box-type E3 ligase in that they facilitate substrate ubiquitination without the formation of a stable Ub intermediate and mimic NEL ligases with an the N-terminal LRR domain to mediate substrate interaction. **SidC**, a *L. pneumophila* T4SS translocated protein, contains a completely divergent N-terminal E3 ligase structure (SNL), unlike any known E3s ligases. The SNL domain relies on host cell E2s to facilitate substrate ubiquitination and a C-terminal domain (P4C) that serves to link SidC to PI(4)P-containing membranes like the *Legionella*-containing vacuole (LCV). Adapted and reproduced with permission from Lin and Machner, 2017[290]. Main panel from figure 1 was combined with figure 2. Smaller panels from figure 1 (E3/DUB enzyme lists and Ub linkage outcomes) were excluded for simplicity.

As mentioned earlier, the addition of a single ubiquitin molecule constitutes monoubiquitination, whereas the addition of a single ubiquitin molecule at several different target residues is termed multi-monoubiquitination. The formation of polymeric ubiquitin chains occurs through ubiquitin attachment to one of the seven-lysine residues in an additional ubiquitin molecule[12,197,257,432,478]. These chains can be composed of two to more than ten ubiquitin moieties and result in homotypic, heterotypic, or branched linkages between lysine residues on subsequent ubiquitin molecules[3,160,257]. These varying topologies and chain lengths trigger distinct outcomes for proteins,

demonstrating ubiquitination versatility as a cellular code for storing and communicating information regarding modified proteins[3,132,247,257,432].

Monoubiquitination and multi-monoubiquitination induce unique responses relative to the various cues from polyubiquitin chains, which are more classically associated with tagging proteins for degradation by the proteasome, lysosome, and initiating signaling cascades/complexes [173,197,209,234,297]. Monoubiquitination plays a role in membrane receptor endocytosis[197,234,257,297,478,515,523], enlargement of vesicles for large cargo transport[234], cell cycle progression[278,446], lipid droplet clustering[297], trafficking between vesicular compartments[421,431], and histone monoubiquitination is important for normal meiosis of a cell[197]. One particularly interesting case of monoubiquitination regulation is through targeting the COPII component, Sec31. Monoubiquitination of Sec31 is believed to control the size and function of a vesicle coat needed to accommodate oversized pro-collagen filaments and other large cargo[234]. This PTM system also has important implications in various pathologies including Fanconi anemia[372,563,564], retroviral budding[197,421], *Listeria* internalization[478,515], and several neurodegenerative diseases, like Parkinson's disease[39,86,376,421]. In the case of Parkinson's disease, the pathology is characterized by death of in dopaminergic neurons and the presence of inclusion bodies, known as Lewy bodies. Monoubiquitinated α-synuclein is a primary component of Lewy bodies and the PTM is believed to act as a seeding event for the formation of these inclusion bodies[119,423]. Furthermore, the α-synuclein monoubiquitination appears to code for different degradation rates dependent on the substrate residue targeted for Ub addition[3]. Monoubiquitination serves as a distinct cellular PTM resulting in circumstance specific protein responses. Due to this system variability, crucial details on how the

monoubiquitin signal serves to alter a protein's structure, localization, and/or enzymatic activity remain to be discovered.

1.3. Autophagy and the ER

Autophagy is an evolutionarily conserved self-degradative/recycling pathway that governs the turnover of long-lived, misfolded, or aggregated proteins and organelles through lysosomal degradation[36,127,235,320,430]. This catabolic pathway traffics substrates, such as cytoplasmic content, dysfunctional organelles, aggregated proteins, and microbial pathogens to lysosomes for degradation by hydrolytic enzymes. Lysosomal degradation generates metabolites that are reused by the cell for energy and the synthesis of new macromolecules[430,451]. Several autophagic pathways exist, exhibiting variations on their cargo and route to lysosomes. They can be categorized as the non-selective degradation pathways of macroautophagy and microautophagy, along with the signal- specific degradation through chaperone-mediated autophagy (Figure 1.9)[147,407]. Macroautophagy, which from here on out will simply be referred to as 'autophagy', is the cellular process of 'self-eating', in which proteins and organelles from the cytoplasm are degraded in a highly coordinated fashion through autophagosome sequestration in a multi-membrane vacuole (Figure 1.9.A)[323,498,552]. On the other hand, microautophagy involves the direct engulfment of cytosolic components by the lysosomes, in mammals, or vacuoles, in plant and fungi[284,434,463]. The lysosome/vacuolar membrane invaginates, engulfing cytosolic components, including organelles like peroxisomes and the nucleus (Figure 1.9.C)[193,205,206,224]. The last autophagic branch is the selective chaperone-mediated autophagy, which is specific for the degradation of soluble cytosolic proteins with a

‘‘KFERQ’’ motif, and no lipid or organelles are turned over via this pathway (Figure 1.9.B)[96,109,283,331,370]. The molecular chaperone, heat shock cognate protein of 70 kDa (Hsc70), interacts with the pathway receptor, the lysosome-associated membrane protein type 2A (LAMP-2A), to facilitate direct transfer of these proteins across the lysosomal membrane (Figure 1.9.B)[19,34,96,243,258,283,362].

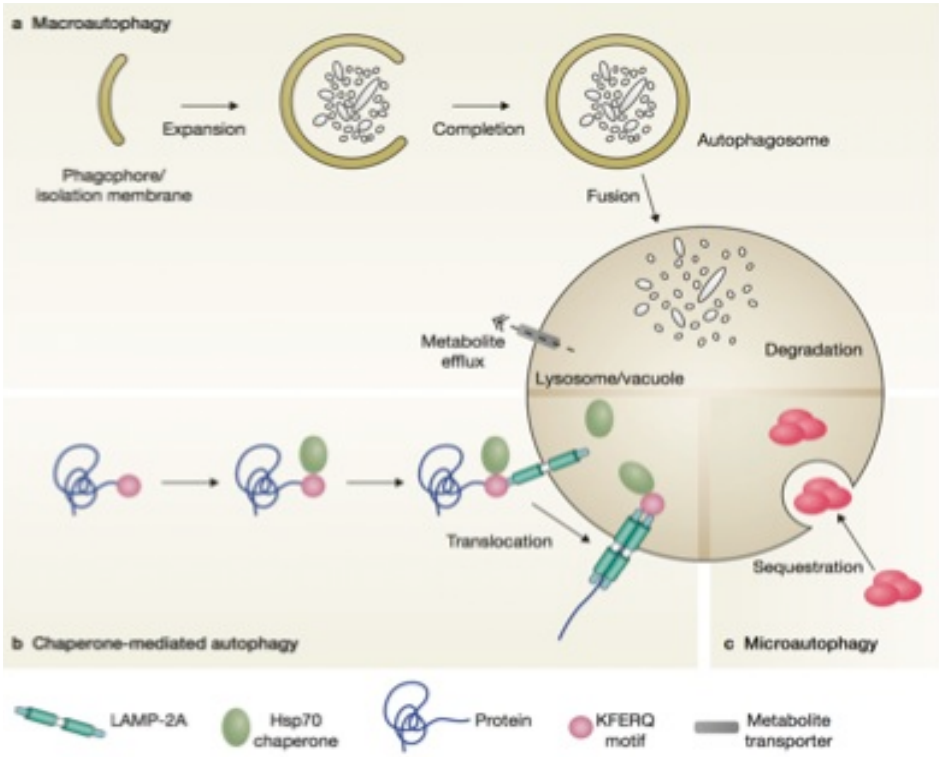

Figure 1.9. Macroautophagy, Chaperone-mediated autophagy, and microautophagy.
The three major classes of autophagy have been described **(a)** macroautophagy, also simply autophagy, is a process in which double-membrane vesicles sequester cytosolic components in an autophagosome compartment. Mature autophagosomes then fuse with lysosomes exposing the luminal contents to lysosomal hydrolytic enzymes. Degraded contents serve as recycled metabolites that are transported back into the cytoplasm for energy or macromolecule building blocks. **(b)** Chaperone-mediated autophagy (CMA) targets proteins carrying the pentapeptide KFERQ-like sequence, which is recognized by the Hsc70 chaperone that then associates with the lysosomal integral membrane proteins LAMP-2A. This interaction triggers LAMP-2 oligomerization, promoting translocation of the KFERQ protein into the lysosome interior through a process that requires Hsc70. **(c)** Microautophagy is a process in which targeted material (red circles) is recruited to in proximity of the lysosomal membrane and the lysosome membrane then invaginates and pinches off bringing the material into the lysosome interior. Reproduced with permission from Boya, Reggiori, and Codogno, 2013[55].

Each of these processes is critical for cellular homeostasis and is considered a survival or adaptive process, since each pathway is induced upon cellular stress, including starvation, chemical perturbations, or the presence of infectious agents. As such, autophagy is linked to numerous physiological and pathological conditions, such as programmed cell death[104,127,136,296,333,346], cancer[20,102,264,269,287,495], innate and adaptive immunity to pathogens[62,105,235,282,318], neurodegenerative maladies[20,436,505], and myopathies[114,438,462].

Macroautophagy has been best characterized in yeast. After signaling initiates the autophagic process in yeast, Atg (autophagy) proteins accumulate at a single specialized site termed the phagophore assembly site or pre-autophagosomal structure (PAS). An equivalent structure in mammalian cells has not been described, as autophagosomes appear to develop at multiple ER-associated sites throughout the cell, potentially explaining the multiple phagophore membrane sources that have been reported in the literature[36,178,460]. Numerous studies have demonstrated an intimacy between autophagosome biogenesis and ER structures, in which the ER provides a membrane platform for scaffolding of autophagosomal machinery, promotes expansion of isolation/autophagosome membranes, and budding of mature autophagosomes[26,165,177]. ERES[165,437], ERGIC[152,171], and ER-mitochondrial contact sites (MAMs)[149,174,177,305,312] have been implicated as preferred phagopore initiation sites as well as membrane source material for developing autophagosomes. During initiation of autophagy by starvation in mammalian cells, the SNARE (soluble N-ethylmaleimide-sensitive factor-attachment protein receptors) protein syntaxin-17 (Stx17) interacts with homo-oligomers of Atg14L, Beclin 1-associated autophagy-related key regulator, to form an autophagy-specific

phosphatidylinositol 3-kinase complex, PI3KC3-C1[128,222,311,338,570]. Atg14L accumulation and oligomerization occurs on the ER at MAM sites (Figure 1.10.A)[177]. The Atg14L relocalization from the Golgi to the ER promotes Atg14 homo-oligomerization, which is important for early autophagosome biogenesis. Studies found both MAM and ERGIC disruption resulted in defuse Atg14L ER localization and subsequent autophagosome formation defects[152,177,334,460].

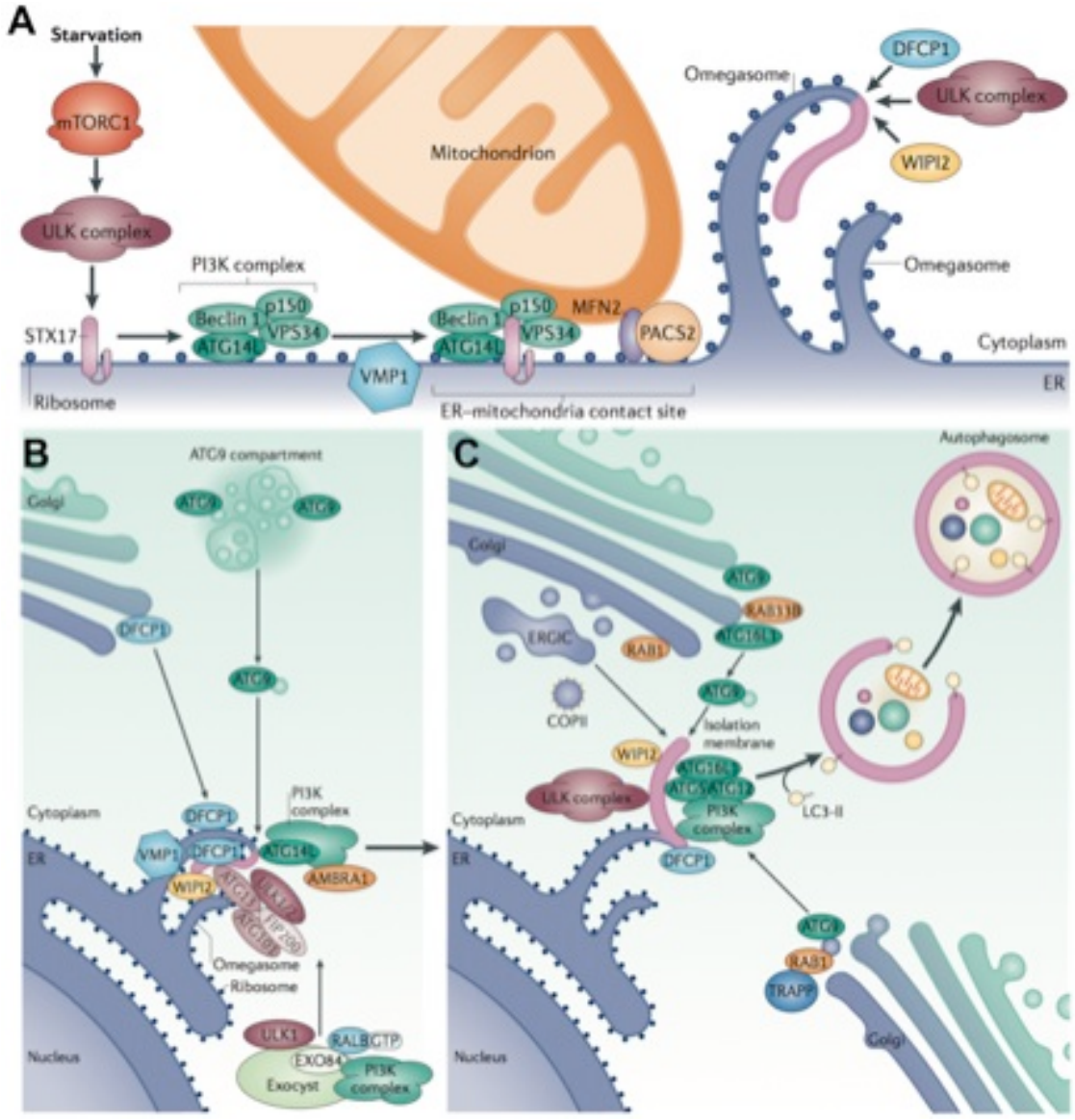

Figure 1.10. Autophagy initiation, formation and expansion of the isolation membrane.

(A) Upon transmission of a starvation signal through the mammalian target of rapamycin complex 1 (mTORC1) – UNC51-like kinase (ULK; comprising ULK1 and ULK2) complex axis, the endoplasmic reticulum (ER) resident protein syntaxin 17 (STX17) is activated and binds autophagy-related 14-like protein (ATG14L), a subunit of the class III autophagy-specific PI3K complex that contains Beclin 1, p150 and the PI3K vacuolar protein sorting 34 (VPS34). This complex then translocates to the ER–mitochondria contact site, where PI3K locally produces phosphatidylinositol-3-phosphate (PtdIns(3)P)81 (not shown). This triggers deformation of the ER membrane, which leads to the recruitment of the ULK complex and PtdIns(3)P effectors such as double FYVE-containing protein 1 (DFCP1) and WD-repeat domain phosphoinositide-interacting g 2 (WIPI2). This results in the formation of the omegasome to create the isolation membrane (pink). This region of the ER membrane also contains vacuole membrane protein 1 (VMP1). Mitofusin 2 (MFN2) and phosphofurin acidic cluster sorting protein 2 (PACS2) are components of the mitochondria contact site and are essential for its formation. **(B)** The initiation of autophagy at the omegasome requires the UNC51-like kinase (ULK) complex (which contains the Ser/Thr kinases ULK1 and/or ULK2, ATG13, FAK family kinase-interacting protein of 200 kDa (FIP200) and ATG101) and the class III PI3K complex. These complexes have been proposed to be delivered to the isolation membrane from a protein scaffold platform that is created by the EXO84-containing exocyst subcomplex, which is activated by GTP exchange on RALB10 . AMBRA1 (activating molecule in Beclin 1-related autophagy 1) is likely to associate with the PI3K complex at the omegasome. The omegasome is a membrane platform that is connected to the endoplasmic reticulum (ER) and is identified by the presence of double FYVE-containing protein 1 (DFCP1). The isolation membrane grows out of the omegasome platform76 (pink). DFCP1 is mobilized from the Golgi. VMP1 (vacuole membrane protein 1) is a multi-spanning ER and Golgi membrane protein that promotes Beclin 1 recruitment to the ER (not shown). WIPI2 (WD-repeat domain phosphoinositide-interacting 2) is an autophagy-related (ATG) protein and a phosphatidylinositol-3-phosphate (PtdIns(3)P) effector that is recruited to the omegasome. ATG9-postitive vesicles that originate from the ATG9 compartment 45–47 provide membrane to the isolation membrane in a manner dependent on ULK1 activity. ATG14L associates with the membrane and helps to direct the PI3K complex to the omegasome. **(C)** Coat protein complex II (COPII) vesicle traffic from the ER– Golgi intermediate compartment (ERGIC) is required for LC3 lipidation (to form LC3-II) and autophagosome formation. Further membrane is contributed to the isolation membrane by vesicles from the Golgi. This vesicular traffic step delivers additional ATG9-positive membranes and may involve a mammalian TRAPP (transport protein particle) complex, as well as possibly RAB1 and RAB11. Additional evidence suggests that RAB33B 100 may also have a role in delivering vesicles to the isolation membrane by interacting with the ATG16L1 complex. Adapted with permission from Lamb *et al*, 2013[274] by combining figures 2 and figure 3.

In mammals, PAS-like sites develops at ER regions enriched in phosphatidylinositol-3-phosphate (PI3P) and accumulate the PI3P-binding protein

DFCP1 (Figure 1.10.A-C)[210,311,490]. The formation of the Atg14L-SNARE complex positively regulates the formation of the DFCP1-positive ER cradle at sites termed omegasomes (Figure 1.10.A). The name was derived from microscopy studies in which DFCP1 localization generated ~1 μm diameter Ω-shaped rings on the ER[26,210,498]. From these PI3P- ATG14L-rich regions of the ER, LC3-positive isolation membranes, also called phagopores or pre-autophagosomes, emerge from within the omegasome ring and extend out from the center. Narrow membrane extensions interconnect ER sheets with the isolation membrane. These sheets were observed tightly sandwiching the forming crescent isolation membrane and are proposed to stimulate and guide isolation membrane development and elongation (Figure 1.10.A)[512,553]. The observation of tight physical links between the ER and developing phagopore, along with the fact that 70% of formed autophagosomes were discovered to contain sections of the ER, support the idea that this ER cradle and the omegasome actually represent the same structure[186,553]. Furthermore, these ER interaction sites with the isolation membrane are proposed to mediate lipid transfer to budding autophagosomes directly from the ER membrane. Although there is strong precedence for the role of the ER in autophagosome biogenesis, other lipid sources including mitochondria, Golgi, and the plasma membrane have also been implicated as membrane donors[152,171,174,177,405].

Two ubiquitin-like systems carefully regulate the autophagic process. The first Ub-like system is the Atg12-Atg5-Atg16L1 complex, which associates with the forming isolation membrane enhancing localized LC3 lipidation. The second Ub-like system is that of LC3 lipidation. In this reaction, the lipid phosphatidylethanolamine (PE) is conjugated to cytosolic ATG8 homologues, as detailed below [153,321,358,497,498]. These Ub-

like systems along with the transmembrane protein Atg9, Rab32, and Rab33b[13,74,200,225,566] promote membrane expansion and elongation allowing the double membrane 'cup' to engulf cytoplasmic components or organelles, including targets such as the ER and mitochondria (Figure 1.10.B,C)[127,158,371,407]. After the isolation membranes fuse together, effectively closing the membranous 'cup', an autophagosome is formed (Figure 1.11). As autophagosomes arise throughout the cytoplasm they traffic along microtubules toward lysosomes amassed around the perinuclear area[130,229]. Once in close proximity, oligomeric ATG14 utilizes its membrane tethering, and fusion-enhancing activities, in complex with SNAREs STX17 and SNAP29 on the cytosolic-facing autophagosome membrane. This complex primes the vacuole for interaction with VAMP8 to induce autophagosome-endolysosome fusion[107,223,489], resulting in the formation of an autolysosome[107,214,224,293]. In this compartment the luminal content of the vacuole is then degraded by lysosomal proteases, generating metabolites for reuse by the cell.

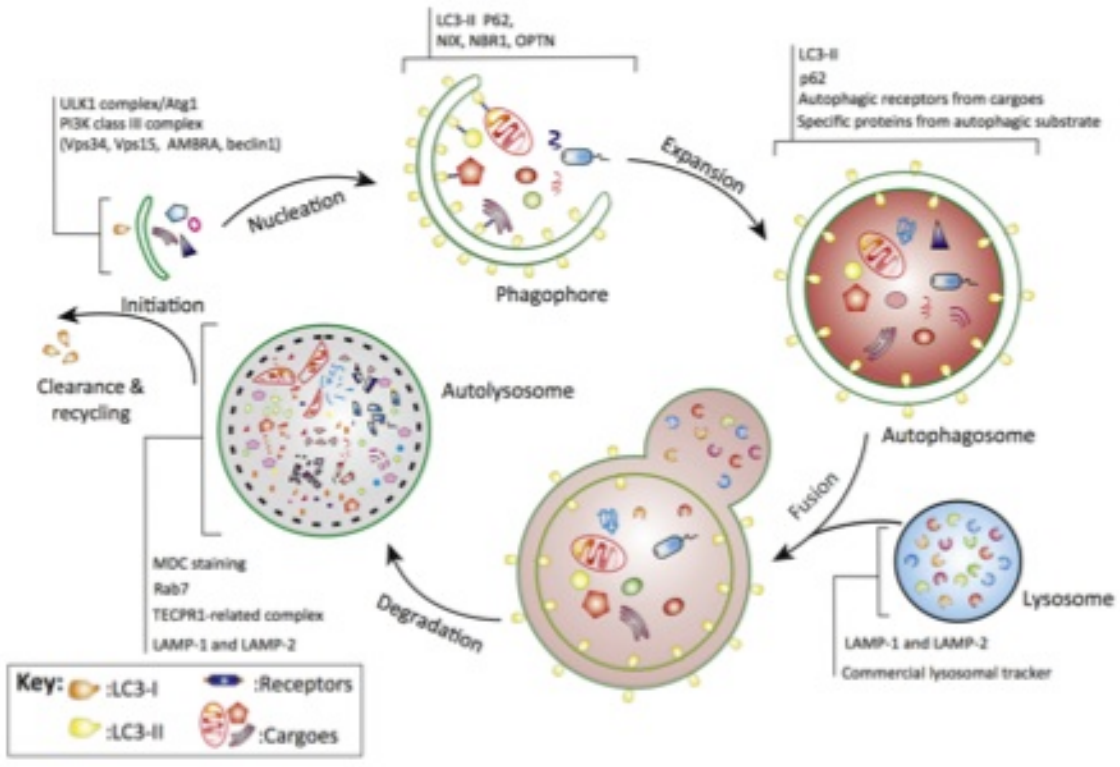

Figure 1.11. The autophagic process with associated marker proteins for each phase. A few protein complexes that specially accumulate in different stages of autophagy can be employed to monitor autophagic flux. At the beginning of autophagy, a phagophore originating from the phagophore assembly site (PAS) with initial complexes containing ULK and PI3K Class III, forming with structures known as omegasomes (see Figure 1.10.). The elongating phagophore membrane is associated with lipidated LC3 (LC3-II) and cargo receptors like p62 and optineurin (OPTN) (see also Figure 1.16.B) and the membrane ultimately fuses with itself to seal cytosolic cargo in a double-membrane structure called an autophagosome. The autophagosome membrane remains associated with lipidated LC3 and cargo receptors. Next, the autophagosome membrane fuses with the lysosome to generate an acidic autolysosome compartment labeled with LAMP-1/LAMP-2 and Rab7. After a degradation of autolysosome contents by lysosomal hydrolases, the degraded components are recycled back to the cell as amino acids, glucose, and lipids, for macromolecule synthesis and maintenance of cellular homeostasis. LAMP, lysosome-associated membrane protein; MDC, monodansylcadaverine; PI3K, phosphoinositide 3-kinase; ULK, Unc-51-like kinase, OPTN, optineurin; LC3-I, cytosolic LC3; LC3-II, membrane associated LC3 conjugated to phosphatidylethanolamine (PE). Reproduced with permission from Wang *et al*, 2017[528].

As mentioned previously, the process of isolation membrane elongation during autophagosome development is regulated by two critical ubiquitination-like

reactions[64,247,321,386,540]. The first reaction employs the Ub-like moiety Atg12, which is conjugated to Atg5 by Atg7, an E1-like Ub-activating enzyme, and by Atg10, E2-like Ub-conjugating enzyme. This complex then interacts with Atg16L1 resulting in association of the protein complex with nascent phagopores (Figure 1.10.C), followed by dissociation from mature autophagosomes[153,247,428]. The second Ub-like reaction regulating autophagy depends on the conjugation of Ub-like molecules from the Atg8 family to the lipid moiety phosphatidylethanolamine (PE). This family of Ub-like modifiers is composed of three subfamilies: LC3, GABARAP and GATE-16. The E1-like Atg7 and the E2-like Atg3, conjugate cytosolic LC3 (LC3-I), also referred to as the microtubule-associated protein 1 light chain 3 (MAP-LC3 or Atg8), to PE, producing a membrane bound LC3-II (Figure 1.10.C). It has also been proposed that the LC3 ligation to PE is enhanced by the E3-like activity of the Atg5–Atg12 complex, which may also help dictate autophagosome synthesis sites. Unlike the Atg5–Atg12–Atg16L1 ternary complex, the lipidated LC3 (LC3-II) remains in association with mature autophagosomes through their fusion with lysosomes. Lysosomal fusion results in the degradation of LC3-II present within the autolysosomes, while cytoplasm-facing LC3-II is recycled back into the system as LC3-I after de-lipidation.

A simplified outlook on this process indicates Atg5–Atg12–Atg16L1-positive LC3-positive structures are phagopores, whereas Atg5–Atg12–Atg16L1-negative LC3-positive vesicles are regarded as mature autophagosomes[451,498]. These streamlined definitions do not account for intermediate structures that arise during the process. Much like the oversimplification of ER structures and subdomains, this simplified classification results in a piecemeal understanding of the structure, shape, and protein composition of

the autophagy membranes during their development[428]. A commonly utilized method for measuring induction of the autophagic pathway employs the LC3-PE ligation process. Increases in LC3-II relative to a housekeeping control protein are frequently used as a readout for autophagy induction[30,322,323,556]. Previously a comparison of LC3-I to LC3-II ratios was also considered a diagnostic readout for autophagy, but a thorough examination of the system revealed that antibodies often show higher affinity for LC3-II species. Consequently the ratio between the two species is not an accurate reflection of the amount of cytosolic to membrane-bound LC3. In addition, the appearance and levels of LC3-I are highly variable by cell type and treatment condition often leading to false positives[233]. Other established tools include the following: electron microscopy (EM) for autophagic structures[43,554], and ELISA[357] for LC3-II levels; immunoblotting for p62 degradation[46,368]; fluorescence microscopy for LC3 puncta[233,391,401]; autophagosome and autolysosome detection using flow cytometry[451,529]. Finally, there is an extensive catalogue of fluorescent reporters used to monitor localization changes in autophagic markers along with pH changes in the vesicular compartment[30,170,233,319,322,357,391,556]. Developing new methods, while improving classic techniques to monitor autophagic flux, is critical to understanding this catabolic process in cellular homeostasis. Most important is using these research tools to unravel the links between autophagy and host immunity or neurodegenerative disorders.

1.4. ADP-ribosylation, a PTM, and bacterial toxin.

ADP-ribosylation, like ubiquitination and the Atg8 lipidation during autophagy, is a reversible post-translational modification, in which ADP-ribose is added to a substrate

protein at an arginine, lysine, cysteine, asparagine, or diphthamide (modified histidine) residue[280,466]. β nicotinamide adenine dinucleotide (β-NAD^+) acts as a cofactor for ADP-ribosyltransferases (ARTs), which cleave ADP-ribose from β-NAD^+, releasing nicotinamide, and transferring the ADP-ribose to a protein substrate (Figure 1.12)[280]. This process can be partially reversed by ADP-ribosylhydrolases, which cleave the ADP-ribose from the substrate protein, leaving an unmodified target and free ADP-ribose, but NAD^+ is not regenerated in the process (Figure 1.12)[93].

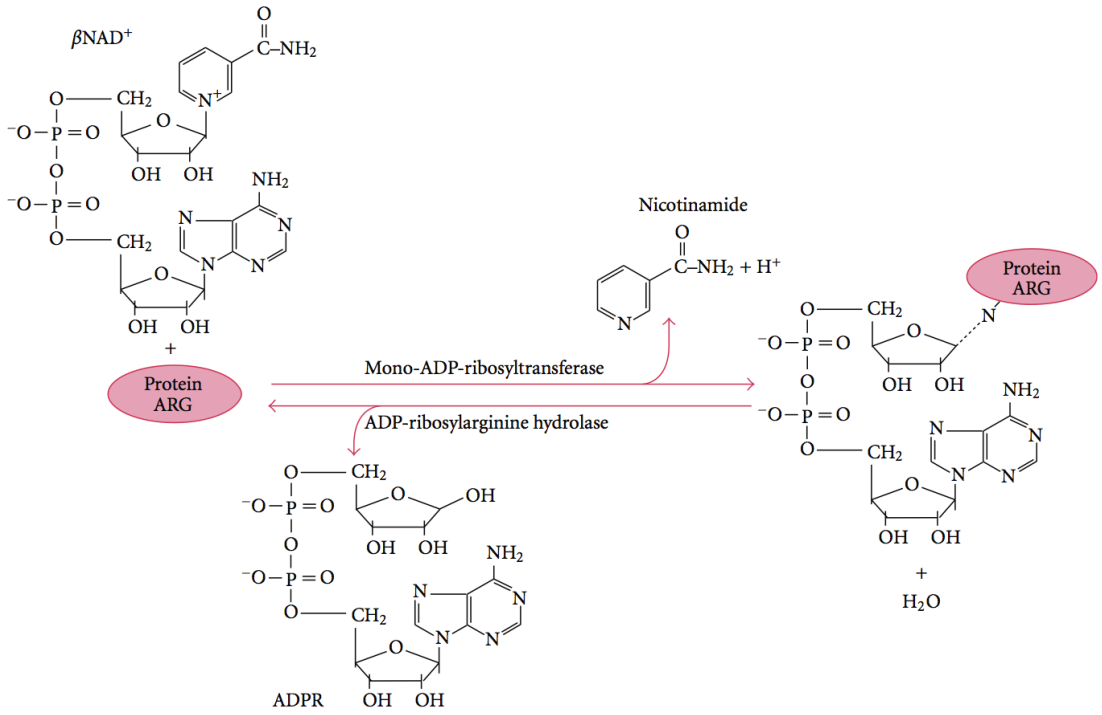

Figure 1.12. ADP-ribosylation of proteins.
Schematic representation of the enzyme-catalyzed reversible mono-ADP-ribosylation reaction. The diagram shows the enzymatic cleavage of β-NAD+ by an ADP-ribosyltransferase facilitating the covalently attachment of ADP-ribose to the guanidine group of an arginine residue and release of nicotinamide. The native arginine residue in a target protein is restored by ADP-ribosylarginine hydrolase cleavage of the α-glycosidic bond, releasing ADP-ribose. Reproduced with permission from Balducci *et al*, 2011 [27].

These enzymes are present in both prokaryotes and eukaryotes. Prokaryotes produce primarily mono ADP-ribosyltransferases. Eukaryotes harbor both poly ADP-

ribosylpolymerases (PARPs) and mono-ADP-ribosyltransferases (mono-ARTs) that add either polymeric ADP-ribose chains or a single ADP-ribose moiety to a protein respectively. Interestingly, enzymes for removal of ADP-ribose, like ADP-ribosylhydrolases (ADH) are curiously absent from certain genomes, including yeast, flies, and worms [159,272,310]. ART activity has been well studied in the context of pathogenesis, since many bacterial pathogens produce ADP-ribosyltransferases that act as toxins, crippling critical host proteins during infection. Actin, vimentin, RhoA, elongation factors, and GTPases are just a few targets of bacterial ARTs[7,263,360,488,5037,263,503]. The addition of ADP-ribose to a substrate protein typically inactivates the target, often by blocking important interaction sites or catalytic activities, such as hindering actin polymerization and GTP-to GDP cycling on GTPases [73,272,396]. Although ADP-ribosylation by prokaryotes is typically considered a means of eukaryotic protein inactivation, there are many examples of the modification activating the target protein, either directly (Cholera toxin) or indirectly by inactivating negative regulatory proteins (Bordetella toxin) [272].

1.5. Glycation, Maillard reactions, and Advanced Glycation End products (AGE).

Glycation "is a chemical reaction involving primary and secondary aliphatic amino groups of amino acids, peptides, amines, proteins, some phospholipids, and carbonyl groups of reducing sugars as well as degradation products of carbohydrates, lipids, and ascorbic acid" ((Nguyen, 2006) Figure 1.13)[345]. The reaction is so prevalent in cooking, food preparation, and biological systems, including diabetes complications, vision loss, and neurodegenerative disorders (Alzheimer's), that you are likely already

readily familiar with the reaction even if you did not know it. Browning bread and charring steaks are both common food science examples of heated sugars reacting with amino acids and undergoing a glycation reaction.

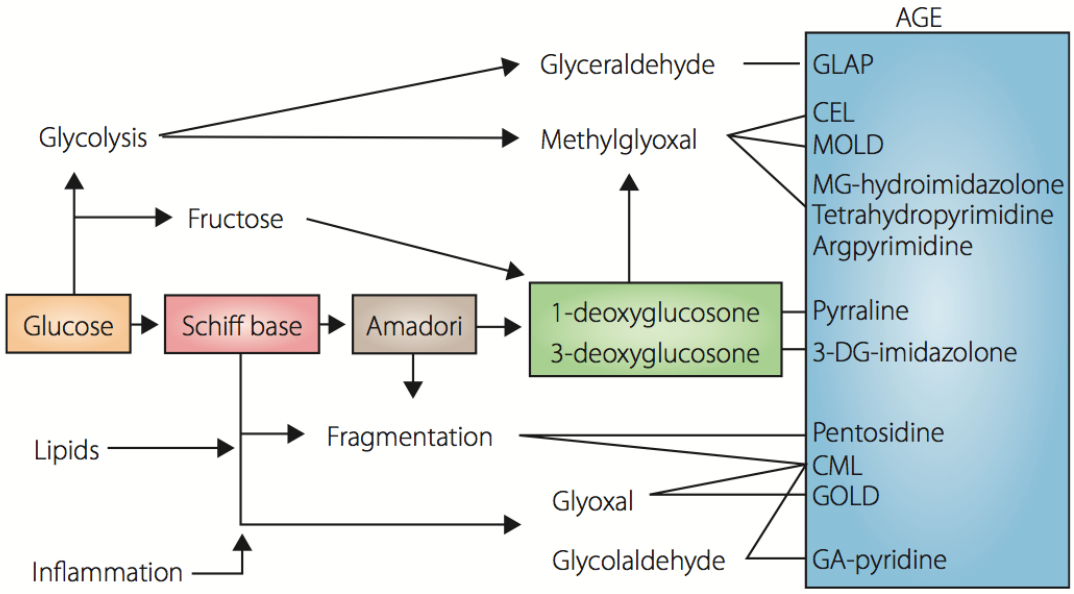

Figure 1.13. Possible pathways of advanced glycation end-products (AGE) formation.
The classical pathway leading to the formation of AGE involves Schiff base and Amadori products. The Amadori products can be transformed into reactive dicarbonyl products, such as glucosones, and can be fragmented by oxidation (glycoxidation) to generate pentosidine and Ne-carboxymethyl-lysine (CML). Reactive dicarbonyls can also be generated from ketones, lipids, glycolysis, and inflammatory pathways. Representative AGEs are presented here. CEL, Ne-carboxyethyl-lysine; 3-DG-imidazolone, 3-deoxyglucosone-imidazolone; GA-pyridine, glycolaldehyde-pyridine; GLAP, glyceraldehyde-related pyridinium; GOLD, glyoxal-derived lysine dimer; MG-hydroimidazolone, methylglyoxal-derived hydroimidazolone; MOLD, methylglyoxal-derived lysine dimer. Reproduced with permission from Yamamoto and Yamamoto, 2012[548].

Of particular interest is the distinct effects glycation can have on the ubiquitin proteasome system (UPS). Research has indicated the carbohydrate-based modification can significantly impair the UPS in a cell, resulting in decreased turnover of targeted proteins. This activity can be mediated by glycation of host proteins, glycation of UPS enzymes, or by glycation of ubiquitin itself. Ub-related glycation significantly impairs

enzymatic processing of ubiquitinated proteins as well as hindered proteasome recognition of modified substrate proteins. This ultimately hinders a cells' attempt to clear glycated products, which can mature into advanced glycation end products (AGE) that are associated with extensive protein crosslinking[345,510]. Glycated ubiquitin was also inefficiently incorporated into ubiquitin conjugates by cellular enzymes blocking ubiquitination initiation.

1.6. Pathogens interaction with the ER

Invasive pathogens such as viruses and intracellular bacteria utilize their host cells to facilitate replication and pathogen expansion. During bacterial subversion of host systems, pathogens interact with various host organelles to generate a replication-competent niche within the cell. Bacterial pathogens, such as *Salmonella enterica*, *Legionella pneumophila*[219,220,492], *Brucella spp.*[70,163,475,476], *Coxiella* burnetti[255,344,507], *Shigella flexneri*[329,440], and *Francisella tularensis*[252,440], invade eukaryotic host cells forming a membrane-bound vacuole that evades or delays endocytic maturation. The pathogens manipulate host trafficking to and from the vacuole to generate a pathogen compartment amenable for growth[70,82,163,220,414,492]. Alternatively, some pathogens promote vacuolar rupture and replicate within the cytosol[138,176,267]. For pathogens that remain within a vacuolar compartment throughout their life cycle, they require a mechanism for interacting with and subverting host pathways and organelles outside their membranous compartment. These intravacuolar pathogens employ secretion systems to translocate proteins into the cytosol and cytosolic face of the vacuole membrane to hijack host systems for the purpose of limiting host defenses and enhancing bacterial

replication. One of the organelles that many pathogens, including viruses, target is the expansive ER network. This compartment offers pathogens access to a nutrient rich environment with seemingly few bactericidal components relative to locations like lysosomes or the cytosol, compartments that are abundant with hydrolytic enzymes and antimicrobial peptides [72]. The role of ER in the biosynthesis of proteins, carbohydrates, and lipids, along with directing transport of these products through the secretory pathway, makes this organelle particularly well suited to serve the needs of an incoming pathogen.

Moreover, the ER is intimately involved in the first phase of infection during phagocytosis of pathogens. The peripheral ER is situated along long stretches of the plasma membrane[155,351,480], and during phagocytosis in macrophages much of the enveloping membrane was remarkably shown to be derived from the ER, not simply the plasma membrane[14,145]. The role of the ER in controlling protein folding and sensing the accumulation of unfolded proteins through the unfolded protein response (UPR) also serves to initiate a series of conserved signal transduction events linked to innate immunity and host defense[72,230,236,445]. This conserved signaling pathway operates as an intracellular pathogen sensor, as their invasion and replication is often associated with induction of ER stress[230,309]. Viral infections, in particular, place an intense demand on a cell's protein synthesis system, and these pathogens have evolved methods to block UPR to promote cell survival during replication[168,558]. Additional evidence of how the ER serves to both promote and counteract proliferation of pathogens is continually developing and represents a critical field of study in both cell biology and pathogenesis.

The bacterial pathogens *Legionella pneumophila* and *Brucella spp.* along with the protozoan parasite *Toxoplasma gondii* are known to target the ER to generate an ER-

derived replication compartment. A *Brucella spp.* infection begins with early endosome markers, such as Rab5 and the transferrin receptor, localizing to the vacuolar face[163]. Then these are shed and the vacuole briefly acidifies prior to the compartment adopting ER and autophagosome features like colocalization with calreticulon, Sec61b, and LAMP-1 markers[267,383,384,476]. ER proteins stably accumulate at the vacuole membrane leading to interaction with ERES[71] and ultimately induction of UPR[395]. For *Toxoplasma gondii*, the parasite forms a specialized non-fusogenic compartment known as the parasitophorous vacuole (PV), which immediately after invasion recruits mitochondria and ER to the vacuolar membrane, while excluding PM proteins. ER association was identified by the presence of reticular membranes that were ribosome studded. Both mitochondria and the ER form a intimate association with the vacuolar membrane, as nearly 75% of PV membrane associated with one of these organelles by 4 HPI[467]. This relationship has been proposed to supply lipids for the PV membrane, as the parasite may be incapable of de novo lipid synthesis[47,467,509,514]. This membrane architecture mimics the lipid transport mechanism utilized by cells to facilitate lipid flipping between opposing membrane faces of the ER and other organelles such as the PM[201,479,480]. Lastly, *Legionella pneumophila* too, generates an ER-derived vacuolar compartment by evading the endocytic-lysosomal pathway and subsequent subversion of the autophagic machinery. The maturation process and details of the *Legionella* containing vacuole (LCV) biogenesis will be discussed in more detail within the next chapter. Each of these pathogens manipulate host ER from within their vacuoles to promote replication and evade host defense systems[50,162,425,533]. The mechanisms that underlie these vacuolar transformations remain unclear, but future studies on the topic offer exciting

opportunities to examine organelle biology and requirements for pathogen development during encapsulation within a host compartment.

1.6.1. *Legionella* and the Icm/Dot T4SS

The Gram-negative intracellular pathogen *Legionella pneumophila* is ubiquitous in aquatic environments and has been isolated from numerous human-made structures associated with water, including cooling towers, air conditioning units, fountains, and spas[343,354]. *L. pneumophila* relies on parasitizing protozoan hosts, which may be free-living or within a biofilm, for survival in the harsh aquatic environment[325,343,535]. In an accidental human host, inhalation of aerosolized water particles contaminated with *Legionella pneumophila* allows the bacterium to be internalized by alveolar macrophages[28,59,151,213,461,546]. Immunocompromised individuals are particularly susceptible to infection by *L. pneumophila*, which can induce a minor flu-like illness, known as Pontiac fever, or a severe and potentially fatal form of pneumonia, known as Legionnaire's disease[124,343,461]. Successful *L. pneumophila* infection and replication within either the human or protozoan host is dependent on successful evasion of the endocytic maturation pathway. *L. pneumophila* remains within a vacuolar compartment and evasion of the endocytic pathway requires a functional type IV secretion system (T4SS) also known as the Dot/Icm system. The T4SS is used to secrete hundreds of bacterial effectors called IDTS (Icm/dot translocated substrates) into the host cytosol for modulation of host pathways. For a successful replication cycle, *Legionella* must generate an endoplasmic reticulum (ER)-derived compartment known as a *Legionella* containing vacuole (LCV), which supports vacuole expansion and bacterial

replication[124,213,151,521]. The Dot/Icm system is predicted to translocate 300 or more effector proteins that target host pathways and engineer its intracellular ER-derived niche. The T4SS is essential for nearly all facets of the *L. pneumophila's* intracellular life cycle, including bacterial entry into the host, formation of the LCV, intracellular replication, and finally bacterial egress[343,426].

1.6.2. *Legionella* targets the endoplasmic reticulum and host trafficking system.

Bacteria engulfed by professional phagocytes are actively transferred into phagolysosomal compartments designed to degrade the invaders[350,447]. *Legionella pneumophila*, like other intravacuolar pathogens, has developed a successful scheme to bypass phagolysosomal maturation and instead create a compartment suitable for bacterial replication (Figure 1.14.). *Legionella's* survival strategy depends on preventing the host from initially trafficking the LCV into an antimicrobial phagolysosome compartment, in which an acidic pH and hydrolytic proteases would degrade intracellular pathogens[114,319]. Notably, within minutes of engulfment by phagocytes, the LCV is decorated with smooth vesicles and the region surrounding the LCV is enriched with mitochondria, regardless of whether the cell is amoebae or mammalian in origin (Figure 1.14.B)[23,240,414,492,504]. These smooth vesicles have been repeatedly observed during early infection, and these structures along with mitochondria become far less prevalent after the LCV transitions to into a rough ER-like compartment[204,504]. These smooth vesicles are postulated to be ER-Golgi vesicles, which *Legionella* hijacks and fuses with the LCV through a cohort of IDTS that target host trafficking and membrane machinery[240,414].

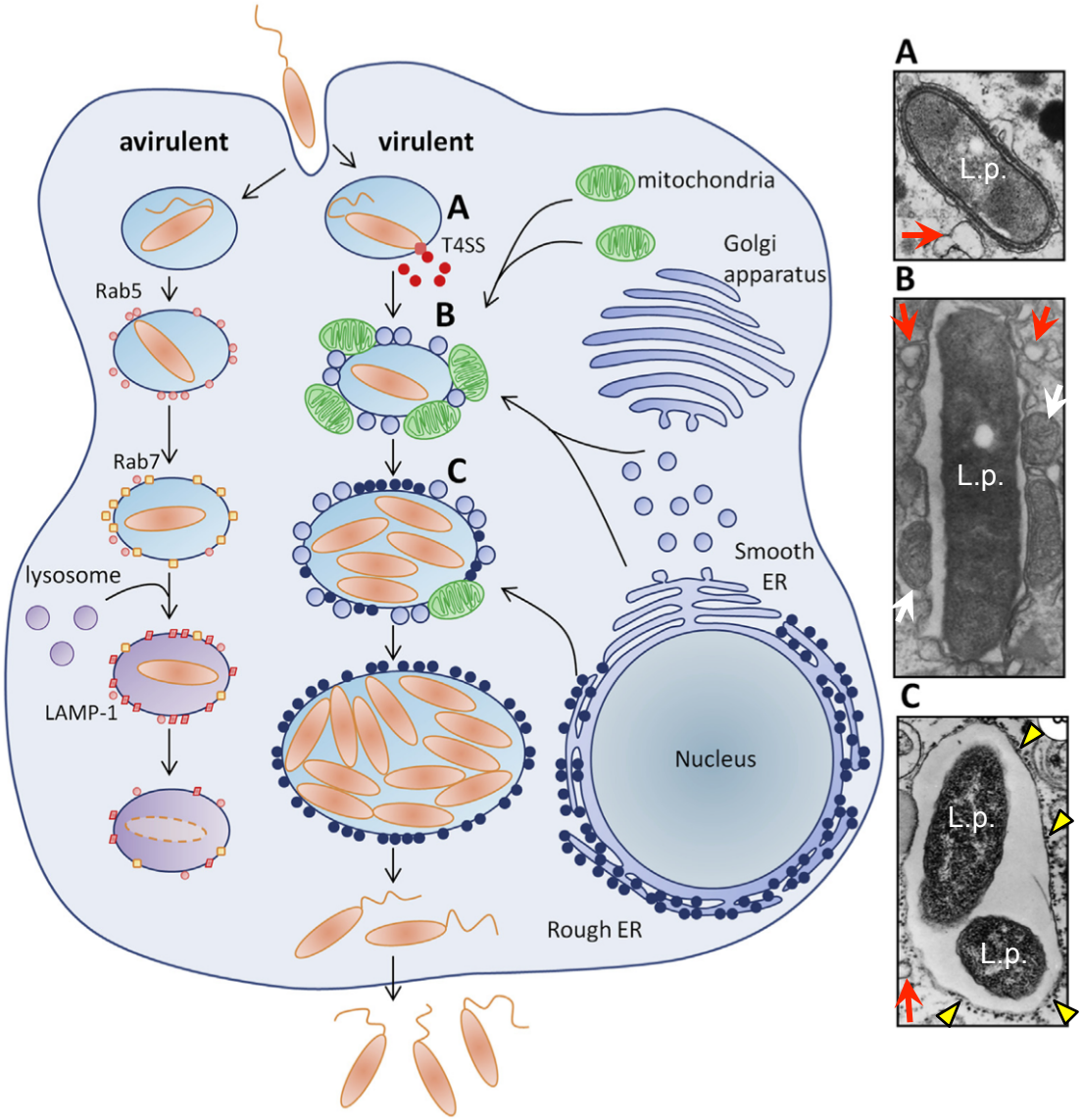

Figure 1.14. *Legionella pneumophila* conserved life cycle with correlative EM of different phases of infection.
LCV biogenesis during *Legionella pneumophila* infectious cycle relies on a functional T4SS for bacterial virulence and the development of an ER-derived replication compartment. *L. pneumophila* is internalized within host cell and resides in a phagosome **(A)**. Virulent *L. pneumophila* injects T4SS effector proteins to control LCV biogenesis and ER manipulation. Mitochondria (white arrow) and smooth ER-derived vesicles (red arrow) are rapidly recruited around LCV **(B)**. Hours later, virulent *L. pneumophila* begins to replicate efficiently within a vacuole decorated with ribosomes (yellow arrow heads) **(C)** rough ER properties. For avirulent *L. pneumophila*, such as Dot/Icm-deficient strains, bacteria lose the ability to recruit mitochondria, ER-derived vesicles and ribosomes and are cleared via endosomal pathway and fusion with lysosomes. Reproduced with permission from Allombert et al, 2013 [10].

As the *Legionella* infection progresses, the LCV membrane appears to resemble the rough ER in thickness, ribosomes studding the membrane, and protein composition[4,204,504]. Interestingly, this vacuolar transformation occurs concurrently with the successful avoidance of the endocytic pathway, as late endosome and lysosomal markers fail to localize to the LCV during productive infection (Figure 1.14, avirulent track)[205]. This engineered bacterial vacuole offers *Legionella* both a safe refuge from the cellular immune system and a compartment supplied with the required nutrients for bacterial expansion.

The ER plays an intimate role in the formation of this LCV compartment. Analyses of the ER targets that are manipulated reveal unique insights into both the regulation of ER function and the details of *Legionella*'s pathogenic life cycle. Consistent with *Legionella*'s need to manipulate host membranes, numerous IDTS were found that both mimic and manipulate host SNARE proteins involved in mediating membrane fusion events [15–17]. Several prevalent bacterial strategies used to manipulate SNARE activity are 1) IDTS mimicry of eukaryotic SNAREs structure and function to promote membrane fusion through interactions with host SNAREs, such as with LseA[251] or proteins such as LegC2/YlfB (yeast lethal factor B), LegC3, and LegC7/YlfA[35,65,133,456]; 2) promotion of eukaryotic SNARE activity by targeting host SNARE interacting proteins, as in the case of DrrA/SidM activating the Rab1 GTPase to promote non-canonical SNARE (Sec22b) pairing between ER vesicles and the plasma membrane[17,569], and finally 3) elimination or inhibition of SNAREs through direct enzymatic targeting as in the case of *L. pneumophila*'s Lpg1137, which acts as a mitochondrial localized serine protease that cleaves the host SNARE syntaxin17 to inhibit ER-mitochondrial

communication and autophagic induction[15].

Small host GTPases cycle between an active membrane-associated form and inactive cytosolic species, dependent on the guanine nucleotide bound, and are essential for proper LCV maturation[341,483]. These GTPases are common *Legionella* IDTS targets. Numerous studies report Rab1, which promotes vesicle trafficking from ER intermediate compartments to the cis-Golgi[385], is subject to a litany of post-translational modifications mediated by *Legionella* IDTS throughout infection (Figure 1.15). At least 9 IDTS have been reported to target Rab1 through the following activities or PTMs: Rab1 GTP/GDP state specific binding to mediate additional IDTS interactions (LidA), guanine nucleotide exchange factor (GEF) activity (SidM), GTPase activating (GAP) activity (LepB), AMPylation (SidM), phosphocholination (AnkX), deadenylylation (SidD), dephosphocholination (Lem3), and ubiquitination ((SidC/SdcA, SidE family) Figure 1.15)[78,181,203,218,332,342,396,482,496,569]. *Legionella* effectively hijacks Rab1 function to serve as a 'master regulator' of the LCV transformation from a PM-like compartment to an ER-derived vacuole. The bacterial tactics utilized to manipulate Rab1 represent several conserved mechanisms of GTPase manipulation. For instance, Lpg0393 displays GEF activity towards a cluster of Rab proteins involved in endocytosis and endosomal maturation, which was proposed to mediate LCV acquisition of ER by increasing endosome-trans Golgi vesicle traffic that feeds into the pathway supplying ER vesicle accumulation at the LCV[470]. The IDTS PieE has been confirmed to interact with numerous Rab proteins, including Rab1, Rab5, and Rab10, but the role for this interaction remains to be discovered[330]. Another important *L. pneumophila* target is the small GTPase Arf1 (ADP-ribosylation factor 1), which controls ER-Golgi and Golgi-PM

vesicle trafficking related

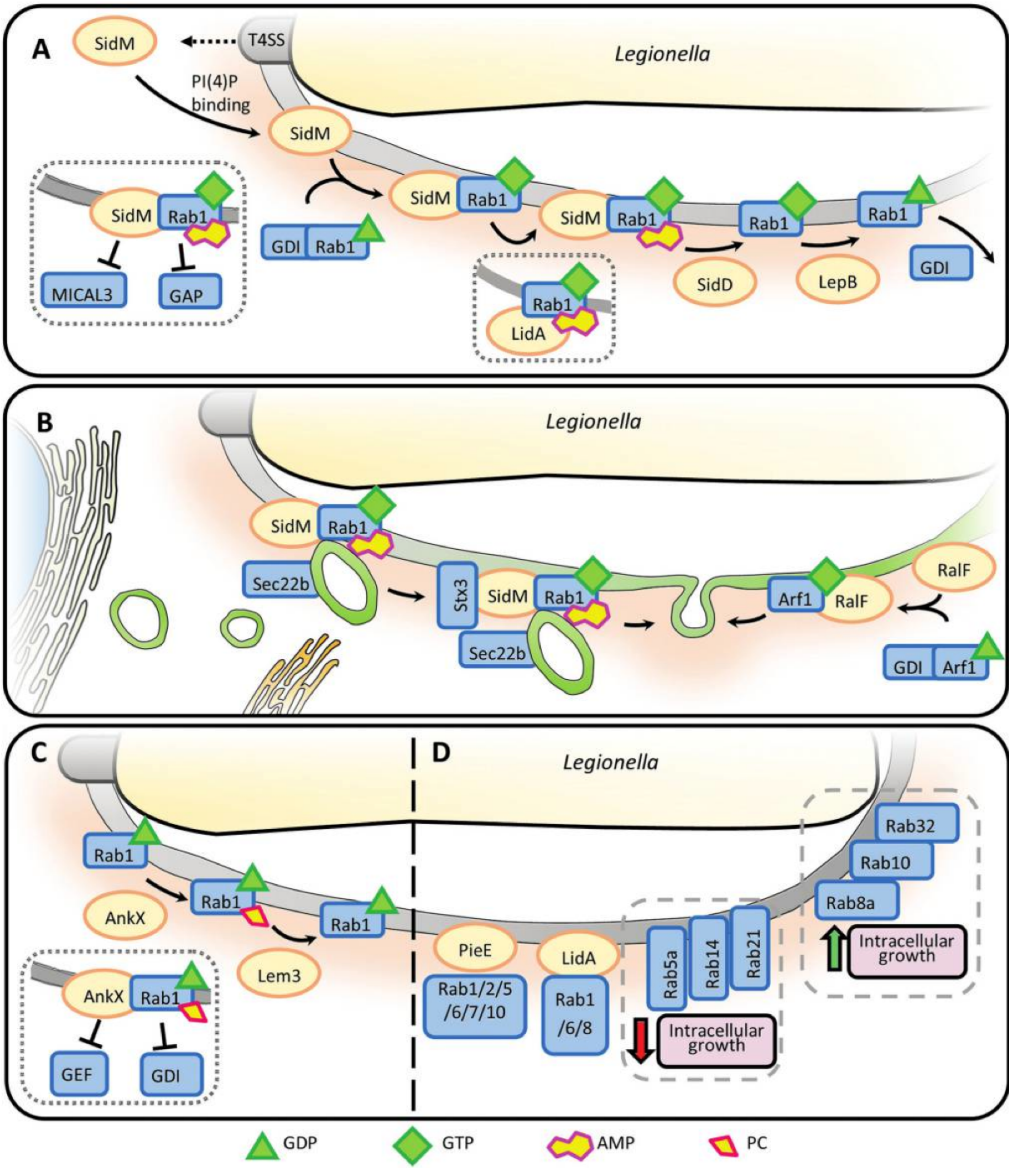

Figure 1.15. A preponderance of *L. pneumophila* IDTS target small GTPases to manipulate trafficking and ER for the generation of a replication permissive vacuole.

Legionella pneumophila effectors subvert Rab GTPases on the *Legionella*-containing vacuole (LCV) to facilitate generation of ER derived intracellular niche. **(A)** Rab1 recruitment and modification by AMPylation. SidM anchors onto the LCV by binding PI(4)P. It activates and recruits Rab1 onto the LCV using its guanine nucleotide exchange factor (GEF) domain and then locks Rab1 in the active state by AMPylation. SidD later deAMPylates Rab1 allowing the GTPase activating protein (GAP) LepB to deactivate Rab1, then GDP dissociation inhibitors (GDIs) extract Rab1 from the LCV. **(B)** Recruitment of Rab1 and ARF1 leads to ER-derived vesicle fusion with the LCV. Rab1 activation by SidM results in tethering of Sec22b containing ER-derived vesicles to the LCV membrane. SidM also recruits syntaxin-3A to promote non-canonical SNARE

(soluble N-ethylmaleimide sensitive factor activating protein receptors) pairing between Sec22b and syntaxin-3A. promoting fusion of ER-derived vesicles with the LCV. RalF acts as an ARF1 GEF to recruit and activate ARF1 onto the LCV where it promotes fusion of ER-derived vesicles. **(C)** Manipulation of Rab1via phosphocholination. AnkX phosphocholinates Rab1 in either its GTP- or GDP-bound form prevents 1) deactivation by GAPs or 2) activation by GEFs and 3) extraction from the LCV by GDIs. Lem3 dephosphocholinates Rab1 to relieve these inhibitions. (D) Additional effectors and Rab GTPases acting on the LCV. PieE and LidA localize to the LCV and interact with additional panels of Rab proteins, potentially allowing precise selection and tethering of particular trafficking vesicles. Secretory pathway Rabs 8a, 10, and 32 are recruited to the LCV and promote intracellular growth, in contrast endocytic pathway Rabs 5a, 14, and 21 negatively impact on *Legionella* proliferation. Reproduced with permission from So *et al*, 2015[469].

to the coat protein complex I (COPI)[79,227,228]. The IDTS RalF utilizes its N-terminal GEF domain to recruit, and then activate Arf1 on cytoplasmic face of the LCV shortly after phagocytosis. Active Arf1 on the LCV then promotes docking and fusion of ER-derived vesicles. Curiously Arf1 recruitment to the LCV, but not the presence of RalF, was found to be critical for a successful intracellular replication[241,337,414]. Another *L. pneumophila* IDTS shown to interact with the host ER through an unknown mechanism is Ceg9. When the bacterial protein was used as bait, the structural ER tubule protein Rtn4 precipitated with Ceg9, but intriguingly during infection Rtn4 would localize and rearrange around LCV independently of Ceg9 expression, indicating there were likely other *Legionella* proteins targeting the reticulons. This will be discussed in further detail within the SidE family section below.

1.6.3. *Legionella* and the autophagy system

As described earlier, autophagy is a host pathway that can serve as a host immune response to infectious agents. As such, numerous pathogens have evolved strategies to inhibit or activate the autophagic system to survive and replicate. Some intracellular

pathogens induce the formation of ubiquitinated aggregates that envelop their replication compartments or tag microbial-induced structures. This accumulation of ubiquitinated products serves as an initiation signal for the autophagic response to clear pathogens through a specific autophagic process termed xenophagy (Figure 1.16)[90,143,317,356]. Ubiquitinated aggregates are bound by several autophagy adaptors proteins, including sequestosome 1 (p62/SQSTM1), neighbor of BRCA1 gene 1 (NBR1), nuclear dot protein 52 kDa (NDP52), and optineurin (Figure 1.16.A,B), which are then designed to deliver the ubiquitinated contents to an autophagosome through Atg8/LC3 mediated signaling[23,46,368,454,517].

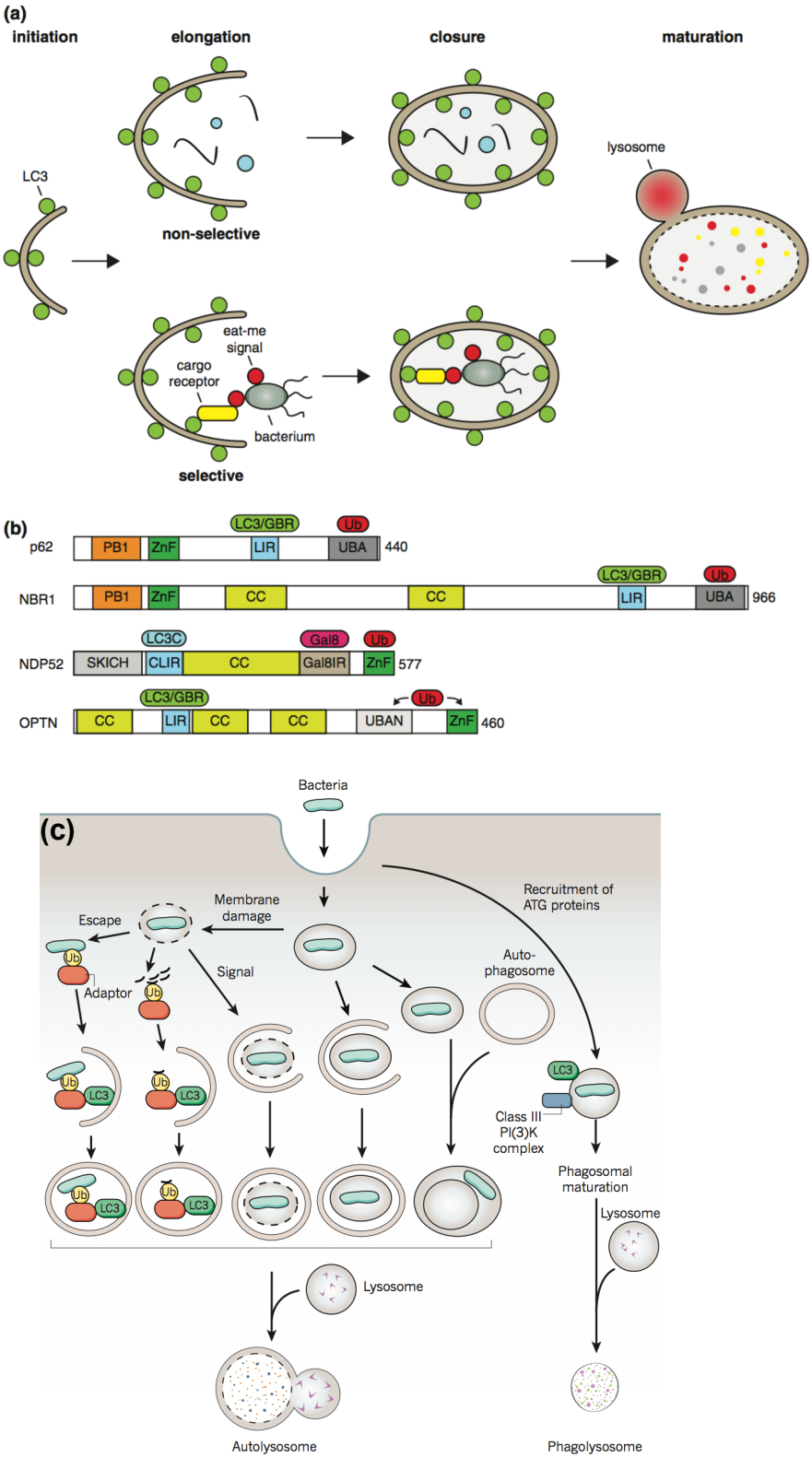

Figure 1.16. Pathogen recognition by the autophagic system and the structure of cargo receptors.

(a) Autophagosome biogenesis is initiated from crescent-shaped double membrane structures termed phagopores, which are studded with LC3 and the related ATG8-like proteins. Phagophore membranes elongate and envelop cytosolic material in a non-selective manner, eventually segregating the cargo from the remainder of the cell in a compartment called an autophagosome. A selective autophagic response occurs when cytosolic components, like a bacterial pathogen, are selectively recognized by autophagic cargo receptors by detecting 'eat-me' signals. 'Eat me' signals like ubiquitination, prompt bound cargo receptors to associate with forming phagopores through LC3/Atg8 binding domains in the receptors. Autophagosome maturation results in fusion with lysosomes causing the degradation of the autophagosome content and its inner membrane. **(b)** Domain structure of important autophagic cargo receptors. Highlighted are binding sites for 'eat-me' signals and LC3/ATG8 family members are indicated. All cargo receptors bind ubiquitin-labeled cargo; NDP52 also detects the 'eat-me' signal Galectin-8 (Gal8). P62, NBR1 and Optineurin (OPTN) bind non-selectively LC3 and Gabarap proteins (LC3/GBR) via their LC3-interactin regions (LIRs), while NDP52 preferentially interacts with LC3C via a LC3C-specific binding site (CLIR). Abbreviations: CC, coiled-coil; CLIR, LC3C-specific LIR; Gal8, Galectin-8; Gal8IR, Galectin-8 interacting region; LIR, LC3-interacting region; OPTN, Optineurin; PB1, Phox and Bem1P; SKICH, skeletal muscle and kidney enriched inositol phosphatase carboxyl homology; Ub, ubiquitin; UBA, ubiquitin-associated domain; UBAN, ubiquitin binding in ABIN and NEMO domain; ZnF, zinc finger domain. **(c)** Potential autophagic routes to target a bacterium (or damaged membranes of bacteria-containing compartment) to the lysosome. Adaptor refers to the known cargo receptor proteins described in (b) as well as additional unknown adaptors may be involved in pathogen recognition through either ubiquitin-dependent or -independent mechanisms. Reproduced with permission from Boyle and Randow, 2013 (Panel A,B)[56] and Levine, Mizushim, and Virgin, 2011 (Panel C)[282].

Legionella subversion of the autophagic pathway appears to be *via* its arsenal of IDTS proteins. Research on the biogenesis of LCV indicate that the bacterium is able to inactivate the autophagic response, specifically in permissive hosts, whereas restrictive hosts, such as C57BL/6, promote prompt LCV fusion with lysosomes, degrading the internalized bacterium. Macrophages derived from a permissive mouse host, such as A/J mice (deficient in Naip5, a NOD-like receptor) are capable of supporting *Legionella* intracellular replication through a process relying on blocking early fusion with lysosomes. In these permissive hosts, the autophagy markers LC3, Atg7, Atg8, have been observed localizing to *L. pneumophila* membrane at early stages of infection in a T4SS dependent manner. These observations support a model where *L. pneumophila* infection

induces the autophagic system to initiate the formation of nascent membranous compartment destined for lysosomal degradation at the LCV. These immature phagopore-like structures are proposed to provide donor membranes and proteins for a developing and expanding bacterial compartment. This system would require tight regulation of the autophagic system to prevent premature progression along the pathway in order to maintain bacterial viability and replication[11]. Consistent with this model, several pro- and anti-autophagic IDTS have been described to date. These factors, including the inhibitory RavZ[83,202,271,550], Lpg1137[15], and likely several other yet to be described factors, effectively delay autophagosome progression for at least 4-6 HPI.

Interestingly, non-permissive hosts challenged with *L. pneumophila* were shown to have increased numbers of LCVs associated with autophagic components relative to LCVs from permissive hosts. It should be noted that chemical inhibition of autophagy in permissive hosts negatively impacts *Legionella* replication. Pretreatment of A/J macrophages with either the autophagy inhibitors BFA or 3MA prior to *Legionella* challenge resulted in a significant increase in degraded bacteria within the first two hours of infection and a notable reduction in recovered CFUs specific to WT *Legionella* challenge[11]. Unfortunately, these autophagy inhibitors do no function within the vacuum of a single signaling process; there are strong caveats with the use of these chemical tools due to off target effects. Genetic analysis of amoeba mutants lacking key autophagy genes was unable to provide any evidence of a direct role for autophagy in *Legionella* intracellular replication. For instance, mutations of the apg1, apg5, apg6, apg7, and apg8 genes in *Dictyostelium discoideum* produce autophagic defects, yet still yield normal levels of *L. pneumophila* intracellular replication[365]. These studies demonstrate the

complex and highly coordinated temporal regulation of the autophagic process by *Legionella* IDTS. The enzymatic activities of these bacterial factors orchestrate autophagic progression, but the importance of this pathway remains elusive, as absence of the autophagy machinery or absence of IDTS autophagy inhibitors rarely affect *L. pneumophila* intracellular replication[238,329].

The transformation of the LCV into an immature autophagosome was shown to heavily rely on autophagic uptake induced by the IDTS LegA9, an ankyrin containing protein of unknown function. Evidence indicates LegA9 functions to tag the LCV for autophagy recognition by the host system, although overall autophagic flux remained unchanged when exposed to LegA9, as indicated by LC3-II induction independent of LegA9 expression. A *Legionella* mutant lacking *legA9* resulted in reduced vacuole ubiquitination and reduced colocalization with the autophagy adaptor p62, which resulted in successful *L. pneumophila* evasion of autophagic delivery to lysosomes in restrictive hosts. An impressive increase in intracellular replication was observed during *L. pneumophila* challenge in a classically restrictive macrophage host. Curiously, the *legA9* deletion strain is the only known *L. pneumophila* mutant, other than the Δ*fla* (flagellin deletion) strains that can successfully replicate in restrictive macrophages or monocytes, again emphasizing the importance of the autophagic system in *Legionella* replication and survival[248].

Contrary to autophagy promotion by LegA9, several *Legionella* effectors, including RavZ and LpSPL, have been shown to inhibit the autophagic process. The *Legionella* IDTS sphingosine-1 phosphate lyase (LpSpl) inhibits host autophagy through modulating sphingolipid metabolism. The bacterial protein mimics the eukaryotic

sphingosine-1-phosphate lyase 1 (SGPL1) in both structure and function. Host sphingolipids function as bioactive membrane components that play a fundamental regulator for critical host processes, particularly autophagy. LpSpl expression, dependent on its lyase activity, reduced sphingomyelin and ceramide levels, but most noticeably LpSpl negatively affected sphingosine levels during infection. The altered sphingolipid metabolism hindered initiation of starvation-induced autophagy and served to counteract the host antibacterial response, enhancing *Legionella* survival[126,417,418]. Another extensively studied autophagy inhibitor produced by *L. pneumophila* is RavZ. This effector specifically cleaves membrane conjugated LC3 (LC3-PE) forming on developing autophagosomes. RavZ targets autophagosomes through membrane and phosphatidylinositol 3-phosphate (PtdIns3P) interactions[202,211,338,369], then extracts LC3-PE from the membrane followed by irreversible LC3 deconjugation from the PE lipid[83,271,550]. The presence of both *lpspL* and *ravZ* within the *L. pneumophila* genome further substantiate the model of *Legionella* developing an immature autophagosomal for a designated period of the infection.

Hours into infection, *Legionella* releases its own autophagosome maturation block through the activity of the IDTS LepB (Figure 1.15.A). This bacterial protein expresses both lipid kinase activity[112,218] and Rab targeting GAP activity. The LepB kinase activity converts PtdIns3P into PtdIns(3,4)P2 and has been suggested to function in collaboration with the bacterial phosphoinositide phosphatase SidF to convert LCV localized PtdIns(3) of unknown origin to PtdIns(3,4)P, and ultimately PtdIns(4)P[112]. LepB Rab1 GAP activity serves to inactivate Rab1, Rab8, Rab13 and Rab15 localized to the LCV membrane in the later hours of infection[218,316,557]. Early during infection SidM GEF

activity specifically activates LCV membrane localized Rab1[218,304,335,444], followed by SidM mediated Rab1 AMPylation[151,181,464,482], which prevents Rab GAP proteins from accessing the constitutively GTP bound Rab1 (Figure 1.15.A,B). Eventually, the IDTS SidD reverses Rab1 AMPylation[181,409,496], facilitating inactivation of Rab1 through LepB GAP activity (Figure 1.15.A)[181,218,316,340,557]. By the final phase of infection at 12-18 HPI, a significant proportion of vacuoles have acidified[487], colocalize with LAMP-1 and cathepsin D proteins, and have the LCV membrane decorated with autophagic proteins[11]. Eventually after several rounds of replication and vacuole expansion to house the increasing bacterial load, the bacteria escape from the vacuolar compartment into the cytoplasm. Then pore-forming toxins lyse the cells releasing intracellular bacteria into the environment to restart the infection cycle within a new host[9,45,324,326].

1.6.4. *Legionella* targets the host ubiquitin system

Like many other intracellular pathogens, *Legionella* needs to rapidly manipulate host systems during infection. To manufacture these dynamic cellular changes, pathogens have found robust success with hijacking the post-translation modification system, which host cells themselves rely on for swift adaptation to changing environments[12,376,431,478]. Ubiquitination is a highly conserved pervasive PTM system utilized by eukaryotes. It was therefore not surprising that several *L. pneumophila* IDTS were discovered to directly target the Ub system by mimicking E3 Ub ligases domains[123,265,376]. Many of these E3 mimics were identified through homology to the eukaryotic F- and U-box domains, which are closely associated with the ligases. Proteins with an F-box constitute one of three components in the SCF complex (Skp, Cullin, F-box containing complex). In this

multi-protein complex the F-box protein serves as a Ub ligase tagging proteins destined for proteasomal degradation with Ub. Alternatively, RING/U-box proteins contain a ~70 amino acid motif (U-box) that was identified as a ubiquitin chain assembly factor in yeast. This motif enables U-box protein to collaborate with an E1, E2, and other potentially other E3s to catalyze ubiquitin chain formation. U-box proteins often serve as bridging partners and may not act as an E3 for the protein complex when an additional Ub ligase is present, but in the absence of additional E3s, U-box proteins can serve in their stead[106,183,377].

To date, at least two RING/U-box family E3 ligases and at least five F-box containing *L. pneumophila* translocated proteins have been described[290]. The *Legionella* effectors LubX (a.k.a. LegU2) and GobX contain two or a central U-box respectively. LubX acts in cooperation with the E2 enzymes UbcH5a or UbcH5c to polyubiquitinate the dual specificity kinase Clk1 involved in pre-mRNA processing. LubX also targets the *Legionella* IDTS SidH for polyubiquitination and subsequent degradation by the proteasome, representing the first described example of a *Legionella* 'metaeffector', in which one bacterial protein regulates another bacterial protein within the host. The second less described U-box protein in *Legionella* is the Golgi localized ligase GobX, which contains a single eukaryotic characteristic U-box. Two of the more intensely studied *Legionella* F-box protein are LegU1 and AnkB (a.k.a LegAU13/Ceg27). LegU1 integrates into a functional SCF complex providing E3 ligase activity to the complex and targets BAT3, a host chaperone that regulates the ER stress response, for ubiquitination. AnkB promotes polyubiquitination of proteins at the LCV and recruit Skp1. It has been proposed that the purpose of AnkB polyubiquitination of target proteins is designed to

promote proteasomal-mediated protein turnover generating necessary metabolites for bacterial replication. The abundance of bacterial effectors that mimic host E3 ligases or F-box domains underscores the importance of exploiting ubiquitination for microbial pathogenesis.

Ubiquitinated proteins localize to the LCV as early as 1hr after uptake by a host cell and may represent a method for *L. pneumophila* to dictate the protein composition of the LCV by modulating protein turnover[213,226]. For instance, the IDTS AnkB ubiquitinates a multitude of host substrates, promoting their proteasomal degradation. It has been proposed that this increases the amino acid pools and energy sources that *L. pneumophila* can commandeer for bacterial proliferation. Labeling of LCV membrane with ubiquitinated conjugates results from a number of other host and bacterial-mediated ubiquitination events, making the model of increased amino acid pools due to a single E3 ligase difficult to explain. In regards to these other ubiquitination pathways, it is likely that each phase of intracellular infection is likely to represent different pools of LCV-driven Ub conjugates. These Ub populations would potentially vary in the levels of conjugated or unconjugated Ub, the types and prevalence of specific Ub chain linkages, and Ub conjugation source (bacterial- vs. host-mediated). Fluorescence microscopy and proteomic studies of ubiquitin fluctuations associated with *L. pneumophila* infection provide substantial evidence for the highly dynamic nature and importance of Ub signaling at the LCV[226,266,389]. Moreover, a number of studies from the *Legionella* field have identified a collection of IDTS that have homology to Ub enzymatic or regulatory domains of eukaryotic or intracellular pathogen origin. These bacterial enzymes often heavily rely on molecular mimicry of eukaryotic enzymatic folds and associated domains,

like E3 Ub ligases and deubiquitinases. This mimicry presumably results from prokaryotes lack of this PTM system and its associated molecular machinery. As such, it is highly likely these bacterial enzymes arose in the genome through horizontal gene transfer over the course of *Legionella* evolution within different eukaryotic hosts[21,199,387,543,567].

Alternatively, there are *Legionella* effectors that employ protein structures notably absent from the eukaryotic ubiquitin toolbox. For instance, bacterial pathogens have developed novel E3 enzyme appropriately termed 'novel E3 ligases or NELs (Figure 1.8.B). The *Legionella* SidC effector family represents a completely divergent class of Ub ligases. SidC was shown to promote ubiquitin accumulation at the LCV concomitant with ER recruitment to the LCV during first two hours of infection[206]. SidC is translocated across the LCV membrane where it associates with the vacuoles cytoplasmic face using its C-terminal phosphatidylinositol-4-phosphate [PI(4)P]- binding domain[111,150,530]. Here, the bacterial protein enhances ER vesicle recruitment and accumulation of polyubiquitinated conjugates at the LCV membrane. These phenotypes were dependent on a canonical catalytic triad, C46-H444-D446, identified within SidC and its homologue SdcA [199,206,216]. This protein is able to produce high-molecular-weight polyubiquitin chains linked through any of the seven lysine residues on Ub. This was determined after single Ub lysine mutants were insufficient to abolish polyubiquitin formation compared with a Ub mutant lacking all lysine residues, which abrogated ubiquitin chain formation[150,203,206,301,399]. Another curious *L. pneumophila* effector found to targets ubiquitin and enhance ER association with the LCV during the first few hours of infection is SidJ. This protein serves as a both a bacterial 'metaeffector' and antagonist

to SidE family activity. This was demonstrated in fluorescence microscopy studies showing SidE localization at the LCV is temporally regulated by SidJ[232] and through co-expression of SidJ and SidE protein in yeast, which alleviated SidE family lethality [184,232]. The studies presented in this thesis, as well as other research groups, discovered the SidE proteins were themselves able to manipulate ubiquitination at the LCV. Of particular note was the panel of Rab proteins that SidE proteins could target for ubiquitination. Amongst this panel of Sde targeted Rab proteins, Rab33b appears to be the preferred target, while Rab1, Rab6, and Rab30 were also targeted to a lesser extent[396]. Rab33 is a Golgi resident GTPase that directly interacts with ATG16L to down regulate autophagosome formation[13,74,225]. This SidE mediated ubiquitination was through a completely novel mechanism and Ub linkage relative to the classic Ub conjugation system, which will be discussed in detail within the results chapters below. The same research group then discovered SidJ contained a DUB domain that targets both K63 and K48 polyUb, but was also able to specifically deconjugate SidE-mediated ubiquitination through a second DUB-like domain that that cleaves the phosphodiester linkage between Ub and the protein substrate. These enzymatic activities were critical for the role of SidJ in recruiting ER to the LCV during amoeba challenge[397]. The relationship between SidJ and the SidE family will be discussed further in the SidE family section below, but highlights the intertwined pathways of ER modulation through the ubiquitin signaling.

In addition to subverting Ub signaling pathways, ER association with the LCV, and proteasome activity, evidence indicates *L. pneumophila* may inhibit dendritic cell aggresome-like induced structure (DALIS) formation as a method to impair antigen presentation [1,226,339]. DALIS structures arise from pathogen-derived molecules, like LPS,

where aggregates of ubiquitinated proteins accumulate and potentially serve as a transient antigen storage system[1,18,66,212,382]. Interestingly, WT *Legionella pneumophila* promotes vacuole ubiquitination, but was able to inhibit DALIS formation unlike a *dotA3* when TLR2 was stimulated to induce DALIS formation[226]. By eliminating a long-lived standing supply of ubiquitinated bacterial antigen[281], *Legionella* can further inhibit host immune responses by limiting cell-surface antigen presentation and prevent dendritic cell activation [1,131,212]. This repertoire of Ub modulating bacterial effectors demonstrates a conserved tactic of *L. pneumophila* to use IDTS to hijack the host Ub signaling system, specifically to promote ER interaction with the LCV.

1.7. SidE family and the Sde operon.

The SidE Family (Substrate of Icm/Dot complex, protein E paralogues) is a family of translocated *L. pneumophila* proteins, of which relatively little was known prior to the initiation (late 2011) of the thesis work described here. The family consists of five proteins, including SidE, SdeA, SdeB, SdeC, and SdeD, although the relationship of SidD to the other SidE proteins is debatable due to the distinct structural and size differences of SdeD. *SdeC, sdeB,* and *sdeA* are organized contiguously, with *sidJ* inserted between *sdeC* and *sdeB* within the genome (Figure 1.17.A). Unlike the *sde* locus, that contains most of the protein family, *sidE* is present at an entirely separate region of the *L. pneumophila* genome[28,294]. The SidE proteins are extremely large, hydrophilic proteins with extensive α-helices in the carboxy-terminal region. The proteins range from an expected molecular weight of 170kDa-217kDa and they have no known orthologues[28].

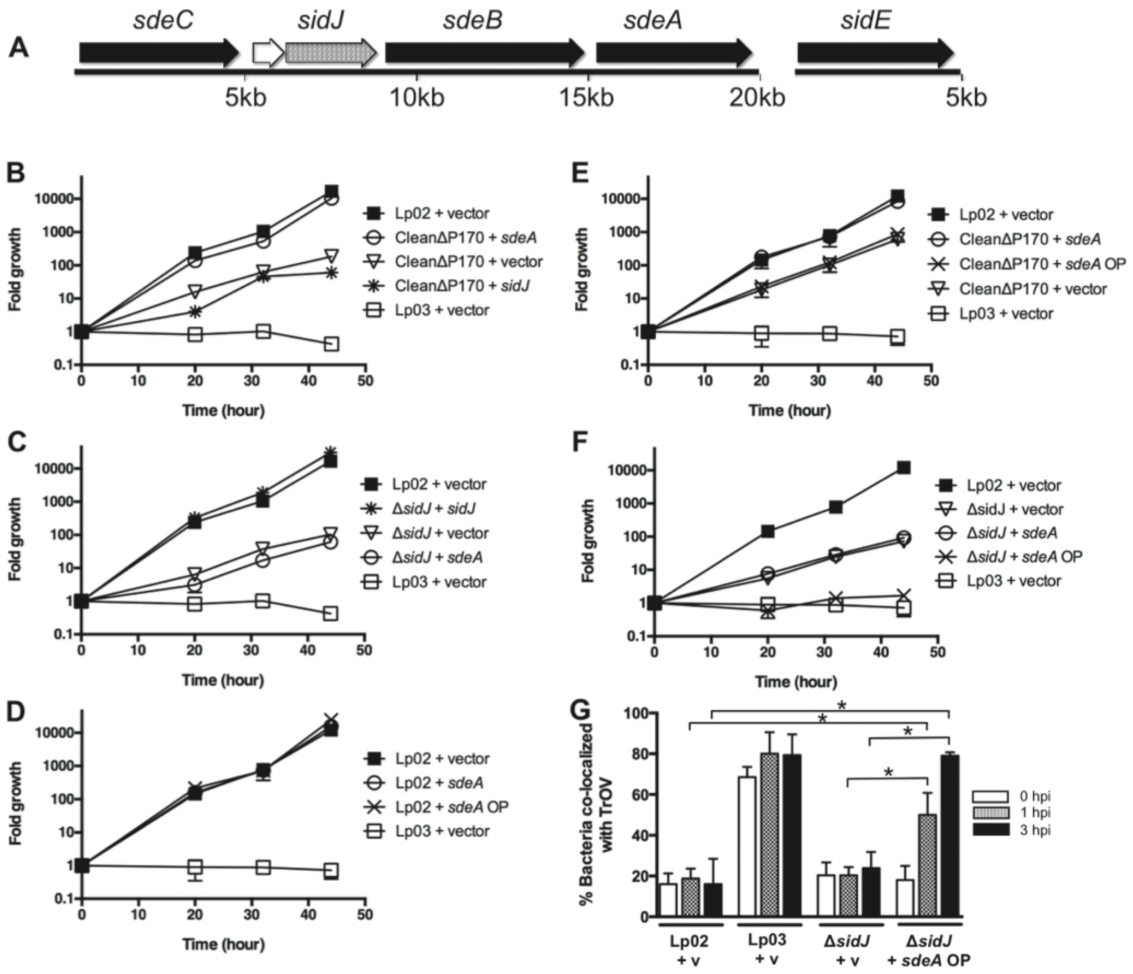

Figure 1.17. SidE and SidJ relationship during *L. pneumophila* amoebae infections. **(A)** *sdeC-sdeA* locus includes five genes (*sdeC, lpg2154, sidJ, sdeB, and sdeA*), whereas the *sidE* gene is located at a separate genetic locus. The SidE family consists of the related proteins SidE, SdeC, SdeB, and SdeA (black arrows). **(B-F)** Replication of various *L. pneumophila* strains in *A. castellanii* was determined at the indicated time points post infection and expressed as fold growth. **(B)** Suppression of the growth defect of the CleanΔP170 (*ΔsidE ΔsdeC ΔsdeB-A*) mutant by expression of low amounts of SdeA. (C) Complementation of the *ΔsidJ* mutant by expression of SidJ. **(D-F)** Overexpression (OP) of SdeA does not inhibit the growth of the wild type strain Lp02 **(D)** or the CleanΔP170 mutant **(E)** but does inhibit the replication of the *ΔsidJ* mutant **(F)**. **(G)** Overproduction of SdeA causes *Legionella* to traffic into the endocytic pathway of amoebae. *A. castellanii* pre-incubated with Texas Red Ovalbumin (TrOV), which labels the endocytic pathway and vacuoles, then infected with Lp02, a dotA mutant (Lp03) and a *ΔsidJ* mutant containing vector (v) or a plasmid over-expressing SdeA (sdeA OP). The percent of bacteria that co-localized with TrOV was quantitated at 0, 1, and 3 hours post infection. Data are means ± SEM of three independent experiments. Approximately 100 bacteria were scored per condition and asterisks indicate statistical difference ($P<0.05$). Reproduced with permission from Jeong *et al*, 2015[232].

Bardill *et al* demonstrated that SdeA-C effectors are secreted within the first minutes of macrophage infection in a Dot/Icm dependent manner[28]. Immunofluorescence microscopy of individual and combination *sidE* family deletions, in addition to CyaA translocation assays, demonstrated rapid SdeA secretion and association with the cytoplasmic face of the LCV membrane during infection. The CyaA translocation assay utilizes a *B. pertussis* calmodulin-dependent adenylate cyclase toxin (CyaA) as a reporter fusion to the N-terminus of SdeA. Translocation into the cytoplasm was monitored through increases in cAMP level, dependent on interaction with calmodulin found exclusively in the eukaryotic cytosol [28,61]. Bardill and colleagues showed that expression of SdeA-C could be observed as early as 5 minutes post infection (mpi) [28]. After challenge of A/J bone marrow-derived macrophages (BMDM) with *L. pneumophila,* SdeA-C localization was observed at the poles of the cytoplasmic face of the LCV[28]. This type of localization has been previously observed with various other confirmed *L. pneumophila* IDTS[92,535]. [231]. SdeA-C levels at the LCV peak around 30mpi, followed by a steady decrease in detectable levels at the LCV over the next several hours[28]. In addition, SdeA-C exhibited growth-phase regulation in liquid medium, with peaks in expression at early stationary phase, a property that is similar to other Dot/Icm substrates[28]. Further confirmation of SdeA-C T4SS-dependent translocation came from affinity chromatography and pull-down studies using the T4SS component IcmS as bait, which targets a number of IDTS for translocation [28,288,347].

Genetic analysis of SidE family has been explored through individual or combination deletions of the effector family. Loss of the entire SidE family produced no observable growth defect in A/J BMDM[28,301]. The absence of a growth phenotype with

IDTS mutants, particularly within mammalian hosts, is a reoccurring theme in the *Legionella* field. Genetic studies indicate that this growth resilience in mammalian host results from IDTS exhibiting overlapping function and/or overlaps in the cell process targeted by the bacterial effector proteins [354,355]. Genetic studies in the several amoebae hosts often offer genetic insights on IDTS classically obscured by mammalian complexity. For instance, challenge of *Acanthamoeba castellanii* or *Dictyostelium discoideum* with a *sidE* family deletion mutant results in at least a 10-fold defect in intracellular replication relative to a WT infection[28,232,452]. This defect could be eliminated by expression *in trans* of individual SidE members from a plasmid, indicating that these proteins function in redundant fashion to promote successful infection (Figure 1.17. B). Deletion of the SidE antagonist, SidJ, also results in a significant impairment of intracellular replication in amoebae (Figure 1.17.C), which was dramatically exacerbated by overexpression of SidE proteins in a *sidJ* deletion mutant (Figure 1.17.F). SidE overexpression only negatively affected intracellular replication in an *Acanthamoeba castellanii* challenge when SidJ was absent (Figure 1.17.D,E). Endocytic labeling experiments in amoeba with Texas Red Ovalbumin (TrOV) reveal that overexpression of SidE proteins in the absence of SidJ promote LCV maturation along the endocytic route leading to decreased bacterial viability (Figure 1.17. F). This suggests that the SidJ-SidE relationship is critical for proper LCV maturation during the first hours of infection. The occurrence of several highly homologous proteins stacked within a bacterial genome, as the *sde* genes are, indicate that gene duplication events resulted from the need to generate specialized effectors for specific hosts or target proteins to ultimately broaden

Legionella's host or IDTS target range for more efficient infection regardless of the host *L. pneumophila* may encounter within its aquatic environment[28,124,354,355].

1.8. Profiling Ceg9-Rtn4 interaction reveals Ceg9-independent Rtn4 structural reorganization and LCV association.

As mentioned earlier, *Legionella* modifies its intracellular compartment to become an ER-derived niche and this process involves manipulating host ER. One of the *Legionella pneumophila* IDTS implicated in mediating LCV interaction with the peripheral ER. This IDTS of unknown function, Ceg9, was found to strongly interact with two isoforms of the structural ER tubule protein Rtn4 (Rtn4b/d) Figure 1.18.A)[172]. This interaction was particularly interesting because it is the first report of a *Legionella* protein to specifically target a peripheral ER tubule protein. Fluorescence microscopy of permissive macrophages infected with WT *L. pneumophila* revealed strong colocalization between Rtn4 and the LCV within minutes of infection. This LCV-associated Rtn4 displayed novel characteristics from the remaining Rtn4 population in the cell after subjecting the cells to detergent permeabilization (Figure 1.18.B). Since Rtn4 is an integral ER membrane protein, treatment with a detergent to permeabilize cells membranes prior to immunofluorescence staining, results in dissolution of the ER lipid bilayer, solubilizing most integral membrane proteins, and extracting the Rtn4 network. In direct contrast to the native membrane extractable Rtn4, a detergent-resistant reticular network of Rtn4 remained around the LCV after Triton X100 permeabilization (Figure 1.18.B). This population of detergent-resistant Rtn4 appears at the LCV within 10 minutes post infection (mpi) and by 40 min, the majority of LCVs are associated with a detergent resistant Rtn4 aggregate (Figure 1.18.C). The association of Rtn4 with LCV

was absent in a T4SS defective strain of *L. pneumophila*, Lp03, also known as *dotA3*, and occurred independently of Ceg9 (Figure 1.18.C). This indicates that a *L. pneumophila* T4SS substrate, other than Ceg9, is responsible for the transformation of Rtn4 at the LCV[172].

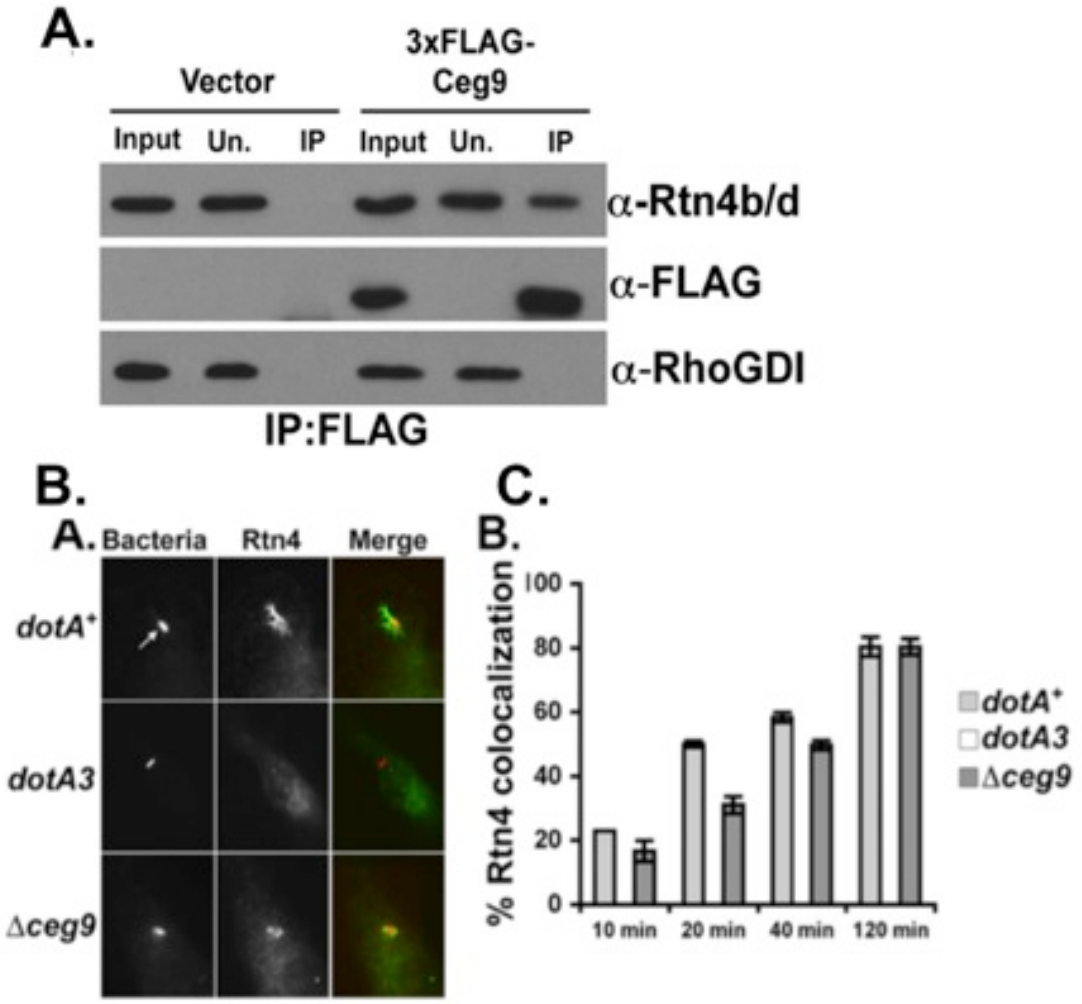

Figure 1.18. *L. pneumophila* T4SS substrate Ceg9 interacts with Rtn4b/d and Rtn4 accumulates at the LCV dependent on T4SS, but independent of Ceg9.
Experiments performed by Eva Haennsler[172]
(A) HEK293T cells were transfected with the 3xFLAG vector control and 3xFLAG-tagged Ceg9, extracted, and subjected to α-FLAG immunoprecipitation, SDS-PAGE fractionation, and immunoblot analysis with the denoted antibodies. Lanes: Input, 0.87% of the starting material; Un., 0.91% of the unbound supernatant; IP, 12.5% of the immunoprecipitation fractions eluted by boiling in 2x SDS sample buffer. **(B)** Representative examples of Rtn4 visualization after infection of A/J mice BMDMs with denoted *L. pneumophila* strains and detergent (Triton X100) extraction, followed by immunofluorescence microscopy. Panels: left, *L. pneumophila*; center, Rtn4; right, merge

images with *L. pneumophila* strains (red) and Rtn4 (green). **(C)** A/J mice BMDMs were challenged at an MOI of 1 with the wild type strain Lp02, the *dotA3* or T4SS deficient strain Lp03, and a *ceg9* deletion mutant. At the denoted time points, the cells were fixed and probed for *Legionella* and Rtn4. The phagosomes surrounded by reticular network or aggregates of Rtn4 with a signal above background were enumerated for each time point. The data represented are the averages and standard errors of three coverslips per data point and is representative of several independent experiments. Adapted from Haenssler *et al*, 2015 by combining select panels from Fig. 1 and Fig. 5.[172]

To investigate the association of tubular ER with the LCV during infection, Haenssler *et al*[172] challenged mammalian cells with *L. pneumophila* and analyzed for Rtn4 association with the LCV using immunofluorescence (IF) microscopy [172]. As shown in the original report of Rtn4-Ceg9 association[172], a detergent-resistant Rtn4 formed a reticular network proximal to the LCV by 40 min post infection[260], which was then observed condensed around the LCV circumferentially at 8 hours post-infection (hpi) in Triton X100-permeabilized samples (Figure 1.18.B, Figure 1.19.A,B)[260]. The inability to detect the well-characterized tubular reticulon network throughout the cell was investigated by changing permeabilization agents. The three agents selected were 1) methanol, an organic solvent that dissolves membrane lipids, while preserving most protein-protein interactions; 2) Triton X100, a non-ionic non-selective detergent that may extract proteins along with lipids depending on the concentration and conditions; and 3) SDS (sodium dodecyl sulfate), a harsh anionic detergent that denatures proteins by disrupting non-covalent bonds within and between proteins. Consistent with the previous report[172], Rtn4 colocalization with the LCV required a functional T4SS (Figure 1.19.C). Strikingly, staining of the entire Rtn4 network could only be detected in methanol treated samples that were permeabilized in the absence of detergent. In contrast, Rtn4 colocalized with the LCV after wild type *L. pneumophila* challenge under all permeabilization conditions tested, even in the presence of 5% SDS (Figure 1.19.C).

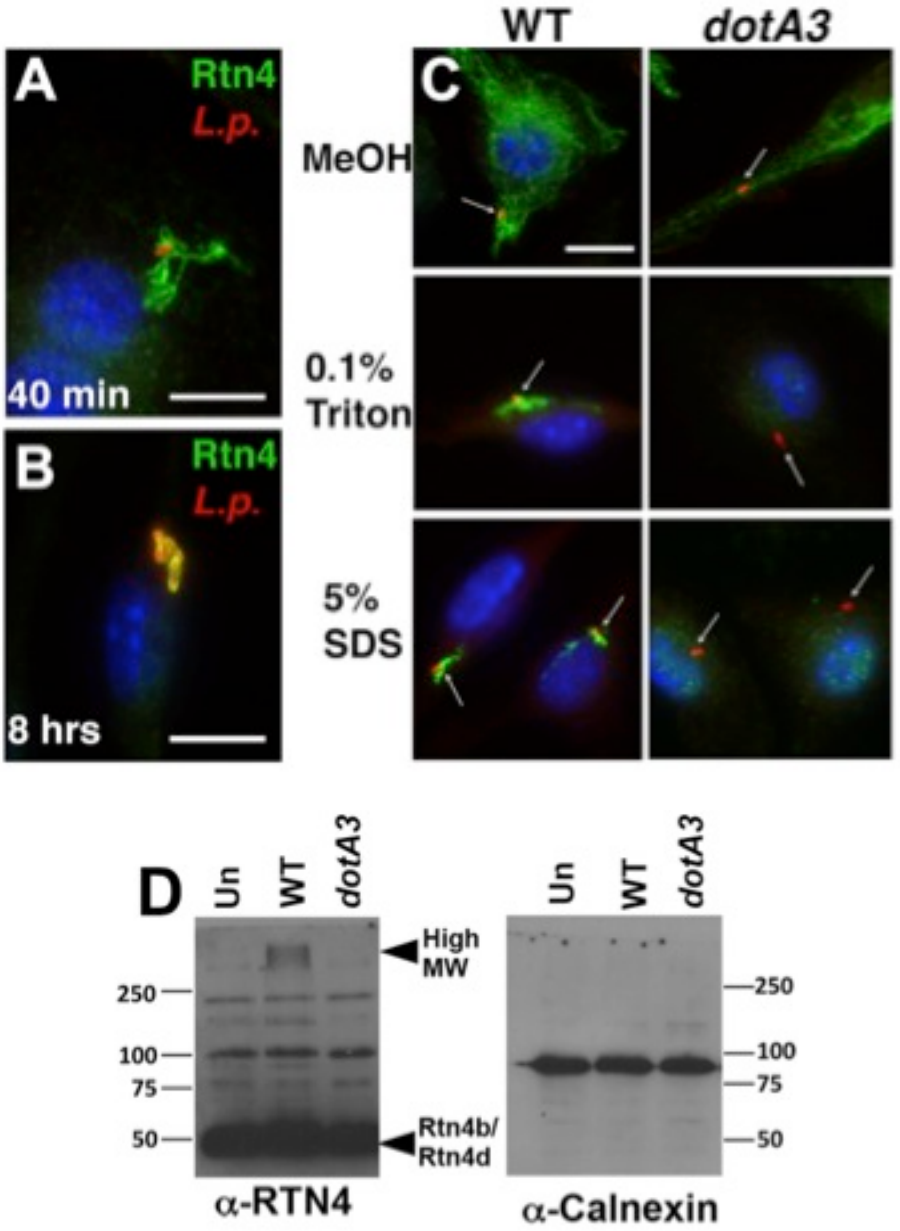

Figure 1.19. *L. pneumophila* challenge promotes Rtn4 transformation.
Experiments performed by Eva Haenssler[260]
(A,B) A/J mice BMDMs were challenged with *L. pneumophila*, followed by fixation, permeabilization with 0.1% Triton X100 and probing with α-Rtn4 (green), α-*L. pneumophila* (red), and Hoechst (blue). Scale bar: 5μm. **(C)** BMDMs challenged for 1 h with Lp02 (WT) or an *icm*/*dot* (*dotA3*) mutant were fixed, permeabilized as noted, and probed. Scale bar: 5μm. Arrows indicate location of bacterium within infected cells. **(D)** Altered electrophoretic migration of Rtn4 after *L. pneumophila* challenge, indicated by pointer and High MW. HeLa cells were challenged for 2 h, solubilized in SDS at room temperature, fractionated by SDS-PAGE, and probed. Lanes: Un, uninfected; WT, Lp02; *dotA3*, *icm/dot*- or T4SS defective. Reproduced with permission from Kotewicz *et al*, 2017[260].

Therefore, the persistent Rtn4 association with the LCV results from structural changes that distinguish this fraction from the cellular pool of Rtn4.

The imperviousness of the Rtn4 to SDS extraction intimated that these structural changes might be detectable on SDS gels. To test this hypothesis, mammalian cells (Cos1, Cos7, or HeLa) were challenged with the WT or *dotA3* strains and SDS extracts were fractionated by SDS-PAGE and analyzed with α-Rtn4 immunoblots. A high molecular weight (HMW) Rtn4 species was identified in extracts from infections with the WT strain, while another ER membrane protein, calnexin, showed no altered migration (Figure 1.19.D). This HMW Rtn4 species was absent in *dotA3* infected cells, just as SDS-resistant Rtn4 was not observed at the LCVs of *dotA3* (Figure 1.19.C,D). Taken together, the co-occurrence of an unextractable Rtn4 population at the LCV, revealed via IF microscopy, and the formation of a HMW, detergent-resistant Rtn4, uncovered by SDS-PAGE fractionation, suggest these novel Rtn4 forms represent the same pool of *L. pneumophila* modified Rtn4.

1.9. Study Aims.

The ability of *L. pneumophila* to target a predominantly tubular ER-localized protein at the earliest moments of infection suggests that the bacterium has adopted an early strategy to interact with peripheral ER prior to acquisition of rough ER components later during infection. From these early clues, we postulated that upon phagocytosis into a host, *L. pneumophila* rapidly interacts with the peripheral tubular network through one or more of its T4SS translocated proteins to facilitate the generation of an ER-derived vacuole, competent for bacterial replication. The study described in the subsequent dissertation was designed to decipher the players in this tubular ER manipulation

strategy, the molecular mechanism underlying the observed Rtn4 transformation, and finally to address the role these distinctive ER transformations play during infection.

Chapter 2:

Materials and Methods

This chapter contains excerpts that have previously been published in (reprinted with permission of publisher):

Kotewicz KM, Ramabhadran V, Sjoblom N, Vogel JP, Haenssler E, Zhang M, Behringer J, Scheck RA, Isberg RR. Cell Host Microbe. 2017 Feb 8; 21(2):169-181. Epub 2016 Dec 29.

2.1. Ethics statement.

This study was carried out in accordance with the Guide for Care and Use of Laboratory Animals of the National Institutes of Health. The Institutional Animal Care and Use Committee (IACUC) of Tufts University approved all animal procedures. The animal work was predominantly used for the isolation of macrophages, but a single experiment did involve *Legionella pneumophila* infections of live female 8-week old A/J mice. IACUC Protocol numbers for studies represented here: B2015-192 (replaced B2013-18) '*Legionella* Growth in Macrophages', B2014-122 (replaced B2011-149) 'Mechanisms of *Legionella pneumophila'*, and B2014-122 (K. Davis) 'Mechanism of *Legionella pneumophila* virulence' in a collaboration with K. Davis (former Isberg post-doctoral associate, currently at Johns Hopkins University in faculty position

2.2. Bacterial culture and media.

L. pneumophila derivatives used in these studies were streptomycin-resistant restriction-defective thymidine auxotrophs derived from a clinical isolate of *Legionella pneumophila*, strain Philadelphia-1 (Lp01). *L. pneumophila* strains were propagated on charcoal–N-(2-acetamido)-2-aminoethanesulfonic acid (ACES)–yeast extract plates, with or without thymidine as needed (CYE/T) and in ACES-yeast extract broth (AYE/T) [37,191,299]. Plasmids were introduced by electroporation [37] or by mating with *Escherichia coli* Tra^+ helper strain RK600 [492]. Luminescent *Legionella* strains were constructed using the *ahpC::luxCDABE* construction as described [[125]]. Strains harboring the pGFP Cm^R or pmCherry Cm^R isopropyl-β-D-thiogalactopyranoside (IPTG)-inducible plasmids were cultured with 5μg/mL Cm, 0.1mg/mL thymidine, and 1mM IPTG during growth in broth. *L. pneumophila ΔsdeC-A* in-frame deletion mutant was generated using a derivative of

the suicide vector pSR47S[115] as previously described [28]. The "clean" *sidE* family deletion, which lacks *sdeC, sdeB-sdeA,* and *sidE* and was previously published as Δ*p170* [[232]], was a kind gift from J. Vogel (Washington University, St. Louis MO). Individual Sde members were expressed without IPTG induction in *L. pneumophila* in a Gateway™ (Invitrogen) cloning compatible pJB908 having an N-terminal PolyHistidine tag, a kind gift of T. O'Connor. The Gateway™ compatible pJB908 was further modified to add an N-terminal *c*-myc epitope tag for double epitope tag protein expression in *L. pneumophila*. QuikChange™ site directed mutagenesis was used to generate point mutations in *sde* genes. For the infection of mammalian cells, *L. pneumophila* strains were grown overnight to post-exponential phase (OD_{600} 3.5-4.5) to a predominantly motile state as described previously [191]. Strain derivations and primers utilized in this study are described below in Tables 2.1.-2.4.

Table 2.1. *Legionella pneumophila* strains used in this study.

Strain	Genotype	Description	Reference
Lp02	(WT) Philadelphia 1, *thyA rpsL hsdR*	Wild type	[38]
Lp03	Lp02 *dotA03*	Translocation deficient	[38]
Δceg9	Lp02 *Δceg9*		[172]
Pentuple	Lp02 *Δlpg1603–lpg1686, Δlpg1104–lpg1128, lpg1136—lpg1169, Δlpg1933–lpg1999Δlpg2369–lpg2465, Δlpg2508–lpg2573*	Strain missing 18.5% of genome	[354]
Lp02 pGFP	Lp02 (pMMB207*Δmob*267*Ptac*::GFP)	Wild type, GFP^+	[193]
Lp02 pmCherry	Lp02 (pMMB207*Δmob*267*Ptac*::mCherry)	Wild type $mCherry^+$	[260]
KK034	Lp02*ΔsdeC-sdeA (Δlpg2153-2157) kan^R P_{ahpC}::lux*	*sdeC-sdeA* deletion, Lux^+	[260]
KK034 pGFP	KK034 (pMMB207*Δmob*267 P*tac*::GFP)		[260]
KK034 pmCherry	KK034 (pMMB207*Δmob*267 Ptac::mCherry)		[260]
KK034 $pSdeC_{WT}$	KK034 (pJB908att-$sdeC_{WT}$)	PolyHis/c-myc::SdeC WT	[260]
KK034 $pSdeC_{C118S}$	KK034 (pJB908att-$sdeC_{C118S}$)	PolyHis/c-myc::SdeC DUB-	[260]
KK034 $pSdeB_{WT}$	KK034 (pJB908att-$sdeB_{WT}$)	PolyHis/c-myc::SdeB WT	[260]
KK034 $pSdeA_{WT}$	KK034 (pJB908att-$sdeA_{WT}$)	PolyHis/c-myc::SdeA WT	[260]
KK050 pvector	Pentuple, *ΔsdeC-sdeA (Δlpg2153-2157) kan^R P_{ahpC}::lux*	Pentuple lacking *sde* operon, contains *sidE*	This study
KK050 $pSdeC_{WT}$	KK50 (pJB908att-$sdeC_{WT}$)		This study
KK050 $pSdeB_{WT}$	KK50 (pJB908att-$sdeB_{WT}$)		This study
KK050 $pSdeA_{WT}$	KK50 (pJB908att-$sdeA_{WT}$)		This study
JV6113	Lp02 *ΔsidE ΔsdeC ΔsdeBA* (*Δlpg0234, Δlpg2153 Δlpg2156-2157*)	*sidE* family deletion	[232]
KK099	JV6113 *kan^R P_{ahpC}::lux*	*sidE* family deletion, Lux+	[260]
KK099 pGFP	KK099 (pMMB207*Δmob*267 *Ptac*::GFP)		[260]

KK099 pmCherry	KK099 (pMMB207*Δmob*267 *Ptac*::mcherry)		[260]
KK099 pvector	*ΔsidE ΔsdeC ΔsdeBA* (pJB908att-empty)	pJB908 Gateway™ vector *ΔccdB* (PolyHis/c-myc epitope tag vector)	[260]
KK099 pSdeC$_{WT}$	KK099 (pJB908att-*sdeC$_{WT}$*)	PolyHis/c-myc::SdeC WT	[260]
KK099 pSdeC$_{C118S}$	KK099 (pJB908att-*sdeC$_{C118S}$*)	PolyHis/c-myc::SdeC DUB-	[260]
KK099 pSdeC$_{H416A}$	KK099 (pJB908att-*sdeC$_{H416A}$*)	PolyHis/c-myc::SdeC NP-	[260]
KK099 pSdeC$_{R763A}$	KK099 (pJB908att-*sdeC$_{R763A}$*)	PolyHis/c-myc::SdeC ART-	[260]
KK099 pSdeC$_{E859A}$	KK099 (pJB908att-*sdeC$_{E858A}$*)	PolyHis/c-myc::SdeC ART-	[260]
KK099 pSdeB$_{WT}$	KK099 (pJB908att-*sdeB$_{WT}$*)	PolyHis/c-myc::SdeB WT	[260]
KK099 pSdeB$_{R763A}$	KK099 (pJB908att-*sdeC$_{R763A}$*)	PolyHis/c-myc::SdeB ART-	[260]
KK099 pSdeB$_{E859A}$	KK099 (pJB908att-*sdeB$_{E859A}$*)	PolyHis/c-myc::SdeB ART-	[260]
KK099 pSdeA$_{WT}$	KK099 (pJB908att-*sdeA$_{WT}$*)	PolyHis/c-myc::SdeA WT	[260]
KK099 pSdeA$_{R766A}$	KK099 (pJB908att-*sdeA$_{R766A}$*)	PolyHis/c-myc::SdeA ART-	[260]
KK099 pSdeA$_{E862A}$	KK099 (pJB908att-*sdeA$_{E862A}$*)	PolyHis/c-myc::SdeA ART-	[260]

Table 2.2 *Escherichia coli* strains used in this study.

E. coli		
BL21 DE3	*F¯ ompT hsdSB gal dcm (DE3)*	
DH5α	*supE44 ΔlacU169(Φ80lacZDM15) hsdR17 recA1 endA1 gyrA96 thi-1 relA1*	
DH5α λpir	*DH5a (λpir) tet::Mu recA*	[256]
MT607 pRK600	*recA56 pro-82 thi-1 hsdR17 supE44* (RK600 XL-1)	[135]

Table 2.3. Oligonucleotides used in this study.

Primers	
Description	**Sequence (5' → 3')**
SdeC flanking primer with *attB1*	GGGGACAAGTTTGTACAAAAAAGCAGGCTTCATGCCTAAATACGTAGAAGGGGTAG
SdeC flanking primer with *attB2*	GGGGACCACTTTGTACAAGAAAGCTGGGTCCTATTAGAAACCATACCTTATGTCATCG

SdeB flanking primer with *attB1*	GGGGACAAGTTTGTACAAAAAAGCAGGCTTAATGCCTAAATATGTAGAAGGGGTAG
SdeB flanking primer with *attB2*	GGGGACCACTTTGTACAAGAAAGCTGGGTCCTATTAAAAGTAACCACTTTCTCGGTG
SdeA flanking primer with *attB1*	GGGGACAAGTTTGTACAAAAAAGCAGGCTTAATGCCTAAGTATGTCGAAGGGGTAG
SdeA flanking primer with *attB2*	GGGGACCACTTTGTACAAGAAAGCTGGGTCCTATTAAAATCCTATAGTTTTTTTATTGG
SdeC – pQE-80L	GGGGGATCCATGCCTAAATACGTAGAAGGG
SdeC – pQE-80L (C-terminus StrepII)	GGGGAGCTCTTATTATTTTTCGAACTGCGGGTGGCTCCAAGCGCTGAAACCATACC
Quickchange: SdeC C118S	GAGCCCGGCCTAAACAAAGGCCTATCTGGCTATTGGGTAGCCTC
Quickchange: SdeC C118S	GAGGCTACCCAATAGCCAGATAGGCCTTTGTTTAGGCCGGGCTC
Quickchange: SdeB C118S	GAAGCAACCCAATAGCCAGATAGCCCCTTGTTTAGGC
Quickchange: SdeB C118S	GGCCTAAACAAGGGGCTATCTGGCTATTGGGTTGCTTC
Quickchange: SdeA C118S	AGGCGACCCAGTAGCCGGATAATCCCATATTCAAACC
Quickchange: SdeA C118S	GGTTTGAATATGGGATTATCCGGCTACTGGGTCGCCTC
Quickchange: SdeC H416A	CAT ATC CTG ATA AAT CAA GGC GCT ATG GTC GAT TTA ATG AGG AC
Quickchange: SdeC H416A	GT CCT CAT TAA ATC GAC CAT AGC GCC TTG ATT TAT CAG GAT ATG
Quickchange: SdeC/SdeB R763A	CTCCGAAAAAACTGTATGCTGGATTAAATCTGCCACAAG
Quickchange: SdeC/SdeB R763A	CTTGTGGCAGATTTAATCCAGCATACAGTTTTTTCGGAGC
Quickchange: SdeC E859A	CATATGGCTGGTTCCGAAGATGCATTTTCCGTTTATTTGC
Quickchange: SdeC E859A	GCAAATAAACGGAAAATGCATCTTCGGAACCAGCCATATG
Quickchange: SdeB E859A	CATATGACTGGATCAGAAGATGCATTTTCCGTTTATTTGCC
Quickchange: SdeB E859A	CAAATAAACGGAAAATGCATCTTCTGATCCAGTCATATGG
Quickchange: SdeA E862A	CATGGCGAAGGCACCGAAAGTGCATTCTCCGTTTATTTGCCG
Quickchange: SdeA E862A	CTCCGGCAAATAAACGGAGAATGCACTTTCGGTGCCTTCGCC

Rtn4-APEX2-GFP-F	GATCGGTACCAGGCTCGAACTCGGGCTCGGGCATGGGAAAGTCTTACCCAACTGTGAGT
Rtn4-APEX2-GFP-R	GATCGGATCCAGGCATCAGCAAACCCAAGCTCGGA

Table 2.4. Plasmids used in this study.

Plasmids		**Ref**
Transfection screen		Table 2.5.
pQE-80L	Expression vector for N-terminal PolyHis tagged proteins	Qiagen
pQE-SdeC^{WT}	pQE-80L *sdeC*, C-terminus StrepII tag	[260]
pQE-SdeA^{WT}	pQE-80L *sdeA*, C-terminus StrepII tag	[260]
pQE-SdeC^{C118S}	pQE-80L *sdeC* C118S, C-terminus StrepII tag	[260]
pQE-SdeC^{H286A}	pQE-80L *sdeC* H286A, C-terminus StrepII tag	[260]
pQE-SdeC^{R342A}	pQE-80L *sdeC* R342A, C-terminus StrepII tag	[260]
pQE-SdeC^{H416A}	pQE-80L *sdeC* H416A, C-terminus StrepII tag	[260]
pQE-SdeC^{R422A}	pQE-80L *sdeC* R422A, C-terminus StrepII tag	[260]
pQE-SdeC^{R763A}	pQE-80L *sdeC* R763A, C-terminus StrepII tag	[260]
pQE-SdeC^{E859A}	pQE-80L *sdeC* E859A, C-terminus StrepII tag	[260]
pRtn4b-GFP	peGFP-N1 *rtn4b*	[172]
pcDNA3 APEX2-NES		
pRtn4b-APEX2-GFP	peGFP-N1 *rtn4b*::APEX2::GFP	[260]
pSR47-P_{ahpC}*::lux*	pSR47 containing *P. luminescens lux* operon	[89]
pSR47s	*oriT*RP4 *ori*R6K *kan sacB*	[314]
pJB2199	SR47S Δ*sdeC-sdeA* (contains region flanking *sdeA* and *sdeC*)	[28]
pJB908	RSF1010 *thyA*$^+$ *bla*$^+$ *Δmob*	[450]
pJB908attR	pJB908 PolyHis/c-myc-*attR1*-[Cm^R *ccdB*]-*attR2*	[260]
pJB908att-empty	pJB908 PolyHis/c-myc-*attB1-attB2*	[260]
pSdeC$_{WT}$	pJB908 PolyHis/c-myc-*attB1-sdeC$_{WT}$-attB2*	[260]
pSdeC$_{C118A}$	pJB908 PolyHis/c-myc-*attB1-sdeC$_{C118A}$-attB2*	This study
pSdeC$_{C118S}$	pJB908 PolyHis/c-myc-*attB1-sdeC$_{C118S}$-attB2*	[260]
pSdeC$_{C293A}$	pJB908 PolyHis/c-myc-*attB1-sdeC$_{C293A}$-attB2*	[260]
pSdeC$_{H286A}$	pJB908 PolyHis/c-myc-*attB1-sdeC$_{H286A}$-attB2*	[260]
pSdeC$_{R342A}$	pJB908 PolyHis/c-myc-*attB1-sdeC$_{R342A}$-attB2*	[260]
pSdeC$_{H416A}$	pJB908 PolyHis/c-myc-*attB1-sdeC$_{H416A}$-attB2*	[260]
pSdeC$_{R422A}$	pJB908 PolyHis/c-myc-*attB1-sdeC$_{R422A}$-attB2*	[260]
pSdeC$_{R763A}$	pJB908 PolyHis/c-myc-*attB1-sdeC$_{R763A}$-attB2*	[260]
pSdeC$_{E859A}$	pJB908 PolyHis/c-myc-*attB1-sdeC$_{E859A}$-attB2*	[260]
pSdeB$_{WT}$	pJB908 PolyHis/c-myc-*attB1-sdeB$_{WT}$-attB2*	[260]
pSdeB$_{C118S}$	pJB908 PolyHis/c-myc-*attB1-sdeB$_{C118S}$-attB2*	This study
pSdeB$_{R763A}$	pJB908 PolyHis/c-myc-*attB1-sdeB$_{R763A}$-attB2*	[260]

pSdeB$_{E859A}$	pJB908 PolyHis/c-myc-*attB1-sdeB$_{E859A}$-attB2*	[260]
pSdeA$_{WT}$	pJB908 PolyHis/c-myc-*attB1-sdeA$_{WT}$-attB2*	[260]
pSdeA$_{C118S}$	pJB908 PolyHis/c-myc-*attB1-sdeA$_{C118S}$-attB2*	This study
pSdeA$_{R766A}$	pJB908 PolyHis/c-myc-*attB1-sdeA$_{R766A}$-attB2*	[260]
pSdeA$_{E862A}$	pJB908 PolyHis/c-myc-*attB1-sdeA$_{E862A}$-attB2*	[260]

2.3. Antibodies, chemicals, and Western blots.

Antibodies and chemicals were purchased from the following sources, and used at the following dilutions. Rat α-*L. pneumophila* (raised as polyclonal serum) was used at 1:5,000-1:15,000 (batch dependent) dilutions while α-Rtn4 used for immunofluorescence was purchased from Lifespan Biosciences (LS-B6516, 1:500 dilution) and was detected with α-rat IgG Alexa Flour 594 (1:500) and goat α-rabbit Alexa Fluor 488 (1:500) (Jackson Laboratories). Hoescht 33342 was purchased from Life Technologies (1:10,000). For generating cross-linked α-Rtn4 resin, α-Rtn4 was purchased from Santa Cruz Biotechnology (Nogo N-18, sc-11027). Either uniform percentage SDS-PAGE gels (made in house with the Hoefer system) or precast gradient gels (Miniprotean TGX 4-20%) were purchased from Bio-Rad to fractionate samples. Gels were then transferred to GE Amersham™ Protran™ nitrocellulose (0.2μm) and blocked with 4% non-fat milk or 2% bovine serum albumin (BSA) in Tris-HCl buffered saline with 0.1% Tween-20 (TBST) for at least 20-30 min prior to incubation with primary antibody. Monoclonal mouse α-HA-probe (F-7; 1:500), α-ethenoadenosine (α-εAdo; 1G4; 1:500 Santa Cruz or 1:1000 Novus Biologicals), α-Ub (P4D1, 1:500 Santa Cruz or 1:2000 Cell Signaling Technologies), rabbit α-GAPDH (1:500; sc-25778), and α-GST (1:500-1000; Z-5) antibodies were purchased from Santa Cruz Biotechnology. Rabbit α-GFP antibody was purchased from Life Technologies (1:2,000; A11122), α-Rtn4 (, 1:5000; LS-B6516 rabbit) from Lifespan Biosciences, and rabbit monoclonal α-LC3a/b (1:2,000; D3U4C)

from Cell Signaling Technologies were used for immunoblots. Rabbit α-actin (1:1,000; A2066) and the monoclonal PolyHistidine antibody for immunoblots were purchased from Sigma (1:1,000-2,000; HIS-1).

ECL-Plus Western blotting reagent (Pierce) was used for chemiluminescent detection. Alternatively, the Li-Cor near-fluorescent secondary antibodies detection system was used for immunoblot detections with the Li-Cor Odyssey CLX scanner. In brief, for the Li-Cor system after SDS-PAGE fractionation, proteins are transferred to nitrocellulose membranes, blots were blocked with 4% non-fat milk in TBST for at least 20 min prior to primary antibody incubation. After blocking, milk in TBST was removed, membrane rinsed with TBST, then primary antibody was diluted into 2% BSA in TBST for 2hr room temperature incubation or overnight incubation at 4°C gently shaking (>75rpm/min). Then after primary removal and at least 3 subsequent TBST washes of 5-10 min on a shaking platform, nitrocellulose membranes were incubated in 4% non-fat milk diluted in TBST for 40-45min with the appropriate Li-Cor secondary antibodies (Li-Cor secondary antibodies, donkey IRDye 680RD α-mouse, Goat IRDye 680RD α-rabbit, and/or donkey IRDye800CW α-mouse, goat IRDye800CW α-rabbit, 1:20,000) followed by 3 additional 5-10min washes in TBST, and a final wash in TBS prior to development on the Li-Cor Odyssey CLX scanner.

Silver staining was performed using SilverQuest kit (Invitrogen) as per manufacturers rapid development protocol. MG-132 was from Calbiochem and was used at 10μM final concentration and chloroquine was used at a final concentration 100μM (Caymen Chemicals). Purified GST-HA-Rtn4b was purchased from MRCPPU (https://mrcppureagents.dundee.ac.uk/reagent-catalogues). Purified recombinant human

ubiquitin, ubiquitin tetramers, HA-ubiquitin, PolyHistidine-ubiquitin, NEDD8, SUMO were purchased from Boston Biochem (R&D systems). Purified recombinant Human p62/SQSTM1 with a C-terminus PolyHistidine tag (AA 1-356-H_6, NBP1-44490) was purchased from Novus Biologics.

2.4. Eukaryotic cell culture.

Bone marrow-derived macrophages (BMDMs) were isolated from femurs and tibias of female 8-10week old A/J mice as previously described [24,25,123] and frozen in fetal bovine serum (FBS) with 10% dimethyl sulfoxide (DMSO). Cells were plated the day before infection in RPMI 1640 (Gibco) supplemented with 10% FBS and 2 mM glutamine at 37°C with 5% CO_2. HeLa, HEK293T, Cos1, Cos7 obtained from ATCC were cultivated in Dulbecco modified Eagle medium (Gibco) supplemented with 10% heat-inactivated (FBS, Invitrogen) (vol/vol), 100U/ml of penicillin-streptomycin (Gibco) at 37°C with 5% CO2. The animal studies were approved by the Institutional Animal Care and Use Committee (IACUC) of Tufts University, see ethics statement for protocol numbers.

2.5. Immunofluorescence of Rtn4-LCV colocalization.

BMDMs were plated on glass coverslips at 1-2x10^5/well in 24-well plates. Cells were challenged at a multiplicity of infection (MOI) = 1 and plates were centrifuged at 1000 x rpm for 5 min. For Rtn4 colocalization assays, BMDMs were challenged for 1 hr at 37°C, unless otherwise indicated. Slides were washed three times with PBS to remove non-internalized bacteria, fixed in PBS containing 4% (wt/vol) paraformaldehyde for 15-20 min at room temperature, and washed 3X with PBS. After blocking in PBS containing 4% (vol/vol) BSA, cells were permeabilized in PBS containing 1% (vol/vol) Triton X-

100 (Tx-100; 0.1% for Cos7 cells) for 30min unless otherwise indicated, then washed 3X in PBS, and then blocked in PBS containing 4% BSA. Cells were then stained in PBS (containing XXBSA??) with α-*L. pneumophila* rat or rabbit serum (1:5,000) and α-Rtn4 (Lifespan Biosciences, LS-B6516, 1:500) for 1hr and detected with donkey α-rat IgG Alexa Flour 594 (1:500) and goat α-rabbit Alexa Fluor 488 (1:500) (Jackson Laboratories) Diluted in PBS (containing XXBSA??). Hoescht 33342 (Life Technologies, diluted 1:10,0000 in PBS) was used to label DNA. The Rtn4 positive *L. pneumophila* vacuoles were visually identified by immunofluorescence microscopy for 50 cells/coverslip, with at least 3 coverslips evaluated per condition. Representative images were taken using Zeiss Axiovert or Nikon inverted phase fluorescence microscopes, and contrast and brightness were adjusted in Photoshop™ (Adobe), using linear corrections.

2.6. Formation of HMW Rtn4 screen.

Cos1 or HeLa cells were seeded at $1x10^5$ the day prior to transfection, and 3μg of pDEST53 (GFP only control) or a vector expressing GFP::*Legionella* Icm/Dot translocated substrates (IDTS) were transfected into cells with Lipofectamine 2000™ (Life technologies) for 40-46h[299]. Cells were collected in PBS and sample buffer (lacking reducing agent) at room temperature, then lysates were sheared with 26 gauge needle and samples were analyzed by SDS-PAGE fractionation coupled with immunoblots. Table 2.5 indicates the GFP::*L. pneumophila* T4SS substrates that were transfected and assayed for changes in Rtn4 migration.

Table 2.5. Known/putative IDTS from *L. pneumophila* Gateway® library screened for altered Rtn4 migration.

Transfection Vector	Protein	Altered Rtn4 Migration
pDEST53	pDEST53 (GFP) Amp^R	−
pDEST_*lpg0008*		−
pDEST_*lpg0012*		−
pDEST_*lpg0030*		−
pDEST_*lpg0035*	Ceg1	−
pDEST_*lpg0038*	LegA10	−
pDEST_*lpg0045*		−
pDEST_*lpg0056*		−
pDEST_*lpg0080*	Ceg3	−
pDEST_*lpg0081*		−
pDEST_*lpg0082*		−
pDEST_*lpg0086*		−
pDEST_*lpg0090*	Lem1	−
pDEST_*lpg0096*	Ceg4	−
pDEST_*lpg0103*	VipF	−
pDEST_*lpg0107*		−
pDEST_*lpg0112*		−
pDEST_*lpg0160*		−
pDEST_*lpg0171*	LegU1	−
pDEST_*lpg0191*	Ceg5	−
pDEST_*lpg0195*		−
pDEST_*lpg0210*		−
pDEST_*lpg0227*	Ceg7	−
pDEST_*lpg0240*	Ceg8	−
pDEST_*lpg0246*	Ceg9	−
pDEST_*lpg0276*	LegG2	−
pDEST_*lpg0279*		−
pDEST_*lpg0285*	Lem2	−
pDEST_*lpg0518*		−
pDEST_*lpg1183*		−
pDEST_*lpg1496*	Lem10	−
pDEST_*lpg1969*	PieE	−
pDEST_*lpg2128*		−
pDEST_*lpg2131*	LegA6	−
pDEST_*lpg2137*	LegK2	−
pDEST_*lpg2143*		−
pDEST_*lpg2147*		−
pDEST_*lpg2148*		−
pDEST_*lpg2153*	SdeC	+
pDEST_*lpg2154*	SidE-like	−
pDEST_*lpg2155*	SidJ	−
pDEST_*lpg2156*	SdeB	+

pDEST_*lpg2157*	SdeA	+
pDEST_*lpg2160*		−
pDEST_*lpg2166*	Lem19	−
pDEST_*lpg2176*	LegS2	−
pDEST_*lpg2182*	AdoMet Transferase	−
pDEST_*lpg2199*		−
pDEST_*lpg2200*		−
pDEST_*lpg2206*	WipC	−
pDEST_*lpg2207*		−
pDEST_*lpg2210*		−
pDEST_*lpg2215*	LegA2	−
pDEST_*lpg2216*	NTPase	−
pDEST_*lpg2222*	IpnE	−
pDEST_*lpg2224*	PpgA	−
pDEST_*lpg2244*		−
pDEST_*lpg2248*		−
pDEST_*lpg2257*		−
pDEST_*lpg2271*		−
pDEST_*lpg2298*	LegC7/YlfA	−
pDEST_*lpg2509*	SdeD	−
pDEST_*lpg2523*		−

2.7. Immunofluorescent microscopy of ubiquitin kinetics at the LCV.

BMDMs were plated on glass coverslips at 1-2x10^5/well in 24-well plates. Cells were challenged at a multiplicity of infection (MOI) = 1 and plates were centrifuged at 1000 x rpm for 5 min. The infection clock was initiated post centrifugation and upon transfer of cells to 37°C CO2 incubator for the indicated time post centrifugation for ubiquitin kinetic assays (e.g., 0, 10, 30, 60 min. post infection (mpi)). Slides were washed three times with PBS to remove non-internalized bacteria, then fixed in PBS with 4% (wt/vol) paraformaldehyde for 20 min at room temperature, and washed 3x with PBS. After blocking in PBS with 4% (vol/vol) bovine serum albumin (BSA), cells were permeabilized in PBS with 1% (vol/vol) freshly diluted TritonX-100 (0.1% Tx-100 for Cos7/Cos1 cells) for 30min, washed 3x in PBS, blocked in PBS containing 4% BSA. Cells were then stained with anti-*L. pneumophila* rat or rabbit serum (1:5,000) and anti-

Rtn4 (Lifespan Biosciences, LS-B6516, 1:500) or anti-polyubiquitin (FK1, Enzo, 1:250) for 1hr and detected with donkey anti-rat IgG Alexa Flour 594 (1:500) and goat anti-rabbit Alexa Fluor 488 (1:500). Hoescht 33342 (Life Technologies, 1:10,0000 in PBS) was used to label DNA. The ubiquitin positive *L. pneumophila* vacuoles were determined for 50 cells/coverslip by immunofluorescent microscopy with at least 3 coverslips assessed per condition. Representative images were taken using a Zeiss AxioObserver Z1 or Nikon Diaphot fluorescence microscopes, and image analysis was performed using Photoshop™ (Adobe), adjusting pixel densities using linear corrections.

2.8. Rtn4 Immunoprecipitations.

For transfections preceding Rtn4 Immunoprecipitations (IP), HEK293T cells were plated in DMEM medium containing 10% fetal calf serum at a density of 4 x 10^6 cells in a tissue culture-treated 10cm dish. The next day, 12µg of pMT123 DNA (pHA::ubiquitin) was transfected into cells using Lipofectamine 2000, following manufacturer's procedure (Life Sciences). The mammalian HA::ubiquitin expression plasmid pMT123 was a kind gifts from D. Bohmann and S. Lippard [123,508]. The next day, transfection medium was removed and replaced with DMEM with 10µM MG132 (Calbiochem) at ~30-60min prior to challenge with *L. pneumophila* at an MOI=10 for the indicated times. Post-challenge, the medium was carefully removed, cells gently washed in PBS, then lifted in PBS, centrifuged at 4°C at 1000 x RPM, resuspended in ice cold PBS, centrifuged at 4°C, and then cell pellets were immediately frozen on liquid nitrogen and stored at -80°C until the immunoprecipitation could be performed (Figure 2.1).

For Immunoprecipitations, anti-Rtn4 resin was generated by disuccinimidyl suberate crosslinking with anti-Rtn4 (Nogo N-18, Santa Cruz sc-11027) to Protein A/G

Plus™ resin at 2µg antibody per µl of packed resin as described in manufacturer protocol (Pierce crosslink IP kit). Samples were lysed in 20 mM Tris (pH=7) containing 1% Triton X-100, 150 mM NaCl, 5 mM $MgCl_2$ and complete protease inhibitor cocktail (Roche/Sigma, Cat. # 11697498001) with end-over-end rotation for 20 min at 4°C. Cell debris was removed by centrifugation at ≥14,000 x *g* for 10 min at 4°C. Cleared lysates were transferred to a microcentrifuge spin column, diluted with an equal volume of detergent-free buffer (20 mM Tris (pH=7), 150 mM NaCl, 5 mM $MgCl_2$), and mixed with 40µl of buffer-equilibrated resin (50% slurry) for each sample. Resin binding was allowed to proceed at 4°C via end-over-end rotation for 4 hrs to 16 hrs. Rtn4 resin washes were performed ≥5 times in cold 20 mM Tris (pH=7) containing 1% Triton X-100, 150 mM NaCl, 5 mM $MgCl_2$ at 4°C. For elution, Rtn4 resin in spin columns was incubated with 0.1M glycine (pH = 2.8) with 0.2% TritonX-100 for 5min, centrifuged at 3000 RPM, eluate was reapplied to resin for additional 5 min incubation at room temperature, then eluate was centrifuged, neutralized with 0.5M Tris (pH=10.55), resuspended with reducing SDS sample buffer, boiled, then fractionated by SDS-PAGE coupled with immunoblot analyses (Figure 2.1).

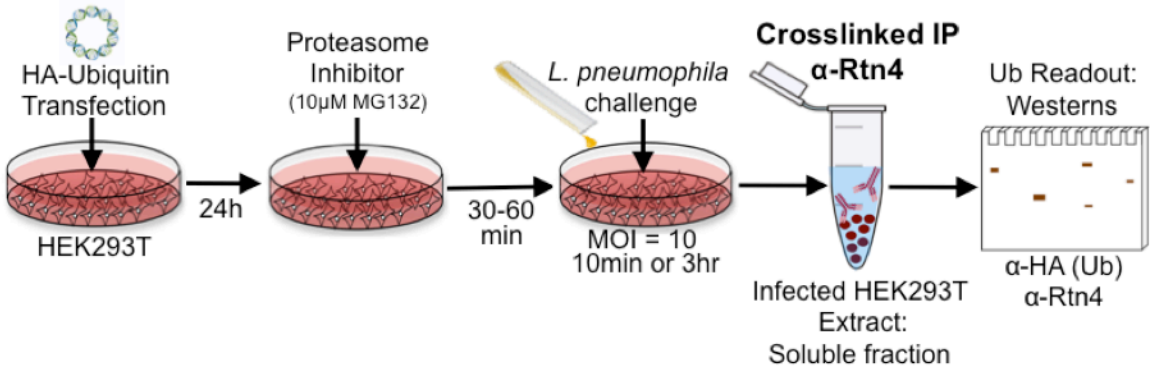

Figure 2.1. Protocol for assessing Rtn4 ubiquitination after *L. pneumophila* challenge of mammalian cells through HA-ubiquitin transfection and α-Rtn4 immunoprecipitation (IP).
A plasmid for mammalian expression of HA-ubiquitin was transfected into HEK293T cells for 24 hrs after which culture medium was removed and replaced with fresh medium containing the proteasome inhibitor MG132 (10μM), to limit protein turn over during infection until Immunoprecipitations could be performed. After cells had been incubated for 30-60 min with MG132, cells were challenged with *L. pneumophila* or associated *sidE* family mutants for 10 min or 3 hrs, washed, and frozen prior to IP. Then infected HEK293T extracts were solubilized with detergent, the soluble fraction was collected and then subject to α-Rtn4 immunoprecipitation. Elutes were fractionated with SDS-PAGE and analyzed for HA-ubiquitin co-migration with Rtn4 species through immunoblots.

2.9. Protein purification.

Full-length *sdeC* or *sdeA* genes were amplified by PCR and cloned into the bacterial expression vector pQE-80L (Qiagen) with *BamHI* and *SacI* restriction sites to generate a 6xHis-SdeC-StrepII fusion construct (Table S1). Wild-type or point mutant SdeC constructs were introduced into in BL21-DE3 and expressed growing cultures in 2X Yeast Tryptone broth (2xYT) overnight at 37°C, back diluted 1:100 in 2xYT, grown to exponential phase (OD_{600} 0.4-0.8), induced with 1mM IPTG, and grown for an additional 4-6 hrs. Bacteria were collected by centrifugation; pellets were subjected to ≥ 4 freeze-thaw cycles in lysis buffer (50mM NaH_2PO_4, 300mM NaCl 10mM imidazole, pH=7.6) followed by sonication. Clarified supernatants were batch purified using sequential double tag purification with Ni-NTA (Thermo) followed by Strep-tactin (IBA) affinity chromatography at 4°C following manufacturers instructions, then dialysis into

20mM Tris (pH = 7.4), 10mM NaCl (1x ART buffer), and concentration with Amicon Ultracel™ 50k (Millipore). Purified aliquots were stored at -80°C in same buffer containing 10% glycerol to minimize or eliminate freeze thaw cycles.

2.10. Deubiquitinase assays.

Recombinant human homotypic-linked ubiquitin tetramers (K63, K48, M1/Linear, Boston Biochemistry, R&D) were incubated with 20nM recombinant SdeC at 37°C in 20mM Tris-HCl (pH=7.4), 10mM NaCl, (1X ART buffer) for the indicated time. A fraction of the reaction was removed and terminated by the addition of reducing sample buffer. Samples were then heated to 50-55°C for 20-30min to avoid Ub chain aggregation as per manufacturer's suggestion, and samples were fractionated by SDS-PAGE and analyzed by silver stain (SilverQuest™ , Invitrogen) or Western blots.

2.11. ADP-ribosylation/nucleotidase assays.

ADP-ribosylation assays were set up on ice in 1X ART buffer with either 10μM HA-ubiquitin, ubiquitin, or PolyHistidine-ubiquitin (Boston Biochem), and 20nM recombinant SdeC/SdeA, 100μM Nicotinamide 1,N6-ethenoadenine dinucleotide or β-Nicotinamide adenine dinucleotide (ε-NAD, Santa Cruz Biotech/Sigma). Reactions were initiated by addition of enzyme and transferred to pre-warmed 37°C thermocycler. Reactions were terminated by addition of reducing sample buffer or freezing with liquid N_2, followed by lyophilization (Labconco Freezone12), resuspension in reducing sample buffer, and boiling. Reactions were analyzed with SDS-polyacrylamide gels coupled with Western blot, silver stain, or Coomassie Blue analysis.

For assays with cell extracts, 293T cells were harvested by lifting in PBS, centrifugation, followed by an additional PBS wash, whereas Cos7 cells were harvested

by lifting in PBS containing 0.05% trypsin, followed by PBS washes. Cells were lysed by passaging **4-5** times with a Dounce homogenizer, and the soluble material, lacking the nuclear fraction, was collected followed by clearing with two 3000 x RCF spins. The soluble protein extract was quantified via Bradford assay (Bio-Rad, 5X Protein Concentrate) and 100 μg of freshly prepped mammalian cell extract was added to reactions. Reactions with cell extract were terminated by freezing in liquid nitrogen, lyophilization, resuspension in 8M urea, and addition of reducing sample buffer prior to SDS-polyacrylamide gels analysis coupled with Western blot, silver stain, or Coomassie analysis.

2.12. Intracellular *L. pneumophila* growth in *Dictyostelium discoideum* and BMDMs.

D. discoideum strain Ax4 was cultured as described [[471]] and cells were plated at 1 x 10^5 in a Nucleon white flat bottomed, white walled treated 96-well plate (Thermo) and given at least 3h to adhere in MB medium (20 mM MES [2(N-morpholino) ethanesulfonic acid, pH 6.9, 0.7% yeast extract, 1.4% BBL thiotone E peptone). Amoeba were challenged with *L. pneumophila* at an MOI=0.5 for 2h, washed 3X in MB, then measured for luciferase expression once every hour for ≥100 hrs in a plate reader (Tecan Infinite 200Pro) at 25.5°C. BMDMs from A/J mice were plated at 1 x 10^5 in a Nucleon white flat bottomed, white walled treated 96-well plate (Thermo) the day prior to infection in RPMI (No phenol red, with glutamine, Life Technologies) with 10% FBS and allowed to adhere overnight. BMDM medium was replaced prior to *L. pneumophila* challenge at an MOI=0.05 for 2 hrs, washed 3x in RPMI, then measured for luciferase expression once every hour for ≥72 hrs in a plate reader (Tecan Infinite 200Pro) at 37°C.

2.13. Rtn4 ubiquitination *in vitro*.

Assays were initiated on ice in 1X ART buffer with 400nM GST-HA-Rtn4 (MRCPPU, https://mrcppureagents.dundee.ac.uk/reagent-catalogues) or GST (Thermo, *E. coli* derived), recombinant human Ub derivatives (Boston Biochem) at 10 μM final concentration, 20nM recombinant SdeC, and 100μM nicotinamide 1,N6-ε-adenine dinucleotide (Santa Cruz Biotech/Sigma) in 50μl. Reactions were initiated by addition of enzyme followed by transfer to a pre-warmed 37°C thermocycler for 1hr, terminated by addition of sample buffer and boiling.

2.14. Electron microscopy.

For analysis of Rtn4b localization about the LCV [273], Cos7 cells were plated in 35mm glass bottom No.2 uncoated gridded dishes (MatTek, catalogue number:P35G-2-14-C-GRID) at 1 x 10^5 cells. The following day, cells were transfected with Rtn4b-APEX2-GFP in Lipofectamine LTX™ reagent for 16-18 hours. 1 hr prior to *Legionella* challenge, the medium with transfection reagent was replaced with DMEM+10% FBS. Cells were then challenged with *L. pneumophila* expressing mCherry or GFP for designated times, washed with PBS, fixed in PBS containing 2% gluteraldehyde solution for at least 1 h on ice, then washed in PBS before further processing. To reveal Rtn4b localization, the fixed cells were incubated in ice-cold PBS containing 20mM glycine for two 5-minute blocking steps before washing in PBS and staining. The washed cells were then incubated on ice for 15 min in 1.5 mls PBS containing SigmaFast DAB tablets, allowing a precipitate to form (2 tablets/5 mls PBS; Sigma-Aldrich, #D4418). The washed cells were stored in PBS prior to processing for transmission electron microscopy (TEM). Thin section analysis of these samples, as well as that of A/J mouse BMDMs that

were challenged with *L pneumophila* were performed as described previously [[492]]. Embedding, sectioning and imaging of samples from both macrophages and Cos7 cells were performed by the Harvard Digestive Diseases Center Imaging Core at Beth Israel Deaconess Hospital (Dr. Susan Hagen, Director). These experiments resulted from a collaboration between V. Ramabhadran, who designed the experiment, and K. Kotewicz, J. Berhinger, and M. Zhang, who were responsible for carrying out and analyzing EM-APEX2 experiments.

2.15. Mass spectrometry.

Identification of Rtn4b/d-modification was performed after IP of Rtn4b/d from extracts of transfected HeLa cells, fractionation on SDS-PAGE followed by silver staining. Rtn4b/d electrophoretic variants were excised, trypsin-digested, and subjected to liquid chromatography tandem mass spectrometry (LC-MS/MS) for modification analysis by the Boston Children's Hospital IDDRC Core, using a Thermo-Fisher Q-Exactive OrbiTrap-type mass spectrometer. To determine molecular masses of Ub derivatives, 10μM Ub monomer was incubated with 20 nM $SdeC_{WT}$ or $SdeC_{H416A}$ and 100 μM ε-NAD for 2 h and 1 h, respectively in ART buffer. Samples were then frozen using liquid N_2 to terminate the reaction. The samples were thawed on ice and buffer exchange was performed into ultrapure water using Illustra Nap5 columns (GE). Samples were diluted with ultrapure water to 1 μM of the Ub derivative and 1 μl was injected for LC-MS analysis. Reversed-phase chromatography was performed on an Agilent 1260 Infinity LC system with a ZORBAX 300SB-C8 column (2.1 x 100mm, Agilent) using a water:acetonitrile gradient mobile phase containing 0.1% formic acid. Mass spectrometry analysis was performed on an Agilent 6530 Accurate-Mass Q-TOF. To determine

deconvoluted molecular masses, data were analyzed using Bioconfirm software.

2.16. Tandem liquid chromatography mass spectrometry.

LC-MS/MS analysis was performed by the Taplin Biological Mass Spectrometry Facility at Harvard Medical School. Excised gel bands were washed with acetonitrile for 10 min., dehydrated *in vacuo*, and rehydrated in 50 mM ammonium bicarbonate (AmBiC) solution prior to incubation with AspN/trypsin (12.5 ng/ml each) at 37^{o}C overnight [[455]]. Peptides were then extracted by removing the AmBiC solution, followed by one wash with a solution containing 50% acetonitrile (ACN) and 1% formic acid (FA). The extracts were then dried in a Speedvac (~1 hr) and stored at 4^{o}C. On the day of analysis, the samples were reconstituted in 5-10 µl of solvent A (2.5% ACN, 0.1% FA). A nano-scale reverse-phase HPLC capillary column was created by packing 2.6 µm C18 spherical silica beads into a fused silica capillary (100 µm inner diameter x ~30 cm length) with a flame-drawn tip [[374]]. After equilibrating the column each sample was loaded via a Famos auto sampler (LC Packings, San Francisco CA) onto the column. A gradient was formed and peptides were eluted with increasing concentrations of solvent B (97.5% ACN, 0.1% FA). As peptides eluted they were subjected to electrospray ionization and then introduced into an LTQ Orbitrap Velos Pro ion-trap mass spectrometer (Thermo Fisher Scientific, Waltham, MA). Peptides were detected, isolated, and fragmented to produce a tandem mass spectrum of specific fragment ions for each peptide. Peptide sequences were determined by matching protein databases with the acquired fragmentation pattern by the software program, Sequest (Thermo Fisher Scientific, Waltham, MA) [[39]]. All databases include a reversed version of all the sequences and the data was filtered to between a one and two percent peptide false

discovery rate.

2.17. Live microscopy.

Cos7 cells were seeded in 35mm glass bottom No.1.5 uncoated dishes (MatTek) at 1 x 10^5 cells. The following day, cells were transfected with ~500ng of plasmid coding for Rtn4b-GFP-APEX2 expression for 16-18 hours and 1hour prior to *Legionella* challenge, the medium with transfection reagent was replaced with DMEM+10% FBS. For bacterial challenge, the transfected cells were placed on the stage of a Zeiss AxioObserver fitted with environmental and temperature controls set at 37^{o}C, 5% CO_2. After allowing 15 min equilibration, either the Lp02 mCherry or the Δ*sdeA-C* mCherry strain was introduced at MOI = 20. Imaging was initiated immediately on a single cell, using a 63X Plan Apochromat 1.40NA lens. Images were grabbed every ~15 s for 10 min using a Hamamatsu Orca-R2 CCD camera and Zeiss AxioVision software. These experiments were designed and performed by V. Ramabhadran (Former Isberg post-doctoral associate).

2.18. LC3 maturation during *L. pneumophila* infection.

BMDMs were plated in 24-well tissue culture treated dishes at 5 x 10^5 and allowed to adhere overnight. The next day, cell medium was exchanged with fresh RPMI containing 10% FBS and glutamine. Chloroquine (100μM, Caymen Chemicals) was added to cells 2 hrs prior to challenge with motile *L. pneumophila* at an MOI=2 and chloroquine remained in the media during infection. After 2 hrs of BMDM challenge with *L. pneumophila,* BMDMs were washed 3X with phosphate buffered saline (PBS) and then lysed in 50μl of reducing sample buffer, boiled, and fractionated with 15% SDS-PAGE followed by immunoblotting with α-LC3 (1:2000, Cell Signaling Technologies)

and α-Actin (1:1000, Sigma) with Li-Cor secondaries (donkey IRDye 680RD α-mouse, Goat IRDye 680RD α-rabbit, and/or donkey IRDye800CW α-mouse, goat IRDye800CW α-rabbit 1:20,000) and Odyssey CLX detection (LI-COR Biosciences). Cos7 cells were seeded in 6-well dishes at 8 x 10^5 cells per well the day prior to bacterial challenge. The next day, medium was replaced with DMEM with 10% FBS and chloroquine (100μM) 2 hrs prior to *L. pneumophila* challenge at an MOI=10 for 2 or 6 hrs. For the 6 hr incubation, after 2hrs of challenge, non-internalized bacteria were washed 3x with DMEM with 10% FBS and fresh DMEM with 10% FBS, then an chloroquine was added back to the cells for the remaining 4 hrs of incubation. At the completion of the 2 or 6 hr challenge, Cos7 cells were washed 2-3x with phosphate buffered saline (PBS), then lysed in 250μl reducing sample buffer and probed with α-LC3 and α-GAPDH (1:500-1000, Santa Cruz Biotechnology) for immunoblots.

2.19. Deubiquitinase assay post Sde modification of polyubiquitin.

His-tagged recombinant full length wild type SdeC, SdeC point mutants (C118S, H416A, E858A), or a no enzyme control were bound to Ni-NTA (Thermo HisPur™) resin at 1ug enzyme per 25μl of packed resin in 1X ART buffer for 1 hr at 4°C with end-over-end rotation. The SdeC-beads were washed 3X with 1X ART buffer to remove non-adsorbed enzyme with microcentrifuge spin filters spun at 3000 x RCF at room temperature. After the final wash, each 25μl of pelleted resin was resuspended with 2μg of recombinant human homotypic-linked polyubiquitin chains (2μg/300μl reaction Ub_{3-7} K63 or K48, Boston Biochem, R&D) and 500μM ε-NAD in 1X ART buffer for 2 hrs with end-over-end gentle rotation at 37°C. After incubation of SdeC and polyUb chains together, the SdeC-bound resin was removed with microcentrifuge spin column filters

and the polyUb reaction mixture was collected. This polyUb fraction was then incubated with either 1) 100nM human recombinant PolyHistidine-otubain 1, isoform 1 (Boston Biochem); 2) 50nM recombinant USP2 catalytic domain (CD) 259-605 (Boston Biochem); 3) 50nM recombinant PolyHistidine-CYLD (Boston Biochem); 4) 50nM recombinant SdeC DUB CD (1-192), or 50nM full length SdeC (1-1533) at 37°C in 20mM Tris 10mM NaCl, pH7.4, (1X ART buffer) for the indicated time. A fraction of the reaction was removed and terminated by the addition of reducing sample buffer to monitor DUB kinetics as needed. Samples were then heated to 50-55°C for 20-30min to avoid Ub chain aggregation, as per manufacturers instruction, and samples were fractionated by SDS-PAGE and analyzed by silver stain (SilverQuest, Invitrogen) or Western blots. Relative DUB activity was determined using Image Studio software (Li-Cor analysis package) after 2 hrs incubation, comparing the efficiency of cleavage of modified Ub relative to unmodified.

2.20. Autophagy adaptors binding of polyUb post Sde-mediated modification of Ub.

His-tagged recombinant full length wild type SdeC, SdeC point mutants (C118S, H416A, E858A), or a no enzyme control were adsorbed to Ni-NTA (Thermo His-Pur™) resin at 1ug enzyme per 25µl of packed resin in 1X ART buffer for 1 hr at 4°C with end-over-end rotation. SdeC conjugated resin was washed 3X with 1X ART buffer to remove non-conjugated enzyme with microcentrifuge spin filters centrifuged at 3000xg at room temperature. After the final SdeC resin wash, each 25µl pelleted resin was resuspended with 4µg of recombinant human homotypic-linked polyubiquitin chains Ub_{3-7} (K63 or K48, 4µg/600µl reaction volume, Boston Biochem, R&D) and 500µM ε-NAD in 1X ART buffer for 2 hrs with gentle end-over-end rotation at 37°C. During incubation of

SdeC and polyUb chains, recombinant autophagy adaptors (either 1µg of recombinant PolyHis-p62, recombinant PolyHis-optenurin, or recombinant PolyHis-Hmp cloned from *Yersinia pseduotuburculosis* and purified from *E. coli* BL21(DE3), kind gift of Connor Murphy, Isberg Lab) were adsorbed to 5µl pre-equilibrated packed Ni-NTA resin (Thermo His-Pur™) through 1 hr with end-over-end rotation at 4°C in low adhesion 1.5ml microcentrifuge tubes. PolyUb chains were then separated from SdeC by collection of SdeC resin in a microcentrifuge column spin filter and then the polyUb fraction was incubated with recombinant autophagy/control proteins on Ni-NTA resin for 1 hr at room temperature with end-over-end rotation. The resin was washed 3-5x with 50mM Tris 0.1% BSA (vol/vol) pH7.5 at room temperature, then resin having adsorbed proteins and bound polyUb chains were eluted from the Ni-NTA beads with 250mM imidazole diluted in 50mM Tris 0.1% BSA (vol/vol) pH7.5. Reducing sample buffer was then added to the elution, and samples were heated to 55°C for 20-30 min, fractionation by SDS-PAGE, and analyzed by immunoblot.

2.21. Sequential modification of Ub by Sde mART and NP domains.

His-tagged recombinant full length SdeC (20nM) was adsorbed to Ni-NTA resin (5µl packed resin) for 1hr at 4°C with end-over-end rotation in 1X ART buffer. After generation of SdeC resin, the beads were washed 4-6x with 500µl 1X ART buffer by centrifugation at 3000 x RCF at 4°C and the supernatant was removed with a 30G needle on a 1ml syringe. Next, SdeC resin was incubated with or without 100µM ε-NAD and 10µM recombinant Ub monomer (Boston Biochem). The mixture was incubated for 1 hr at 37°C with end-over-end rotation. The Ub and ε-NAD mixture was separated from SdeC resin by centrifugation at 3000 x RCF for 1min at 4°C, and then the reaction

supernatant was collected with a 30G needle and kept on ice through additional processing. The supernatant was centrifuged in a fresh pre-chilled low adhesion tube and the supernatant was once again collected into a fresh pre-chilled low adhesion tube to guarantee no residual Ni-NTA resin was passed through to the final collection tube. Finally, ~400-660nM recombinant human GST-HA-Rtn4b was added to the ubiquitin mixture and incubated at 37°C in a pre-warmed thermocycler for 1 hr. Reactions were terminated by the addition of reducing sample buffer, boiling, SDS-PAGE fractionation, and silver stain or immunoblot analysis.

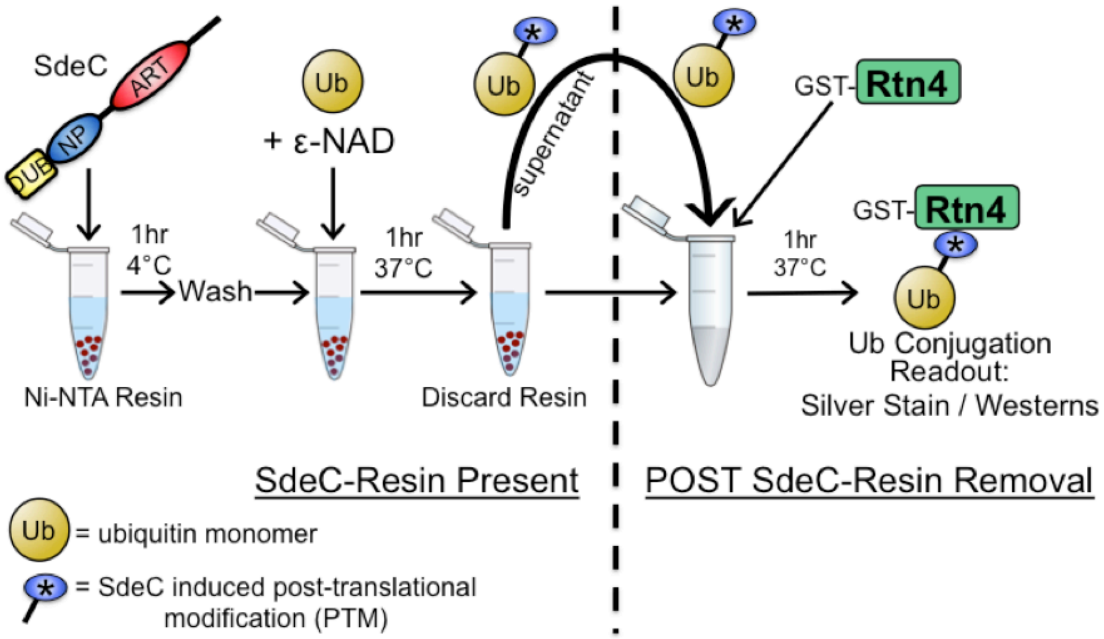

Figure 2.2. Cartoon schematic of process to assess sequential steps of SdeC mediated Rtn4-ubiquitination *in vitro*.
Recombinant full length SdeC (1-1533) or mutant full length point mutant SdeC (H416A or E858A) constructs are attached to Ni-NTA resin, then incubated with ε-NAD+ and ubiquitin monomer (yellow orb) to post-translationally modify ubiquitin (PTM is represented as a blue ball attached to Ub). After allowing time for Ub modification, SdeC resin is removed, and the post-translationally modified or native ubiquitin remains in the supernatant, which is transferred to a fresh eppendorf tube where recombinant GST-HA-Rtn4 is added to the supernatant. In some experiments fresh recombinant SdeC or SdeC point mutants were added at the point of GST-HA-Rtn4 addition (not shown in model above) to assess the utility of modified Ub as a SdeC substrate for conjugation to Rtn4. After the Ub supernatant fraction was allowed to react with GST-HA-Rtn4 for an hour at 37°C, the reaction was terminated with SDS sample buffer, then Rtn4 ubiquitination was

assessed by SDS-PAGE fractionation coupled with silver staining or immunoblot analysis.

2.22. Clearance of *L. pneumophila* from A/J mice after intranasal infection.

For single *L. pneumophila* strain infections, 2 groups of approximately 8-week-old male or female A/J mice (Jackson Laboratories, ME) were inoculated separately to assay the virulence of *ΔsidE ΔsdeC ΔsdeB-A pvector* compared to *ΔsidE ΔsdeC ΔsdeB-A psdeC$_{WT}$* strain. *L. pneumophila* strains were cultured overnight in a series of AYE dilutions to allow a motile, infectious, post-exponential population of each *L. pneumophila* mutant to be available for mouse inoculation. After determining the motility and A_{600}, each strain was washed 2x in sterile room temperature PBS and was diluted to generate a 20µl PBS *L. pneumophila* mixture with 2 x 10^4 CFU in total. Mice were anesthetized and *L. pneumophila* was inoculated intranasally (i.n.) by slowly pipetting a drop of inoculum onto one nostril and waiting for inhalation, then repeating slowly until the entire 20µl inoculum was taken down the nasal passage. At 4 hrs and 48 hrs post inoculation, mice were sacrificed; 1ml of sterile PBS was used to wash mice lungs, BAL (Bronchoalveolar lavage) fluid was collected, and plated for CFU. Serial dilutions of BAL fluid were plated onto both CYET and CYE agar plates to determine the number of viable bacteria and to confirm plasmid retention in bacteria colonizing the lung. Lung CFU were determined 72-96 hrs after plating. Kim Davis (Formerly of the Isberg Lab, currently at Johns Hopkins University) was responsible for the development and implementation of animal infections for the *L. pneumophila* pulmonary mouse model of infection. Enumeration of *L. pneumophila* CFUs from BAL fluid of *ΔsidE ΔsdeC ΔsdeB-A pvector* or *ΔsidE ΔsdeC ΔsdeB-A psdeC$_{WT}$* infected mouse lungs was carried out by K. Kotewicz. These infections, from Dec. 2016, offer preliminary results on the importance

of the SidE family during pulmonary mouse infections and would require significant numbers of additional animal infections to fully assess the virulence differences in a *ΔsidE* family infection, wild type infection, and *ΔsidE* family infection with *in trans* expression of individual SidE proteins. This experiment represents a single replicate with 5 mice per infecting strain per infection time point (4 vs. 48 hrs). A general schematic of the infection protocol is diagramed below in figure 2.2.

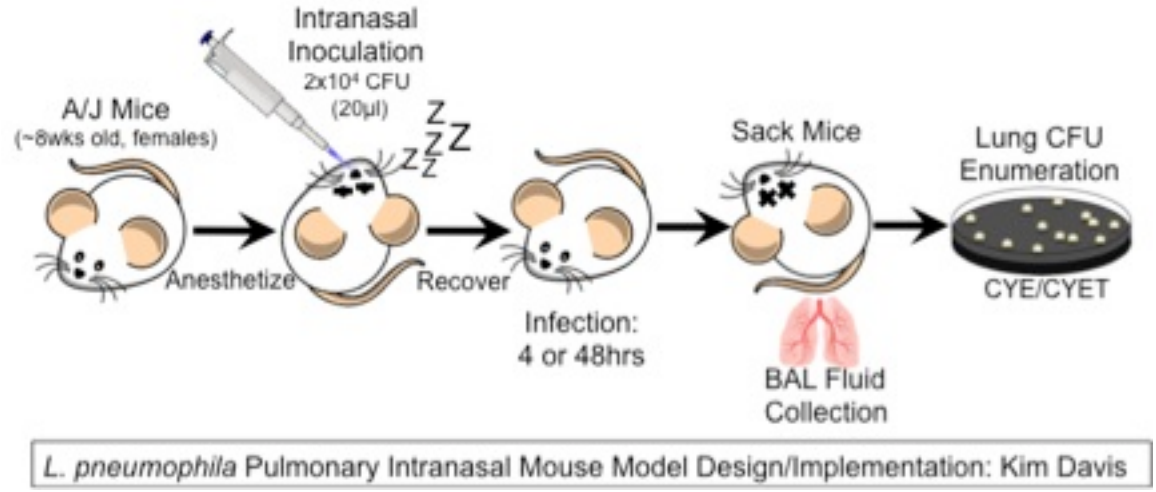

Figure 2.3. Cartoon representation of the protocol used to assess *L. pneumophila* virulence in a mouse pulmonary infection model (Designed by K. Davis).
To assess the importance of the SidE family during a mouse pulmonary model of infection, A/J mice were anesthetized and intranasally (i.n.) inoculated with 2 x 10^4 *L. pneumophila* in PBS containing either *ΔsidE ΔsdeC ΔsdeB-A pvector* (KK099) or *ΔsidE ΔsdeC ΔsdeB-A psdeC*$_{WT}$ (KK099 pSdeC$_{WT}$). The infection groups were housed separately after inoculation and After 4 or 48 hrs, mice were killed, BAL fluid was collected, and plated on CYE and CYET plates for CFU enumeration from the lungs.

Chapter 3:

Sde proteins are a family of *Legionella* IDTS that ubiquitinate and reorganize the tubular endoplasmic reticulum.

This chapter contains excerpts that have previously been published in:
(reprinted with permission of publisher)

Kotewicz KM, Ramabhadran V, Sjoblom N, Vogel JP, Haenssler E, Zhang M, Behringer J, Scheck RA, Isberg RR. Cell Host Microbe. 2017 Feb 8; 21(2):169-181. Epub 2016 Dec 29.

3.1. Targeted transfection screen of *L. pneumophila* T4SS substrate protein(s) reveals Sde proteins promote Rtn4 reorganization.

The intracellular pathogen *Legionella pneumophila* generates a host-derived vacuolar compartment that supports bacterial replication within a cell. This intracellular niche ultimately resembles the rough endoplasmic reticulum, but the purpose and mechanisms underlying the vacuole transformation to an ER-like compartment remain focus of intense study in the *Legionella* field. Although the *Legionella* containing vacuole (LCV) resembles rough ER hours after phagocytosis, the peripheral tubular ER network is perfectly situated to immediately interact with an incoming intracellular pathogen. In many cases tubular ER would likely be the second structure an incoming intracellular pathogen would encounter, after the plasma membrane, since extensive regions of the plasma membrane remain in close association with tubular ER, particularly during phagocytosis[351,379,561]. Early evidence for this line of reasoning within the *Legionella* field arose from a study showing that the *L. pneumophila* T4SS substrate Ceg9 forms a tripartite complex with atlastin-1 and Rtn4 isoforms, Rtn4b/Rtn4d (Figure 1.18.)[172]. Infection with *L. pneumophila* was observed to produced an aberrant accumulation of detergent resistant Rtn4 at the LCV, dependent on a functional T4SS (Figure 1.X)[172,260]. To decipher which of the *L. pneumophila* T4SS substrate(s) was responsible for altering Rtn4, we employed our ability to detect the detergent resistant Rtn4 from immunoblots of infection extract by challenging HeLa cells with different *L. pneumophila* mutants. Cells were challenged for 2 hrs with either *L. pneumophila* lacking Ceg9, a T4SS substrate previously shown to interact with Rtn4[172], a minimalized *L. pneumophila* strain lacking 12.7% of the genome (*Δpent*)[354], WT *Legionella*, or a T4SS defective strain, *dotA3*. Infected cell extracts from both *Δceg9* and *Δpent* strain challenge resulted in a HMW

Rtn4 species similar to a WT infection (Figure 3.1. WT, *Δpent*, *Δceg9*) Consistent with previous observations, a *dotA3* infection did not alter Rtn4 and the immunoblot mimicked an uninfected cell extract (Figure 3.1. *dotA3*, Un).

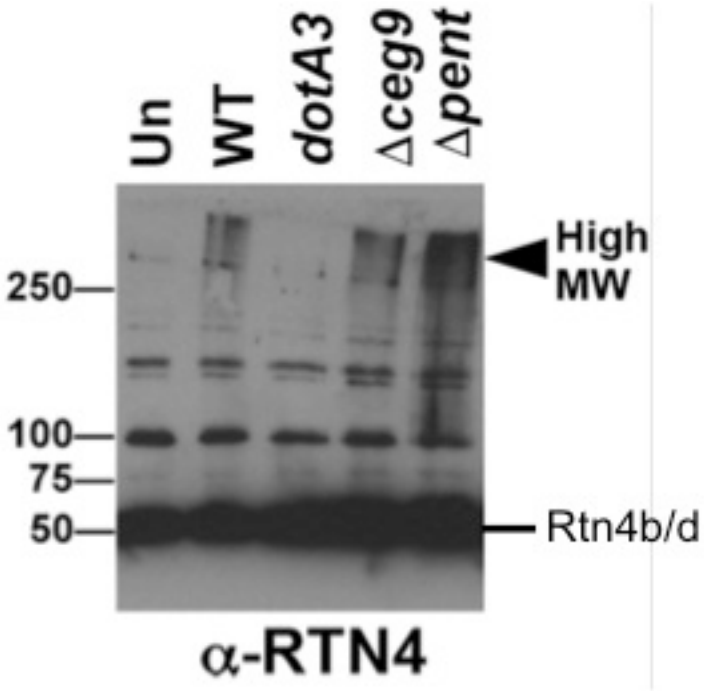

Figure 3.1. Rtn4 HMW species forms independently of Ceg9 and still develops in an effector minimalized mutant, *Δpentuple* strain.
Experiments performed by Eva Haenssler[260]
Altered electrophoretic migration of Rtn4 after *L. pneumophila* challenge, indicated by black arrowhead and High MW label. HeLa cells were challenged for 2 h, solubilized in SDS at room temperature, fractionated by SDS-PAGE, and probed with α-Rtn4. Rtn4b/d monomers are the prominent bands at 50kDa, Rtn4 dimers are present at 100kDa, and higher order oligomers such as tetramers can be observed at 200kDa and above. Lanes: Un, uninfected; WT, Lp02; *dotA3*, *icm/dot*⁻ or T4SS defective; *Δceg9*, Ceg9 deletion strain; *Δpent*, pentuple deletion strain[354].

From these results, we designed a targeted transfection screen to assay the effect of individual *L. pneumophila* proteins on Rtn4, by selectively screening gene candidates located outside the *Δpent* deletion regions. Plasmids encoding individual GFP-tagged *L. pneumophila* T4SS substrates were transiently transfected into mammalian cells for 40-46 hrs, then cell extracts were fractionated by SDS-PAGE and probed with α-Rtn4

(Figure. 3.2. A). Of the >60 *L. pneumophila* substrates examined (Table 2.5), three members of the Sde family, SdeC, SdeB, and SdeA, generated an HMW Rtn4 species. In addition, a modified form of Rtn4 that migrated just above the abundant Rtn4b/d monomers (~50kDa) was observed (Figure 3.2.A; modified). Interestingly, transient expression of two additional SidE family homologues, *sidE* (*lpg0234*) and *sdeD* (*lpg2509*), was unable to induce the transformation of Rtn4. These three large *L. pneumophila* T4SS substrates that were capable of targeting Rtn4 are organized in a contiguous locus with *lpg2154* and *sidJ*, a known antagonist/regulator of SidE family function (Figure 3.2. B).

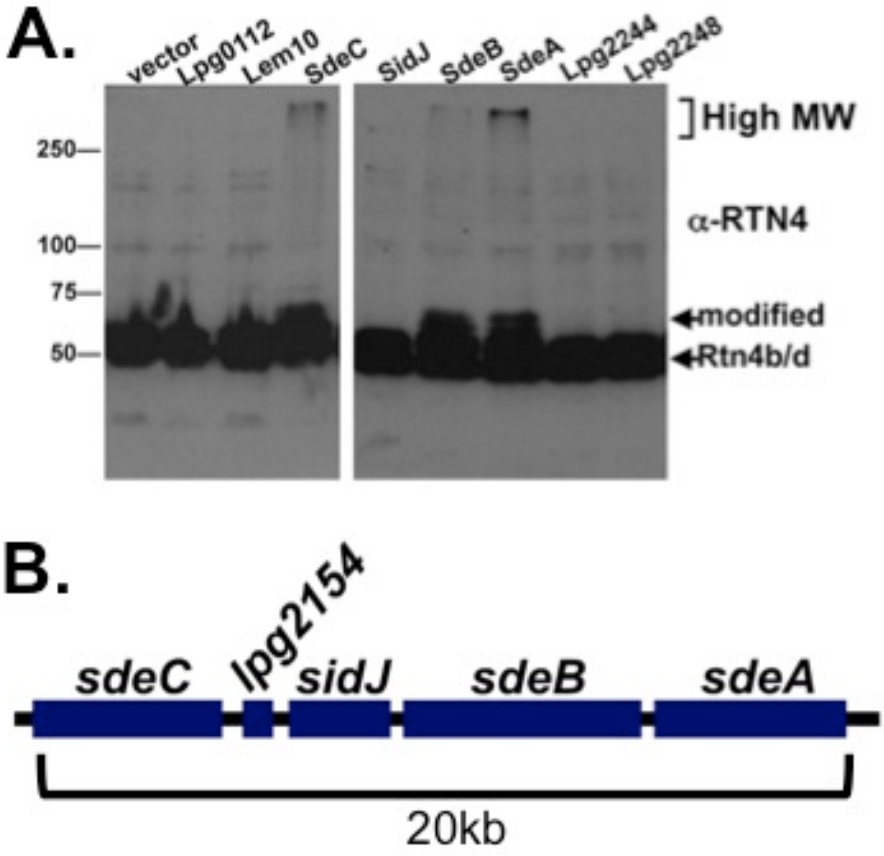

Figure 3.2. Three *Legionella* homologues from the SidE family are individually capable of altering electrophoretic migration of Rtn4 during transient overexpression.

(A) Sde family members result in Rtn4 electrophoretic variants after transient transfection into mammalian cells. Cos1 cells were transfected for 40-46 hrs with plasmids expressing GFP fusions to the indicated *L. pneumophila* T4SS substrates, then cells were extracted, gel fractionated and blots probed with α-Rtn4. **(B)** The chromosomal arrangement of the *sde* genes in a 20kb operon-like structure with antagonist/regulator *sidJ* (*lpg2155*).

3.2. SdeA, SdeB, SdeC are each independently responsible for Rtn4 transformation during *L. pneumophila* infection.

To determine if *L. pneumophila* lacking the *sde* family was capable of inducing colocalization of detergent-resistant Rtn4, BMDMs were challenged for 1 h with *L. pneumophila* and analyzed by immunofluorescence microscopy (Figure 3.3. A-C). More than 70% of wild type (Lp02) LCVs were associated with Rtn4, while no colocalization was observed with *dotA3* (Lp03) vacuoles (Figure 3.3. A-C). Both a complete *sde* family deletion (*Δsde*, KK099, *ΔsdeC ΔsdeB-A ΔsidE*; Table 2.1)[232] and a *sde* locus deletion (*ΔsdeC-A*, KK034; Table 2.1) were unable to induce Rtn4 association with the LCV (Figure. 3.3. A,B). Comparison of the results between these two different genetic backgrounds indicates the ER-LCV association was independent of other *sidE* family homologues still present in the genome, including *sidE* (*lpg0234*) and *sdeD* (*lpg2509*). Furthermore, the Rtn4 transformation did not require other *sde* locus genes, including *lpg2154* and *sidJ* (*lpg2155*). Expression of plasmid-encoded SdeC or SdeB was able to completely restore Rtn4-LCV association to WT levels in either *sde* deletion background, while there was partial restoration with expression of SdeA (Figure 3.3. A-C).

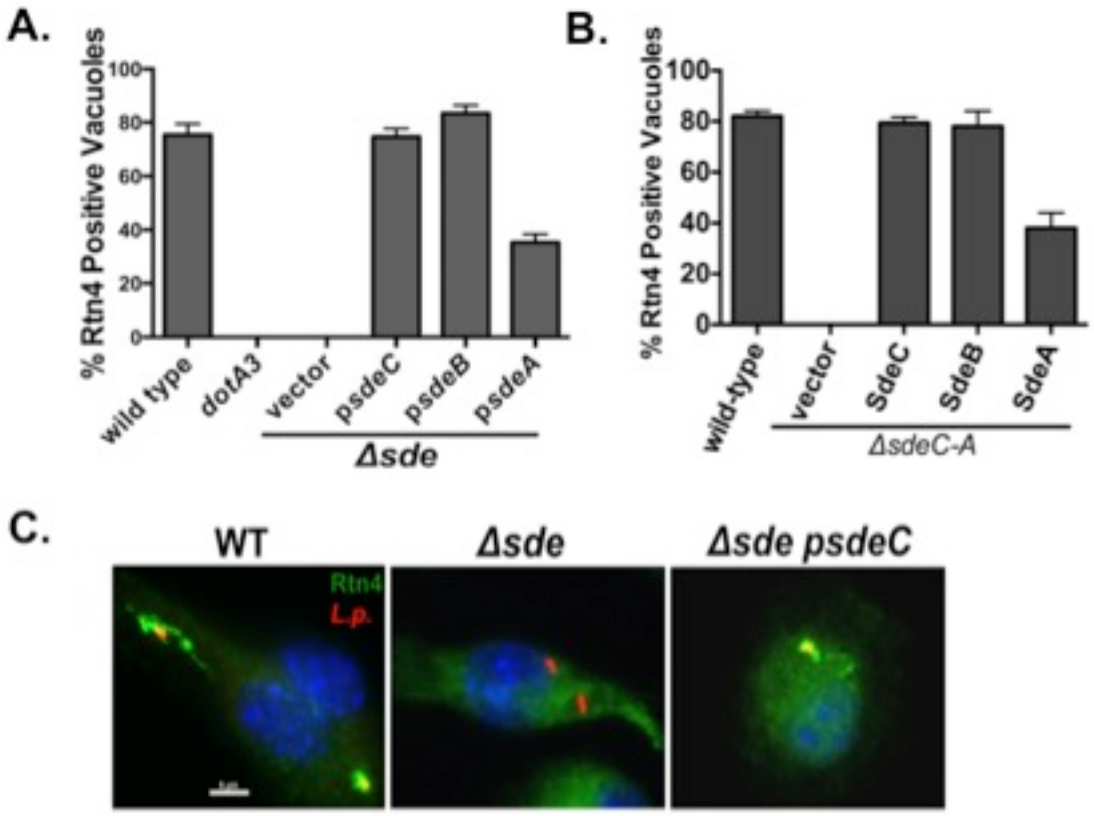

Figure 3.3. Sde proteins are responsible for Rtn4 reorganization during infection. **(A,B)** BMDMs from A/J mice were challenged at an MOI =1 for 1 hr with denoted *L. pneumophila* strain, followed by fixation, permeabilization with 1% Triton X100 and probing with α-Rtn4 (green), α-*L. pneumophila* (red), and Hoechst (blue) for nuclear DNA staining. LCVs associated with Rtn4 signal above background were considered positive, represents at least three independent experiments with 50 LCV/coverslip counted with 3 coverslips per condition evaluated. Wild type, Lp02; *dotA3,* T4SS defective or an *icm*/*dot*-; *Δsde*, *ΔsidE ΔsdeC ΔsdeB-A* or *Δlpg0234 Δlpg2153 Δlpg2156-2157* (KK099); *ΔsdeC-A*, *Δlpg2153-2157* (KK034). **(C)** Representative immunofluorescent micrographs of BMDMs infected with noted *L. pneumophila* strain. Deletion of *sde* family (KK099) prevents Rtn4 rearrangements about the LCV, which can be complemented by expression of individual Sde proteins. Scale bar: 5μm.

3.3. Live microscopy of Rtn4b-GFP during *L. pneumophila* infection reveals rapid Rtn4 nucleation outward from LCV.

The prior immunofluorescence microscopy studies of Rtn4 at the LCV provide static images of the relationship between these two highly dynamic structures[172,260]. The interpretation of these images typically occurs in the absence of the native tubular ER network, due to paraformaldehyde fixation followed by detergent extraction of membrane. This limits the amount of information we could acquire on the dynamics of Rtn4 at the LCV and the interactions between the transformed Rtn4 with the peripheral ER network. To address these experimental blind spots, we surveyed the dynamics of Rtn4-LCV association in real-time. Cos7 cells were transfected with Rtn4b-GFP, then challenged with WT *L. pneumophila* or *Δsde* (KK034 pvector) strains expressing mCherry and monitored over a 10 min period (Figure 3.4. A,B). The Rtn4b-GFP signal illustrates a high-resolution outline of the ER network, which strongly contrasts with the poor resolution of endogenous Rtn4 in prior micrographs after concentrated detergent extraction (Figure 1.18.B. and 3.3.C). In response to the WT infection, an Rtn4 signal intensified around the vacuole membrane, enveloping the entirety of the LCV. Then the Rtn4 signal dramatically nucleated outward from the LCV in several directions in Rtn4-rich tubular protrusions. These intense Rtn4 projections were observed branching, some of which formed junctions with other Rtn4 protrusions (Figure 3.4. A). The protrusions appeared to both move along existing ER tubule pathways, as well as forge novel ER tubule extensions and new connections with the existing ER network. In a *Δsde* challenge, there was no observable change in Rtn4 localization or intensity (Figure 3.4. B).

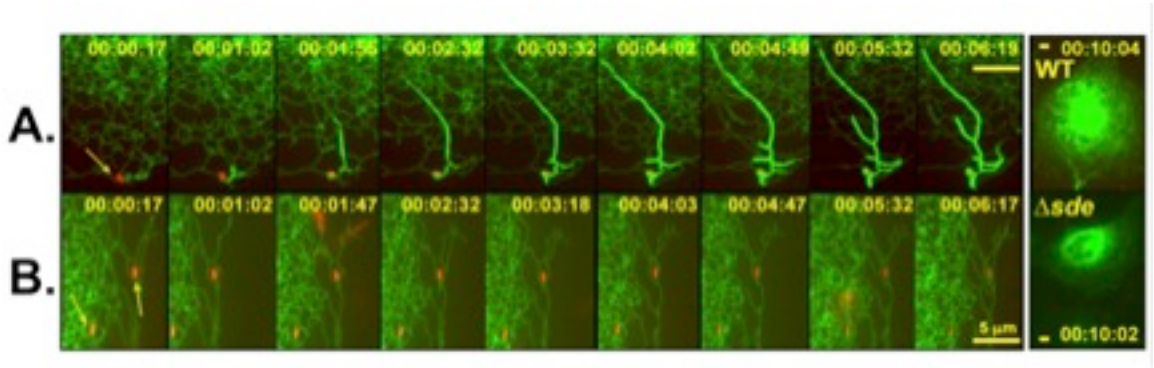

Figure 3.4. Sde family members promote immediate Rtn4 rearrangements after host cell contact.

Experiments performed by Vinay Ramabhadran[260]

Cos7 cells, which were transiently transfected to express Rtn4b-GFP, were challenged with **(A)** wild type (WT, Lp02 pmcherry) *L. pneumophila* or **(B)** *Δsde* (*ΔsdeC-A*, KK034 pmcherry) and images from live cells were captured over a 10 min period. Scale bar: 5µm. Images displayed at 1.15X the captured sizes.

3.4. Sde-dependent ER rearrangements result in distinct morphological changes.

To further resolve the transformation of tubular ER during *L. pneumophila* infection, we devised a method for high resolution probing of Sde-mediated ER structural changes. First, an Rtn4b-APEX2-GFP fusion protein was generated (V. Ramabhadran and J. Berhinger, Figure 3.5), where GFP served as a marker for transfected cells. The APEX2 fusion allows Rtn4 localization to be determined by coupling the protein of interest to an engineered peroxidase reporter, which can be detected by transmission electron microscopy (TEM) after addition of the substrate diaminobenzidine (DAB). This peroxidase reaction precipitates fusion proteins in place to generate an electron dense signal providing sub-organelle resolution of the fusion protein localization[81,273,279,306]. Cos7 cells were transiently transfected with an Rtn4b-APEX2-GFP fusion then challenged with the WT or *Δsde* strains expressing mCherry for 1 h, and analyzed for deposition of DAB by microscopy. Bright-field microscopy revealed strong DAB depositions associated with WT LCVs, mimicking the Rtn4b structures previously observed by fluorescence microscopy (K. Kotewicz, M. Zhang, and J. Behringer, (Figure 3.5).

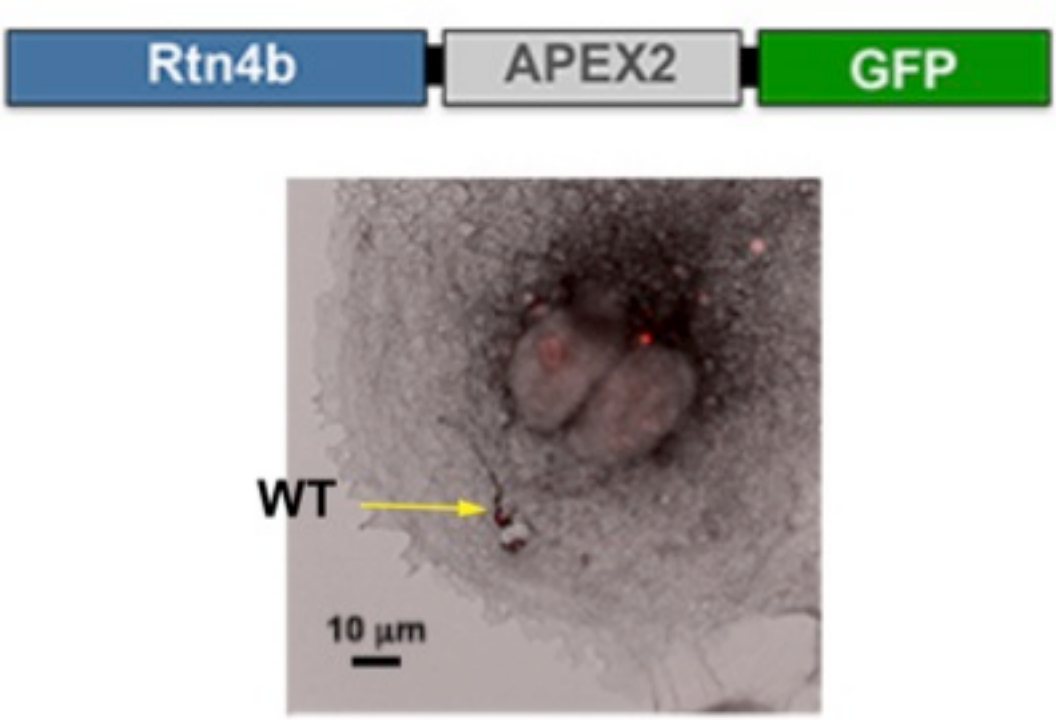

Figure 3.5. Rtn4b-APEX2-GFP accumulation and deposition at WT *L. pneumophila* LCVs.
(Top) Map of the Rtn4b-APEX2-GFP construct. **(Bottom)** DAB deposition mimics topology of Rtn4 rearrangements in response to *L. pneumophila*. Cos7 cells harboring Rtn4b-APEX2-GFP were challenged with wild type (WT) *L. pneumophila* (pmCherry) for 1 hr, then fixed, subject DAB precipitation. Yellow arrow indicates the site of *L. pneumophila* (red) with localized DAB deposition mimicking patterns observed with immunofluorescence microscopy. Scale bar: 10µm. Special thanks to Jess Behringer for the image acquired during her rotation through the lab.

One hour after infection, TEM images of WT LCVs revealed vesicle-mimicking structures (termed pseudovesicles) with dense DAB deposition about their surface in close proximity to the vacuole (Figure 3.6. A-C, red arrows). Furthermore, DAB-rich depositions formed numerous projections extending out perpendicularly from the cytoplasmic face of pseudovesicles often towards the surface of other pseudovesicles (Figure. 3.6. A,C,D, white arrow heads). These bridge-like structures were reminiscent of the proteinacious bridges observed between tubular ER and mitochondria at membrane contact sites[95]. LCV membranes adjacent to the WT were darkly stained by DAB

depositions, indicating high levels of Rtn4 contiguous with the vacuole membrane (Figure. 3.6. A). In contrast, vacuole membranes encompassing the *Δsde* mutant had little evidence of either pseudovesicles or DAB staining (Figure. 3.6. E-G). To determine if the pseudovesicular structures observed were specific to the presence of the fusion protein, TEM of bone marrow-derived macrophages (BMDMs) challenged with WT *L. pneumophila* was performed (V. Ramabhadran). Analogous pseudovesicular structures, as well as linear projections from these structures were observed surrounding the LCV (Figure 3.7. A-E). There is strong precedence for this observation, as pseudovesicular structures occurring immediately after infection have been observed numerous times in the literature (Table 3.1). There were no pseudovesicular structures in BMDMs challenged for 1 h with *L. pneumophila* mutants lacking *sde* (Figure 3.8. A-I). Instead, the LCV was associated with long membranous ribosome-rich structures that resembled irregularly stacked rough ER sheets, indicating premature association of rough ER with the LCV (Figure 3.8. A,B,D,E,G,H,I). Rough ER association with the LCV during the earliest phase of infection has rarely, if ever, been observed in the literature (Table 3.1.), and was only occasionally observed in micrographs of cells challenged with WT (Figure 3.7. D).

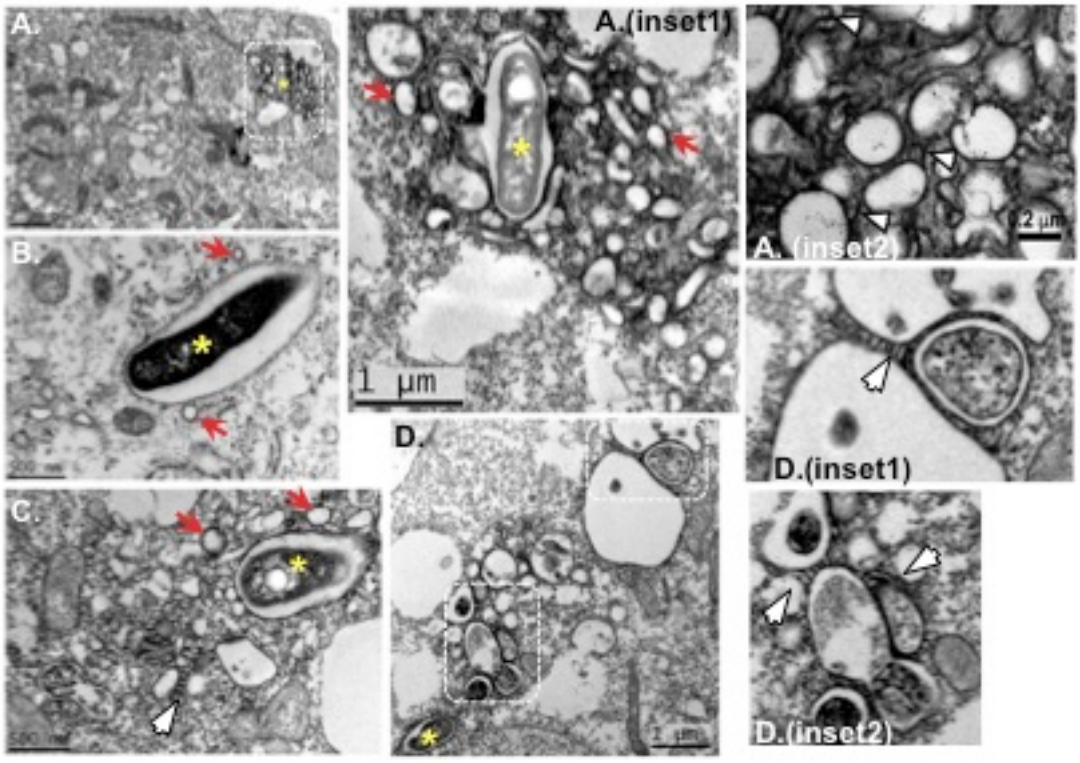
A.
A.(inset1)
A. (inset2)
2 µm
B.
1 µm
D.
D.(inset1)
C.
D.(inset2)

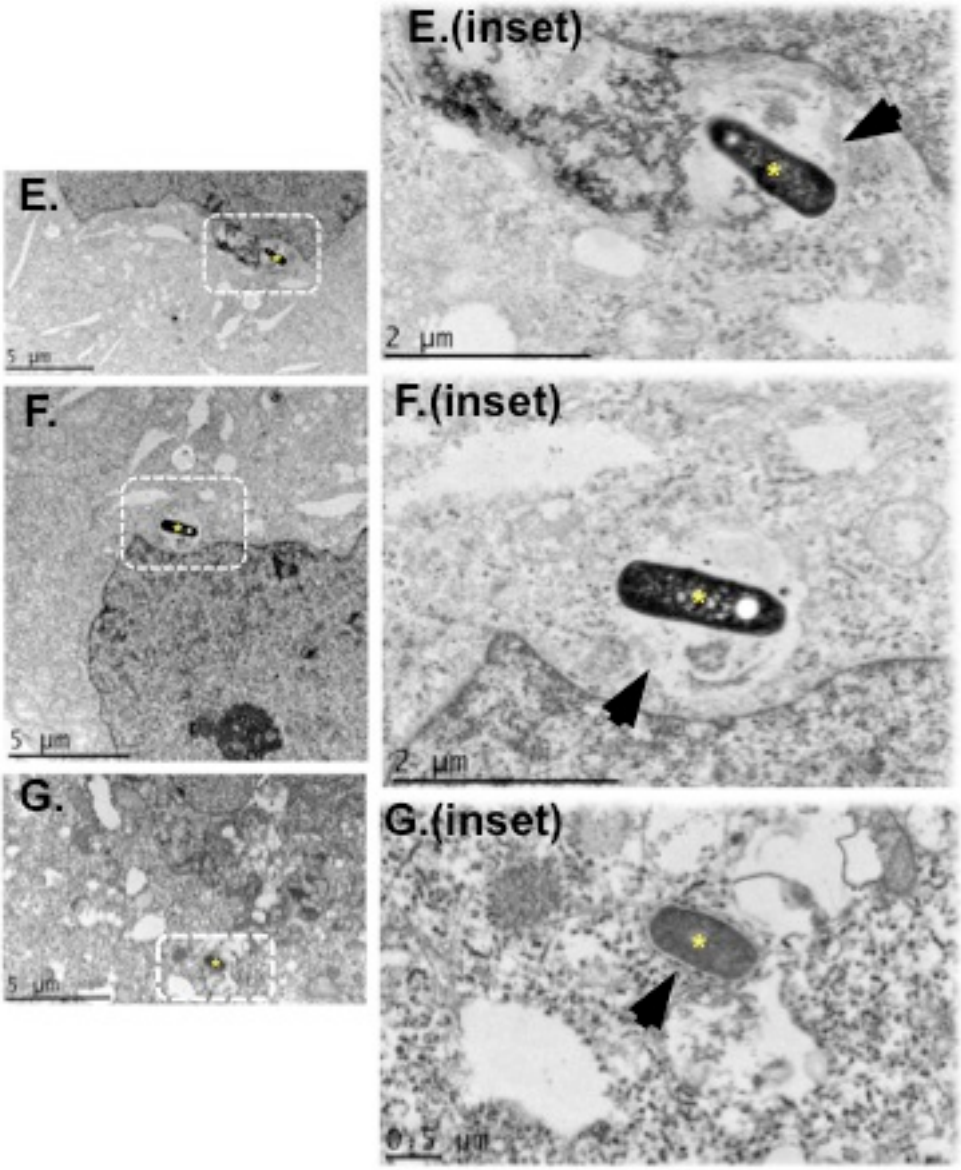

Figure 3.6. TEM of *L. pneumophila* infection of Cos7 cells with Rtn4b-APEX2-GFP reveals Rtn4 rich 'pseudovesicles' and proteinacious bridges linking them dependent on Sde family.

Sde-dependent ER rearrangements generate Rtn4-staining pseudovesicles or linear stacks. **(A-G)** Cos7 cells harboring Rtn4b-GFP-APEX2 challenged for 1 h with either LP02 **(A-D)** WT or **(E-G)** the Δ*sde* strain (KK099), subjected to DAB staining followed by TEM. **(A(inset1/2)** are TEM images of different sections from the same cell. Panels **(A/D inset)** are a high magnification image of Rtn4-rich region abutting a bacterium that can be seen in panel A/D. **(E-G)** Δ*sde* strain results in poorly defined LCV membrane, note absence of Rtn4 staining and 'pseudovesicles'. Inset regions are highlighted with white dashed box, yellow stars indicate location of bacterium, red arrows indicate Rtn4-rich 'pseudovesicles', white arrowheads indicate membrane projections or proteinacious bridges, black arrowheads point to weakly defined membranes in direct apposition to the LCV.

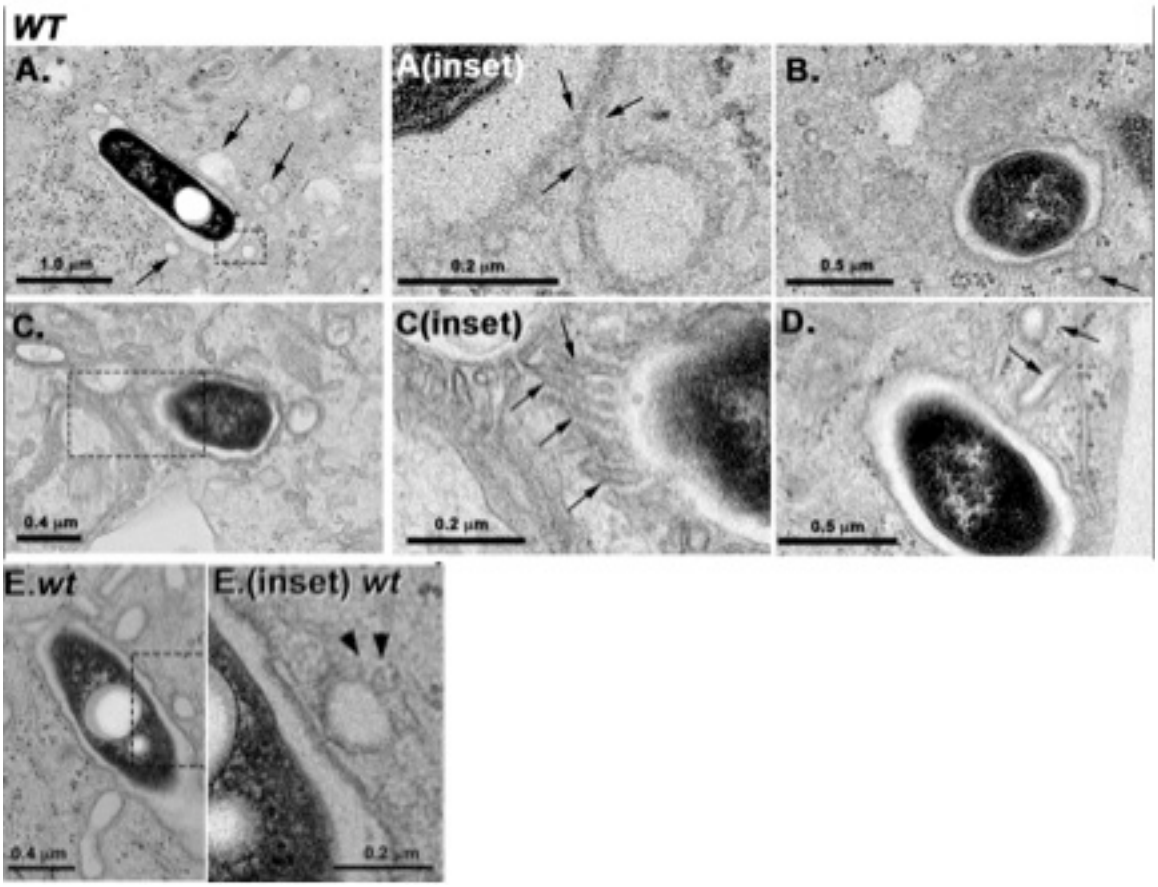

Figure 3.7. TEM of WT *L. pneumophila* infected BMDMs reveal Rtn4 rich 'pseudovesicles' and membrane stacks that accumulate at the LCV.

Shown are transmission electron micrographs of BMDMs from the A/J mouse challenged for one hour with Lp02 (WT) strain. **(A,B)** Arrows point to pseudovesicles, with boxed area noting region in interest displayed in next panel. **(A(inset))** Region of interest noted in panel A. Arrows point to projections from pseduovesicle to LCV. Dashed boxes are displayed to show regions displayed in partner images at different magnifications. **(C)** Prominent stacks emanating from LCV. Boxed area refers to region on interest displayed in next panel. **(C(inset)).** Region of interest from panel C. Arrows point to stacks of membranous compartments extending from LCV. **(D)** Pseduovesicles noted by arrows. Image shows apparent rough ER sheet recruitment at early infection time points. **(E)** BMDM challenged for 1 h with LP02 (WT). **(E(inset))** Boxed area at higher magnification. Arrowhead points to projections from round structure.

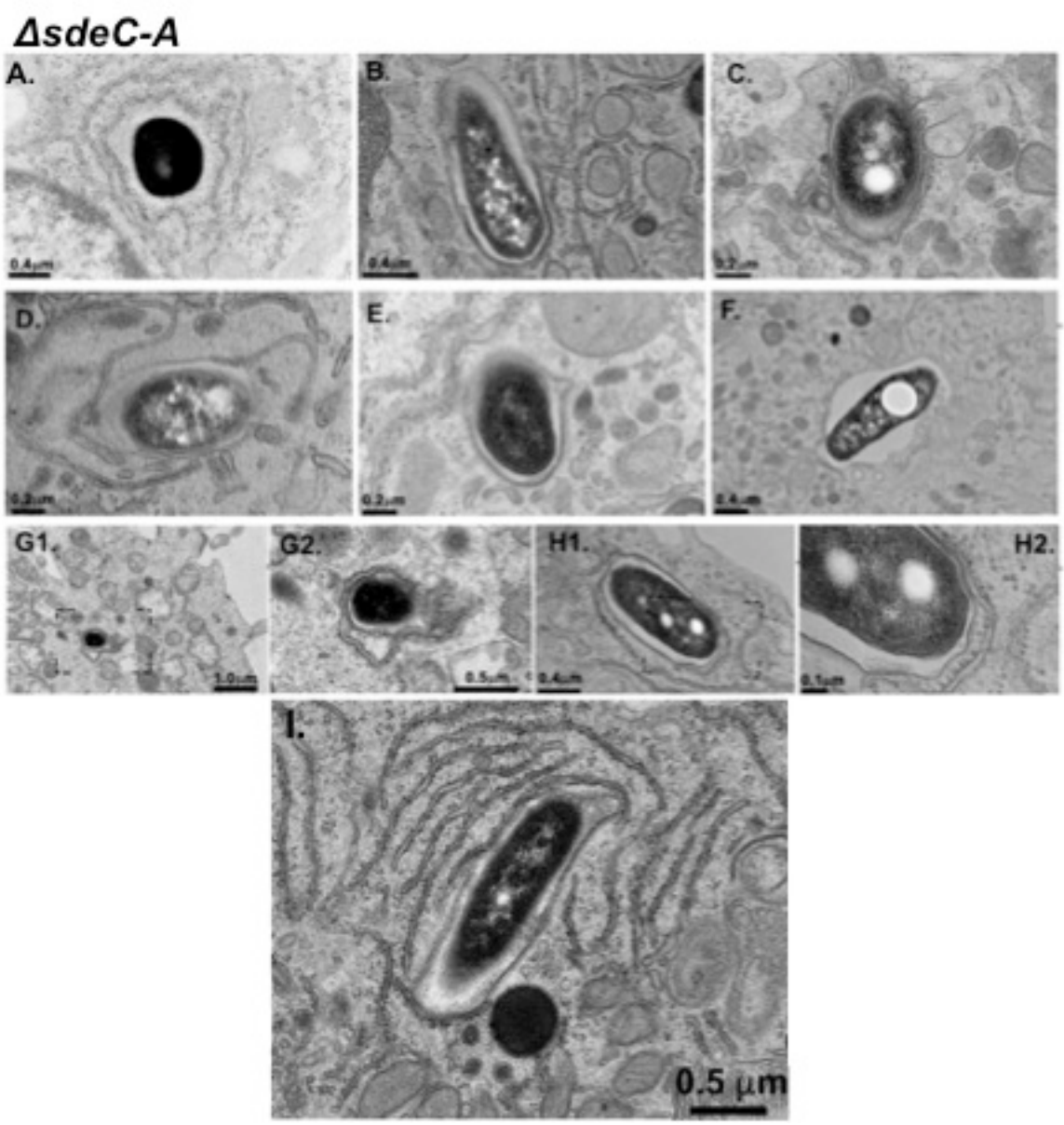

Figure 3.8. TEM of *ΔsdeC-A* infected BMDMs results in premature ER sheet association with the LCV.

Experiments performed by Vinay Ramabhadran[260]

Lack of pseudovesicle and accumulation of endoplasmic reticulum sheets surrounding LCVs of *Δsde or ΔsdeC-A* mutants. **(A-F)** Shown are transmission electron micrographs of bone marrow derived macrophages from the A/J mouse challenged for one hours with *L. pneumophila* mutants lacking the Sde family. Macrophages challenged with *sde* mutants **(A)** KK099, clean *sidE* family deletion or **(B-I)** KK034, *sde* locus deletion *ΔsdeC-A* strain. Note long ribosome-studded membranes (ER sheets) and lack of pseudovesicles.

Table 3.1. Survey of published electron micrographs that analyze *L. pneumophila* intracellular replication.

Compiled by Ralph Isberg[260]

Organism	FIGURES				Host Cells	Ref
Legionella pneumophila	Fig. 1C: 2.5 hpi. Large number of round structures ("vacuoles") (100+nm) surround replication compartment. Appears very similar to Rtn4-APEXII stain.	Fig. 1E: 8 hpi. See rough ER.	Fig. 3: 5 hpi. See Bip (ER marker) in large "Vacuole."		Hartmannella vermiformis	(Abu Kwaik, 1996)
Legionella pneumophila	All in presence of cycloheximide. Fig. 1A: flattened round vacuoles tightly associated. Fig. 1C: 4 hpi. Ribosomes, ER. Fig. 1D: 6 hpi. See round structures (100-400 nm.) Fig. 1E: 8 hpi. Numerous round structures.	Fig. 2B: 8 hpi. Rough ER.			U937 cells	(Abu Kwaik, 1998)
Legionella pneumophila	Fig. S1: WT. 6 hpi. Multiple large vacuolar structures associated with bacterial vacuole.				*A. polyphaga*	(Al-Khodor et al., 2008)
Legionella pneumophila	Fig. 3: TEM shows images of large number of bacteria in cells. Associated compartments cannot be evaluated.				U937 cells	(Alli et al., 2000)
Legionella pneumophila	Fig. 3: 4 hpi. Clear view of large vacuoles near replication vacuole.	Other figures, all later time points (16- 24 hpi) showing filled up amoebae.			Acanthamoeba palestinensis	(Anand et al., 1983)
Legionella pneumophila	Fig. 8: Round 200 nm "vacuoles" with thickened membrane.	Other figs: too many bacteria to interpret.			Guinea Pig pulmonary macrophages	(Baskerville et al., 1983)
Legionella pneumophila	Fig. 2: 6 hpi. Multi-bacterial compartments surrounded by rough ER.	Fig. 7: 6 hpi. Multi-bacterial vacuoles surrounded by rough ER, with evidence of quashed "vacuole" next to replication compartment.			U937 Cells	(Berger and Isberg, 1993)
Legionella pneumophila	Fig. 3A: 6 hpi. Squished electron dense "vacuoles" associated with bacterial compartment.				U937 Cells	(Berger et al., 1994)
Legionella pneumophila Legionella longbeachae	Fig 4: TEM of extracellular bacterium.				Extracellular only	(Cazalet et al., 2010)
Legionella pneumophila	Fig. 1: Single bacterium. No apparent structures associated.				HeLa cells	(Daisy et al., 1981)
Legionella pneumophila	Fig. 3: 36 hrs co-culture show cells with serpentine ER around replication compartments. >10 bugs/cell				*Acanthamoeba castellani*	(Dey et al., 2009)
Legionella pneumophila Escherichia coli Staphylococcus aureus	Fig. 1B: 24 hpi. Large numbers of bacteria.				Guinea pig alveolar macrophages	(Elliott and Winn, 1986)

Legionella pneumophila	Fig. 1: a: appears to be ribosomes around vacuole, 4 hpi (difficult to resolve)	Fig. 6: a, b: Appears to be "Vacuoles" around replication compartment 4 hpi (difficult to resolve)	Fig. 7: a(U937), appears to be "Vacuoles" around replication compartment. b(WI-26): appears to be RER around replication compartment 4 hpi (difficult to resolve)		WI-26 human type I alveolar epithelial cells and U937	(Gao et al., 1998)
Legionella pneumophila	Fig. 2A: 21 hpi. See single bug vacuole (reinfection?) with multiple large vacuoles surrounding it. 2D: 45 hpi. See ER whorls.				HeLa cells	(Garduno et al., 1998)
Legionella pneumophila Legionella longbeachae	Fig. 1A: 5 hpi. Replication compartments associated with large vacuoles. Fig. 1B: 24 hpi. Replication compartment associated with rough ER, ribosomes.				MM6 macrophage-like cell line	(Gerhardt et al., 2000)
Legionella pneumophila	Fig 3a: 3 hpi. Large thick membraned compartments associate with replication compartment. Fig. 3c: 24 hpi. Ribosomes associated with compartment.				HeLa cells	(Goldoni et al., 1995)
Legionella pneumophila	Fig. 5: In presence of cytocholasin; not scored.				HeLa cells	(Goldoni et al., 1998)
Legionella pneumophila	48 hr infections? Fig. 1C: See solo bacterium in vacuole with associated large vesicles.				*Hartmannella vermiformis*	(Greub and Raoult, 2003)
Legionella pneumophila	Fig. 8: Six day infection of *C. elegans*. See intestinal cells with internal bacteria and multiple vesicle associated. Unclear if vesicles near replication compartment induced by bacteria or in uninfected as well.				*C. elegans*	(Hellinga et al., 2015)
Legionella pneumophila	Fig. 5: 48 hpi. Stretched out "vacuoles' about 300+ nm in length.				A. castellanii	(Holden et al., 1984)
Legionella pneumophila Streptococcus pneumonia E. coli Pseudomonas aeruginosa Pseudomonas alcaligenes Neisseria gonorrhoeae Neisseria meningitidis	Fig. 1G: 3.5 min pi. 100 nm + "vacuoles" associated with compartment with monocytes. Coiling phagocytosis.	Other figures: very early time points, as well as analysis of E. coli and antibody-coated bacteria.			monocytes, alveolar macs, neutrophils	(Horwitz, 1984)
Legionella pneumophila	Fig. 3A: 1 hpi. Stretched out vesicles and vacuoles. Fig. 3B: 1 hpi. Large vesicles, mitochondria. Fig. 3C: 6 hpi. Ribosomes accumulate.	Fig. 4A: 1 hpi. Large vesicles, spikes coming from replication vacuole. 4B: 6 hpi. Lined by ribosomes.				(Horwitz, 1987)
Legionella pneumophila	Fig. 8B: 2 days pi. Ribosome studded replication compartment. 10 nm 'Filaments."				Human Monocytes	(Horwitz and Silverstein, 1980)

Legionella pneumophila Escherichia coli	Fig. 1A: 30 min. pi. Large smooth vesicles in human PMN.				Human polymorphs	(Horwitz and Silverstein, 1981)
Legionella Pseudomonas Mycobacterium Chlamydia	Fig. 4C: *Legionella* micrograph difficult to interpret.				Acanthamoeba keratitis	(Iovieno et al., 2010)
Legionella pneumophila Escherichia coli	Fig 5a: 1 hpi. Difficult to discern morphology. Fig 5B: 48 hpi. Large replication vacuoles.				Pigtail monkey alveolar macrophages	(Jacobs et al., 1984)
Legionella pneumophila	Figs. 2 and 4: Guinea pig lung infections, 3 days pi, macrophages show ribosomes surrounding replication vacuole.				Guinea pig lungs, macrophages and neutrophils	(Katz and Hashemi, 1983)
Legionella pneumophila	3 hour infection; Fig. 8: larger numbers of bacteria in a single vacuole				Tetrahymena thermophila	(Kikuhara et al., 1994)
Legionella pneumophila Hartmannella vermiformis	3 day co-culture; Fig.2: Multi-bacterial vacuoles.				*Hartmannella vermiformis*	(King et al., 1991)
Legionella pneumophila	48 hpi?: Fig. 2: Large numbers of bacteria. Rough ER.				A/J mouse peritoneal macrophages.	(Klein et al., 1991)
Legionella pneumophila Dictyostelium discoideum	Fig. 7: 6 hpi. Large spacious vacuole with nearby vesicle.				*D. discoideum*	(Li et al., 2005)
Legionella dumoffii Legionella pneumophila	*L. dumoffi,* only. Fig. 2B: 3 hpi. See round Vesicle (ER-like double membrane), rough ER. Fig 1C: 6 hpi. Clear rough ER and clusters of large vesicles: Figs 2D,E: 12 hpi. Ribosome studded and rough ER as well as persistent vacuole.				Vero cells	(Maruta et al., 1998a)
Legionella dumoffii Legionella pneumophila	dumoffi only				Alveolar epithelial	(Maruta et al., 1998b)
Legionella pneumophila	Large numbers of bacteria in vacuole? Cytoplasm?				*Acanthamoeba*	(Michel et al., 1998)
Legionella pneumophila	Fig. 3: 6 hpi. Single bacterium with mitochondrion.				Rat alveolar epithelial cells	(Mody et al., 1993)
Legionella pneumophila Acanthamoeba polyphaga	Fig. 7: 6 hpi. TEM of heavy metal labeling. Too low power to observe morphology.				*A. polyphaga*	(Molmeret et al., 2002)
Legionella pneumophila	Fig. 1: 8 hpi. Fig. 1B: Several large vacuoles, and clear evidence of stacks of rough ER. Fig. 1C: Huge stacks of ER, plus "rough ER fingers" extend from a round structure. Fig. 1D: Rough ER-encompassed "vacuole" adjacent to replication compartment.					(Molmeret et al., 2004)
Legionella pneumophila	Fig. 1: 1 hpi. Vacuoles associated with compartment. 8 hpi. Rough ER (U937.) Fig. 2A: Large vacuoles associated (MDM.)				U937 cells; human monocyte-derived macrophages	(Molmeret et al., 2007)

Legionella pneumophila Escherichia coli	Fig. 2: 24 hpi. Large replication compartments, some ribosomes.				Human alveolar Macrophages	(Nash et al., 1984)
Legionella pneumophila	Fig 4b, MRC-5 cells (1-2 hpi?), "Vesiculated" cytoplasmic membrane associated with *Legionella*-containing vacuole; Fig. 4d, MRC-5 cells, rough-ER like structures about replicating bacteria				MRC5, Vero and HeLa cells	(Oldham and Rodgers, 1985)
Legionella pneumophila Dictyostelium	Fig. 7B: Panel 2, large number of associated vesicles. Panel 1, ER and stretched "vesicle."				RAW 264.7	(Ragaz et al., 2008)
Legionella pneumophila L. micdadei	Figs 5 and 6: 3.5 min. pi. Pseudopod coils. An ER structure near coil. Monocytes.	Figs. 7 and 8: PMNs pseudopod coils.			PMN and human monocytes	(Rechnitzer and Blom, 1989)
Legionella pneumophila	Fig. 1: 1 hpi. Large numbers of large vesicles (100nm +) associated. No clear ER.	Fig. 3A, B: Vesicles surrounding replication vacuole stain intensely for G6Pase, ER marker.	Fig. 4A: 1 hpi ER fragments surrounding replication vacuole stain intensely for G6Pase,ER marker. Figs 4C,D,E: See clear ER-like labeling at 3 and 8 hours. Fig. 4D: See heavy staining of membrane around "Vesicle" consistent with associated "vesicles" having a double membrane.	Fig. 5C,D: 1 hpi. See GTPase staining of finger-like projections similar to those seen in micrograph displayed in attached manuscript.		(Robinson and Roy, 2006)
Legionella pneumophila	6 hpi: Fig. 1C multiple bacteria in a single compartment with clear rough ER associated around *Legionella*-containing vacuole				U937 cells	(Rodgers and Gibson, 1993)
Legionella pneumophila	Fig. 1: Large multi-bacterial vacuoles. Late time points.				Human tropoblast cell line	(Schmid et al., 1991)
Legionella pneumophila Dictyostelium discoideum L. hackeliae	Fig. 2: Purified *L. pneumophila* compartments have clear association with large vacuoles.					(Shevchuk et al., 2009)
Legionella pneumophila	*Legionella pneumophila*	Fig. 3D; ribosome studded replications vacuoles.			Infected guinea pig lungs; macrophages	(Surgot et al., 1988)
Legionella pneumophila	Fig. 7: 7 hpi. 7A: Human monocytes. Heavy ER immunoperoxidase staining of flattened "vacuole" (200 nm +). 7B: Human monocytes. ER staining of ER-like structures. 7c: Murine macrophages. ER-like staining associated with compartment.				human monocytes and murine bone marrow macrophages	(Swanson and Isberg, 1995)

Legionella pneumophila	Fig. 1: 5 min. pi. "ER-derived" vesicles as much as 300 nm in length. Membrane thicker than vacuolar membrane. Fig. 2: 15 min. pi. See flattened vesicles of similar size and filaments connecting them.	Fig. 4: 19 hpi. See ribosomes around replication vacuole. Fig 5: See at two hours little evidence of RER, but evidence of continued associate of "ER vesicles."			U937 Cells	(Tilney and Roy, 2001)
Legionella pneumophila						(Vandenesch et al., 1990)
Legionella pneumophila Legionella micdadei	Fig. 6B: 18 hpi. ER closely associated.				Human monocytes	(Weinbaum et al., 1984)
Legionella pneumophila	Fig. 9: Large compartments containing bacteria in alveolar guinea pig macrophages from infected animals				Guinea pig lungs	(Williams et al., 1987)
Legionella pneumophila	Fig. 2: Large numbers of bacteria in late infection (2-3 days pi.)				Human embryonic lung fibroblasts	(Wong et al., 1980)
Legionella pneumophila	Fig. 1: 24 hpi. Large bacterial compartments.	Fig. 2: 24 hpi. Large bacterial compartments.			Murine macrophages	(Yamamoto et al., 1992)

3.5. Sde family members induce Rtn4 monoubiquitination

As mentioned previously, transfection of individual Sde proteins resulted in the formation of both a HMW Rtn4 species and a modified Rtn4 species that migrated just above the Rtn4b and Rtn4d monomers. In hopes of deciphering the mechanism underlying Sde-mediated Rtn4 transformation, we designed a method to isolate and identify this modified Rtn4 species. First, GFP-SdeC was transiently transfected into cells to produce modified Rtn4. Then Rtn4 was immunoprecipitated using a crosslinked α-Rtn4 resin, which prevents the elution of antibody chains from the resin. This step was crucial, since the heavy chain of antibodies fractionate at ~50kDa, which would co-migrate with Rtn4 monomers obscuring down-stream analysis. After immunoprecipitation, the modified Rtn4 species was excised from SDS gels for LC-MS/MS analysis (Figure 3.9. A). The modified Rtn4 sample showed almost complete coverage of Ub, although curiously the classic Gly-Lys isopeptide diagnostic of

ubiquitination and Ub linkage type could not be detected (Tables 3.2. and 3.3.). Several peptides present in the control Rtn4 monomer samples were noticeably absent from the modified Rtn4 species, consistent with those peptides containing residues targeted by the modification (Table 3.3). Furthermore, the migration of the modified Rtn4 was consistent with monoubiquitination (8.5 kDa) of one or both Rtn4 isoforms (Rtn4b/Rtn4d). The minor difference in molecular weight (~2kDa) between the two Rtn4 isoforms along with their simultaneous recognition by Rtn4 antibodies made distinguishing between them difficult. To confirm the identity of the Rtn4 modification as monoubiquitin, HA (hemagglutinin)-tagged Ub was transiently co-expressed with either GFP-SdeC or a GFP control in cells. Then transfected cell extracts were subject to Rtn4 immunoprecipitation (IP) and immunoblot analysis. Eluates of immunoprecipitates from SdeC-transfected cells revealed two prominent HA positive bands above 50kDa (Figure 3.9. Panel B, compare each of the E lanes). The migrations of the two species were consistent with single and double Ub modification of Rtn4 in response to SdeC. No ubiquitination of Rtn4 was observed in eluates from GFP control transfections (Figure 3.9. B, Eluate lanes). The HMW species previously observed by α-Rtn4 immunoblots could not be detected by silver stain analysis, suggesting this population was not present at a high enough concentration for silver stain visualization or else this HMW Rtn4 was not immunoprecipitated, potentially due to removal of the insoluble fraction of cell extract prior to Rtn4 IP.

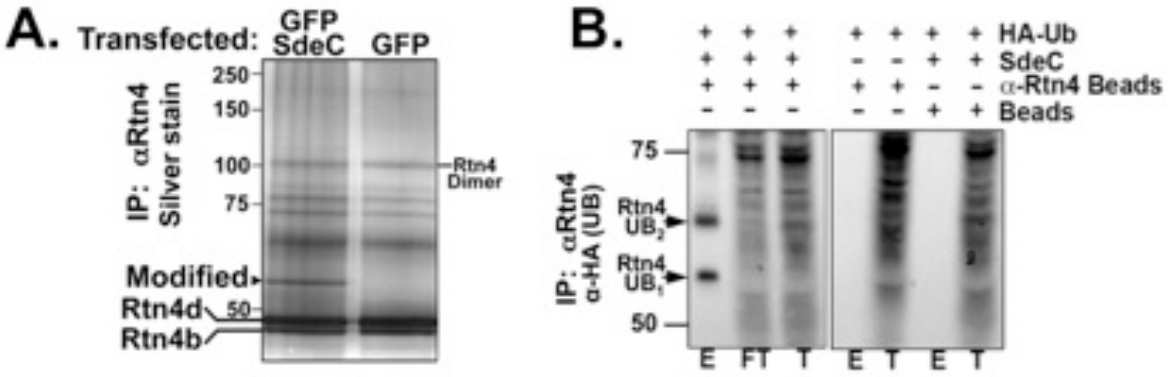

Figure 3.9. Expression of Sde family members promote Rtn4 monoubiquitination. **(A)** GFP-SdeC or GFP (vector) were transiently expressed in HeLa cells for 24 h, followed by Rtn4 IP. Eluates were fractionated by SDS-PAGE and stained. **(B)** HA-Ub was transiently co-expressed with either GFP or GFP- SdeC in HeLa cells for 24 h, then subjected to IP with α-Rtn4 IP, fractionated by SDS-PAGE, and probed for Ub-modified Rtn4 with α-HA (E=Eluate, FT=Flow-through, T=Total).

Table 3.2. Mapping of Rtn4 peptides identified by LC-MS/MS, see Figure 3.9.

Rtn4b (GFP)

MEDLDQSPLVSSSDSPPRPQPAFKYQFVREPEDEEEEEEEEEEDEDEDLEELEVLERKPAAGLSAAPVPTA
PAAGAPLMDFGNDFVPPAPRGPLPAAPPVAPERQPSWDPSPVSSTVPAPSPLSAAAVSPSKLPEDDEPPA
RPPPPPPASVSPQAEPVWTPPAPAPAAPPSTPAAPKRRGSSGSVVVDLLYWRDIKKTGVVFGASLFLLLSL
TVFSIVSVTAYIALALLSVTISFRIYKGVIQAIQKSDEGHPFRAYLESEVAISEELVQKYSNSALGHVNCTIKELR
RLFLVDDLVDSLKFAVLMWVFTYVGALFNGLTLLILALISLFSVPVIYERHQAQIDHYLGLANKNVKDAMAKIQ
AKIPGLKRKAE

Modified Rtn4b (GFP-SdeC)

MEDLDQSPLVSSSDSPPRPQPAFKYQFVREPEDEEEEEEEEEEDEDEDLEELEVLERKPAAGLSAAPVPTA
PAAGAPLMDFGNDFVPPAPRGPLPAAPPVAPERQPSWDPSPVSSTVPAPSPLSAAAVSPSKLPEDDEPPA
RPPPPPPASVSPQAEPVWTPPAPAPAAPPSTPAAPKRRGSSGSVVVDLLYWRDIKKTGVVFGASLFLLLSL
TVFSIVSVTAYIALALLSVTISFRIYKGVIQAIQKSDEGHPFRAYLESEVAISEELVQKYSNSALGHVNCTIKELR
RLFLVDDLVDSLKFAVLMWVFTYVGALFNGLTLLILALISLFSVPVIYERHQAQIDHYLGLANKNVKDAMAKIQ
AKIPGLKRKAE

Rtn4d (GFP)

MEDLDQSPLVSSSDSPPRPQPAFKYQFVREPEDEEEEEEEEEEDEDEDLEELEVLERKPAAGLSAAPVPTA
PAAGAPLMDFGNDFVPPAPRGPLPAAPPVAPERQPSWDPSPVSSTVPAPSPLSAAAVSPSKLPEDDEPPA
RPPPPPPASVSPQAEPVWTPPAPAPAAPPSTPAAPKRRGSSGSVDETLFALPAASEPVIRSSAVVDLLYWR
DIKKTGVVFGASLFLLLSLTVFSIVSVTAYIALALLSVTISFRIYKGVIQAIQKSDEGHPFRAYLESEVAISEELVQ
KYSNSALGHVNCTIKELRRLFLVDDLVDSLKFAVLMWVFTYVGALFNGLTLLILALISLFSVPVIYERHQAQID
HYLGLANKNVKDAMAKIQAKIPGLKRKAE

Modified Rtn4d (GFP-SdeC)

MEDLDQSPLVSSSDSPPRPQPAFKYQFVREPEDEEEEEEEEEEDEDEDLEELEVLERKPAAGLSAAPVPTA
PAAGAPLMDFGNDFVPPAPRGPLPAAPPVAPERQPSWDPSPVSSTVPAPSPLSAAAVSPSKLPEDDEPPA
RPPPPPPASVSPQAEPVWTPPAPAPAAPPSTPAAPKRRGSSGSVDETLFALPAASEPVIRSSAVVDLLYWR
DIKKTGVVFGASLFLLLSLTVFSIVSVTAYIALALLSVTISFRIYKGVIQAIQKSDEGHPFRAYLESEVAISEELVQ
KYSNSALGHVNCTIKELRRLFLVDDLVDSLKFAVLMWVFTYVGALFNGLTLLILALISLFSVPVIYERHQAQID
HYLGLANKNVKDAMAKIQAKIPGLKRKAE

Ubiquitin (GFP-SdeC)

MQIFVKTLTGKTITLEVEPSDTIENVKAKIQDKEGIPPDQQRLIFAGKQLEDGRTLSDYNIQKESTLHLVLRLR
GG

Yellow = Peptide coverage
Red = Peptide missing in modified Rtn4 (High Frequency, HF, Peptide, ≤5)
Gray = Peptide missing in modified Rtn4 (Low Frequency, LF, Peptide, >5)
Underline = Rtn4b/d predicted transmembrane regions

Table 3.3. Rtn4 and ubiquitin peptide prevalence identified by LC-MS/MS.

		RTN4 Peptides	Modified Rtn4 (GFP-SdeC)	Rtn4b/d (GFP-SdeC)	Rtn4b/d (GFP)
		MEDLDQSPLVSSSDSPPRPQPAFK	2	6	10
		MEDLDQSPLVSSSDSPPRPQPA	2	3	6
		MEDLDQSPLVSSSDSPPR	0	1	3
		SDSPPRPQPAFK	0	0	3
		SPPRPQPAFK	0	2	0
		QPAFKYQFVREPEDEEEEEEEEEEDEDEDLEELEVLER	0	2	0
		FKYQFVR	0	2	2
		FKYQFVREPEDEEEEEEEEEEDEDEDLEELEVLER	0	1	0
		YQFVREPEDEEEEEEEEEEDEDEDLEELEVLER	0	3	2
		REPEDEEEEEEEEEEDEDEDLEELEVLER	0	0	2
		EPEDEEEEEEEEEEDEDEDLEELEVLER	8	29	50
		EDEEEEEEEEEEDEDEDLEELEVLER	0	2	2
		EEEEEEEEEDEDEDLEELEVLER	0	1	0
		EEEEEEEEDEDEDLEELEVLER	0	0	3
		EEEEEEEDEDEDLEELEVLER	2	1	0
		EEEDEDEDLEELEVLER	0	3	3
		EDEDEDLEELEVLER	0	1	4
		EDEDLEELEVLER	0	2	2
		EDLEELEVLER	0	2	0
		DLEELEVLER	0	5	8
Missing in Modified Rtn4	**HF**	KPAAGLSAAPVPTAPAAGAPLMDFGNDFVPPAPR	0	31	71
	LF	KPAAGLSAAPVPTAPAAGAPLMDFGN	0	0	2
	LF	KPAAGLSAAPVPTAPAAGAPL	0	0	2
	LF	KPAAGLSAAPVPTAPAA	0	0	2
	HF	KPAAGLSAAPVPTAPA	0	0	5
	LF	PAAGLSAAPVPTAPAAGAPLMDFGNDFVPPAPR	0	4	4
	HF	AAGLSAAPVPTAPAAGAPLMDFGNDFVPPAPR	0	13	26
	HF	SAAPVPTAPAAGAPLMDFGNDFVPPAPR	0	7	4
	HF	MDFGNDFVPPAPR	0	5	9
	LF	DFGNDFVPPAPR	0	3	2
	LF	FGNDFVPPAPR	0	2	5
	LF	DFVPPAPR	0	2	2
		GPLPAAPPVAPER	24	72	105
		PLPAAPPVAPER	2	7	8
		LPAAPPVAPER	4	13	13
		PAAPPVAPER	0	10	17
		APPVAPER	0	5	2
		PAAPPVAPERQPSWDPSPVSSTVPAPSPLSAAAVSPSK	0	2	7
		APPVAPERQPSWDPSPVSSTVPAPSPLSAAAVSPSK	0	1	0
		PVAPERQPSWDPSPVSSTVPAPSPLSAAAVSPSK	0	1	0
		QPSWDPSPVSSTVPAPSPLSAAAVSPSK	6	128	156
		QPSWDPSPVSSTVPAPSPL	0	4	4
		SWDPSPVSSTVPAPSPLSAAAVSPSK	0	16	18
		SWDPSPVSSTVPAPSPL	0	2	2
		DPSPVSSTVPAPSPLSAAAVSPSK	2	10	21
		PSPVSSTVPAPSPLSAAAVSPSK	4	8	28
		PSPVSSTVPAPSPL	0	3	5
		SPVSSTVPAPSPLSAAAVSPSK	0	2	7
		TVPAPSPLSAAAVSPSK	0	0	4
		VPAPSPLSAAAVSPSK	0	0	2
		PAPSPLSAAAVSPSK	0	2	2
		SAAAVSPSK	4	4	6
Missing in Modified Rtn4	**HF**	LPEDDEPPAR	0	2	7
	HF	TPPAPAPAAPPSTPAAPK	0	3	8
	LF	PAAPPSTPAAPK	0	0	2
Rtn4b Specific		PAAPKRRGSSGSVVVDLLYWR	0	0	1
		RGSSGSVVVDLLYWR	0	5	2
		GSSGSVVVDLLYWR	1	22	25
		SGSVVVDLLYWR	0	1	3
		GSVVVDLLYWR	0	1	0
		SVVVDLLYWR	0	1	3

		VVVDLLYWR	0	1	3
Rtn4d Specific		ASEPVIRSSAVVDLLYWR	0	0	1
		PVIRSSAVVDLLYWR	0	1	0
		SSAVVDLLYWR	1	2	3
		AVVDLLYWR	0	1	1
		KGVIQAIQK	0	0	2
		GVIQAIQKSDEGHPFR	0	0	2
		GVIQAIQK	2	7	10
		VIQAIQK	0	1	2
		SDEGHPFRAYLESEVAISEELVQK	0	1	5
		SDEGHPFR	2	9	25
		EGHPFR	0	1	0
		AYLESEVAISEELVQK	30	137	190
		EVAISEELVQK	0	0	2
		ISEELVQK	0	2	2
		YSNSALGHVNCTIK	2	15	24
		YSNSALGHVN	2	11	10
		YSNSALGH	2	3	5
		SALGHVNCTIK	0	2	0
		VNCTIK	0	2	0
		RLFLVDDLVDSLK	0	6	10
		LFLVDDLVDSLK	8	21	33
		PVIYERHQAQIDHYLGLANK	0	1	0
		HQAQIDHYLGLANKNVK	0	0	2
		HQAQIDHYLGLANK	26	145	206
		HQAQIDHY	0	0	2
		QAQIDHYLGLANK	2	6	12
		AQIDHYLGLANK	0	2	4
		QIDHYLGLANK	0	2	2
		IDHYLGLANK	2	4	10
		DHYLGLANK	0	4	0
		HYLGLANK	0	2	5
		YLGLANK	0	1	0
Missing in Modified Rtn4	LF	NVKDAMAKIQAK	0	1	2
	HF	DAMAKIQAK	0	6	14
	LF	IQAKIPGLKR	0	0	3
	HF	IQAKIPGLK	0	5	9
	LF	IPGLKR	0	2	2
		TOTAL	**140**	**862**	**1295**

UBIQUITIN Peptides	**Modified Rtn4 (GFP-SdeC)**	**Rtn4b/d (GFP-SdeC)**	**Rtn4b/d (GFP)**
MQIFVK	3	0	0
TITLEVEPSDTIENVK	6	2	0
IQDKEGIPPDQQRLIFAGK	3	0	0
IQDKEGIPPDQQR	3	0	0
EGIPPDQQRLIFAGK	2	0	0
LIFAGKQLEDGR	1	0	0
TLSDYNIQK	3	1	0
ESTLHLVLR	2	0	0
TOTAL	**23**	**3**	**0**

To analyze if Rtn4 ubiquitination occurs during *L. pneumophila* infection, cells were transiently transfected with HA-Ub and challenged with WT or *Δsde L. pneumophila*, then subjected to Rtn4 IP. Immunoprecipitates from WT challenge predominantly resulted in ubiquitination of what appeared to be the smaller Rtn4b isoform within 10 min of infection (Figure 3.10; WT, 10 MPI). By 3 hrs (180 MPI), both Rtn4b and Rtn4d isoforms were robustly monoubiquitinated, with evidence of HMW ubiquitinated forms accumulating (Figure 3.12. WT 180 MPI). The absence of the Sde family resulted in the complete loss of Rtn4 ubiquitination, similar to mock-infected cells (Figure 3.10; vector, mock). The *Δsde* strain harboring SdeC showed inefficient complementation of monoubiquitination, but evidence of HMW ubiquitinated forms were present, whereas complementation of ubiquitination with either SdeB or SdeA was robust, producing substantial Rtn4b/d mono- and multi-ubiquitination (Figure 3.10). The pattern of Rtn4 ubiquitination in these strains was broadly reminiscent of a WT infection, with an abundance of detectable mono- and di-Ub modified Rtn4.

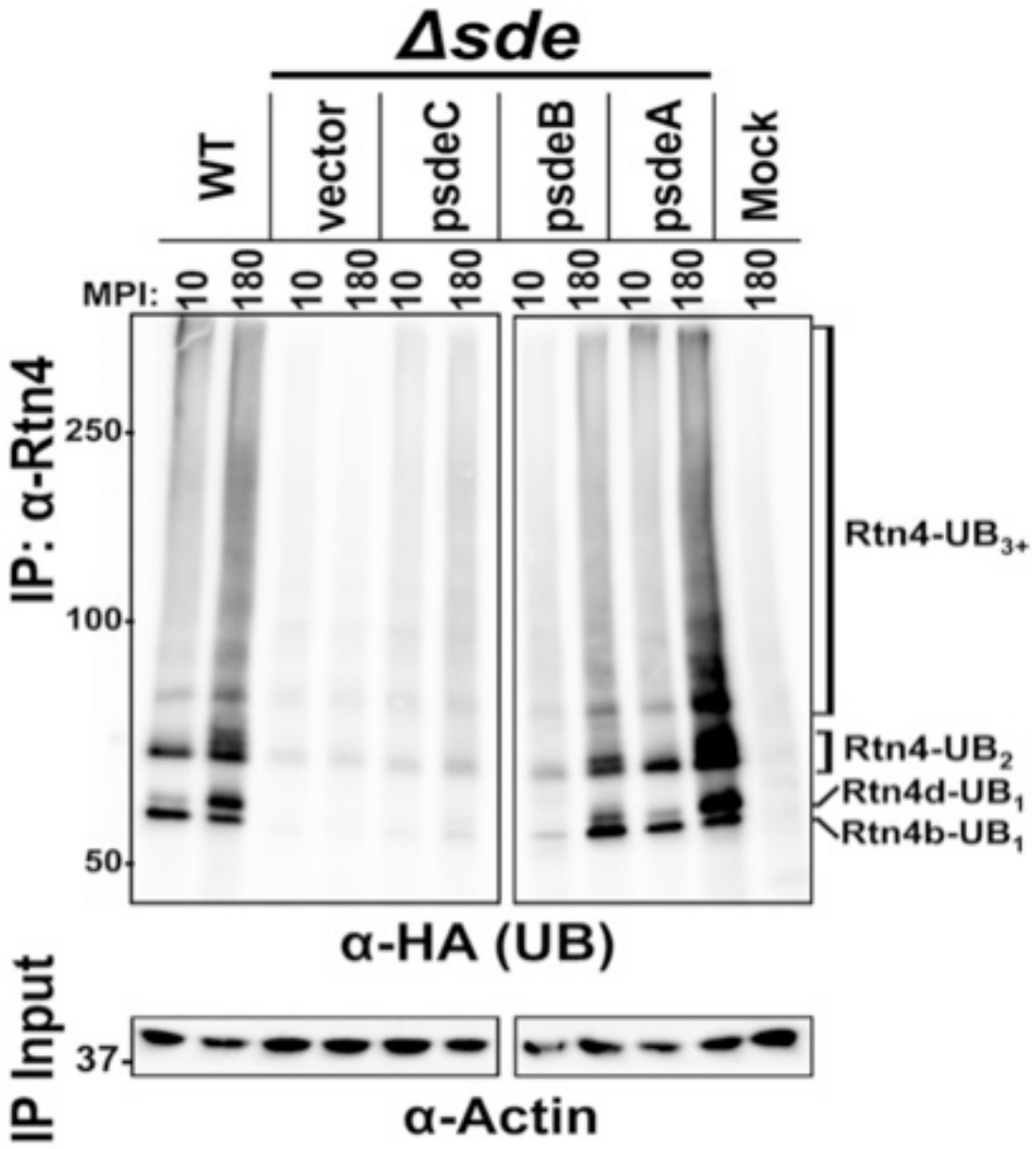

Figure 3.10. Sde proteins promote Rtn4 ubiquitination within minutes of *L. pneumophila* infection.
HEK293T cells were transiently transfected with HA-Ub for 24 hrs, the cell culture medium was replaced with 10μM MG132 (Millipore) medium 30-60 min. prior to challenge with indicated *L. pneumophila* strains and the infection was allowed to proceed for 10 MPI or 180 MPI (MPI, minutes post infection), prior to IP with α-Rtn4. Rtn4 IP elutes were fractionated with SDS-PAGE and Rtn4 ubiquitination was probed with α-HA immunoblots. Cell extract used for the IP was probed with α-actin to control for comparable levels of protein in the IP input.

Chapter 4:

Sde proteins contain an N-terminal deubiquitinase (DUB) domain that preferentially cleaves K63-polyubiquitin.

4.1. Sde proteins contain deubiquitinase (DUB) domain that limits polyubiquitination of the LCV early during infection.

To understand how the Sde proteins promote Rtn4 ubiquitination, we used Phyre2 and HHPred software to search for the presence of any secondary structure or sequence homology to Ub related domains[245]. Three prominent conserved enzymatic domains were apparent in the N-terminal half of the Sde proteins (Figure 4.1; panel A). The first high confidence domain predictions contained homology to a cysteine protease fold within the most extreme amino terminus 200 amino acids in each Sde protein (Figure 4.1; panel A). We along with another research group found that this Sde domain had homology to ubiquitin proteases, specifically deubiquitinating enzymes (DUBs)[452]. The Sde proteins contain a conserved set of residues, HW-D-C (histidine-tryptophan - - - aspartic acid - - - cysteine), which has been experimentally demonstrated to serve as the catalytic site for homologous protease folds, including in the sentrin-specific protease 8 that targets the ubiquitin-like modifier NEDD8, ubiquitin carboxyl-terminal hydrolase 14 (UCH14), and ubiquitin carboxyl-terminal hydrolase 8 (UCH8) (Figure 4.1; panel B). To understand the role of this ubiquitin hydrolase domain in promoting Rtn4 ubiquitination and ER structural transformation, each predicted catalytic residue of SdeC DUB domain was mutated in *sdeC*, as was the catalytic cysteine in *sdeB* and *sdeA*. To determine if the Sde DUB domain plays a role in the Rtn4 structural transformation, BMDMs were challenged with *L. pneumophila* and individual *sde* mutants to assay the percentage LCV that colocalize with detergent-resistant Rtn4. As previously described, BMDMs were challenged for 1 hr with *L. pneumophila* and analyzed by immunofluorescence microscopy after detergent extraction. Infections with *Δsde* strain expressing individual Sde mutants, where the predicted catalytic cysteine residue was mutated to a serine,

resulted in a drop of Rtn4-positive vacuoles by 50% or more relative to Rtn4 positive LCVs associated with the corresponding wild type Sde protein (Figure 4.1; panel C).

Next, we examined if the DUB domain were important for intracellular replication in the amoebal host *Dictyostelium discoideum*. Luciferase expressing *L. pneumophila* was used to challenge the amoeba for 2 hrs, then bacterial replication was monitored hourly by luciferase expression over the next 4-5 days. Infection with *Δsde* strain resulted in a significant replication defect relative to WT infection (Figure 4.1; panels E,F). Plasmid encoded *sdeC* or *sdeB* allowed *L. pneumophila* replication as well, or better, than WT. Plasmid encoded *sdeC* or *sdeB* DUB domain point mutants produced similar growth curves to their WT counterparts, with the $SdeB_{C118S}$ mutant apparently growing better than WT (Figure 4.1; panel F, compare *Δsde* $psdeB_{C118S}$ with Lp02). This demonstrates that the Sde DUB activity is not essential for the bacterial protein family's role during intracellular growth. We have found that the Sde ubiquitin protease domain contributes to the transformation of Rtn4 and its association with the LCV, but this domain is not ultimately required for this transition, nor is the deubiquitinase domain critical for the Sde protein's role during infection, as the absence of the domain has no effect on growth within *Dictyostelium discoideum*.

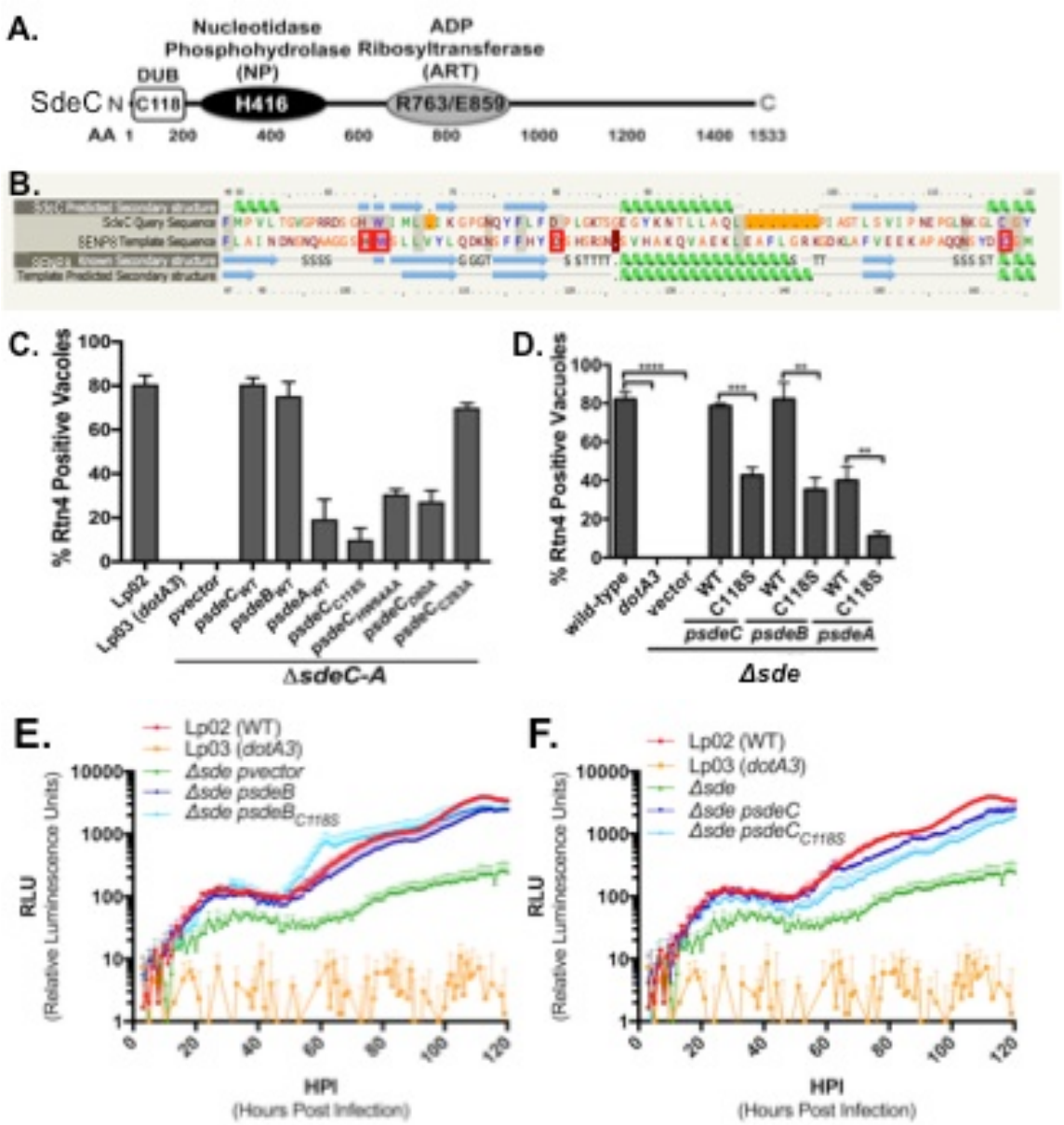

Figure 4.1. Sde DUB domain activity enhances Rtn4 transformation, but is not required for intracellular growth in *Dictyostelium discoideum.*

(A) Cartoon schematic of the three conserved Sde family domains predicted by Phyre2 and HHPred, online secondary structure homology prediction software[245]. The domain organization and predicted catalytic residues for each domain are indicated for SdeC. **(B)** The SdeC DUB catalytic core (query line) aligned to sentrin-specific protease 8 fold (SENP8, template line) by Phyre2[245]. Red boxes indicate known catalytic residues in sentrin-specific protease 8[453], template line maroon highlight indicates insertion relative to template, orange highlight indicated deletion relative to template, grey highlight indicate homologous residues, secondary structure predictions are indicated by green spirals for α-helices and blue arrows for β-sheets[245]. **(C-D)** BMDMs from A/J mice were challenged at an MOI =1 for 1 hr with denoted *L. pneumophila* strain, followed by fixation, permeabilization with 1% Triton X100 and probing with α-Rtn4 (green), α-*L.*

pneumophila (red), and Hoechst (blue) for nuclear DNA staining. LCVs associated with Rtn4 signal above background was considered positive, represents at several independent experiments with at least 50 LCV/coverslip counted with 3 coverslips per condition evaluated. Wild type, Lp02; *dotA3,* T4SS defective or an *icm*/*dot*$^{-}$; *Δsde*, *ΔsidE ΔsdeC ΔsdeB-A* or *Δlpg0234 Δlpg2153 Δlpg2156-2157* (KK099). **(E-F)** *Dictyostelium discoideum* was challenged with luciferase-expressing *L. pneumophila* mutants for 2 hrs at an MOI=0.5 and then intracellular bacterial growth was monitored every hour for the next 120+ hrs in a plate reader. Growth curves are representative of at least 3 independent experiments with a single experiment and ±SD shown.

To address whether the Sde DUB domain serves as an ubiquitin hydrolase that functions during infection, we challenged BMDMs with *Δsde* expressing individual Sde members or their corresponding DUB domain point mutants and analyzed the kinetics of polyubiquitination accumulation at the LCV using immunofluorescence microscopy. Over the first 30 min of WT *L. pneumophila* infection starts with very few if any vacuoles staining positively for polyUb, but by 30 MPI ~20-40% of WT LCVs stain polyUb positive (depending on the experiment) with the FK1 monoclonal antibody, which is specific for polyubiquitin and does not recognize other Ub forms (Figure 4.2; wild-type, 0-30 MPI). Without a functional T4SS, *L. pneumophila* did not elicit polyubiquitination of the replication vacuole (Figure 4.2; *dotA3*). In the absence of *sde* members, the majority of LCV were polyubiquitin-positive within 15 MPI and a significant percentage of LCVs were positive after a mere 5 min centrifugation of bacteria onto BMDMs and immediate fixation (Figure 4.2; vector, 0-15 MPI). This demonstrates the rapid effect that Sde proteins have on host ubiquitination immediately upon phagocytosis. Plasmid expression of individual Sde proteins in a *Δsde* background was able to partially reduce the LCV hyper-ubiquitination observed in the *Δsde pvector* strain (Figure 4.2; compare vector with *psdeC* or *psdeB* at 0 MPI). This polyUb reduction by Sde protein was most pronounced at 0 MPI where less than 20% of LCVs remained

polyUb positive. At 10 to 30 MPI infection of BMDM challenged with *Δsde psdeC* or *Δsde psdeB* resulted in a large increase in positive LCVs, often with more than 60% of vacuoles positive, which was higher than even WT infection levels (Figure 4.2; compare Wild-type to *Δsde psdeC* or *Δsde psdeB,* 30 MPI). Intriguingly, plasmid expression of SdeA in a *ΔsdeC-A* background resulted in constitutively low levels of LCV polyubiquitination, whereas expression of SdeA in a clean *Δsde* background, which retains the *sidJ* gene, produced polyUb kinetics similar to *Δsde psdeC* or *Δsde psdeB*. Under conditions of maximum complementation, at 0 MPI, polyUb-positive LCVs are rarely seen, but within 10 to 30 MPI polyUb levels rise above those observed in WT infections (Figure 4.2; panel A,B, compare *ΔsdeC-A psdeA* with *Δsde psdeA,* 0-30 MPI). The Sde proteins ability to limit polyUb at the LCV is dependent on an active DUB domain in the Sde proteins, as the SdeC(C118S) DUB mutant is wholly unable to reduce polyUb levels, resulting in rapid stable polyubiquitination of the majority of vacuoles at 0 MPI, similar to what was observed with the *Δsde pvector* strain (Figure 4.2; *psdeC C118S* 0 MPI).

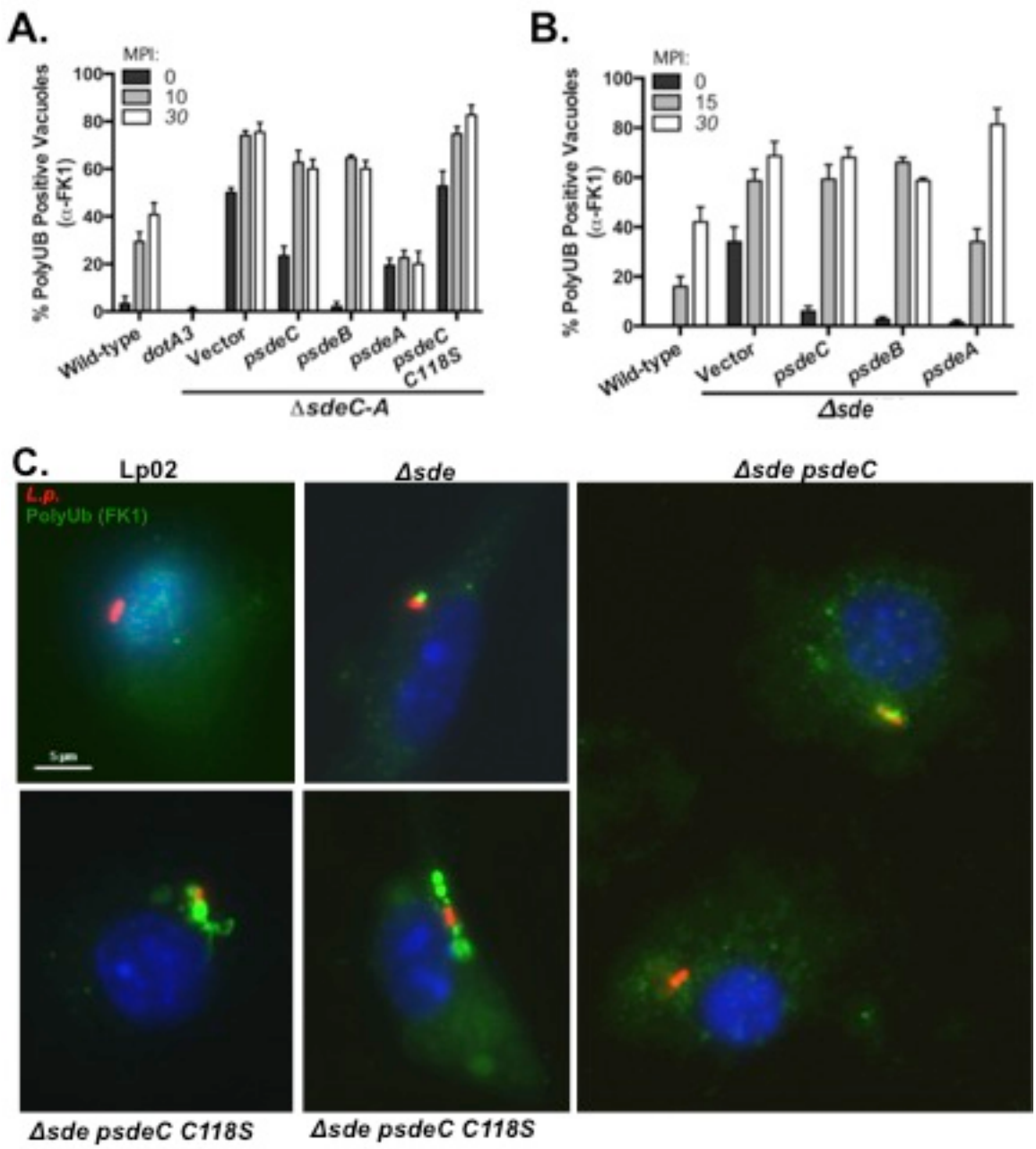

Figure 4.2. Sde proteins limit LCV polyubiquitination early during infection dependent on their DUB domain.

(A,B) BMDMs from A/J mice were challenged at an MOI =1 for indicated infection times (after 5 min centrifugation of bacteria onto BMDMs) with denoted *L. pneumophila* strain, followed by fixation, permeabilization with 1% Triton X100 and probing with α-polyUb (α -FK1, green), α-*L. pneumophila* (red), and Hoechst (blue) for nuclear DNA staining. Wild type, Lp02; *dotA3,* T4SS defective or an *icm*/*dot*$^-$; *Δsde*, *ΔsidE ΔsdeC ΔsdeB-A* or *Δlpg0234 Δlpg2153 Δlpg2156-2157* (KK099); *ΔsdeC-A*, *Δlpg2153-2157* (KK034). **(C)** Representative images from 20 MPI are shown for the indicated strains in part A/B are shown. SdeC C118S, DUB deficient; scale bar=5μm.

4.2. Sde proteins react with a DUB specific probe *in vitro.*

To further profile the Sde family DUB domain we examined the Sde proteins reactivity with a broad spectrum cysteine DUB inhibitor that serves as a biotin labeled probe[116,117,146]. The probe includes a biotin tag with an aminohexanoic acid (Ahx) linker to ubiquitin containing a DUB reactive C-terminal PA (propargylamide) group (Figure 4.3; panel A). The C-terminal carboxylate of Ub substituted with propargylamide serves as an alkyne reactive group in a selective reaction with the active-site cysteine residue of deubiquitinating enzymes (Figure 4.3. A)[117]. Proteomic studies confirmed the probes selectivity toward deubiquitinating enzymes along with reactivity across all major eukaryotic DUB families, UCH, USP and OUT, which other traditional DUB probes, such as VME, cannot easily achieve[116,117]. Sde proteins were expressed from a plasmid in *E. coli* followed by incubation of the bacterial lysates with or without the DUB probe, biotin-Ub-PA. Lysates were then probed for biotin incorporation above background to detect the presence of a cysteine DUB. Expression of full length SdeC, SdeB, and SdeA resulted in lysates with the DUB probe producing numerous biotin reactive species starting above 150kDa with lower reactive fragments scattered across the lower molecular weights to ~50kDa (Figure 4.3; panels B,C). These biotin labeled species were unique to reactions containing both Sde proteins and the biotin-Ub-PA probes, as reactions lacking either component produced only 2-3 cross-reacting background biotin bands on immunoblots (Figure 4.3; panels B,C, vector, Biotin-Ub-PA: −). Consistent with C118S representing the catalytically active DUB cysteine residue, all C-terminal SdeC truncations assayed were still reactive with the biotin DUB probe (Figure 4.3; panel C, 1-831, 1-675, 1-269). A SdeC N-terminal construct containing only the first 269

amino acids showed robust biotin labeling just below the 37kDa marker. The biotin labeling of the DUB active site in Sde proteins was also monitored using recombinant SdeC or a recombinant SdeC DUB fragment, 1-192. Recombinant SdeC was incubated with increasing concentrations of the DUB probe and the covalent linking of the two proteins was monitored by changes in SdeC migration. Since the probe contains Ub, an increase in SdeC migration of 10 kDa would be indicative of the bacterial protein reacting with the probe. SdeC DUB fragment migrates at ~28kDa, while the DUB probe alone corresponded with a faint smear at about 10kDa. With increasing levels of the probe incubated with SdeC 1-192 an increasingly prominent band just above 35kDa appeared (Figure 4.3; panel D).

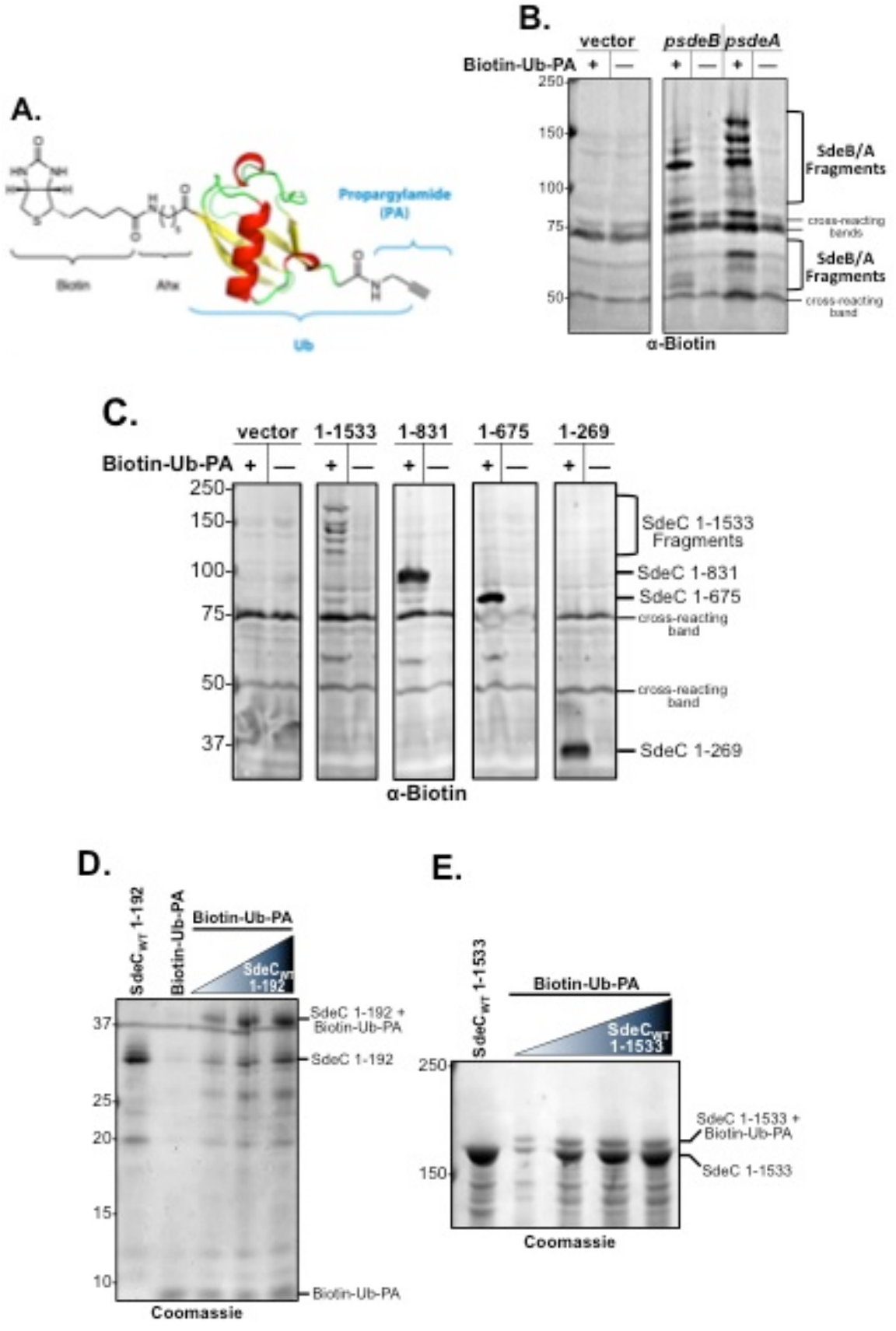
A.
Propargylamide (PA)
Biotin
Aha
Ub
B.
vector
psdeB psdeA
Biotin-Ub-PA + — + — + —
250
150
100
75
50
SdeB/A Fragments
cross-reacting bands
SdeB/A Fragments
cross-reacting band
α-Biotin
C.
vector
1-1533
1-831
1-675
1-269
Biotin-Ub-PA + — + — + — + — + —
250
150
100
75
50
37
SdeC 1-1533 Fragments
SdeC 1-831
SdeC 1-675
cross-reacting band
cross-reacting band
SdeC 1-269
α-Biotin
D.
SdeC WT 1-192
Biotin-Ub-PA
Biotin-Ub-PA
SdeC WT 1-192
37
25
20
15
10
SdeC 1-192 + Biotin-Ub-PA
SdeC 1-192
Biotin-Ub-PA
Coomassie
E.
SdeC WT 1-1533
Biotin-Ub-PA
SdeC WT 1-1533
250
150
SdeC 1-1533 + Biotin-Ub-PA
SdeC 1-1533
Coomassie

Figure 4.3. Sde proteins react with a biotin labeled cysteine DUB probe.
(A) Diagram of the DUB inhibitor/probe structure with a biotin head, an aminohexanoic acid (Ahx) linker, ubiquitin moiety (Ub) with a PA (propargylamide) group at the Ub C-terminus[117]. **(B)** DH5α *E. coli* were induced to express full-length SdeB or SdeA from a plasmid, then cells were sonicated and bacterial lysates were incubated with 1μM biotin-Ub-PA for 30 min at 37°C. Reactions were terminated by the addition of reducing SDS sample buffer, then samples were fractionated by SDS-PAGE and probed for biotin labeling of bacterial DUBs with α-biotin immunoblots. **(C)** Plasmids encoding *sdeC* C-terminal truncations were induced, reacted, and analyzed for biotin labeling as in part B indicating covalent modification of Sde with Biotin-Ub-PA probe. **(D,E)** Recombinant SdeC DUB domain, 1-192, **(D)** or full length SdeC, 1-1533, **(E)** concentrations were titrated from 200nM-1μM with 1μM biotin-Ub-PA and reacted at 37°C for 30 min, then analyzed for altered SdeC migration by Coomassie staining.

4.3. Sde proteins contain a highly preferential K63 deubiquitinase domain.

To further explore Sde family DUB enzymatic activity, a recombinant DUB fragment (1-192) and full-length SdeC construct were produced, along with their corresponding catalytically inactive DUB point mutants (C118S). To assess SdeC DUB activity, we incubated the DUB domain in a Ub chain cleavage assay using K63 or K48 homotypic ubiquitin tetramers (Ub_4) as the substrate. $SdeC_{WT}$ 1-192 concentration was titrated in 10-fold increments and incubated with 200μM of Ub_4 for 40 min at 37°C. Cleavage was monitored by SDS-PAGE fractionation and silver staining to unveil the formation of smaller Ub chains and Ub monomer (~8kDa). The SdeC DUB domain (1-192) was able to produce detectable, but low levels of Ub cleavage in reactions with SdeC concentrations as low as 0.2nM. In these low SdeC concentration reactions the faint appearance of a K63 Ub trimer (Ub_3) could be detected compared to a no SdeC control reaction (Figure 4.4; lanes 2,4). At SdeC concentrations of 20-200nM the majority of K63 Ub tetramers had been cut into smaller Ub fragments, with the majority of Ub chains cleaved into Ub monomers in the 200nM SdeC reaction ; 4.4. lanes 6,7). Consistent with this cleavage resulting from SdeC DUB activity rather than an undefined contaminant, no

cleavage was observed with a non-hydrolyzable K63 Ub tetramer, even with high concentrations of SdeC ((200nM) Figure 4.4. Lanes 3,8). Contrary to K63 Ub chain cleavage, SdeC was unable to cut K48 Ub tetramers at low concentrations, 0.2nM to 2nM (Figure 4.4; lanes 10,11), and very limited cleavage was observed at high SdeC concentrations of 20-200nM (Figure 4.4; lanes 12,13). This demonstrates the strong preference of SdeC for a specific ubiquitin linkage and that linkage specificity is encoded within the 200 amino-terminal DUB region.

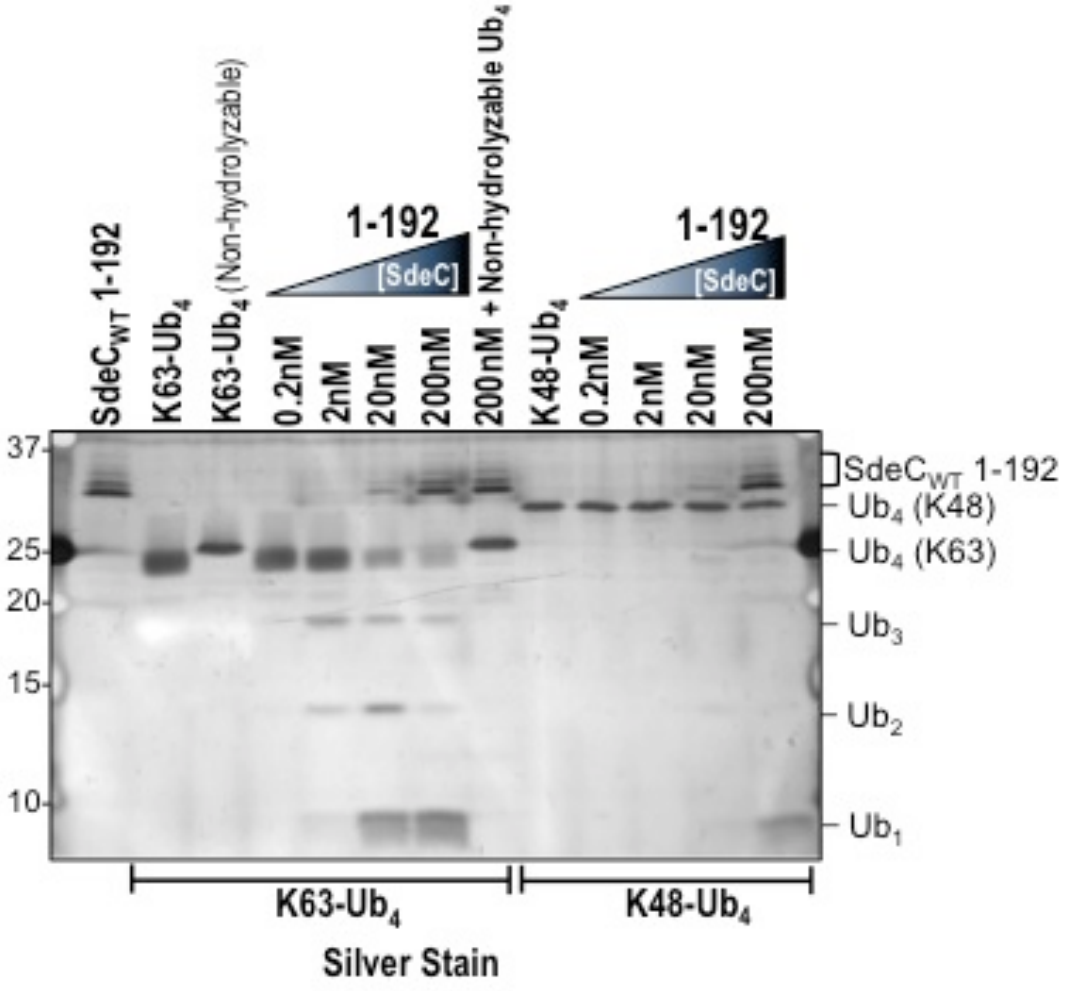

Figure 4.4. SdeC DUB domain rapidly cleaves K63-polyUb, but not K48-polyUb at low nanomolar levels.
SdeC$_{WT}$ 1-192 was incubated with 200nM Ub$_4$ for 40min at 37°C and cleavage of Ub chains, either K63 or K48 linked polyUb, was monitored by SDS-PAGE fractionation and silver staining for the formation of smaller Ub products and loss of Ub$_4$.

To further profile this linkage specificity, the SdeC DUB fragment was incubated with di-ubiquitin representing each of the seven possible lysine linkages as well as the methionine 1 linkage (M1/linear). Cleavage of the 200ng of the di-ubiquitin probe by either 4ng of SdeC 1-192 or by 40ng of the non-specific Ub protease, Usp2 catalytic domain (CD) that served as a positive control, was examined after a 30 min reaction. This was followed by SDS-PAGE fractionation and silver stain analysis for the loss of di-ubiquitin and the formation of Ub monomer. SdeC 1-192 was able to cleave the K63 di-ubiquitin probe and to a far lesser extent, K48 and K33 cleavage could be detected relative to the no enzyme control (Figure 4.5; $SdeC_{WT}$ 1-192, 30 min, K63, K48, K33). No discernable cleavage was observed in assays containing K11 or M1/Linear di-ubiquitin. Unfortunately assessment of DUB cleavage for K29, K27, and K6 di-ubiquitin probes was difficult due to the high concentration of Ub monomers contaminating the sample prior to incubation with a DUB (Figure 4.5; $SdeC_{WT}$ 1-192, 0 min, K29, K27, K6). As such, only a comparison of di-ubiquitin levels could be used as cleavage efficiency readout. In these problematic reactions, there appeared to be a slight reduction in di-ubiquitin levels after 30 min incubation with $SdeC_{WT}$ 1-192 compared to no enzyme or $SdeC_{C118S}$ 1-192 control reactions, but no changes in Ub monomer concentrations could be readily observed, indicating that there was little evidence for extensive SdeC cleavage of these Ub linkages.

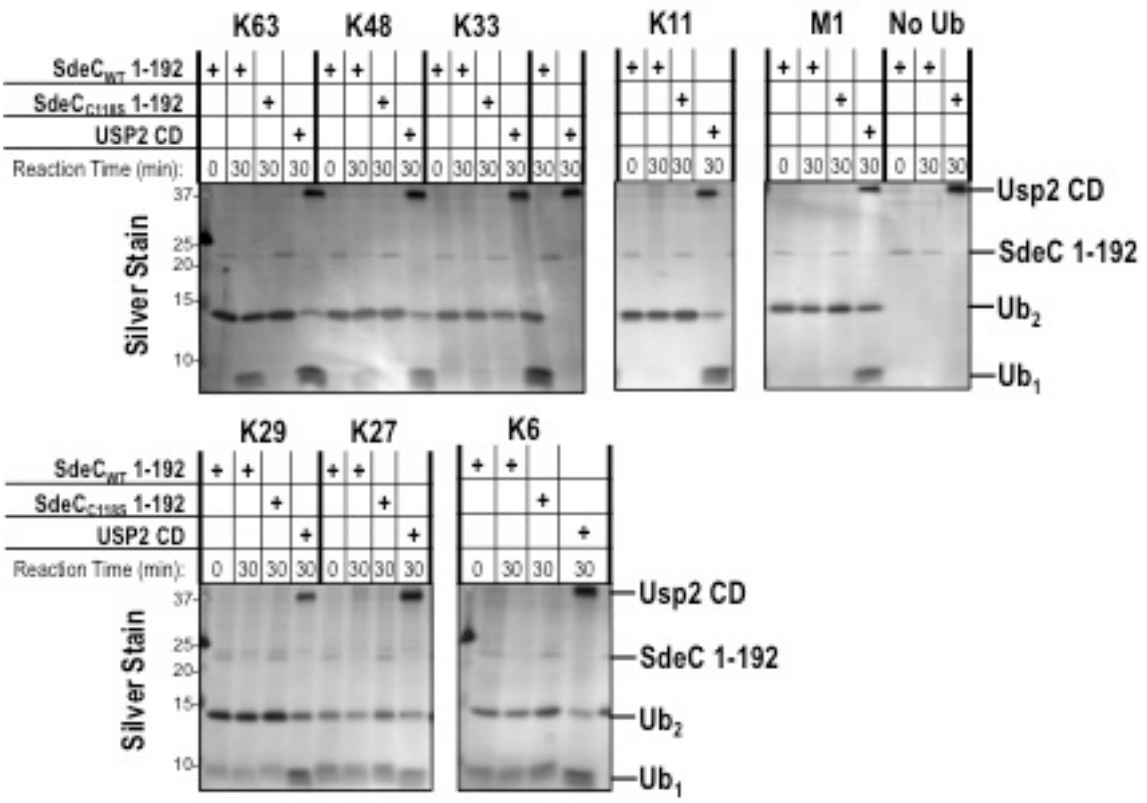

Figure 4.5. Di-ubiquitin probes of different linkage confirm Sde DUB domain strong preference for K63-Ub.

Di-ubiquitin chains of all possible chain linkages were incubated with SdeC$_{WT}$ 1-192, SdeC$_{C118S}$ 1-192, or Usp CD for 30 min at 37°C. Reactions were fractionated by SDS-PAGE and silver stained to reveal formation of Ub monomer indicating cleavage. USP2 CD is a non-specific Ub protease and serves as a cleavage positive control, SdeC$_{C118S}$ 1-192 and SdeC$_{WT}$ 1-192 at 0 min serves as a no cleavage control. Ub$_1$, ubiquitin monomer; Ub$_2$, Ub dimer; Usp2 CD, Ubiquitin Specific Protease 2 Catalytic Domain.

The amino-terminal DUB domain represents only ~1/8 of the entire SdeC protein, so to understand the role of the rest of the SdeC protein, DUB cleavage kinetics were compared between the DUB domain alone and full length SdeC. Either K63 or K48 ubiquitin tetramers (Ub_4) were incubated with either 20nM of the DUB fragment of SdeC, 1-192, or full-length SdeC, 1-1533, aliquots of the reactions were then removed throughout the 2 hr incubation to monitor the kinetics of Ub_4 disappearance and development of Ub_3, Ub_2, and Ub_1 products. Cleavage of K63 Ub tetramers by SdeC DUB domain 1-192 was rapid and at 2 hrs no Ub_4 remained, only Ub_3-Ub_1 species were visible (Figure 4.6; top left panel). In reactions containing K48 Ub_4, a large amount of Ub_4 remained after 2 hr incubation with either $SdeC_{WT}$ 1-192 or $SdeC_{WT}$ 1-1533 and a limited amount Ub_3 and Ub_2 was formed (Figure 4.6; compare bottom panels, WT 0-120 min). Even after a 2 hr incubation with $SdeC_{WT}$ 1-192 and K48 Ub_4, no Ub monomers arose (Figure 4.6; bottom left panel). The K48 Ub_4 cleavage by the SdeC DUB domain fragment mimicked the cleavage pattern observed in reactions with full-length SdeC. Fascinatingly, the $SdeC_{WT}$ 1-192 cleavage of K63 Ub_4 was far more efficient than the full-length $SdeC_{WT}$ 1-1533 cleavage (Figure 4.6; compare top panels, WT 0-120 min). Reactions with $SdeC_{WT}$ 1-1533 and K63-Ub_4 contained a large population of Ub_4 that remained untouched after 2 hrs at 37°C (Figure 4.6; top right panel). This indicates the SdeC regions outside the DUB domain may modulate the activity of the N-terminal DUB domain, specifically during K63-ubiquitin cleavage. In all reactions with either $SdeC_{C118S}$ 1-192 or $SdeC_{C118S}$ 1-1533, regardless of the ubiquitin linkage assayed as a substrate or the reaction time allotted, no ubiquitin cleavage was ever observed (Figure 4.6; $SdeC_{C118S}$

1-192/1-1533 (120min)). This result confirms the identity of C118 as the catalytic cysteine required for DUB protease activity in the Sde family.

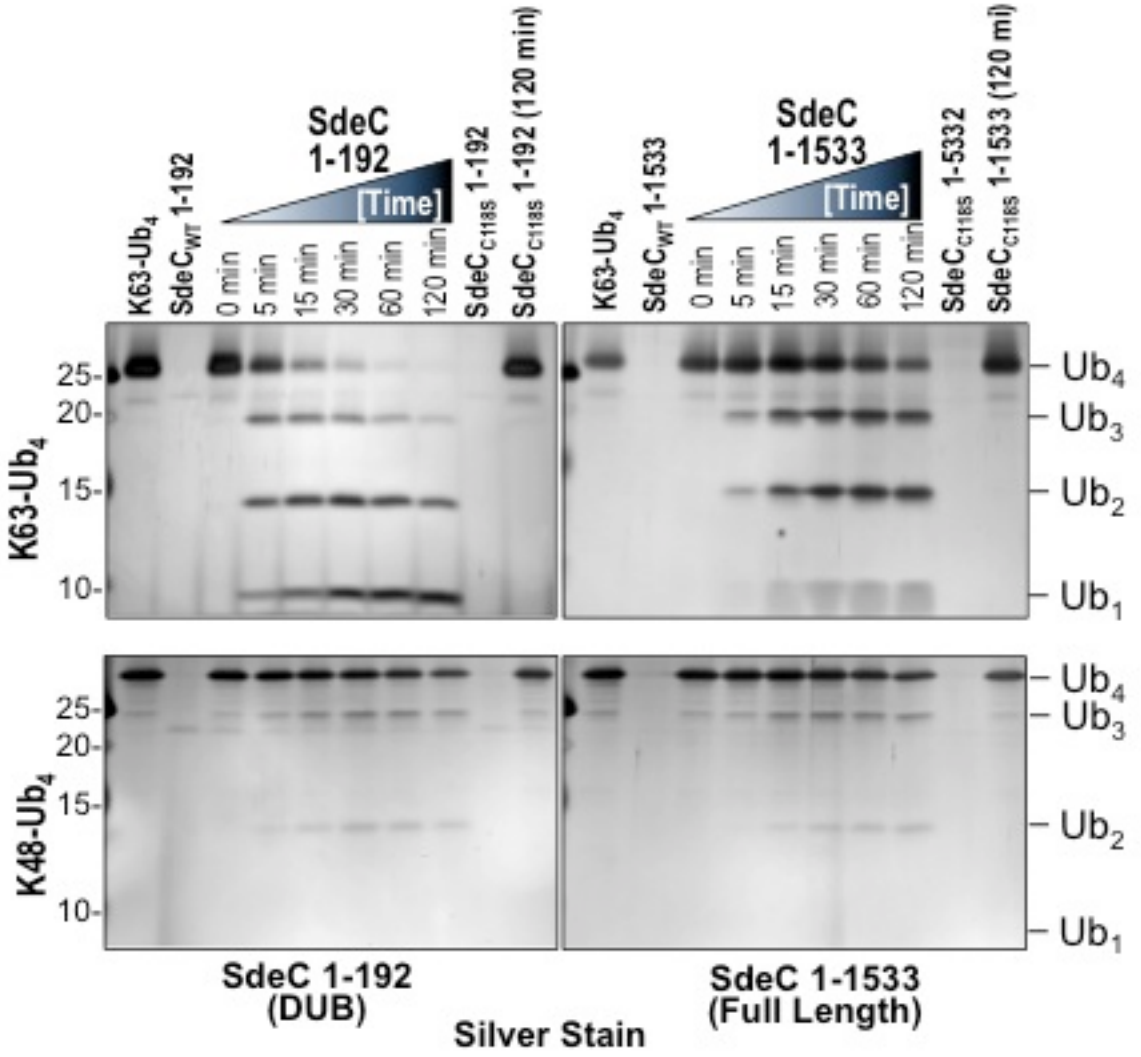

Figure 4.6. Sde K63-preferential DUB activity is limited by other Sde domains. Kinetics of SdeC 1-192 or SdeC 1-1533 (full length) cleavage of K63 (Top panels) or K48 (bottom panels) Ub_4 (1μM) was monitored over 2 hr incubation at 37°C by SDS-PAGE fractionation and silver staining. Loss of Ub_4 and formation of smaller Ub products was monitored as a readout for Ub cleavage efficiency by DUBs. Lines indicate location of each Ub. K63-Ub_4 and K48-Ub_4 only reactions or $SdeC_{C118S}$ 1-192 and $SdeC_{C118S}$ 1-1533 with Ub_4 served as a no cleavage control.

Chapter 5:

Sde proteins contain a mono-ADP-ribosyltransferase that is essential for Rtn4 reorganization, intracellular growth in amoeba, and Rtn4 ubiquitination.

This chapter contains excerpts that have previously been published in:
(reprinted with permission of publisher)

Kotewicz KM, Ramabhadran V, Sjoblom N, Vogel JP, Haenssler E, Zhang M, Behringer J, Scheck RA, Isberg RR. Cell Host Microbe. 2017 Feb 8; 21(2):169-181. Epub 2016 Dec 29.

5.1. Sde ART activity is required for Rtn4 rearrangements.

We and other research groups identified an arginine-mono ADP-ribosyltransferase (ART) domain conserved across the Sde family proteins[40,396]. The Sde DUB domain was not essential for Rtn4 transformation, so we probed the connection between the ART domain and ER reorganization. Conserved residues in Sde family members that aligned with catalytic ART residues from other bacterial mono-ART were targeted for alanine mutagenesis (**R**-STS/T-EX**E**), as the arginine and the second glutamic acid in the EX**E** motif are absolutely essential for function[29,148,179,263,272]. Then BMDMs were challenged with a panel of *L. pneumophila* strains deleted for the Sde family, but harboring plasmids with Sde ART domain point mutations, and analyzed for Rtn4-LCV association by IF microscopy. The predicted enzymatic residues were mutated to alanine in each Sde member and expressed in *Δsde* background (Figure 5.1. SdeB/C E859A or R763A; SdeA E862A). Each Sde ART mutant was completely unable to restore Rtn4 association with the LCV, consistent with the Sde ART domain being essential for Rtn4 reorganization (Figure 5.1. A,B).

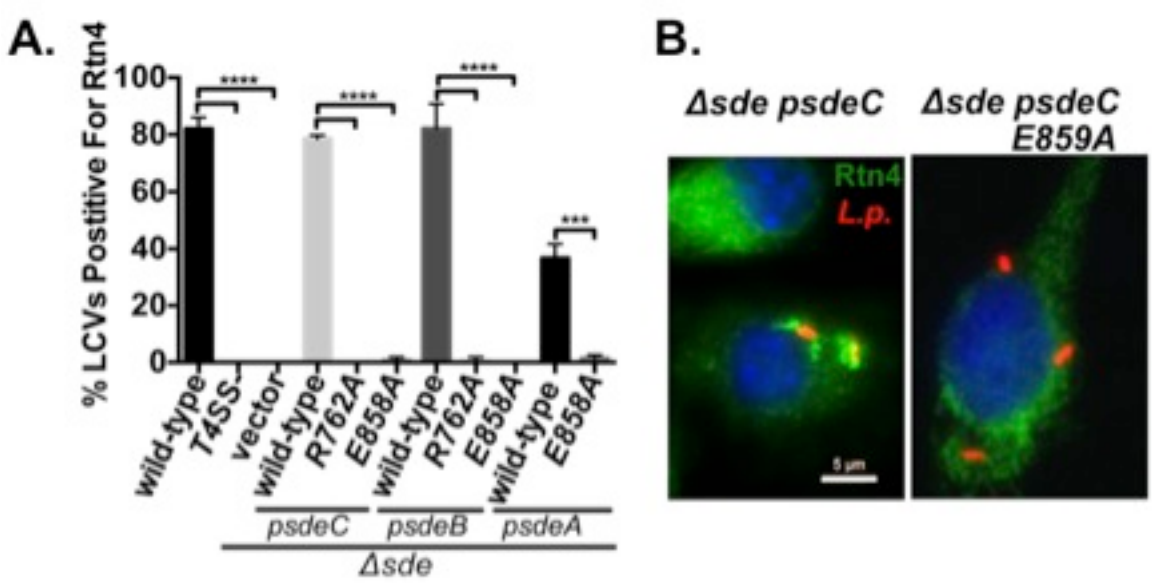

Figure 5.1. Sde family mono ADP-ribosyltransferase activity is required for Rtn4 restructuring.
(A) A/J BMDMs were challenged for 1 h, fixed, permeabilized with 1% Triton X100 and probed with α-Rtn4 (green), α-*L. pneumophila* (red), and Hoescht (blue). 50 *L. pneumophila* vacuoles were assessed for Rtn4 colocalization per coverslip with at least 3 coverslips per condition. **(B)** Representative micrographs of Rtn4 association with the LCV at 1hpi (hour post infection), scale bar = 5μm.

5.2. Sde family ART domain is required for *L. pneumophila* intracellular growth in *Dictyostelium discoideum.*

The Sde family is not required for intracellular replication in BMDMs[28,452], but the family is important for growth in an amoebal host, both *Acanthamoeba castellanii*[28] and *Dictyostelium discoideum*[260,396,452]. We and other research groups observed that the Sde DUB module was not required for the Sde family function during intracellular growth in *D. discoideum*[452] (Figure 5.2), nor was the DUB domain required for the formation of Rtn4 rearrangements (Figure 4.1, panels C,D)[260], but the ART domain was essential for Rtn4 rearrangements (Figure 5.1). These results indicated that the ART domain would be critical for the Sde function during infection. To test this, *D. discoideum* was challenged at an MOI of 0.5 for 2 hrs with luciferase expressing WT *L.*

pneumophila and *Δsde* mutants, then their intracellular replication was monitored by enumeration of luciferase levels over the next 120 hrs (4-5 days)[89,125]. WT *L. pneumophila* grew robustly and *Δsde* strain harboring plasmids with individual wild-type *sde* genes was able to replicate to WT levels of growth (Figure 5.2. A). Infection with a *Δsde* strain resulted in a significant decrease in intracellular growth after 100 hr challenge (Figure 5.2. A). Plasmids harboring the ART mutant $SdeC_{E859A}$, $SdeB_{E859A}$, or $SdeA_{E862A}$ were unable to restore *L. pneumophila* intracellular growth to levels observed with either the WT strain or the *Δsde* strain harboring $SdeC_{WT}$ (Figure 5.2. B). Plasmids harboring an alanine mutation at the predicated catalytic arginine residue of the ART domain, $SdeC_{R763A}$, $SdeB_{R763A}$, or $SdeA_{R766A}$, also failed to fully restore *L. pneumophila* intracellular growth (Figure 5.2. C). Therefore, the Sde ART domain is essential for promoting bacterial replication during an amoebal challenge.

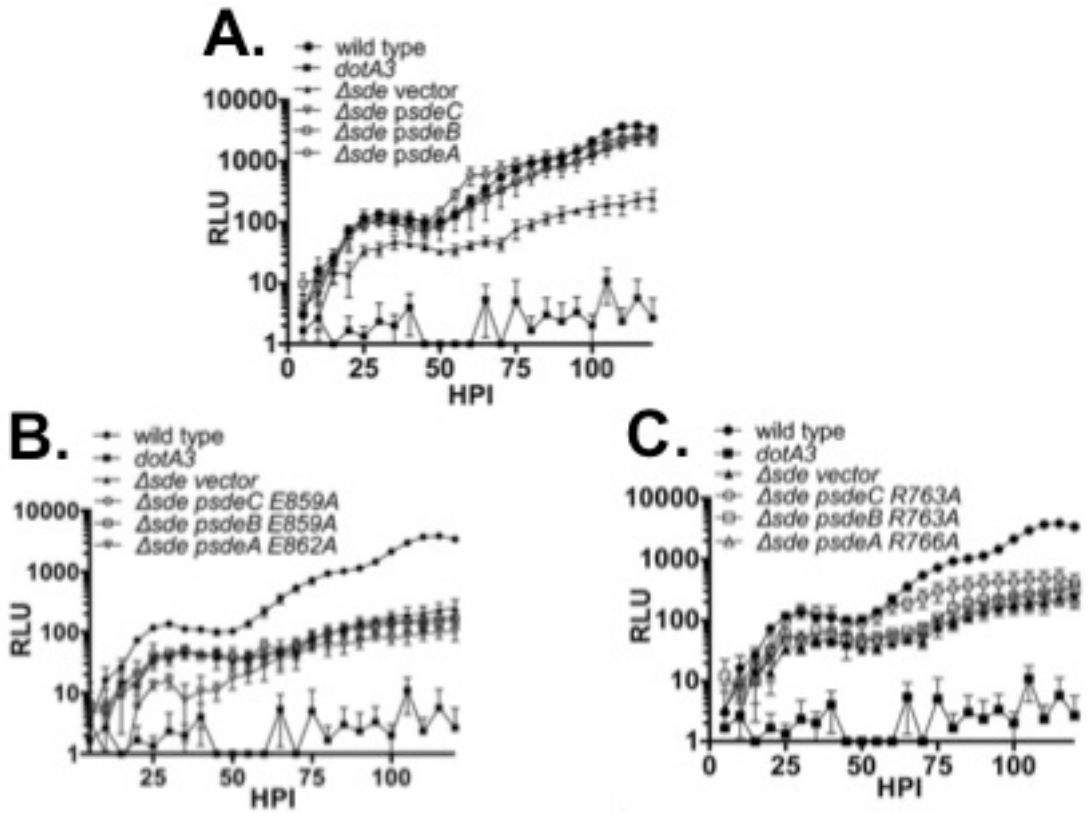

Figure 5.2. Sde family ART domain is required for *L. pneumophila* intracellular growth in *Dictyostelium discoideum*

A-C) *Dictyostelium discoideum* was challenged with WT (Lp02) or mutant *L. pneumophila* expressing luciferase (*PahpC::lux*). *L. pneumophila* intracellular growth (luminescence) was monitored hourly. Mean ± SEM for every 5 h increment; results representative of ≥3 replicate experiments. Panels represent the breakdown of strain by group from a single experiment **(A)** Individual WT Sde protein expression restores *Δsde* infection to WT levels. **(B)** Individual Sde expression of ART arginine catalytic residue mutants are unable to restore *Δsde* infection to WT levels. **(C)** Individual Sde expression of ART glutamic acid catalytic residue mutants are unable to restore *Δsde* infection to WT levels.

5.3. Rtn4 ubiquitination requires Sde ART activity.

We next evaluated the role of the Sde ART activity in promoting Rtn4 ubiquitination during *L. pneumophila* challenge of HEK293T cells. As previously described, this was assayed through HA-ubiquitin transfection, followed by *L. pneumophila* challenge, and α-Rtn4 IP. WT *L. pneumophila* infection promoted Rtn4 ubiquitination whereas the *Δsde* mutant was clearly defective (Figure 5.3. Compare WT to vector). Expression of WT SdeB in a *Δsde* background was able to complement Rtn4 ubiquitination, albeit to lower levels, whereas the ART mutant, SdeB R763A, was indistinguishable from a *Δsde* infection, indicating that the ART is required for Rtn4 ubiquitination (Figure 5.3. compare R763A to SdeB WT).

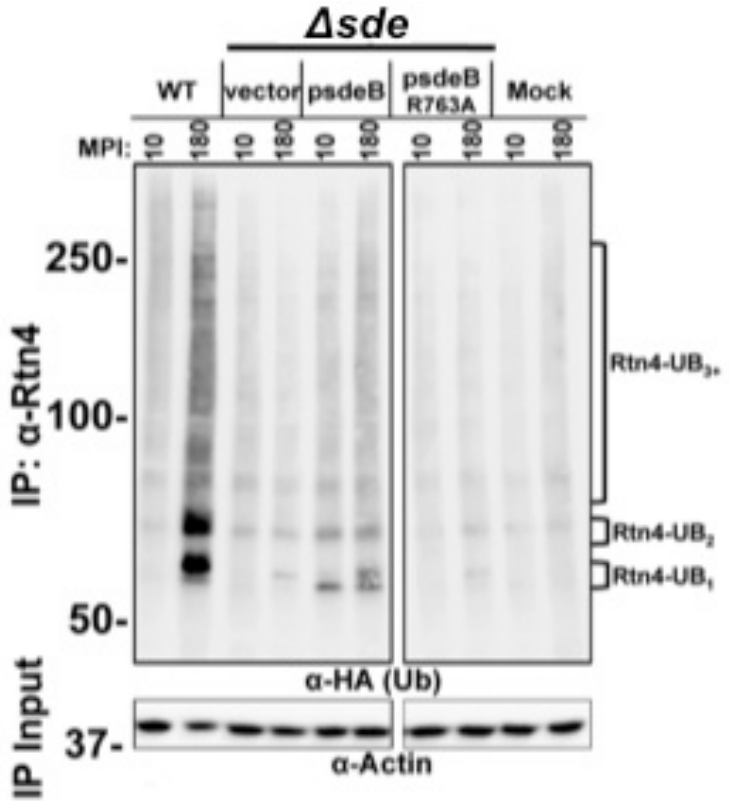

Figure 5.3. Sde family mono ADP-ribosyltransferase activity is required for Rtn4 ubiquitination. HEK293T cells transiently transfected with HA-Ub were challenged with *L. pneumophila*, and extracts were subjected to IP with α-Rtn4. Eluates were analyzed for Rtn4 Ub by probing immunoblots with α-HA. An α-actin immunoblot illustrates comparable protein extract input for the Rtn4 IP.

5.4. Sde proteins transiently ADP-ribosylate host proteins.

We hypothesized that any ADPr modifications were either inefficient or unstable. To address this problem, we devised an ADPr assay that exploited an analogue of β-NAD, ethenoNAD (εNAD)[156,262], in which ADPr of substrates could be monitored by Western blotting with α-ethenoadenosine (α-εAdo)[156,254,262]. To assay for SdeC ART activity directed against mammalian proteins, while simultaneously monitoring cellular ubiquitination changes in response to Sde proteins, recombinant full-length SdeC was incubated with cell extracts and recombinant HA-Ub in the presence of εNAD. A 5 min reaction with either WT SdeC or a DUB-defective derivative resulted in robust laddering of ADPr-substrates, in a pattern reminiscent of polyubiquitin chain laddering (Figure 5.4. α-εAdo, 5 min WT and C118S). By 60min, evidence for the εAdo (ADPr, ADP-ribosylation) signal was greatly reduced, with the only remaining signal being above 250kDa (Figure 5.4. 60 min, WT and C118S). Probing with α-HA revealed that both $SdeC_{WT}$ and $SdeC_{C118S}$ induced robust HA-Ub polymerization, but the Ub polymerization was unchanged over time, unlike the εAdo signal (Figure 5.4. α-HA WT and C118S). In contrast, there was no ADPr or HA-Ub polymerization by the $SdeC_{E859A}$ ART mutant (Figure 5.4. α-εAdo, α-HA). In the absence of HA-Ub, a HMW species above 250kDa was recognized by α-εAdo and this signal disappeared over time (Figure 5.4. α-εAdo, WT-No HA-UB). These results indicate that SdeC promotes ubiquitination of host proteins dependent on the ART domain, and the addition of excess monoubiquitin in the form of HA-Ub enhances the detection of transient ADPr modification of host proteins.

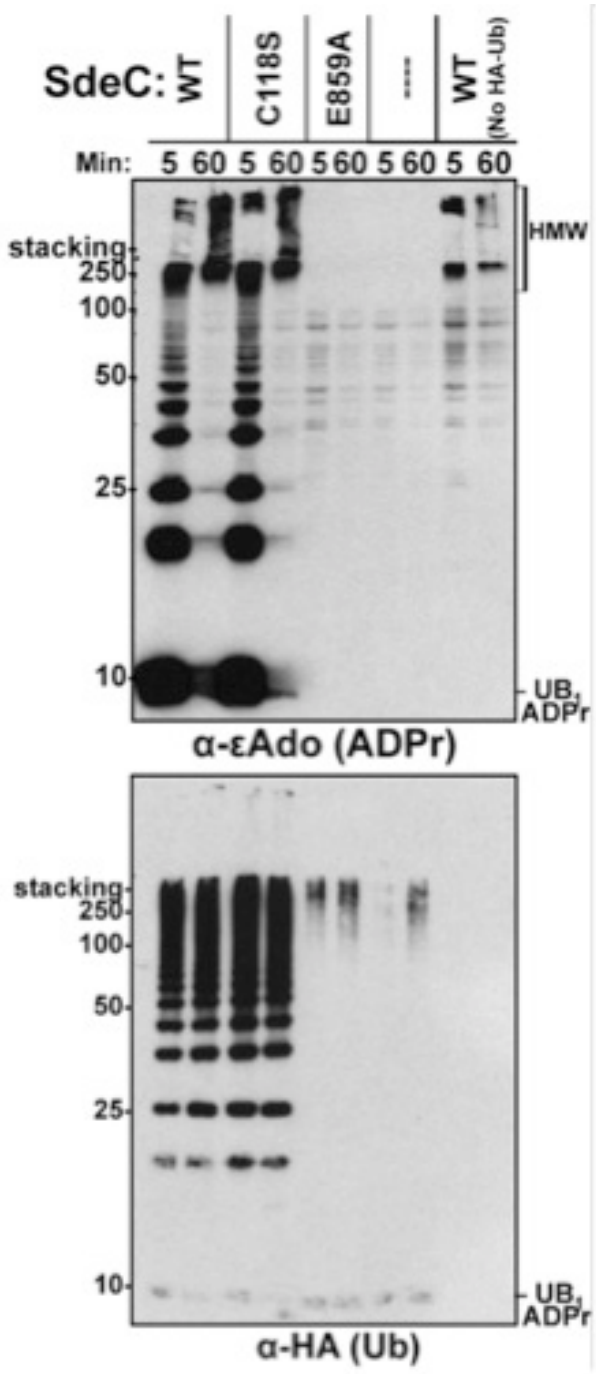

Figure 5.4. SdeC promotes transient ADP-ribosylation of host proteins and persistent HA-ubiquitin polymerization.
HEK293T extract (100μg) was incubated at 37°C for the indicated time with recombinant SdeC (10nM), εNAD (100μM), and recombinant human HA-Ub (20μM). Ubiquitination changes and εADPr were assessed by immunoblot with indicated antibodies. UB_1 ADPr, ADP-ribosylated ubiquitin monomer; HMW, high molecular weight species; stacking, indicates from this line and above represents the SDS-PAGE stacking gel region transferred to the immunoblots. Lanes; WT: WT SdeC; C118S: DUB mutant; E859A: ART mutant; ---: No SdeC; WT(No HA-UB): WT SdeC, No HA-Ub added.

5.5. Antagonistic relationship between Sde ART and DUB domain activities.

We have demonstrated that the Sde proteins modulate ubiquitination through both their ART and amino terminal DUB domain, but the connection between these two activities remains cryptic. To simultaneously analyze ADPr modification and deubiquitination by the SdeC DUB domain, we simplified the εADPr assay by excluding cell extracts and instead using recombinant polyubiquitin chains as a substrate. Recombinant K63, K48, or M1-linked Ub tetramers and εNAD were incubated at 37°C with either $SdeC_{WT}$ or ART deficient mutant $SdeC_{E859A}$. Addition of $SdeC_{WT}$, followed by immediate introduction of SDS buffer to terminate the reaction, resulted in the appearance of a prominent ADP-ribosylated Ub (ADPr-Ub) tetramer regardless of ubiquitin chain linkage (Figure 5.5. 0 min, α-εAdo). This signal was dramatically reduced, however, if incubations were allowed to continue further prior to termination of the reaction (Figure 5.5. 120 min, α-εAdo). This indicates that ADPr modification by SdeC is rapid and transient, explaining why previous studies were unable to detect the modification with full-length protein[396]. The ADPr signal required an intact ART domain, as no εADPr signal was observed in $SdeC_{E859A}$ reactions (Figure 5.5. α-εAdo E859A). The *in vitro* assay also explained why we were unable to detect SdeC DUB activity, as reduced Ub_4 cleavage occurred when SdeC was incubated with εNAD in assays utilizing K63 or K48 tetramers (Figure 5.5. WT, 0-120 min, silver stains). When the assay was repeated using the SdeC ART mutant, the DUB activity was restored with K63-Ub chains and enhanced cleavage of K48-Ub chains (Figure 5.5. E859A, 0-120 min, silver stains). A 120 min incubation of K63-Ub_4 and $SdeC_{E859A}$ resulted in the elimination of Ub_4 and an accumulation of Ub monomer (Figure 5.5. E859A, left panel (K63), silver stain).

Reactions with $SdeC_{WT}$ and K48-Ub tetramers resulted in low levels of Ub_3 and Ub_2 within the first 5 min, but these ratios remain predominantly static through the 120 min incubation. On the other hand, $SdeC_{E859A}$ DUB activity showed a slow progression of K48 Ub cleavage over the course of a 2 hr incubation. This was visualized as a slow increase in Ub_3, Ub_2, and Ub_1 levels over the course of the reaction (Figure 5.5. E859A, middle panel (K48), silver stain). No cleavage was observed with M1-linked ubiquitin tetramers regardless of SdeC ART activity (Figure 5.5. compare WT and E859A left panel (M1/Linear), silver stain). In the presence of WT SdeC, after the initial appearance of an ADPr signal, a slower migrating Ub tetramer appeared relative to the unmodified Ub tetramer (Figure 5.5. Compare WT 0 min or E859A 0-120 min with WT 5-120 min), and this form persisted without a detectable change in migration, even as the ADPr signal disappeared. These migration changes were present across all linkages, but were most visible in K63-Ub_4 reactions (Figure 5.5). These observations are consistent with Ub chains being ADPr-modified by Sde proteins followed by additional processing indicating the Sde family generates ADPr-Ub as reaction intermediate prior to further modification observed as the loss of the εAdo epitope. Furthermore, these experiments demonstrate that the ART activity and/or the subsequent ADPr processing strongly interfere with the deubiquitinase cleavage.

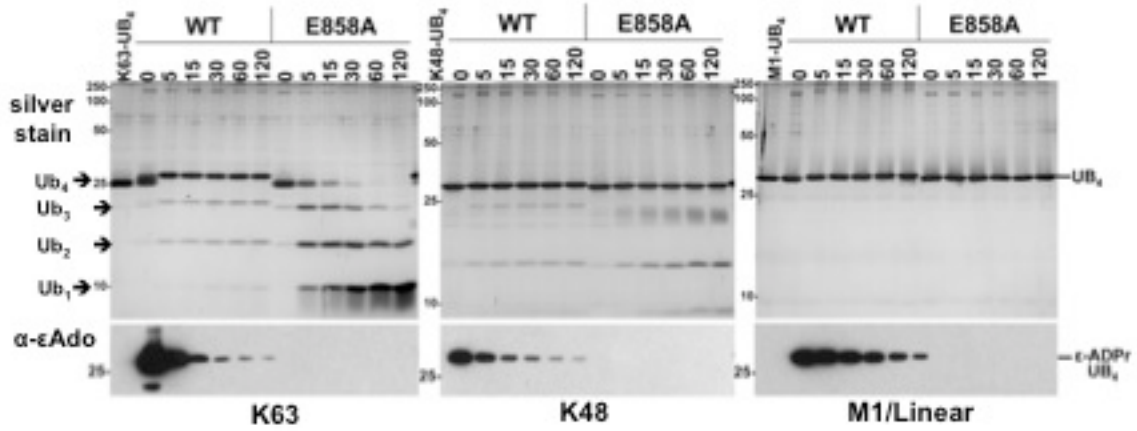

Figure 5.5. SdeC transiently ADP-ribosylates ubiquitin chains and this activity interferes with SdeC DUB activity.

Recombinant SdeC derivatives (20nM) was incubated with K63 (left), K48 (middle), or M1/Linear (right) Ub tetramers (1μM) and εNAD (100μM) at 37°C for the indicated minutes post enzyme addition. Reactions were fractionated by SDS-PAGE, and assayed for altered migration and ADPr of Ub, by silver staining and immunoblotting (α-εAdo). Lanes; WT: WT SdeC; E859A: ART mutant. Arrows indicate Ub tetramers (Ub_4), Ub trimers (Ub_3), Ub dimers (Ub_2), and Ub monomers (Ub_1).

Chapter 6:

Sde family Nucleotidase/Phosphohydrolase domain is required for ER reorganization, intracellular replication in *Dictyostelium discoideum*, and Rtn4 ubiquitination.

This chapter contains excerpts that have previously been published in:
(reprinted with permission of publisher):

Kotewicz KM, Ramabhadran V, Sjoblom N, Vogel JP, Haenssler E, Zhang M, Behringer J, Scheck RA, Isberg RR. Cell Host Microbe. 2017 Feb 8; 21(2):169-181. Epub 2016 Dec 29.

6.1. Sde family Nucleotidase/Phosphohydrolase domain is required for Rtn4 reorganization and intracellular replication in *Dictyostelium discoideum*.

The Sde proteins contain a region between the DUB and ART domains (Figure 4.1. A) with sequence similarity to the *Legionella* IDTS Lem10 (*lpg1496*), which has recently been crystalized by two independent research groups, revealing structural similarities of the domain to nucleotidases and other phosphohydrolases[327,542]. We hypothesized that this nucleotidase/phosphohydrolase (NP) domain could be responsible for processing of ADPr-Ub, resulting in the loss of εAdo, while leaving a modification that retarded Ub migration (Figure 5.5. Left panel (K63), silver stain, α-εAdo). To explore this possibility as well as the potential role of this domain in the Sde associated infection phenotypes, including ER reorganization and Rtn4 ubiquitination, several potential NP catalytic residues in SdeC were selected for site-directed alanine mutagenesis (kindly advised by Kathy Wong who communicated information regarding the Lem10 structure)[542]. The targeted residues were selected based on sequence similarity to the nucleotide-binding pocket in Lem10, and the NP mutants were introduced on plasmids into a *Δsde* background. The SdeC NP mutant $SdeC_{H416A}$ was completely incapable of generating Rtn4 structures associated with the LCV after 1 h challenge, in contrast to the behavior of the $SdeC_{WT}$ derivative, which fully restored Rtn4-LCV association (Figure 6.1, panels A and B).

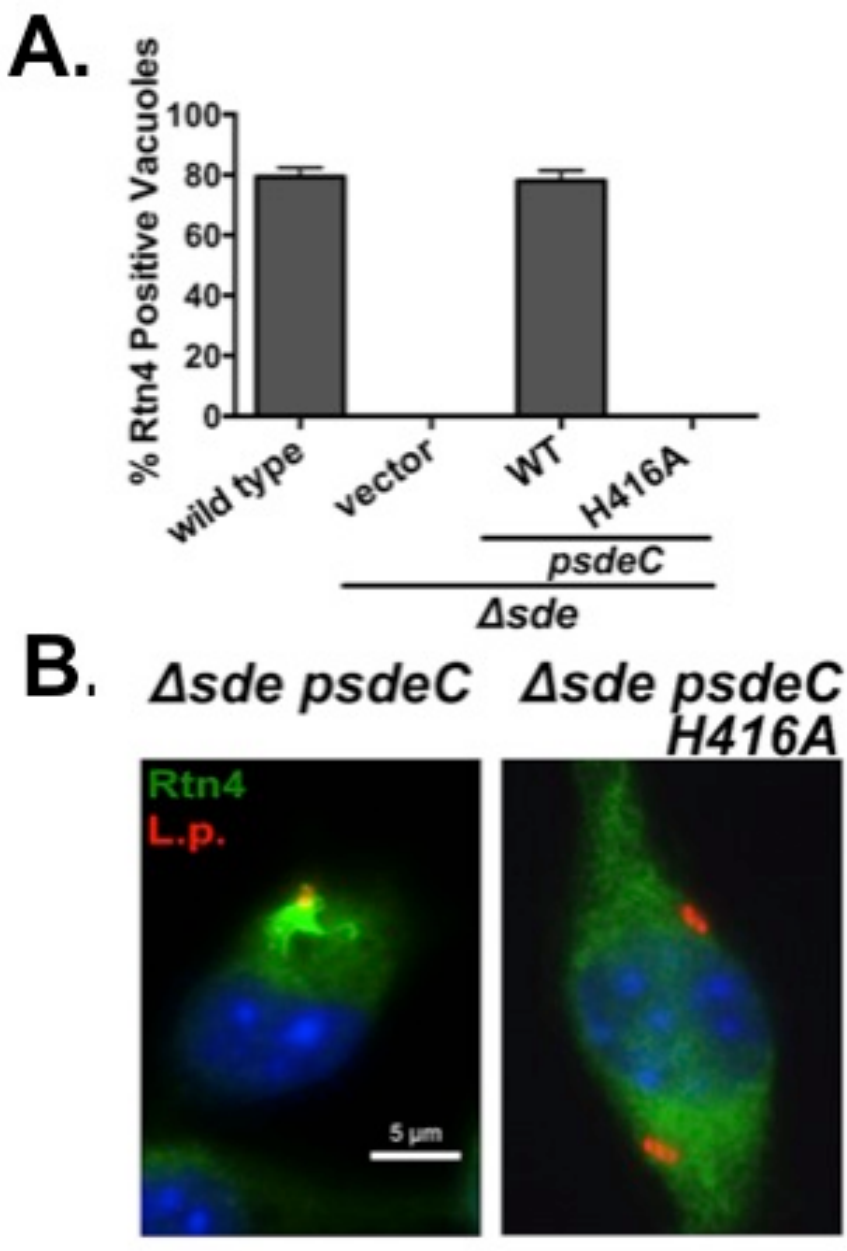

Figure 6.1. Sde family NP domain is required for Rtn4 rearrangements.
(A,B) A/J BMDM were challenged for 1 h followed by fixation, 1% Triton X100 permeabilization, and probed as in Figure 3.3 and 5.1. *L. pneumophila* vacuoles were assessed for Rtn4 colocalization with at least 50 LCV per coverslip and 3 coverslips per condition. **(B)** Representative micrographs of Rtn4 association with the LCV from part A, L.p. (red), α-*L. pneumophila*; α-Rtn4 (green), Reticulon 4b/d; scale bar = 5μm.

To determine if the Sde NP domain was required for promoting intracellular replication in its natural hosts (Figure 5.2.), WT or mutant *L. pneumophila* strains expressing luciferase were used to challenge the amoebal species *Dictyostelium discoideum,* and bacterial replication was monitored over 4-5 days. A plasmid harboring $SdeC_{H416A}$ in a Δ*sde* strain could not restore *L. pneumophila* intracellular growth to levels observed with either the WT or the deletion strain harboring $SdeC_{WT}$. Instead, expression of the SdeC NP mutant more closely mimicked the poor intracellular growth observed with *Δsde* infection (Figure 6.2.). Therefore, the Sde NP domain is required for promoting bacterial replication during amoebal challenge.

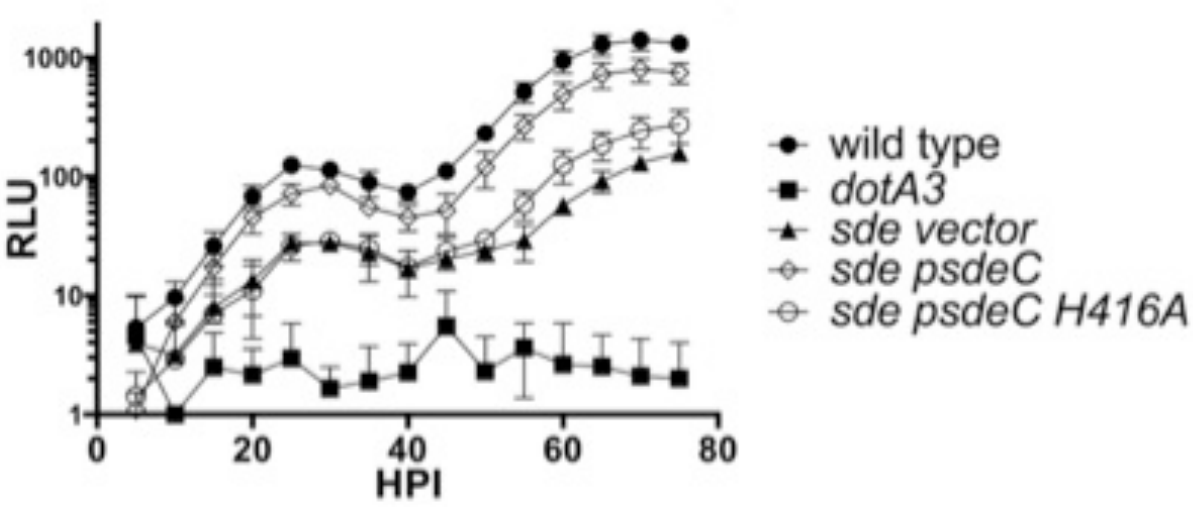

Figure 6.2. Sde NP activity is required for robust intracellular replication in *Dictyostelium discoideum.*
Dictyostelium discoideum was challenged with WT (Lp02) or mutant *L. pneumophila* expressing luciferase (*PahpC::lux*) at an MOI of 0.5 for 2 hrs, then non-internalized bacteria were removed and bacterial replication was monitored for luciferase expression, as a readout for bacterial replication, on a plate reader every hour for the next 4-5 days. Mean ± SEM for every 5 h increment; results representative of ≥3 replicate experiments

6.2. Sde NP activity responsible for transient nature of ADPr modification; NP and ART activity are required for Rtn4 ubiquitination (*in vitro*).

To probe the biochemical role of the NP domain, ADP-ribosylation and Rtn4 ubiquitination changes due to Sde proteins were simultaneously monitored in cell extracts incubated in the presence of recombinant SdeC derivatives. Reactions with $SdeC_{WT}$ produced several altered Rtn4 migration species consisting of ~9kDa incremental shifts, consistent with the addition of one or more Ub moieties being added to the two prominent Rtn4 isoforms, Rtn4b and Rtn4d (Figure 6.3. α-Rtn4). This Rtn4 migration pattern was mimicked in reactions with $SdeC_{C118S}$. Interestingly, both $SdeC_{WT}$ and $SdeC_{C118S}$ reactions had nearly all of the native Rtn4 monomer (50kDa) transformed into the higher migrating Rtn4-Ub species, present within 5 min of SdeC addition (Figure 6.3. α-Rtn4 WT and C118S). After a 1 hr incubation with either $SdeC_{WT}$ or $SdeC_{C118S}$, a notable increase in the amount of native unmodified Rtn4 species reappeared, while the amount of higher order Rtn4 species was noticeably reduced. This signals that either Sde enzymatic activity or undefined enzymes within the cellular extract were removing Sde-mediated Rtn4 modifications regenerating unmodified Rtn4 over the course of the *in vitro* reaction. These higher migrating species of ubiquitinated Rtn4 were not observed in reactions: 1) lacking recombinant SdeC, 2) containing the SdeC ART mutant, $SdeC_{E859A}$, or 3) containing the SdeC NP mutant, $SdeC_{H416A}$ (Figure 6.3, α-Rtn4, ---, E859A, H416A), indicating that the ART and NP domains collaborate to promote Rtn4 ubiquitination *in vitro*. When these reactions were probed with α-εAdo, a HMW ADP-ribosylated species was apparent only in $SdeC_{WT}$ or $SdeC_{C118S}$ reactions that dissipated over a 1 hr incubation (Figure 6.3. WT and C118S). At 5min post SdeC addition, weak

laddering of ADPr proteins was also observed. This may have resulted due to the addition of excess un-tagged Ub monomer (10μM) to the reactions, which supplements the Sde ADPr substrate pool long enough to detect endogenous ubiquitination targeted for Sde-mediated ADP-ribosylation (Figure 6.3. α-εAdo). The $SdeC_{E859A}$ mutant phenotypically mimicked reactions lacking recombinant SdeC, with the residual ADPr signal dependent on endogenous enzymes active within the extract (Figure 6.3. α-εAdo). Strikingly, the NP mutant $SdeC_{H416A}$ construct, which showed no evidence of Rtn4 ubiquitination (Figure 6.3. α-Rtn4) and produced robust stable ADPr of numerous cell extract proteins, including a protein that migrated at the size predicted for Ub (Figure 6.3. α-εAdo at ~9kDa). Therefore, the presence of persistent ADPr modification in the NP mutant negatively correlated with Rtn4 ubiquitination.

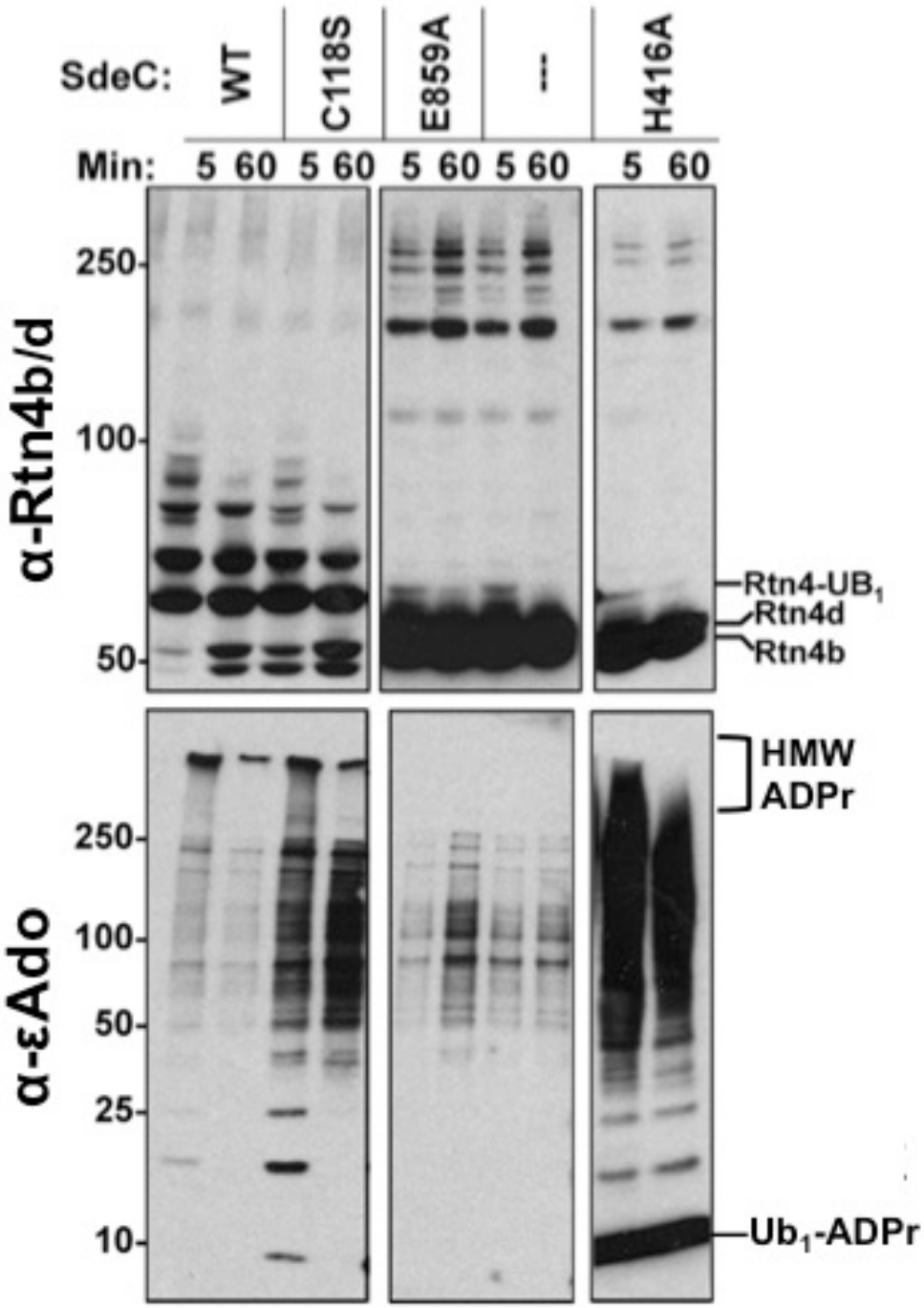

Figure 6.3. Rtn4 ubiquitination requires Sde ART and NP domains, ADP-ribosylation is targeted NP domain.
HEK293T extract (100μg) was incubated at 37°C for the indicated time with recombinant SdeC (20nM), εNAD (100μM), and recombinant human Ub monomer (10μM). Rtn4 Ub and εADPr were assessed after the indicated incubation time by immunoblot with either α-Ado or α-Rtn4.

6.3. Sde DUB Aids in Rtn4 Ubiquitination during *L. pneumophila* infection.

The Sde DUB domain plays a role in the formation of detergent resistant Rtn4 and is important for limiting polyubiquitination at the LCV during the earliest minutes of infection, but it remains unclear why DUB activity would be associated with a bacterial protein that induces Rtn4 ubiquitination. In the *in vitro* ADP-ribosylation and Rtn4 ubiquitination assays with $SdeC_{C118S}$ added, robust Rtn4 ubiquitination occurred, mimicking WT SdeC (Figure 6.3. C118S α-Rtn4). This indicates that under ideal *in vitro* conditions, in which excess exogenous ubiquitin monomer is added, there exists a reaction environment that reveals no DUB domain effect on Rtn4 ubiquitination. We therefore hypothesized that under infection conditions the DUB domain serves to both limit ubiquitin chains (K63) from associating with the LCV and providing a LCV-localized pool of free ubiquitin for use in Sde ubiquitin targets during the earliest stages of infection. We utilized the Sde DUB mutants to determine if Rtn4 ubiquitination occurs independently of this domain during infection by transfecting HEK293T cells with HA-Ub followed by *L. pneumophila* challenge with WT, *Δsde*, and *Δsde* with WT or DUB defective Sde members. Infected cell extracts were then subjected to Rtn4 IP and immunoprecipitates were probed with α-HA to reveal Rtn4 ubiquitination (Figure 2.1 and 4.1). No change in ubiquitination was detectable with *Δsde psdeC-C118S* infection as compared to elutes from *Δsde psdeC* infected extracts, which had previously been shown to induce very low levels of Rtn4 ubiquitination (Figure 6.4 and 4.1, compare vector with pC^{WT} and pC^{C118S}). Since SdeC did not robustly induce Rtn4 ubiquitination, we constructed *Δsde* $psdeB_{WT}$ and *Δsde* $psdeB_{WT}$ strains, both of which efficiently monoubiquitinate Rtn4. Elutes from *Δsde* $psdeB_{WT}$ challenge produce a strong HA (Ub)

doublet, consistent with monoubiquitination of Rtn4b and Rtn4d isoform (Figure 6.4. B, compare *psdeB WT* with *psdeC WT*). A second band corresponding with a second ubiquitination modification was also visible along with a faint HA smear through the higher molecular weights. In contrast, *Δsde psdeB*$_{C118S}$ challenge results in no Rtn4 ubiquitination above the negligible levels observed in a *Δsde pvector* strain infection (Figure 6.4. B, compare *Δsde psdeB*$_{C118S}$ to *Δsde pvector*). The reduction in detergent resistant Rtn4 present at LCVs (Figure 4.1.C,D) and loss of Rtn4 monoubiquitination provides further evidence for the linkage between these two phenotypes associated with Sde family function.

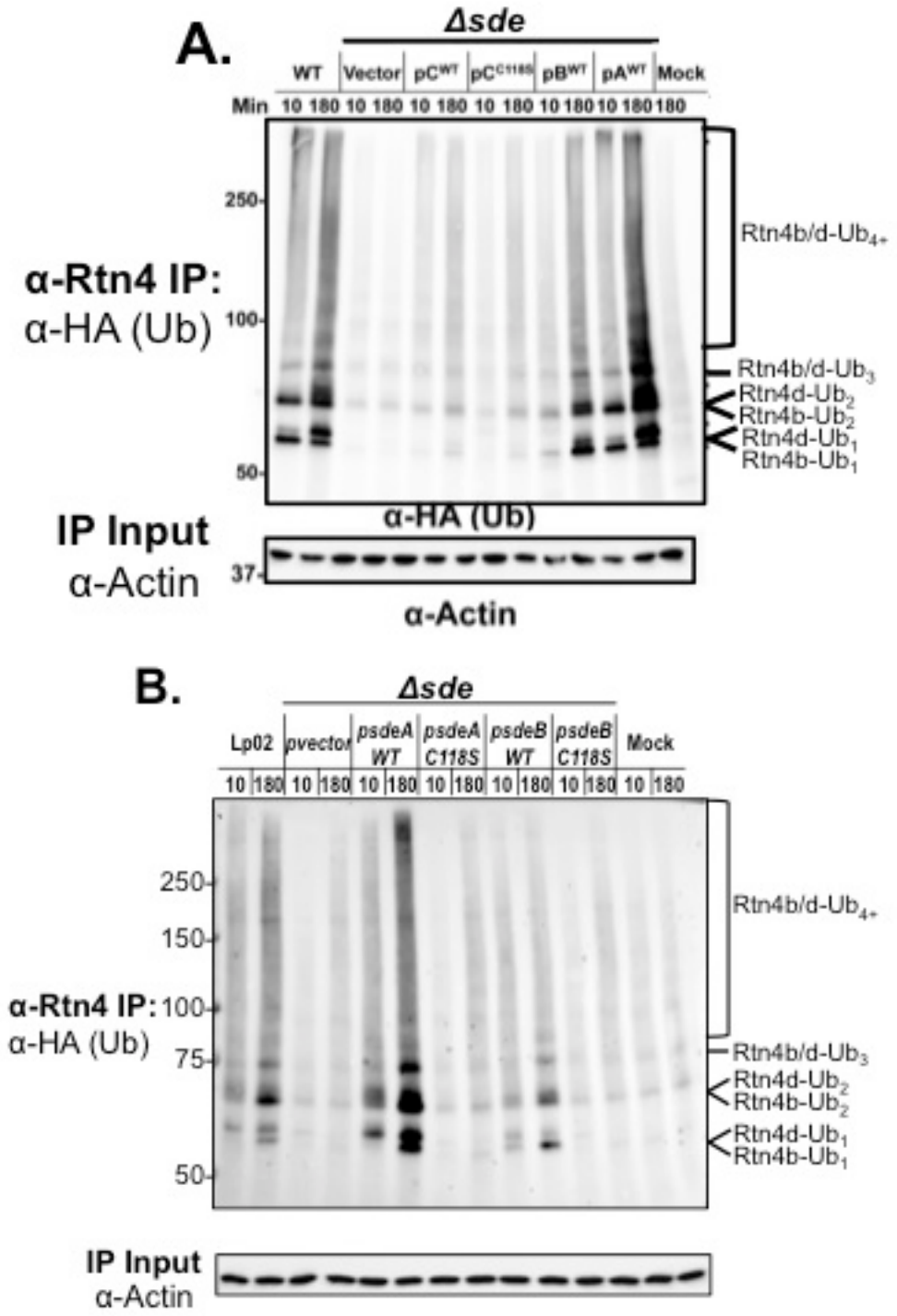

Figure 6.4. Sde DUB activity augments Rtn4 ubiquitination during infection. **(A,B)** HEK293T cells were transiently transfected with HA-Ub for 24 h, the cell culture medium was replaced with 10μM MG132 (Millipore) medium 30-60 min prior to challenge with *L. pneumophila* and the infection was allowed to continue for the indicated time (MPI, minutes post infection) prior to IP with α-Rtn4 and immunoblot of Rtn4 ubiquitination with α-HA. An α-actin immunoblot illustrates comparable protein extract input for the Rtn4 IP.

As the $SdeC_{H416A}$ NP domain mutant appeared to cause accumulation of ADPr-Ub (Figure 6.3), the effect of the NP domain on the modification of Ub was analyzed in an *in vitro* system free of cell extract. $SdeC_{H416A}$ was able to robustly ADP-ribosylate both PolyHis-tagged and untagged Ub over a 60min reaction, with no loss of the εAdo signal (Figure 6.5. α-εAdo). In contrast, WT SdeC showed a weak ADPr-Ub signal after only 1 min, and by 2 hrs the ADPr-Ub signal was undetectable, indicating that the NP activity efficiently removed εAdo (Figure 6.5. α-εAdo). These results indicate that even in the absence of a target to ubiquitinate, both the ART and NP domains collaborate to post-translationally modify ubiquitin, transitioning sequentially from ADPr-Ub to a second modification, which lacks the εAdo epitopes.

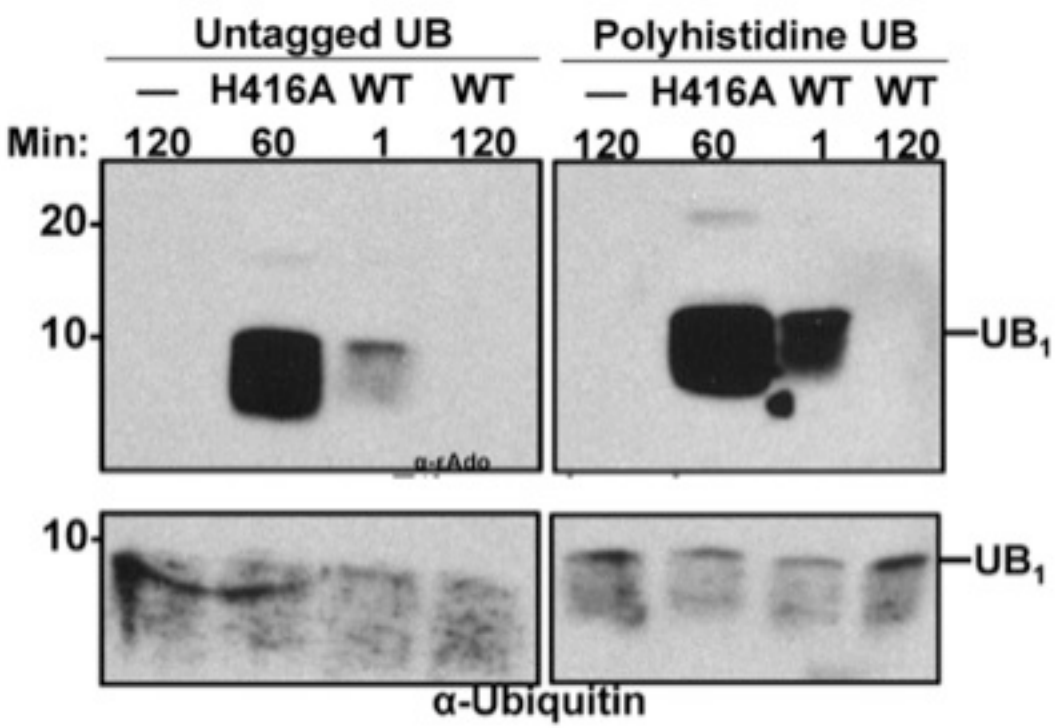

Figure 6.5. ART and NP domains collaborate sequentially to post-translationally modify ubiquitin.
Recombinant Ub or Poly-His-Ub monomers were incubated with εNAD and recombinant SdeC at 37°C for the indicated time. Reactions were terminated by addition of SDS sample buffer and then Ub ADP-ribosylation was assessed by immunoblot.

6.4. Sde proteins covalently polymerize HA-ubiquitin dependent on NP and ART domain and independently of cysteine residues.

In earlier experiments designed to explore the activity of the Sde ART domain, where HA-ubiquitin, cell extracts, εNAD, and recombinant SdeC were combined, resulted in the simultaneous occurrence of a stable HA-ubiquitin polymerization and a transient εAdo signal laddering. This rapid covalent HA-ubiquitin polymerization coupled with its dependence on ART activity suggested this HA-ubiquitin ligation was mediated directly by Sde proteins. To examine this hypothesis, cell extract was excluded from the *in vitro* ADP-ribosylation assay and recombinant SdeC derivatives were incubated with only εNAD and HA-ubiquitin monomers. Anti-εAdo immunoblots of $SdeC_{WT}$ or $SdeC_{C118S}$ reactions mimicked earlier ADPr experiments that had cell extract present (Compare Figure 5.4 and Figure 6.3). The εAdo signal generated a laddering pattern beginning at 10kDa and increasing in ~9kDa increments to between 50-100kDa, while the α-HA blot produced similar laddering within 5 min except the α-HA signal extended beyond 250kDa with a significant increase around 250kDa that may represent ubiquitinated SdeC. The α-HA laddering persisted at 1 hr post SdeC addition, unlike the α-εAdo signal, which was almost completely gone after 1 hr with $SdeC_{WT}$ or $SdeC_{C118S}$ incubation (Figure 6.6. lanes 1-4). $SdeC_{E859A}$ incubation with HA-ubiquitin did not produce any εAdo signal and was unable to polymerize HA-ubiquitin, consistent with ADP-ribosylation of ubiquitin being essential for Ub ligation. Interestingly, this Ub polymerization was only observed with HA-ubiquitin, as no Ub self ligation occurs with untagged recombinant human ubiquitin or PolyHistidine-ubiquitin, indicating this

polymerization was probably due to crosslinking between Ub and a residue on the HA epitope (Figure 6.6).

Ubiquitin ligation classically relies on catalytic cysteine residues and to evaluate Sde proteins ability to serve as a Ub ligase, we individually targeted predominantly cysteine residues that were conserved across Sde proteins for alanine mutagenesis. SdeC C293A was excluded due to previous experiments demonstrating that this alanine mutation had no effect on Rtn4 rearrangements (Figure 4.1. C). Of the seven recombinant cysteine mutant constructs assayed for HA-polymerization, each mutant was still capable of inducing HA-ubiquitin laddering ((special thanks to Kelsey Barraso on assisting with the cloning of cysteine mutants during her 1st year rotation) Figure 6.6. α-HA). Although all of the SdeC cysteine mutants were capable promoting HA-ubiquitin polymerization, there were slight HA-ubiquitin polymerization kinetic differences. $SdeC_{C566S}$ $SdeC_{C617S}$ induced noticeably less HA-ubiquitin polymerization by 5 min when compared to WT or other SdeC cysteine mutants (Figure 6.6. Compare WT to C566S and C617S, 5 min, α-HA). After a 1 hr incubation with $SdeC_{C566S}$ $SdeC_{C617S}$ the level of ubiquitin polymerization was indistinguishable (Figure 6.6. Compare WT to C566S and C617S 60 min α-HA). These same mutant reactions also had lower levels of εAdo signal at 5 min relative to $SdeC_{WT}$ reactions and rather then the εAdo signal disappearing, the amount of protein laddering increased to levels resembling the $SdeC_{WT}$ or $SdeC_{C118S}$ 5 min reactions (Figure 6.6. Compare WT/C118S to C566S and C617S, 5 min, α-εAdo). These mutants suggest that a delay in ADP-ribosylation limits the Ub ligation kinetics, further supporting the idea of ADPr-Ub as an intermediate substrate for Sde mediated ubiquitination.

With SdeC cysteine residues eliminated as the catalytic source of Sde-mediated Ub ligation, we utilized a panel of recombinant SdeC NP mutants in the *in vitro* HA-ubiquitin polymerization assay to probe the effect of this domain on Ub ligation. $SdeC_{R342A}$, $SdeC_{H416S}$, and $SdeC_{R422}$ reactions all produce a conspicuous εAdo signal at ~10kDa and a faint εAdo signal at ~20kDa associated with contaminating Ub dimer, but no Ub polymerization into higher order chains was observed (Figure 6.6. R342A, H416A, R422A α-εAdo). This was confirmed by examining α-HA blots of these reactions in which the only signal present was ~10kDa species consistent with the monomeric HA-Ub (Figure 6.6. R342A, H416A, R422A, α-HA). The other NP domain mutant examined, $SdeC_{H286A}$, produced a α-HA and α-εAdo pattern reminiscent of $SdeC_{C566S}$ $SdeC_{C617S}$, where slower HA-Ub polymerization was associated with persistent ADP-ribosylation. This HA-Ub polymerization appeared extensive by immunoblot and to further inspect this phenomenon a WT SdeC reaction with HA-Ub was examined by silver stain. This revealed that most of the HA-Ub remains monomeric or dimeric in the reaction with only a small fraction of higher order polymers present. The concentration of HA-Ub oligomers dissipated with increasing size, suggesting that the reaction was not very efficient in spite of the fact that the immunoblot appeared to show robust polymerization. These results demonstrate that the NP domain, just like the ART domain, is essential for Sde Ub ligase capabilities.

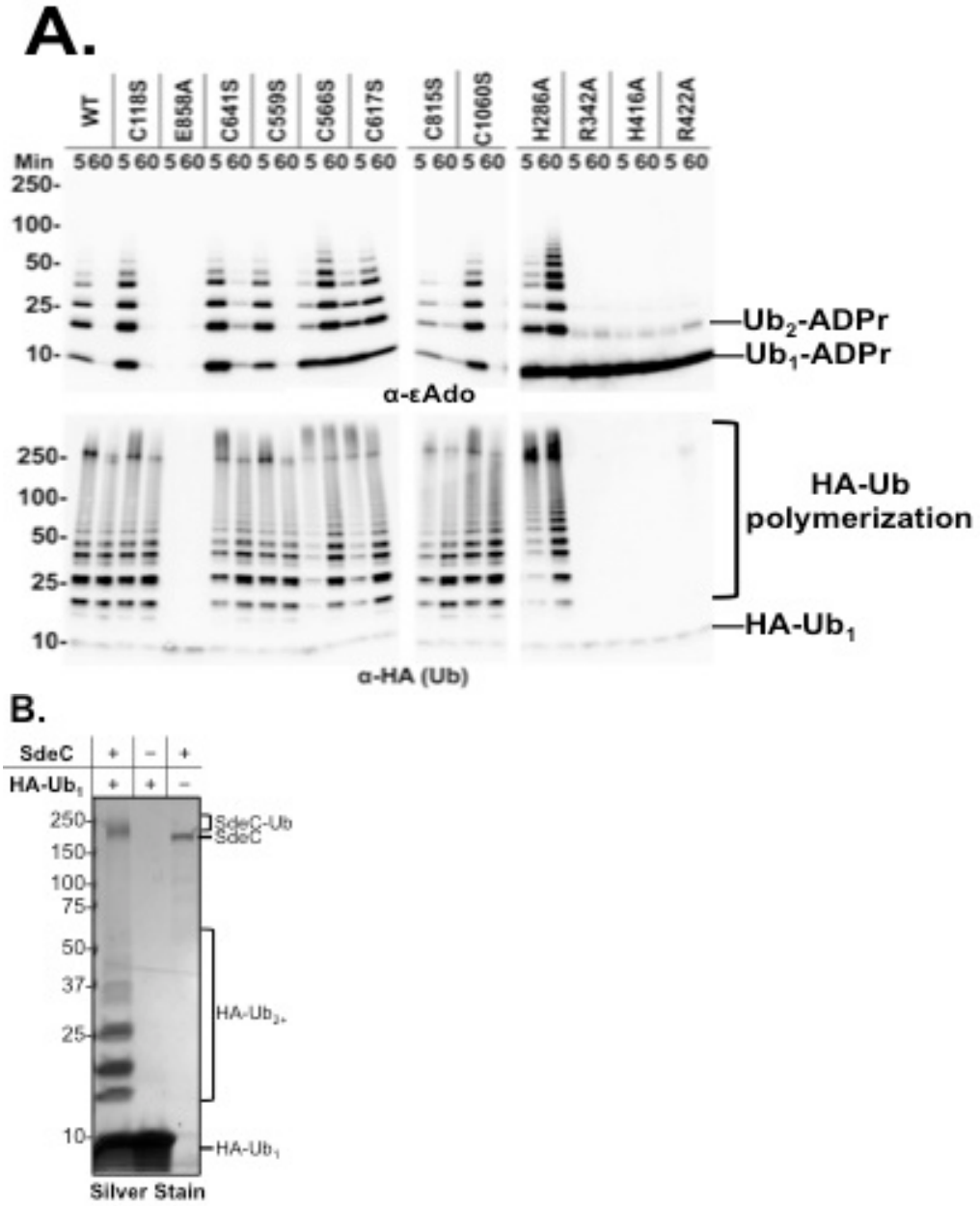

Figure 6.6. SdeC serves as an Ub ligase that promotes HA-ubiquitin polymerization dependent on the ART and NP domain.

(A) Recombinant SdeC derivatives (20nM) were incubated with 10μM HA-ubiquitin and 100μm εNAD at 37°C for 5 to 60 min reactions. After SDS buffer termination, reactions were fractionated with 4-20% SDS-PAGE and probed for α-εAdo (ADPr) and α-HA (Ub). Lanes: WT, $SdeC_{WT}$ 1-1533; C118S, DUB defective SdeC; E859A, ART defective SdeC; C641S/C559S/C566S/C617S/C815S/C1060S, cysteine residues throughout SdeC; H286/R342A/H416A/R422A, NP domain residues of SdeC predicted from Lem10/*lpg1496*[327,542]. **(B)** Recombinant SdeC (20nM) was incubated with HA-Ub (10μM) for 60 min at 37°C, reactions terminated by liquid nitrogen freezing, lyophilization, resuspension in reducing SDS sample buffer, SDS-PAGE fractionation, and silver staining.

6.5. SdeC ubiquitinates Rtn4 in the absence of any other ubiquitin-related enzymes.

To demonstrate that Ub modification of Rtn4 by SdeC occurs catalytically on a natural substrate in the absence of any host components, SdeC derivatives were incubated with a 20X molar excess of GST-Rtn4 in the presence or absence of εNAD. Impressively, within 1 hour, nearly the entire Rtn4 population was mono- or multi-ubiquitinated, with resulting species migrating ~8k – 24kDa larger than GST-Rtn4, and no detectable modification of unfused GST (Figure 6.7. A-C). Upon closer inspection of the modified Rtn4 species using a 5% acrylamide gel to generate more separation of the 70+ kDa Rtn4 products, reveals between 6-8 Rtn4 modification species (Figure 6.7. D,E). Ubiquitination of Rtn4 required both the NP and ART domains, as neither $SdeC_{H416A}$ nor $SdeC_{E859A}$ could promote any Rtn4 ubiquitination (Figure 6.7. E859A, H416A). The loss of either NP or ART activity, however, could be overcome by mixing the two mutant proteins together in the presence of GST-Rtn4, with extremely efficient ubiquitination after 1 hr (Figure 6.7. E859+H416A). These results are consistent with ADPr-Ub being a substrate of the SdeC NP domain, in which trimming of ADPr and transfer of Ub to Rtn4 requires the NP activity.

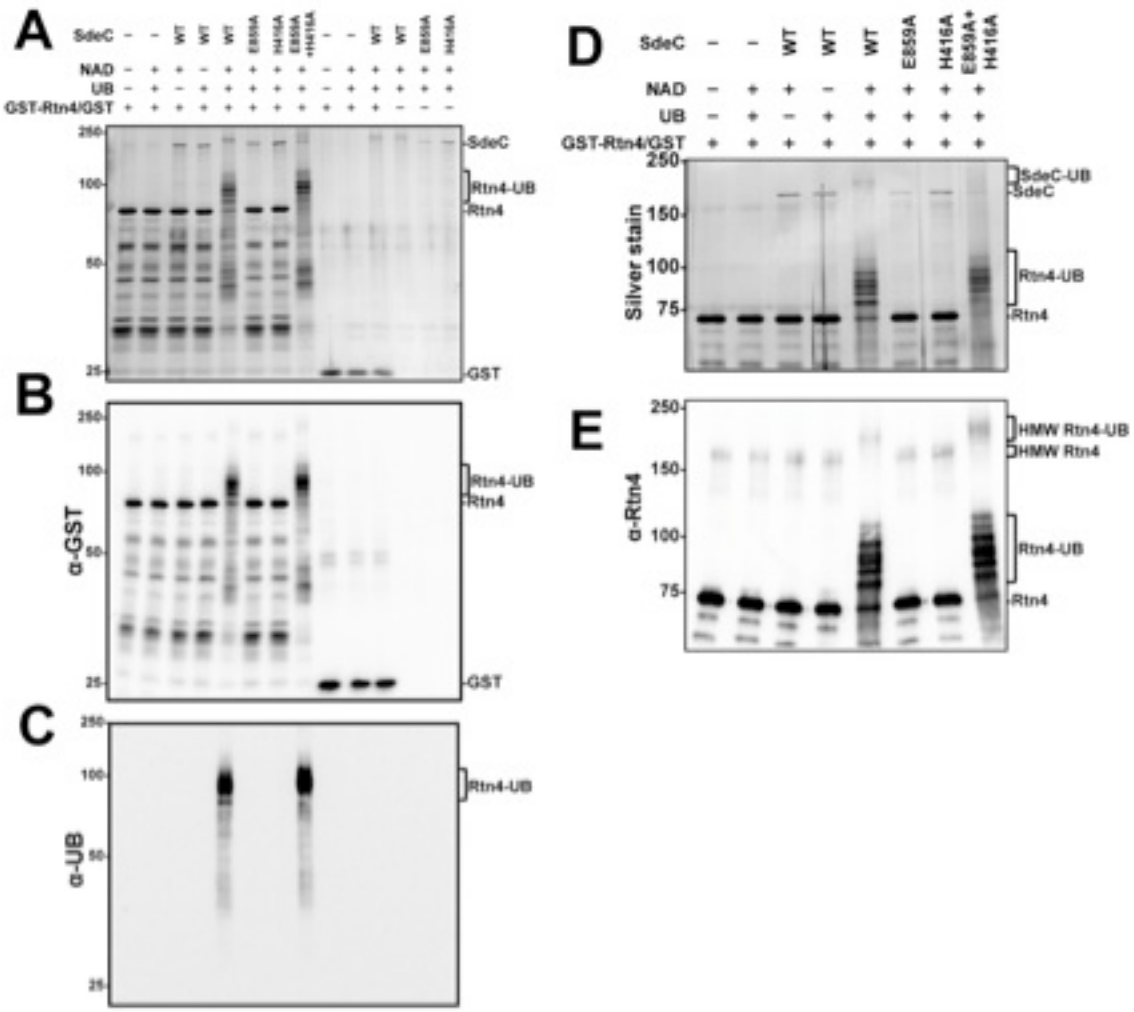

Figure 6.7. *In vitro* SdeC ubiquitinates Rtn4 dependent on ART and NP activity, but independent of other Ub factors.
GST-HA-Rtn4 or GST was incubated at 37°C for 1 h with SdeC, εNAD and recombinant human Ub monomer. Reactions were separated by 10% SDS-PAGE and assessed for altered Rtn4 migration by **(A)** silver stain or immunoblot for **(B)** α-GST and **(C)** α-Ub. **(D,E)** Reactions were separated by 5% SDS-PAGE to examine each altered Rtn4 migration event by **(D)** silver staining and **(E)** immunoblot for α-Rtn4. Lanes: -, No SdeC; WT, wild-type SdeC; E859A, SdeC ART inactive; H416A, NP inactive. 20nM SdeC derivatives added.

6.6. Sde ubiquitination pathway requires the sequential enzymatic activity of the ART and then the NP domain.

The evidence above suggests that the ART and NP domain of Sde proteins collaborate to modify ubiquitin and facilitate Ub ligation to a substrate protein, such as Rtn4 or ER associated Rabs[396]. The experiments above do not distinguish between Sde-mediated ubiquitination being a result of enzymatic ligation or generation of a reactive ubiquitin byproduct that undergoes non-enzymatic glycation of Ub to a substrate protein through a Maillard-like reaction. To distinguish between these possibilities, recombinant SdeC, SdeA, or SdeC mutants were conjugated to Ni-NTA resin and incubated with ubiquitin monomers and εNAD. After a 2 hr incubation, the Sde resin was removed and the ubiquitin/εNAD mixture was incubated for an additional hour with GST-HA-Rtn4b and additional recombinant Sde proteins, if indicated (post resin), and monitored for Rtn4-ubiquitination by SDS-PAGE fractionation and silver staining (Figure 6.8.A). When recombinant SdeC (WT) or SdeA was pre-incubated with Ub in the presence of εNAD+, and then the modified Ub was separated from SdeC conjugated beads and incubated with GST-HA-Rtn4b, no ubiquitination was observed (Figure 6.8, panel A; panel B, lane 5,7; panel C, lane 4). Ubiquitin pre-incubation in the presence of εNAD+ with SdeC ART (E859A), NP (H416A), or a combination of both mutants, followed by Sde resin removal and Rtn4b incubation with the Ub mixture, similarly did not promote ubiquitination (Figure 6.8, panel A; panel B, lane 8-10). In contrast, when SdeC or SdeA was incubated directly with GST-HA-Rtn4b in the presence of Ub and εNAD+, 6-8 Rtn4b ubiquitination species arose as well as several ubiquitinated SdeC forms (Figure 6.8, panel A; panel B, lane 6; panel C, lane 5). These results are strong evidence that a glycated Ub form is not the precursor for transfer of Ub to Rtn4.

The ubiquitination pattern observed after SdeC/A_{WT} and Rtn4 co-incubation was reproduced by reactions in which $SdeC_{H416A}$ (ART active/NP defective) was pre-incubated with Ub to induce Ub-ADPr and then transferred to a reaction with $SdeC_{E859A}$ (ART defective/NP active) and GST-HA-Rtn4b present (Figure 6.8, panel B, lane 12). In contrast, the reverse incubation sequence, pre-incubation of $SdeC_{E859A}$ (ART defective/NP active) with Ub followed by transfer to a mixture with $SdeC_{H416A}$ and GST-HA-Rtn4b (ART active/NP defective) was unable to promote any Rtn4 or SdeC ubiquitination. Therefore, these results argue strongly that ADPr-Ub serves as the substrate for the NP domain to transfer Ub to the Rtn4 target (Figure 6.8, panel B, lane 11).

We next asked if the Ub modification that is left after Sde mediated processing of Ub-ADPr could serve as a substrate for Sde-mediated Ub conjugation, just as ADP-ribosylated ubiquitin does (Figure 6.8, panel B, lane 12). To assay for this, $SdeC_{WT}$ was pre-incubated with Ub_1 and εNAD, then SdeC was removed and GST-HA-Rtn4b was added to the Ub mixture with fresh $SdeC_{WT}$, $SdeC_{E859A}$, or $SdeC_{H416A}$ added. In reactions in which fresh $SdeC_{WT}$ or $SdeC_{E859A}$ was added in the post incubation step, very little SdeC and Rtn4b ubiquitination were observed, consistent with the $SdeC_{WT}$ pre-incubation terminally modifying nearly the entire Ub population, preventing it from serving as a substrate for SdeC-mediated ligation to Rtn4b (Figure 6.8, panel D, lane 8,9). When the modified Ub was then incubated with $SdeC_{H416A}$ and Rtn4 (the post step), absolutely no Rtn4 ubiquitination was visible, consistent with the NP domain being required for ADPr processing and Ub ligation (Figure 6.8, panel D, lanes 10). If this were not the case, we would have expected to see similar weak Rtn4 ubiquitination as in the previous two

reactions, in which fresh $SdeC_{WT}$ or $SdeC_{E859A}$ was added in the presence of Rtn4b. There was no evidence of substrate competition limiting Rtn4b ubiquitination in reactions that used resin-immobilized $SdeC_{H416A}$ or $SdeC_{E859A}$ in the pre-incubation step, with $SdeC_{WT}$ present in the post reaction, consistent with either Ub or ADPr-Ub serving as acceptable Sde ligation substrates (Figure 6.8, panel D, lane 11,12). Using these substrates, the reactions had robust Rtn4b ubiquitination reminiscent of Rtn4b co-incubation with WT SdeC (Figure 6.8. panel D, lanes 11,12 vs. 7).

To further demonstrate that Rtn4b ubiquitination results from SdeC enzymatic activity, rather then a non-enzymatic glycation we increased the incubation time of the Sde_{WT}-modified Ub with Rtn4b, as glycation reactions kinetics can vary[345,494]. GST-HA-Rtn4b was incubated with native Ub or $SdeC_{WT}$ modified Ub for 18 hrs at 37°C in the presence or absence of fresh SdeC. After 18 hrs with native Ub and GST-HA-Rtn4b in a reaction, no ubiquitination was detected, but a increase in the amount of Rtn4 dimers and trimers was visible as a faint wide band at ~150 and ~225kDa (Figure 6.8. panel D, lane 15). The same result was observed when modified Ub ($SdeC_{WT}$ Pre-incubation) was incubated with Rtn4b for 18 hrs in the absence of SdeC. If unmodified Ub was incubated with Rtn4 in the presence of $SdeC_{WT}$ for 18hrs, Rtn4 ubiquitination was observed, but at notably reduced levels compared to a 1 hr $SdeC_{WT}$ incubation with Rtn4b (Figure 6.8, panel D, compare lane 16 with 7 or 13[control reaction present within same gel]). These experiments demonstrate that there is a sequential ubiquitin modification pathway catalyzed in which the ART domains acts to modify Ub, while the NP domain acts as the transferase that uses the modified Ub as the substrate for transfer to Rtn4.

We further investigated the kinetics of Sde mediated Rtn4 ubiquitination using this simple recombinant protein *in vitro* system consisting of GST-HA-Rtn4b, SdeC, Ub_1, and εNAD. We previously observed the disappearance of higher order ubiquitinated Rtn4 species over time in reactions with cell extract and recombinant SdeC. This suggested to us that Sde proteins might be able to remove their own Ub modification to substrate proteins (Figure 6.8, $SdeC_{WT}$ or $SdeC_{C118S}$ at 0 vs. 60 min). To further probe this concept, we co-incubated GST-HA-Rtn4b and $SdeC_{WT}$ at either 20nM or 200nM in the presence of εNAD and monitored the kinetics of Ub addition and potential Ub removal in an *in vitro* system. At either concentration of SdeC assayed, Rtn4b ubiquitination was extremely rapid, as evidenced by notable Rtn4b monoubiquitination in 20nM SdeC reactions and high levels of multi-ubiquitinated Rtn4b in reactions with 200nM of SdeC for the period of time necessary to add enzyme and immediately quench reactions with SDS (Figure 6.8, panels E, F, 0 min). Strikingly, in reactions with 20nM of SdeC, a reduction in higher order Rtn4 ubiquitinated species could be detected by the reappearance of native Rtn4b within 15 min post enzyme addition (Figure 6.8, panel E, 15 min). These higher order Rtn4-Ub species collapsed back down to primarily native and monoubiquitinated Rtn4 at the conclusion of an18 hr incubation. This same highly rapid appearance and progressive disappearance of ubiquitinated Rtn4 species was observed in reaction with 200nM SdeC. These higher enzyme concentrations also revealed that the SdeC ubiquitination followed a nearly identical pattern as Rtn4 ubiquitination. First, SdeC ubiquitinated species appear rapidly, then slowly disappeared with time (Figure 6.8. panel F, SdeC-Ub 0 vs. 18hr). These experiments demonstrate the

highly active nature of the Sde proteins and their ability to both conjugate and deconjugate their own post-translational modification.

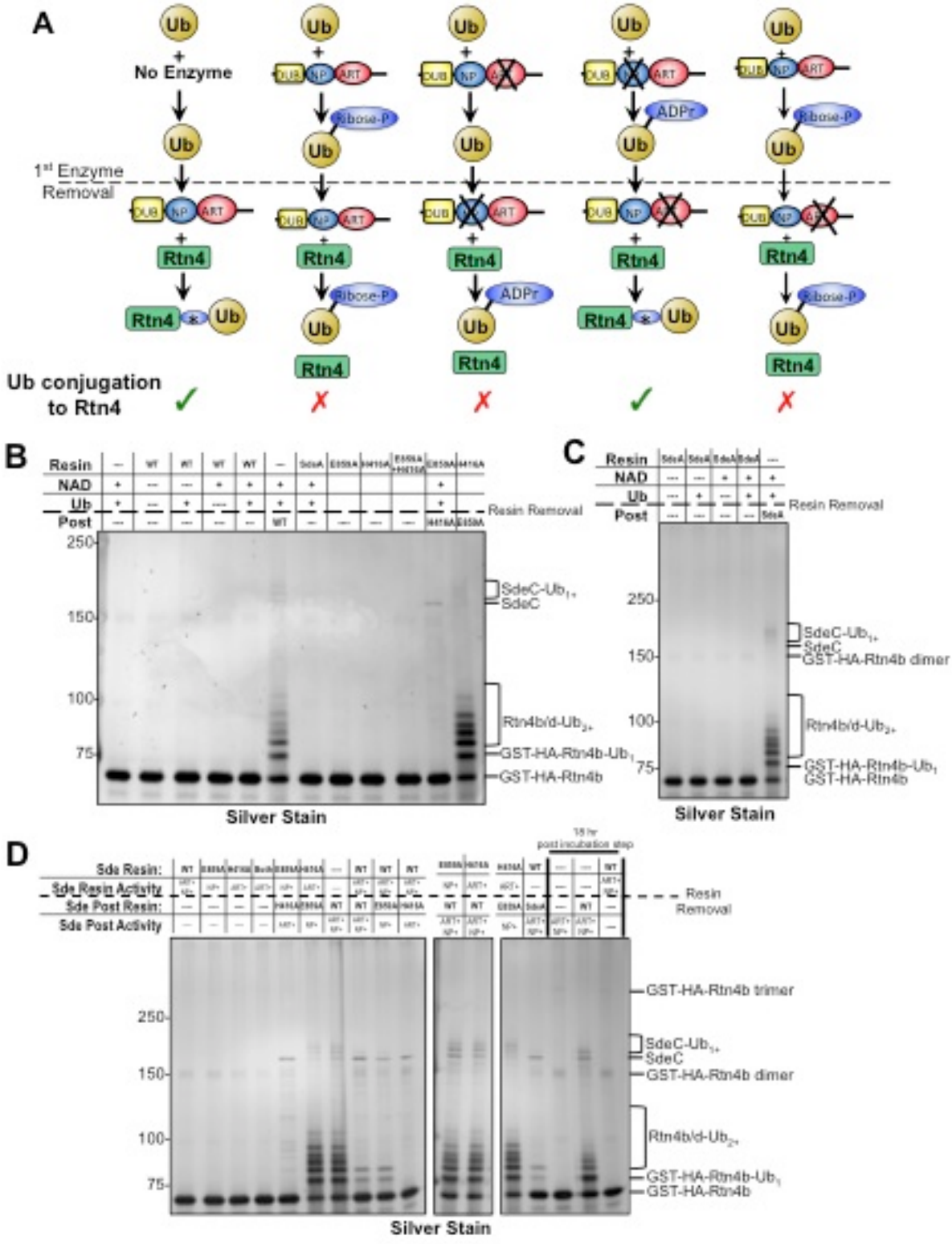
A
No Enzyme
1st Enzyme Removal
Ub
DUB
NP
ART
Ribose-P
ADPr
Rtn4
Ub conjugation to Rtn4
B
Resin
NAD
Ub
Post
Resin Removal
SdeC-Ub1+
SdeC
Rtn4b/d-Ub2+
GST-HA-Rtn4b-Ub1
GST-HA-Rtn4b
Silver Stain
C
Resin
NAD
Ub
Post
Resin Removal
SdeC-Ub1+
SdeC
GST-HA-Rtn4b dimer
Rtn4b/d-Ub2+
GST-HA-Rtn4b-Ub1
GST-HA-Rtn4b
Silver Stain
D
Sde Resin:
Sde Resin Activity
Sde Post Resin:
Sde Post Activity
Resin Removal
GST-HA-Rtn4b trimer
SdeC-Ub1+
SdeC
GST-HA-Rtn4b dimer
Rtn4b/d-Ub2+
GST-HA-Rtn4b-Ub1
GST-HA-Rtn4b
Silver Stain

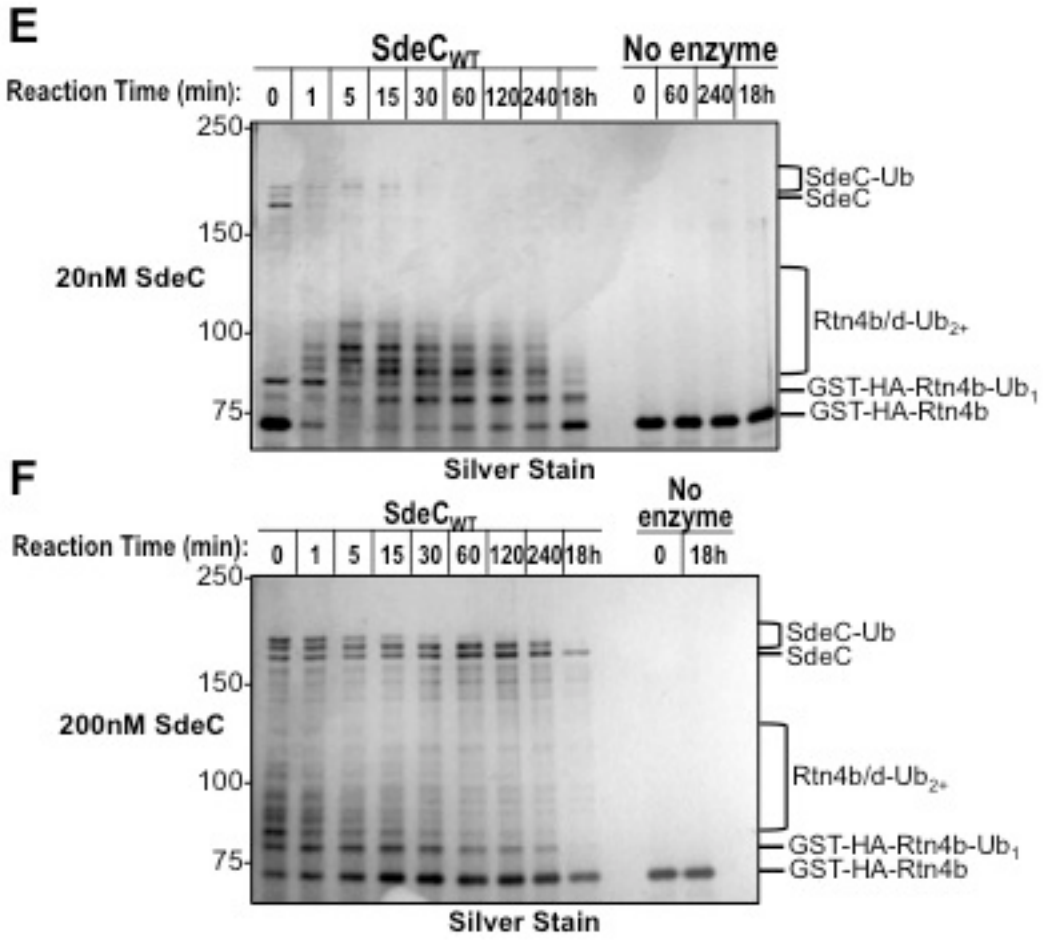

Figure 6.8. ***In vitro*** **SdeC ubiquitinates Rtn4 dependent on sequential ART then NP activity.**
(A) Schematic diagram of sequential *in vitro* reactions showing the indicated Ub modification status at each phase along with whether reactions were sufficient to ubiquitinate Rtn4. **(B-D)** SdeC derivatives (20nM) were conjugated to Ni-NTA resin and then incubated at 37°C for 1 h with εNAD (100μM) and recombinant human Ub monomer (10μM). SdeC resin was removed and the Ub mixture combined with GST-HA-Rtn4b and fresh enzyme where indicated below the dotted line in the 'Post' or 'Sde Post Resin' section. Reactions were separated by 5% SDS-PAGE and assessed for altered Rtn4 migration by silver stain. Lanes: -, No SdeC; WT, wild-type SdeC; E859A, SdeC ART inactive; H416A, NP inactive. 20nM SdeC derivatives added. **(E-F)** Recombinant $SdeC_{WT}$ (20 or 200nM) was incubated with Ub_1 (10μM), GST-HA-Rtn4b (400nM), and εNAD (100μM) for the indicated time and reactions were separated by 5% SDS-PAGE and assessed for altered Rtn4 migration by silver stain.

6.7. A Sde-promoted biochemical pathway leads to ribose-monophosphate modified ubiquitin.

Our results argue that Ub conjugation to Rtn4 by the Sde family is a consequence of covalent ADPr modification of Ub followed by enzymatic processing of the ADPr modification and ultimately Ub ligation to targets. To understand the nature of the transient Ub-modified intermediate and its apparent trimming, monomeric Ub was incubated with SdeC derivatives in the presence of εNAD and analyzed by liquid chromatography-mass spectrometry (LC-MS). In the absence of SdeC, the molecular mass of monomeric Ub was 8564.57 Da, but after 1 h incubation with the $SdeC_{H416A}$ mutant, ≥90% of Ub population increased by a mass of 565.05 to 9129.62 Da (Figure 6.5. and Figure 6.9. A), consistent with a single εADP-ribose moiety added. Incubation of $SdeC_{WT}$ with Ub, on the other hand, resulted in ≥90% of the Ub population converted to 8776.5 Da (Figure 6.5. and Figure 6.9. A). This 212 Da mass increase is consistent with ribose-monophosphate modification of Ub, as a consequence of cleavage at the diphosphate bridge between adenosine and ribose (Figure 6.9. A, B). Therefore, in the absence of a Ub recipient, the ART domain recognizes and modifies Ub, followed by diphophohydrolase processing to ribose-monophosphate by the NP domain (Figure 6.9. B). The proposed reaction is similar to a subset of nucleotidases that show diphosphohydrolase activity toward ADPr-modified proteins[100,367].

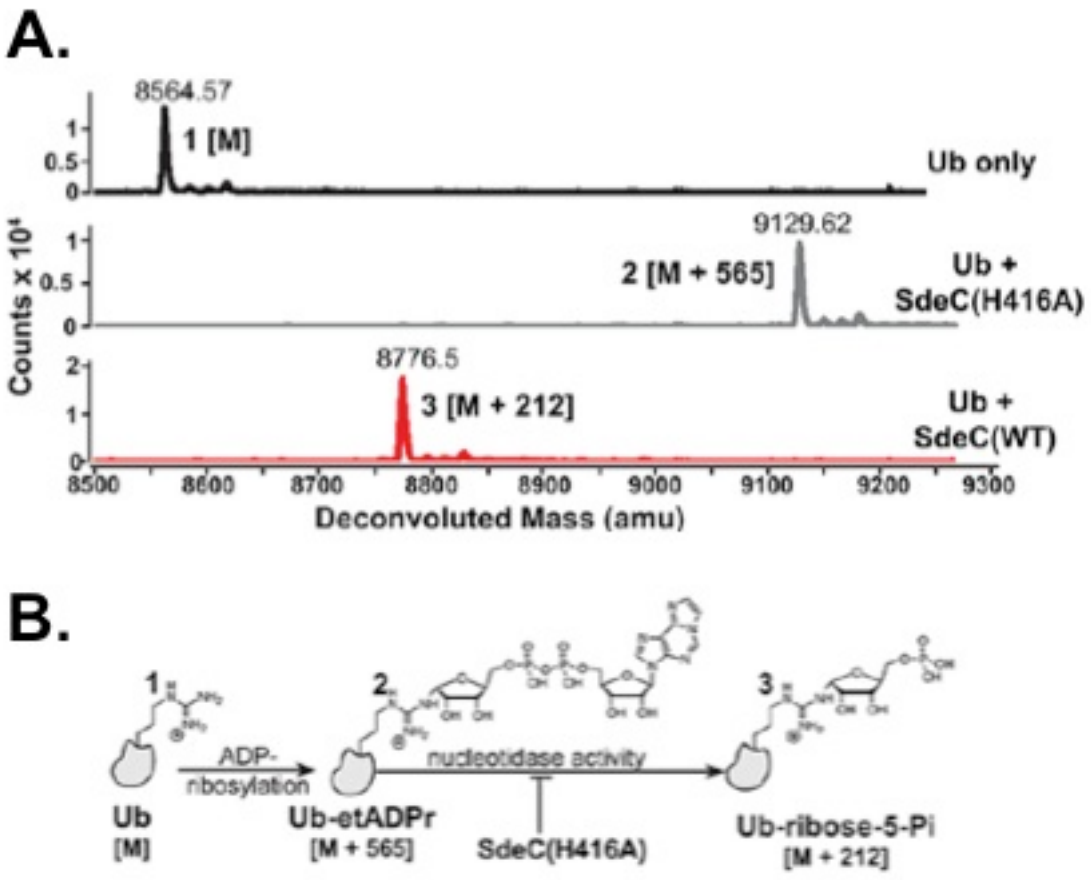

Figure 6.9. ART and diphosphohydrolase-dependent ribose-monophosphate modification of Ub.
(A) Recombinant Ub was incubated with $SdeC_{WT}$ (bottom panel) or without SdeC (top panel) for 120 min or for 60 min with $SdeC_{H416A}$ (middle panel), then subject to LC-MS analysis and the deconvoluted masses of the peaks for each sample displayed. $SdeC_{WT}$ reaction results in a modification of 212 amu. [M] = mass of native Ub; Ub (black), No SdeC present; SdeC((H416A) grey), SdeC ART active, NP defective; SdeC((WT) red) wild type SdeC, ART active NP active. Sample verification, see Figure 6.5., recombinant Ub or poly-His-Ub monomers were incubated with εNAD and recombinant SdeC derivatives at 37°C for the indicated time. Rtn4 Ub and εADPr were assessed by SDS-PAGE fractionation and immunoblot with indicated antibodies. **(B)** Proposed pathway to generated modification of 212 amu.

6.8. Both Sde mediated ADP-ribose and ribose monophosphate modification to ubiquitin occurs at R42.

To determine if the final reaction product is found on Ub residue R42[396], as predicted by diphosphohydrolase action on R42-εADP, the modified Ub species were gel extracted, subjected to trypsin/AspN double digestions and analyzed by liquid chromatography-tandem mass spectrometry (LC-MS/MS). The double digestion generated a 10 amino acid fragment with an expected m/z(+2) = 694.334 for the ribose-monophosphate modified form, and m/z(+3) = 580.91 for the εADPr modified form (5ure 6.10. A, B). When extracted ion chromatograms (XIC) were analyzed for the m/z(+2) expected for the ribose-monophosphate modified form, only Ub incubated with $SdeC_{WT}$ could generate significant amounts (Figure 6.10. A). Similarly, XIC from the m/z(+3) predicted for the εADPr modified Ub fragment showed that only the diphosphohydrolase mutant $SdeC_{H416A}$ could generate significant levels of this product (Figure 6.10. B).

To gain further evidence for a diphosphohydrolase activity, Ub was incubated with $SdeC_{WT}$ for two hours, and then treated with alkaline phosphatase (AP) to remove the predicted phosphate group. The +212 Da modification by SdeC was reduced to a +132 Da modification (Figure 6.10. C, Ub+SdeC+AP), predicted for phosphatase processing to simple ribose (Figure 6.10. D). Therefore, in the absence of a ubiquitination substrate, the ART and diphosphohydrolase collaborate to promote phospho-ribosylation of Ub.

To conclusively demonstrate the proposed biochemical pathway, the AspN/trypsin 10 amino acid fragment spanning R42 was subjected to b- and y-ion analysis after LC-MS/MS. If the ribose-monophosphate modification occurs on R42, beginning with the b_4 ion, each of the successive ions should have an increase in mass of

+212.01 (Figure 6.10. E, noted as $R^{\#}$). We were able to identify ions with high resolution that matched the predicted b_4 through b_9 ions, each with the expected mass increase (Figure 6.10. E). In addition, we were able to identify an ion predicted to be the intact peptide with neutral loss of the modification (Figure 6.10. E, m/z=588.330), which has been observed in ribose phosphate-modified peptides previously[367]. Therefore, SdeC ART activity, followed by diphosphohydrolase processing of ADPr occurs on the R42 residue.

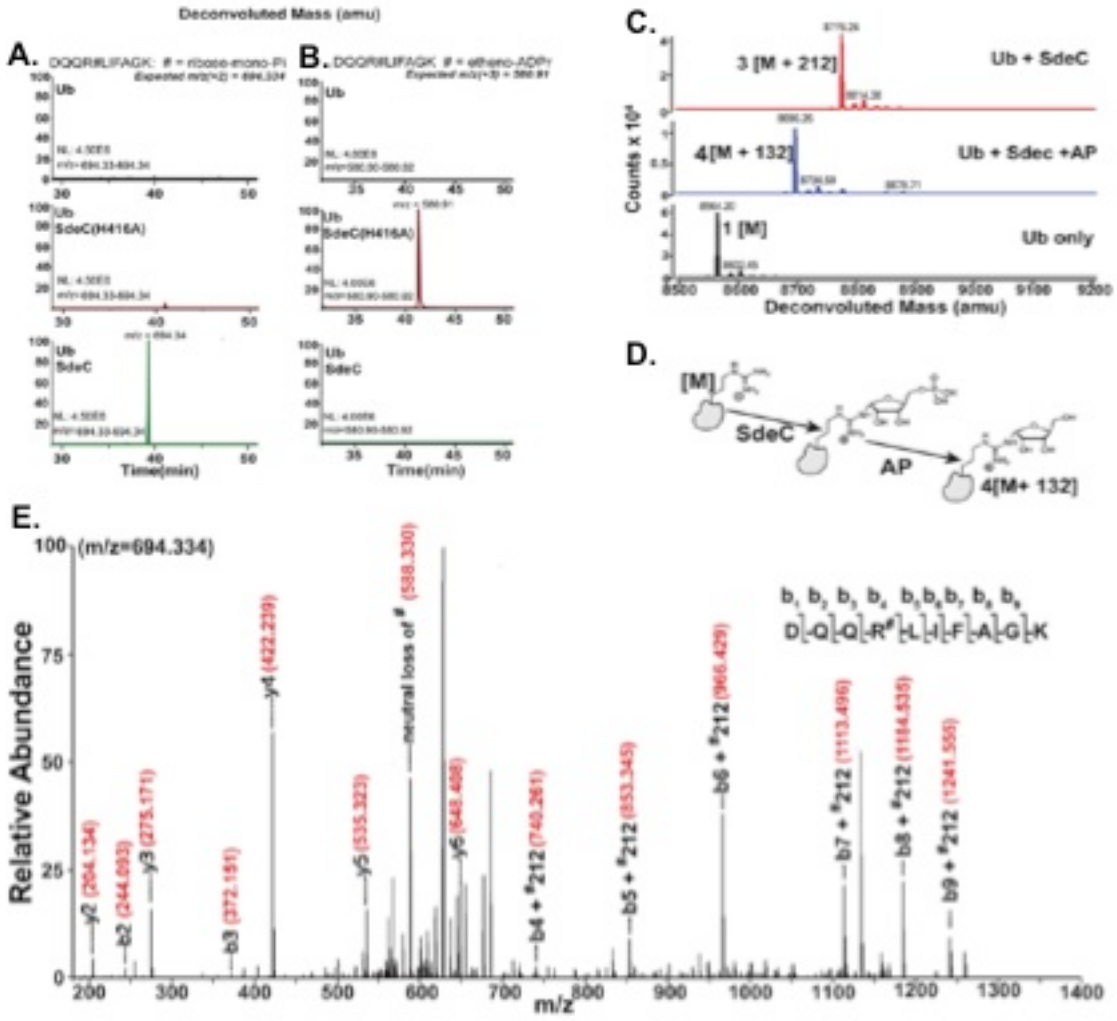

Figure 6.10. Sde ART and phosphohydrolase activity both target Ub at arginine 42 (R42).

(**A,B**) Trypsin/AspN treatment of modified Ub species followed by extracted ion chromatography (XIC) analysis reveals predicted modifications. Shown are XIC chromatograms of species having displayed m/z values for both major modifications displayed in panel B. (**C**) Treatment of species 3 with alkaline phosphatase results in a product predicted for ribosylated Ub. Ub was treated with noted enzymes, followed by LC- MS, and the deconvoluted masses of the peaks for each sample are displayed. (**D**) Likely products that lead to the generation of 132 amu modification. (**E**) Electrospray ionization MS/MS spectrum of trypsin/AspN Ub fragment having +212 amu modification resulting from SdeC treatment. The b-type ion fragments are displayed above the trypsin/AspN peptide that has an increase of 212.01 amu over the predicted size of the unmodified Ub peptide. Each predicted b-type ion was identified and displayed along with identified y-type ion fragments. Ions marked #212 denote fragment sizes that correspond to the predicted b-type ions having an added 212 amu. Panels **(A,B,E)** LC-MS/MS was performed a Harvard Medical School by Ross Tomanino; Meng Zhang preformed sample prep for panel **(C)** with analysis and LC-MS assistance from Nicole Sjoblom and Rebecca Scheck.

Chapter 7:

Evidence that Sde modification of Ub elicits a hyper-ubiquitination response at the LCV, and inhibits host autophagy

7.1. Sde ADP-ribosylation of ubiquitin induces rapid hyper-ubiquitination of the LCV.

To further understand the effect of Sde modification of host Ub with either ADP-ribose or phosphoribose on ubiquitin levels at the LCV, we monitored polyubiquitination intensity and kinetics at the LCV during the first hours of infection in macrophages. A/J BMDMs were challenged with *L. pneumophila* and *Δsde* strains expressing SdeC ART and NP mutants at an MOI = 1 for 0, 10, 20, or 60 min, then LCV polyubiquitin was monitored with the α-FK1 antibody that specifically detects conjugated polyubiquitin. As previously observed, very little polyubiquitin is associated with the LCV early in WT infection and no polyubiquitination was observed in a T4SS defective mutant during the first hour (Figure 7.1, panel A, Lp02, Lp03). This indicates that the LCV ubiquitination present at the LCV in this early infection phase results from the T4SS and its IDTS. Without the Sde family, more than 40% of the LCVs were polyUb positive as early as 0 MPI compared with nearly none in a WT infection (Figure 7.1, panel A, compare Lp02 with *Δsde pvector*). Expression of plasmid encoded SdeC was able to reduce the percentage of polyUb positive LCVs throughout the first hour of infection (Figure 7.1, panel A *Δsde pvector*). Again, this polyUb reduction was dependent on the Sde DUB domain, as the expression of Sde DUB mutant, $SdeC_{C118S,}$ was unable to reduce polyUb levels and mimicked or rose above levels observed in *Δsde* challenge. The polyUb increase observed in *Δsde psde*C_{C118S} above *Δsde* during the first hour would be expected, as expression of the DUB mutant SdeC remove an important source of Ub removal. Furthermore, we have shown the Sde DUB mutants are still completely capable of acting as a Ub ligase *in vitro*, indicating that this SdeC mutant is still actively ubiquitinating

host proteins during infection. We do not believe Sde-mediated ubiquitination is recognized with the polyUb antibody, as nearly all experimental evidence points indicates Sde proteins promote monoubiquitination or multi-monoubiquitination as the primary PTM to ubiquitin.

Infection of BMDMs with the NP SdeC mutant, $SdeC_{H416A}$, would be expected to ADP-ribosylate Ub chains and monomers around the LCV, but be unable to serve as a Ub ligase itself. In addition, although this mutant is DUB competent, I would predict from my results in Chapter 5 that this mutant would still be incapable of removing polyUb chains if the chains were modified as rapidly as they were during the *in vitro* ADP-ribosylation coupled with DUB cleavage assays (Figure 5.5). Expression of plasmid encoded SdeC NP mutant, $SdeC_{H416A}$, resulted in more than 70% of LCVs being polyUb positive within 10 min, and this level was maintained through the first hour (Figure 7.1. A). The percentage of polyubiquitinated LCVs was similar to $SdeC_{C118S}$ levels at 20 and 60 MPI, but there was a significant increase in the ubiquitin intensity observed at LCVs in $SdeC_{H416A}$ infections (Figure 7.1 B). Using Volocity software, 15-25 polyUb positive LCV images were selected and analyzed for Ub intensity around the LCV above background levels in each cell. Measurements of polyUb intensity at individual LCVs from *Δsde psdeC*$_{H416A}$ infections were associated with significantly higher levels of polyUb when compared against LCVs from *Δsde psdeC*$_{WT}$, *Δsde psdeC*$_{C118S}$, *Δsde psdeC*$_{E859A}$, or the very few polyUb positive LCVs we captured during a WT infection (Figure 7.1. B). This high intensity hyper-polyubiquitination observed at the LCVs during *Δsde psdeC*$_{H416A}$ infections was temporally stable within the first hour, as comparing polyUb intensity between 20 min and 60min showed no significant differences (Figure

7.1. C). These observations taken together indicate the dramatic effect the Sde proteins can have on ubiquitination of the LCV. Furthermore, the SdeC NP mutant reveals that limiting Sde family's activity to ADP-ribosylation of Ub induces a robust, rapid, and sustained ubiquitination of the LCV, likely a host Ub response to Sde activity.

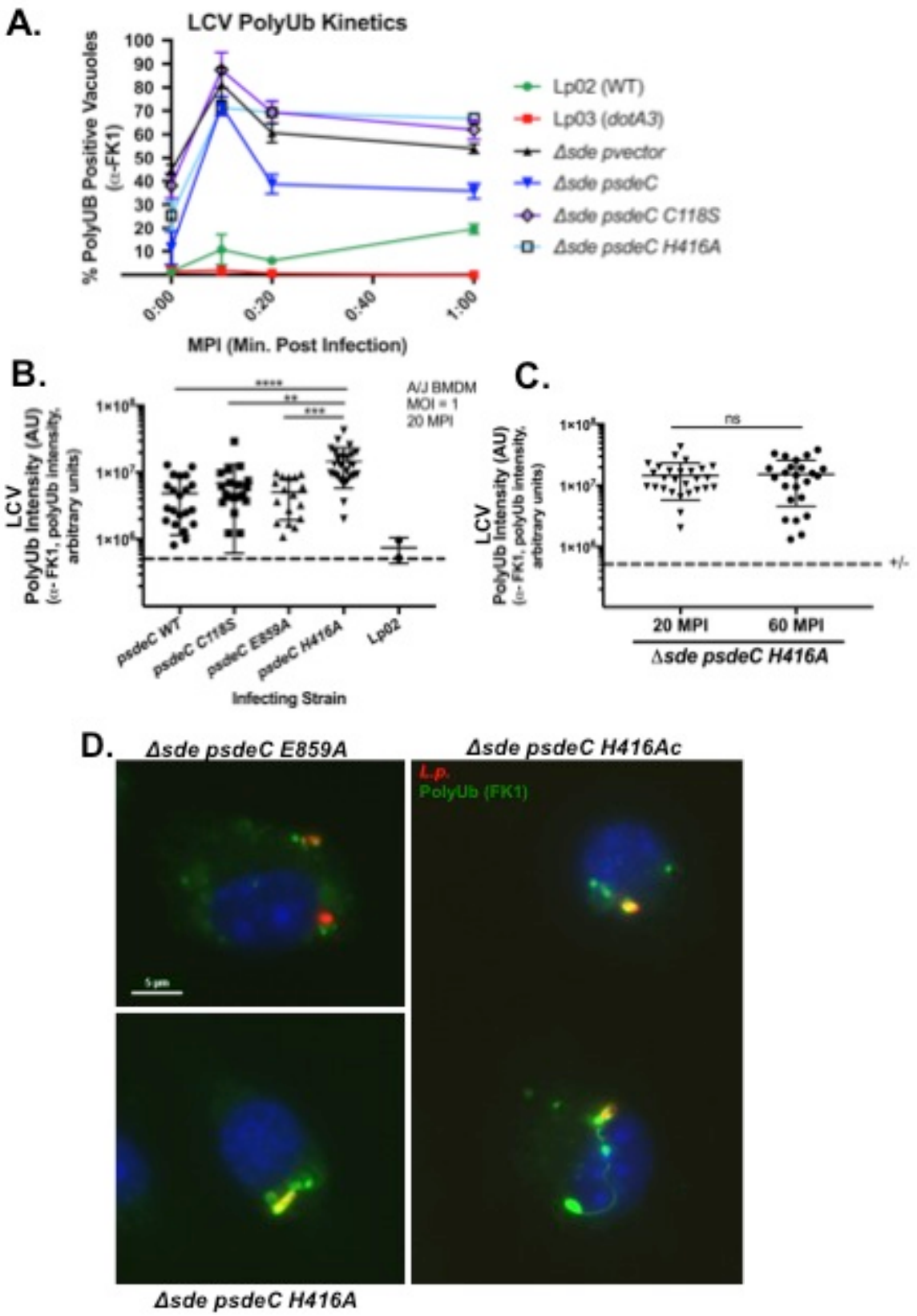

Figure 7.1. SdeC NP mutant, which ADP-ribosylates ubiquitin and cannot serve as Ub ligase, induces hyper-polyubiquitination of LCV.

(A) BMDMs from A/J mice were challenged at an MOI =1 for indicated infection time (post the 5 min centrifugation of bacteria onto BMDMs) with denoted *L. pneumophila* strain, followed by fixation, permeabilization with 1% Triton X100 and probing with α-polyUb, α-*L. pneumophila*, and Hoechst. **(B)** PolyUb intensity was measured by selecting 14x12μM oval around a single *L. pneumophila* vacuole and then enumeration of signal above background within the selected region. **(C)** PolyUb intensity was measures as in part B and intensity was quantitated for LCVs of *Δsde psdeC*$_{H416A}$ at either 20 or 60 MPI. **(D)** Representative immunofluorescent images of LCV after 20 MPI in BMDM, as described in (A). Wild type, Lp02; *dotA3,* T4SS defective or an *icm*/*dot*-; *Δsde*, *ΔsidE ΔsdeC ΔsdeB-A* or *Δlpg0234 Δlpg2153 Δlpg2156-2157* (KK099); *Δsde psdeC*$_{WT}$, SdeC WT (DUB+/ART+/NP+); *Δsde psdeC*$_{C118S}$, SdeC DUB mutant (DUB-/ART+/NP+); *Δsde psdeC*$_{E859A}$, SdeC ART (DUB+/ART-/NP+); *Δsde psdeC*$_{H416A}$, SdeC WT (DUB+/ART+/NP-). Scale bar=5μM.

7.2. Sde modification of polyUb (ADPr-Ub or Phosphoribose-Ub) inhibits deubiquitinase cleavage.

Post-translational modifications of Ub are known to significantly alter protein-protein interactions and signaling cascades[242,244,261,358,361,491,534]. We showed previously that SdeC modification of Ub tetramers with εADPr or ribose phosphate interfered with the SdeC DUB activity (Figure 5.5.), consistent with these Sde-mediated Ub PTMs also acting to inhibit host DUBs during infection[51,207,534]. Both ADP-ribose and phosphoribose modifications would serve as large bulky charged PTMs on Ub chains[100,272]. These PTMs of Ub could serve to disable or perpetuate particular host signaling pathways by making existing chains impervious to cleavage[51,194,534]. To test this hypothesis, polyUb chains were modified by SdeC$_{WT}$ or SdeC$_{H416A}$ to generate phospho-ribosylated polyUb or ADP-ribosylated polyUb, respectively, which was then incubated with a panel of eukaryotic DUBs or the SdeC DUB domain, and Ub cleavage efficiency was then assessed after a 2 hr incubation with the DUBs. SdeC derivatives (1μg) were adsorbed to resin for 1 hr at 4°C, then incubated with either K63 or K48 polyUb$_{3-7}$ (2μg) for 2 hrs at 37°C to promote Ub modification, then SdeC resin was removed, and polyUb$_{3-7}$ was then incubated with

either 1) human recombinant PolyHistidine-otubain 1, isoform 1 (100nM); 2) recombinant USP2 catalytic domain (CD) 259-605 (50nM); 3) recombinant PolyHistidine-CYLD (50nM); or 4) recombinant SdeC DUB CD (1-192, 50nM at 37°C for 2 hr. Cleavage was monitored by immunoblot comparison of the polyUb staining after incubation with SdeC derivatives or a no enzyme control against the polyUb staining after a 2 hr incubation with a DUB. In the absence of SdeC modification, the linkage non-specific DUB, USP2 CD, efficiently cleaves K63 into Ub dimer and monomer (Figure 7.2. Top panels, no enzyme resin, ---). Although the K48-polyUb chains stained less efficiently with α-UB, K48 cleavage was also observed by the disappearance of the higher order polyUb chains (Figure 7.2. Top left pane, no enzyme resin, ---). Curiously, modification of $polyUb_{3-7}$ with either phosphoribose or ADP-ribose enhanced α-Ub immunoblot staining making comparisons across different reactions more challenging (Figure 7.2. Within any panel, compare 0, no enzyme, ---, with either 0, H416; 0, WT; 0, C118S). The K63-specific DUB CYLD and the K48-preferential DUB Otubain-1 efficiently cleaved their preferred Ub chains and showed minor cleavage of their low efficiency substrates (Figure 7.2. No enzyme resin CYLD-K48 or Otubain-1-K63). When $polyUb_{3-7}$ was incubated with $SdeC_{H416A}$, $SdeC_{WT}$, or $SdeC_{C118S}$ beads to produce ADPr-polyUb or phosphoribose-polyUb, cleavage was severely impaired, regardless of the DUB utilized. The only evidence of Ub cleavage in Sde-modified Ub reactions was a slight reduction in the largest polyUb chains present above ~40kDa, which may result from some Ub within a chain escaping Sde-mediated modification. DUB inhibition occurred for both the K48 and K63 $polyUb_{3-7}$ linkages assayed. Cleavage of Sde-modified polyUb by the SdeC DUB fragment displayed a similar pattern to USP2, in

which cleavage of both K63 and K48 polyUb occurred on unmodified ubiquitin, but this DUB activity was almost completely eradicated by either ADP-ribose ($SdeC_{H416A}$) or phosphoribose ($SdeC_{WT/C118S}$) modifications (Figure 7.2, bottom panels, SdeC 1-192, compare no enzyme resin with $SdeC_{H416A}$, $SdeC_{WT}$, or $SdeC_{C118S}$). Regardless of DUB species origin or specificity, the ability of Sde proteins to generate either of two PTMs on polyUb has the potential for strongly interfering with host DUBs and stabilizing poly-Ub chains about the LCV. This model is consistent with the data presented in Fig. 7.1, which argued strongly for the NP and ART partners to enhance poly-Ub localization. It should be noted that Dikic and coworkers have hypothesized that Sde-mediated modification of Ub interferes with poly-Ub formation, but their model is inconsistent with the infection data presented here, and supported by the *in vitro* DUB inhibition assays.

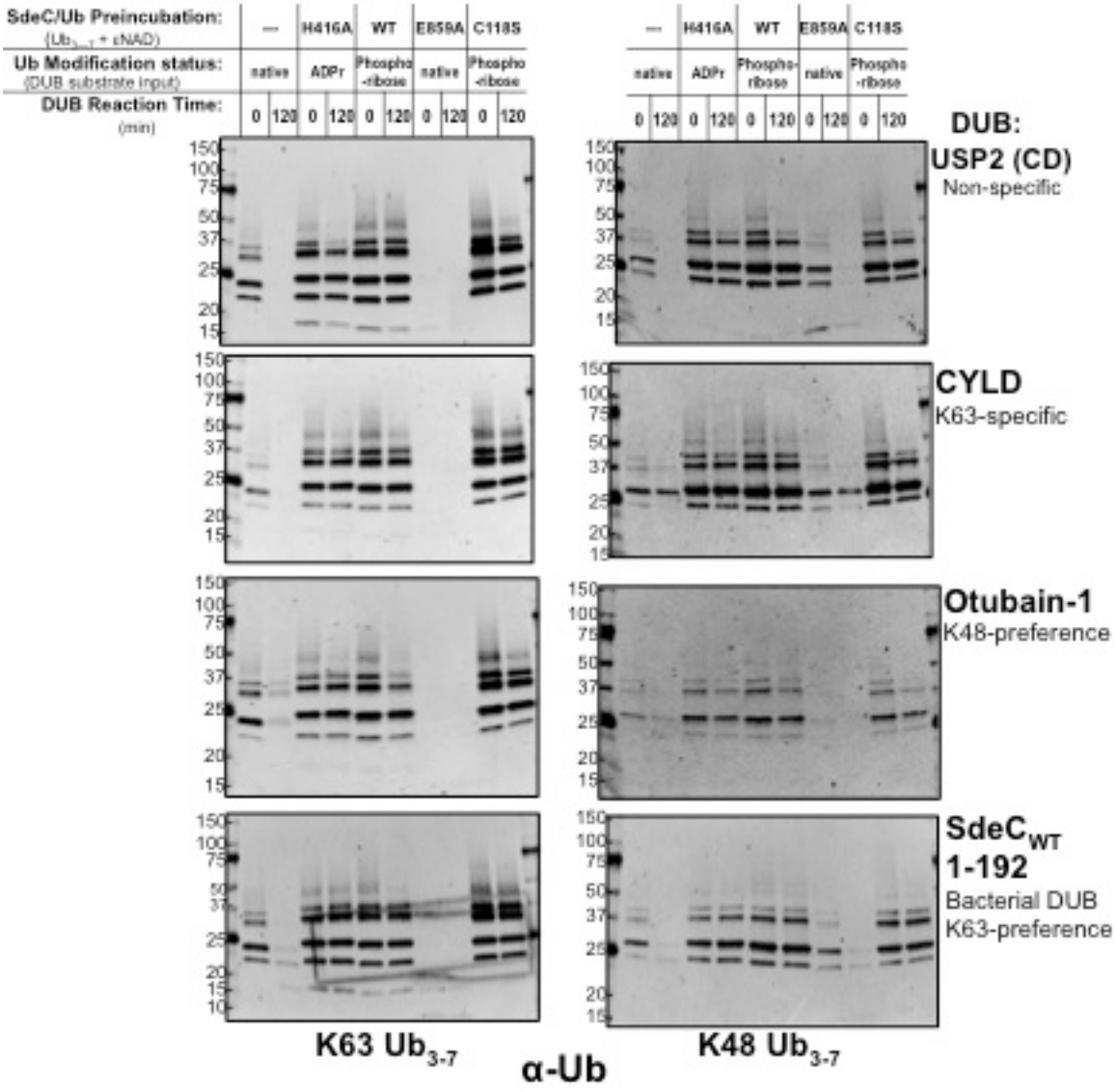

Figure 7.2. Either ADP-ribosylated or phospho-ribosylated polyUb is highly resistant to DUB cleavage (preliminary).
SdeC derivatives (1µg) were adsorbed to Ni-NTA resin for 1 hr at 4°C, then incubated with either K63 or K48 polyUb$_{3-7}$ (2µg) for 2 hrs at 37°C to promote Ub modification, then SdeC resin was removed, and polyUb$_{3-7}$ was then incubated with either 1) human recombinant PolyHistidine-otubain 1, isoform 1 (100nM); 2) recombinant USP2 catalytic domain (CD) 259-605 (50nM); 3) recombinant PolyHistidine-CYLD (50nM); or 4) recombinant SdeC DUB CD 1-192 (50nM) at 37°C for 2 hr. Cleavage was monitored by immunoblot comparison of the polyUb staining after incubation with SdeC derivatives or a no enzyme control against the polyUb staining after a 2 hr incubation with a DUB.

7.3. Evidence that Sde modification of polyUb (ADPr-Ub or Phosphoribose-Ub) inhibits binding by autophagy adaptor, p62

The Sde proteins both limit polyUb at the LCV during infection with the DUB domain and enhance ubiquitination through Sde-mediated Ub ligation and addition of PTMs to resident polyUb, generating a DUB resistant population. We postulated that the Sde-mediated PTM of Ub serves as ubiquitin camouflage, offering a new mechanism for autophagy evasion during infection. Autophagy adaptors, such as optineurin (OPTN) and p62 rely on polyUb binding to facilitate the formation of protein scaffolds and downstream signaling[85,291,298,368,408,448,454,544]. To test this concept, recombinant SdeC was adsorbed to beads to modify K63 or K48 polyUb$_{3\text{-}7}$ chains, then SdeC resin was discarded, and modified polyUb was incubated with p62 adsorbed to Ni-NTA resin. After p62 elution from the resin, the binding efficiency of modified polyUb or native polyUb was evaluated with α-Ub immunoblots. p62 was able to efficiently bind either K63 or K48 polyUb chains that had not been exposed to SdeC (Figure 7.3. ---). If the Ub chains were phosphoribosylated with WT or C118S SdeC, p62 was dramatically reduced with K63-Ub chains and eliminated with K48-Ub chains (Figure 7.3. WT or C118S). The same trend was observed with ADP-ribosylated ubiquitin, p62 binding to K63-Ub chains was radically reduced and with K48-chains the p62 binding was all but eliminated (Figure 7.3. H416A). These results provide an explanation for how Sde-mediated post-translation modifications could serve as inhibitors of polyubiquitin binding, potentially delaying or eliminating signaling pathways such as autophagy that rely on Ub binding to initiate downstream events.

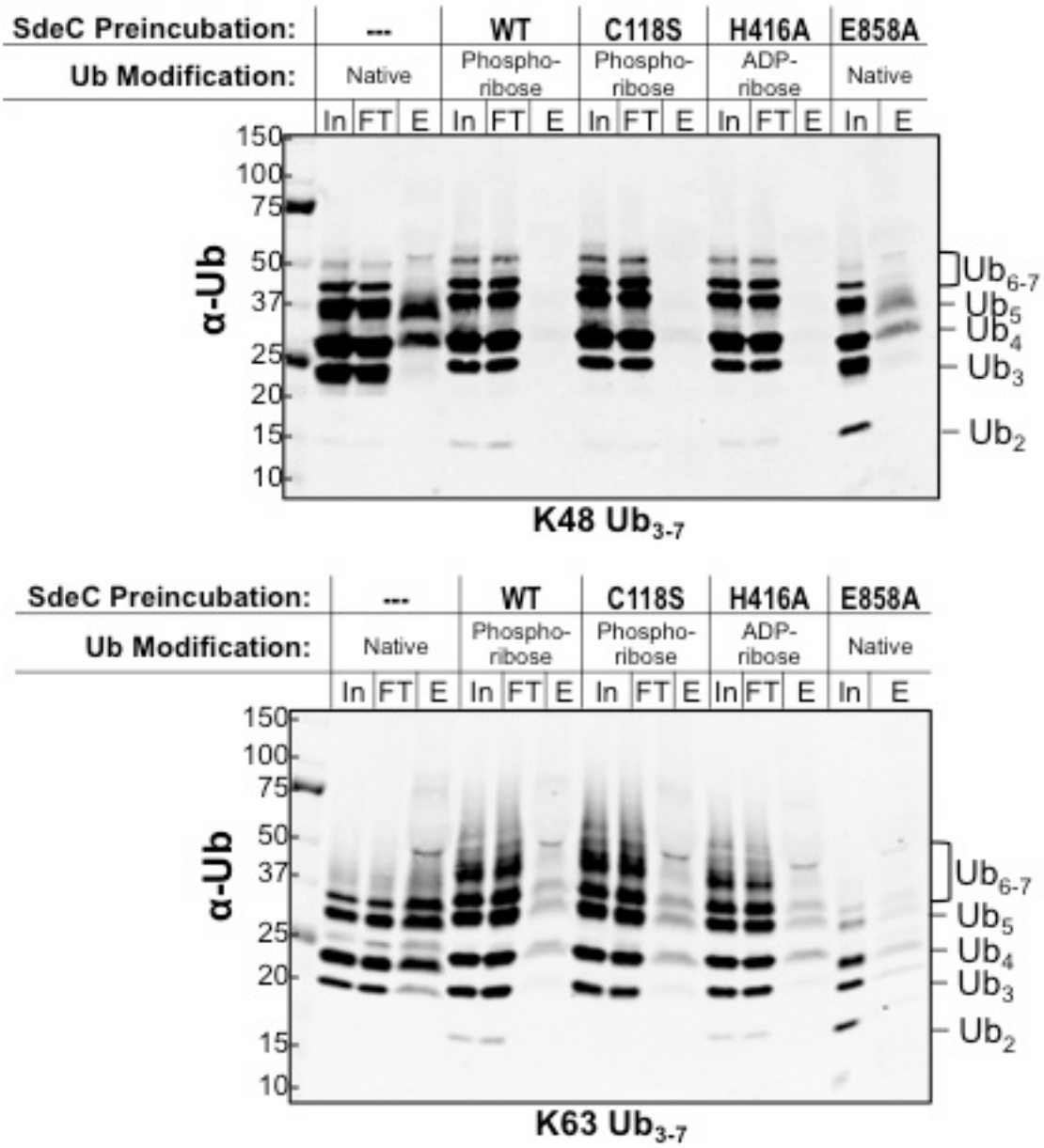

Figure 7.3. Sde modification of polyUb chains with ADPr or phosphoribose severely limits p62 binding to polyUb (preliminary).
SdeC derivatives (1µg) were adsorbed to Ni-NTA resin for 1 hr at 4°C, then incubated with either K63 or K48 polyUb$_{3-7}$ (2µg) for 2 hrs at 37°C to promote Ub modification. Then SdeC resin was removed and polyUb$_{3-7}$ was then incubated with p62 at room temperature for 1 hr. p62 and any bound Ub were eluted with 250mM imidazole and bound polyUb was measured by SDS-PAGE fractionation and α-Ubiquitin (Ub). In, input (2.5%); FT, flow-through (2.5%); E, elute (25%).

7.4. Evidence that Sde proteins work in collaboration with unknown *L. pneumophila* factors to limit host autophagy.

As Sde family members manipulate the host ubiquitin system and the endoplasmic reticulum, we investigated whether they were involved in *L. pneumophila* subversion of the host autophagy system, which sits at the intersection of interactions between the ER, ubiquitin signaling, and innate immunity to intracellular pathogens[177,235,333,484]. *L. pneumophila* is notorious for utilizing multiple strategies to target the same critical host pathways, such as autophagy. The *L. pneumophila* IDTS RavZ is a well-characterized anti-autophagy factor that irreversibly deconjugates lipidated LC3 (LC3II)[202,271,550] . However, even in the absence of RavZ, there is no autophagic response to the highly ubiquitinated LCV, in spite of the fact that Ub targeting of compartments is a first signal that leads to autophagic clearing. Clearly, there must be other factors that prevent recognition of the LCV. To investigate the possibility that modification of Ub is tied to autophagy inhibition, we employed the minimalized *L. pneumophila* genome strain*, Δpentuple*[354], which lacks *ravZ*, but contains the Sde family. We then utilized a *Δpentuple ΔsdeC-A* strain for comparison to the *Δpentuple* background (strains were gifts from Dr. Tamara O'Connor).

We first assessed the importance of the Sde operon in a *Δpentuple* background by monitoring intracellular growth in A/J BMDMs. Both the *Δpentuple* and *Δsde* strains are fully competent for intracellular replication in BMDMs[28,354], but if there were bacterial IDTS within the pentuple strain deletion regions that target the same or compensatory pathway as the Sde family, then we would expect to observe a replication defect specifically in the double mutant background. Wild type and *Δpentuple L. pneumophila*

strains both grew to similar levels over the course of a 74-76 hr challenge of macrophages. Interestingly, a *ΔsdeC-A Δpentuple* strain showed reduced intracellular replication (Figure 7.4. A). In preliminary studies using CFU enumeration to monitor bacterial growth rather than luciferase expression, the defect in fold growth between the WT or *Δpentuple* strain relative to *ΔsdeC-A Δpentuple* mutant was as much as a 10X by 72 HPI (Figure 7.4. B). We next examined autophagy induction during infection with these mutant strains by monitoring differences in LC3 maturation across *L. pneumophila* mutant strains by surveying LC3-II increases relative to LC3-I or a loading control (α-actin), as a readout for induction of the host autophagic response[113,497]. LC3-II resides within autophagosomal membranes that originate from ER membranes and is rapidly degraded upon fusion with lysosomes during autophagic maturation[286,287]. We used chloroquine pretreatment of cells to inhibit endosome fusion with lysosomes, effectively blocking LC3-II degradation so that LC3-I:II ratios could be measured. Without chloroquine treatment LC3-I and LC3-II levels were nearly undetectable in uninfected and *L. pneumophila* infected Cos7 cells (Figure 7.4, panel C, Mock α-LC3a/b). In uninfected Cos7 cells treated with chloroquine, a notable increase in LC3-II relative to an actin control was observed when compared with mock treatment of uninfected cells (Figure 7.4, Panel C, Compare chloroquine-uninfected to mock-uninfected). During Lp02 infection with chloroquine treatment, the increase in LC3-II was slightly diminished compared to uninfected cell extracts, consistent with *L. pneumophila* factors limiting LC3 lipidation. This was due to *L. pneumophila* IDTS, as infection with the T4SS mutant, Lp03, resulted in LC3-II levels above those observed in uninfected cells (Figure 7.4. C, chloroquine Lp03 vs. uninfected, Lp02). This indicates the *Legionella* infection induced

an autophagic response without any additional inhibitors to limit LC3 maturation. Both *Δsde* and *Δpentuple* infections resulted in a slight increase of LC3-II relative to WT infection and the levels appeared comparable between the two mutants (Figure 7.4, panel C, chloroquine *Δsde* and *Δpentuple*). Challenge with *Δsde Δpentuple* compounded these effects resulting in more than twice the amount of LC3-II present in these extracts relative to *Δsde* or *Δpentuple* infected extracts (Figure 7.4, panel C, chloroquine *Δsde Δpentuple*). In fact, the LC3-II levels from *Δsde Δpentuple* infection relative to an actin loading control approximate the LC3-II levels observed in a T4SS mutant infection (Figure 7.4, panel C, Compare *Δsde pvector*, *Δpentuple*, and Lp03 to *Δsde Δpentuple* LC3-II levels α-LC3a/b). Expression of plasmid-encoded SdeC or SdeB, but not SdeA, in a *Δsde Δpentuple* background was capable of partially reducing LC3-II levels relative to levels with the *Δsde Δpentuple* parent strain infection (Figure 7.4. C, *Δsde Δpent psdeC* and *Δsde Δpent psdeB* vs. *Δsde Δpent psdeA*). Comparison of LC3-II levels between these strains at 2 compared to 6 hrs produced largely consistent trends, although overall levels of LC3-II appeared slightly lower at 6 hrs relative to 2 hr infections (Figure 7.4. C, 2 vs. 6 hr). To examine this autophagic flux in a well-established host, A/J BMDMs were substituted for Cos7 cells and the same strains were used to challenge the macrophages for 2 hrs in after a 2 hr pretreatment with chloroquine. In this experiment, LC3-II levels were largely reminiscent of those observed in Cos7 cells. A *Δsde Δpentuple* infection produced more LC3-II relative to a *Δpentuple* infection (Figure 7.4. D, compare *ΔsdeC Δpentuple* with *Δpentuple*). Expression of any one Sde protein from a plasmid showed minimal or no reduction in LC3-II levels compared to a *Δsde Δpentuple* challenge (Figure 7.4. C, *Δsde Δpent psdeC, psdeB*). These experiments will need to be repeated, and

further exploration of the Sde role during infection in a *Δpentuple* background likely would necessitate generation of a strain lacking all SidE family members, but which retain SidJ, in the *Δpentuple* background due to the previously described toxicity of Sde expression in the absence of SidJ[232].

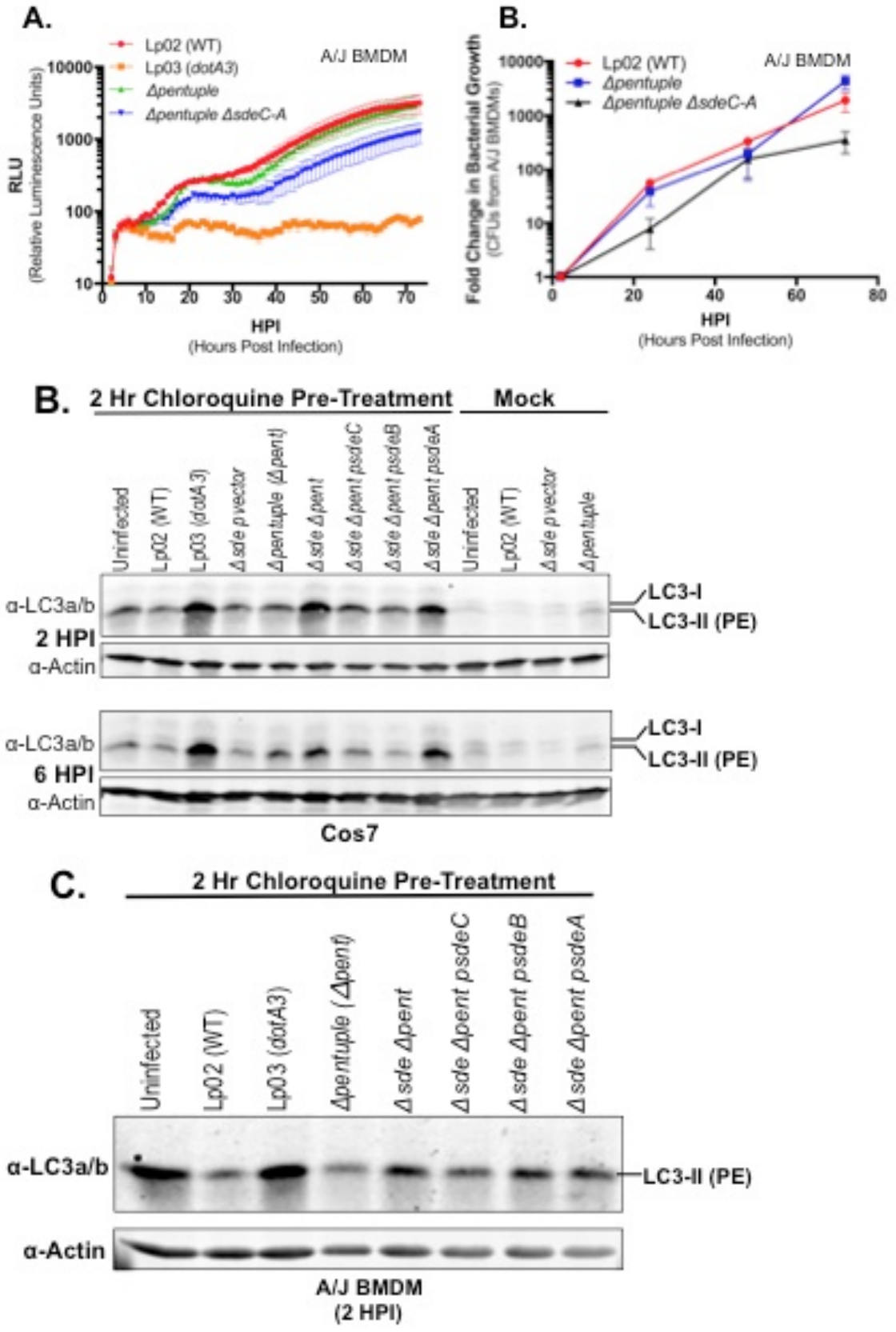
A.
Lp02 (WT)
Lp03 (dotA3)
Δpentuple
Δpentuple ΔsdeC-A
A/J BMDM
RLU
(Relative Luminescence Units)
HPI
(Hours Post Infection)
B.
Lp02 (WT)
Δpentuple
Δpentuple ΔsdeC-A
A/J BMDM
Fold Change in Bacterial Growth
(CFUs from A/J BMDMs)
HPI
(Hours Post Infection)
B. 2 Hr Chloroquine Pre-Treatment
Mock
Uninfected
Lp02 (WT)
Lp03 (dotA3)
Δsde pvector
Δpentuple (Δpent)
Δsde Δpent
Δsde Δpent psdeC
Δsde Δpent psdeB
Δsde Δpent psdeA
α-LC3a/b
LC3-I
LC3-II (PE)
2 HPI
α-Actin
6 HPI
Cos7
C.
2 Hr Chloroquine Pre-Treatment
Δsde Δpent psdeC
Δsde Δpent psdeB
Δsde Δpent psdeA
α-LC3a/b
LC3-II (PE)
α-Actin
A/J BMDM
(2 HPI)

Figure 7.4. The Sde family is important for *L. pneumophila* growth in A/J BMDMs and limiting autophagy during *L. pneumophila* infection in a minimalized genome background (preliminary).
(A) A/J BMDM were challenged with the indicated *L. pneumophila* strains expressing luciferase (*Δsde* backgrounds are operon deletion *ΔsdeC-A* with *sidE* still present in the chromosome) at an MOI=0.05 for 2 hrs, then bacterial growth was monitored by luminescence expression (RLU, relative luminescence units) in a plate reader over the next 74 hrs. **(B)** A/J BMDM were challenged with indicated *L. pneumophila* strain for 2 hrs, then non-internalized bacteria were washed away and bacterial fold replication relative to 2 HPI were determined at 24 hr intervals up to 72 hrs using saponin lysis of macrophages and plating extracts for CFU enumeration on CYET plates at each time point indicated. **(C)** Cos7 cells (8×10^5) were pretreated with chloroquine (100μM) for 2 hrs prior to *L. pneumophila* challenge at an MOI=10 for 2 hrs or 6 hrs. For the 6 hr challenge, after 2hrs of challenge non-internalized bacteria were washed 3x and then fresh medium with chloroquine was added back to the cells for the remaining 4 hrs of challenge. At the completion of 2 or 6 hr *L. pneumophila* challenge, Cos7 cells were lysed in SDS buffer, fractionated, and probed with α-LC3 and α-actin immunoblots. **(D)** BMDMs (5×10^5) were pretreated with chloroquine (100μM) for 2 hrs prior to *L. pneumophila* challenge at an MOI=2 and chloroquine remained in the media during the 2 hr infection. After 2 hrs of BMDM challenge with *L. pneumophila,* BMDMs were analyzed as in panel A.

7.5. Pulmonary model of *L. pneumophila* infection within A/J mice reveal an *in vivo* role for the Sde family.

The Sde proteins have been shown to be dispensable for *Legionella* growth in a tissue culture macrophage model of infection although they are required for efficient growth in amoebae[28]. This prompted the question of whether the Sde family may have a role in a pneumonia model of infection, since their may be important events during disease in the mouse that are not reproduced in BMDM. Macrophages only represent a subset of bacterial-host interactions that occur during a pulmonary infection model. To address this knowledge gap we utilized a pulmonary A/J mouse model of infection developed by Kim Davis (Former Isberg post-doc, currently Johns Hopkins University) in which anaesthetized mice were inoculated with 2×10^4 CFU and BAL fluid was collected at 4 and 48 HPI to determine bacterial load by CFU. In a WT *Legionella*

infection the bacterial load at 4 HPI represents the initial inoculum levels for mice with CFUs near 10^4. A slight increase in bacterial load can be observed at 24 HPI, but by 48 HPI this level approximates CFU/ml at 4 HPI. No increases in bacterial loads of the lungs were observed after *Δpentuple* or *dotA3* challenge (Figure 7.5. A). In fact a comparison between 4 HPI and 48 HPI of *Δpentuple* or *dotA3* reveal a 10 to a nearly 100-fold loss in bacterial load, respectively (Figure 7.5. A). When A/J mice were challenged with *Δsde* (KK099 pvector), a comparison between the 4 and 48 HPI time points revealed a nearly 10-fold reduction in BAL CFUs, similar to the bacterial reduction observed in a *Δpentuple* infection. During a mouse infection with *Δsde* mutant expressing WT SdeC from a plasmid, a partial increase in bacterial load was observed relative to *Δsde* infection loads at 48 hrs (Figure 7.5. B). It should be noted that expression of SdeC was under the control of an IPTG-inducible promoter, so expression of this protein was due to the high baseline expression in the absence of induction. These results suggest the Sde family plays a significant role during a mammalian pulmonary model of infection and that BMDMs do not always represent a definitive paradigm for *L. pneumophila* infection.

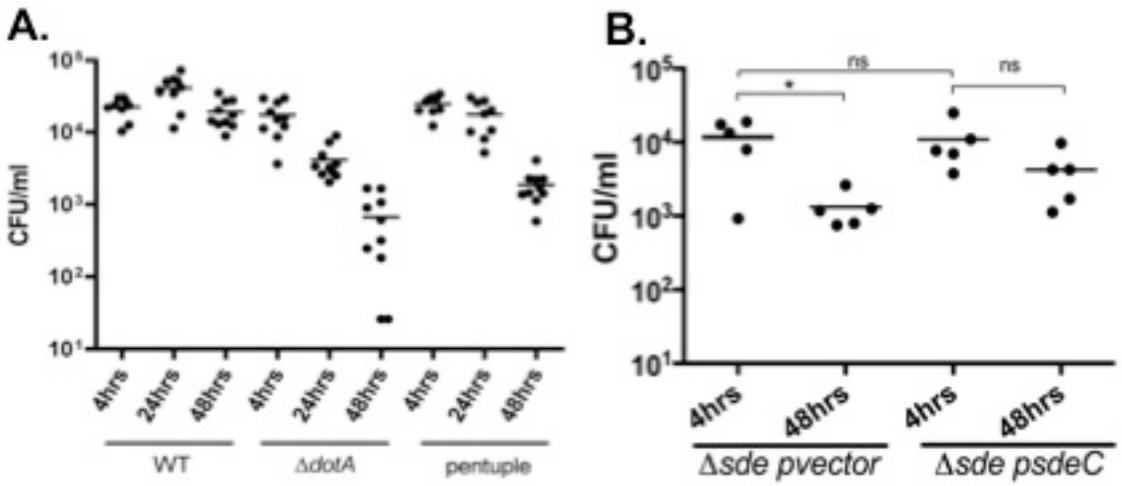

Figure 7.5. Absence of the Sde family results in a defect in *Legionella* survival within a mouse pulmonary model of infection.
(A, B) Anesthetized Female A/J mice were challenged with *L. pneumophila* (2 x 10^4 CFU) through intranasal inoculation. Mice were sacked and BAL fluid was collected and plated for CFUs at 4, 24 (where indicated), and 48 hours post infection.

In the studies described here, we have shown how the intracellular pathogen *Legionella pneumophila*, translocates a family of T4SS substrates known as the Sde family that are involved in the subversion of the endoplasmic reticulum to generate an ER derived replication compartment. We've shown the Sde proteins can target the tubular ER membrane protein Rtn4 and in the absence of these bacterial proteins there is a premature association of rough ER sheets with the vacuole. The Sde proteins promote Rtn4 rearrangements associated with detergent insolubility around the replication compartment and integration of Rtn4 with the LCV membrane. We uncovered that the Sde mediated mechanism of ER rearrangement is through Sde-promoted ubiquitin transfer to Rtn4, which occurs almost immediately after bacterial uptake. Ubiquitin ligation by Sde proteins requires two sequential enzymatic activities from a single polypeptide: an ADP-ribosyltransferase and a nucleotidase/phosphohydrolase. The ADP-ribosylated moiety of ubiquitin is a substrate for the nucleotidase/phosphohydrolase,

resulting in either transfer of ubiquitin to Rtn4, or phospho-ribosylation of ubiquitin in the absence of a ubiquitination target. This represents the discovery if a single bacterial protein drives a multistep biochemical pathway to control ubiquitination and tubular ER function independently of the host ubiquitin machinery. Furthermore, the Sde family modulate LCV ubiquitination through the N-terminal DUB domain and the Ub ligase activity from ART and NP domain collaboration during infection. The Sde proteins ability to PTM ubiquitin chains with phosphoribose or ADP-ribose also serves to confound the host system, where Sde modifications inhibit DUB cleavage and obscure polyubiquitin binding proteins, such as the autophagy adaptor p62, from interactions with Ub chains. These studies indicate the incredible capacity of *Legionella* to recognize and subvert a crucial host signaling system, like ubiquitination, for the bacterium's own purpose in a manner that also confounds and camouflages the bacterial hijacking of the system.

Chapter 8:

Discussion

This chapter contains excerpts that have previously been published in:
(reprinted with permission of publisher)

Kotewicz KM, Ramabhadran V, Sjoblom N, Vogel JP, Haenssler E, Zhang M, Behringer J, Scheck RA, Isberg RR. Cell Host Microbe. 2017 Feb 8; 21(2):169-181. Epub 2016 Dec 29.

8.1. SidE family members manipulate ER structures at the LCV

The generation of an intracellular compartment capable of hosting pathogen replication is a critical early step in the life cycle of intravacuolar pathogens[427,461,469]. In this dissertation I show that *Legionella* specifically targets tubular ER within minutes of infection through the Sde family of T4SS substrates. These proteins exploit ubiquitin (Ub) signaling to restructure tubular ER surrounding the LCV. Tubular ER rearrangements occur with rapid kinetics (Figure 1.18.C, Figure 3.4.A) and the proteins required for these rearrangements are necessary for robust amoebal growth (Figure 5.2, Figure 6.2).

Previous work has shown that as early as 10 min post-bacterial challenge, vesicle-like structures approximately 200 nM in diameter associate with the LCV [4,240,504]. These structures have been called ER-derived vesicles, based on the fact that ER vesicle-associated proteins rapidly associate with the LCV [240,504]. Using high-resolution and fluorescence microscopy studies of the LCV during the first 2 hrs of infection in mammalian cells we demonstrated that these vesicle structures consist of Rtn4-rich membranes derived from peripheral tubular ER (Figure 3.5-3.7). We termed these membranous structures rich in Rtn4 ‘pseudovesicles’. These vesicular structures were often observed in association with Rtn4-rich appendages extending out from the cytoplasmic face of their membranes, frequently towards other nearby ‘pseudovesicles’ (Figure 3.6). These appendages were reminiscent of proteinacious bridges observed between the ER and mitochondria at MAM sites or intercisternal bridges in Golgi stacks[88,95,187,375]. We propose that Rtn4 ubiquitination by the Sde biochemical ubiquitination pathway promotes structural transformations of ER tubules, potentially

through enhanced Rtn4 oligomerization or generation of a scaffold to form tubule matrix-like structures (Figure 8.1)[348].

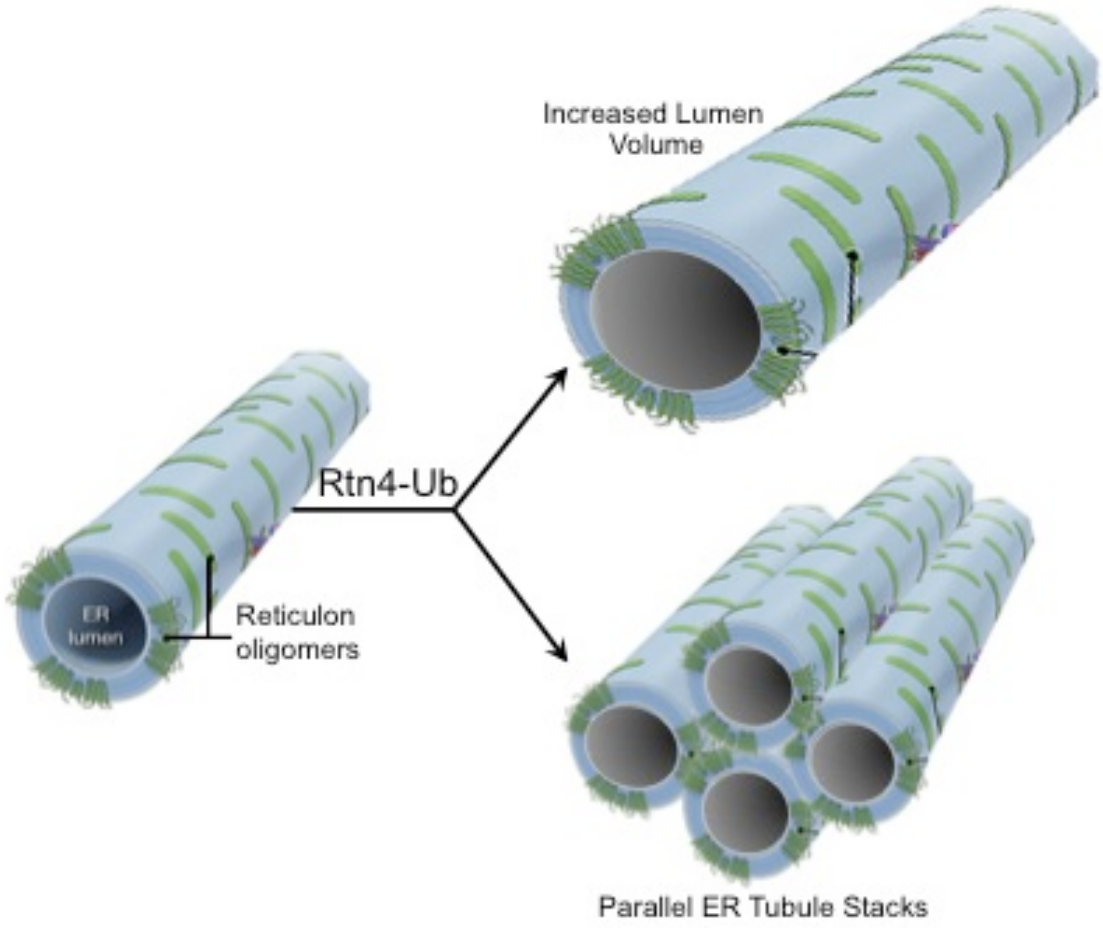

Figure 8.1. Potential ER tubule structure changes mediated by Sde ubiquitination of Rtn4.
ER tubules are formed by phospholipid bilayer with reticulon oligomers (green) inserting into the membrane (blue) to generate curvature, cross section shown. After Rtn4 is ubiquitinated by Sde, Rtn4 accumulation or inhibited membrane traffic promote increased tubule size with an increase in ER lumen diameter (top branch), consistent with the large size of LCV 'pseudovesicles'. Rtn4 oligomers form proteinacious bridges between ER tubules facilitating membrane interaction and formation of stable parallel ER tubule stacks. Adapted from Goyal and Blackstone, 2013[164]. ER tubule image at far left was isolated from figure 2 and the cartoon image was repurposed to indicate possible ER structures transformations generated by Sde ubiquitination.

Although these proteinacious appendages have not garnered much interest within the field, they have been previously observed at early infection time points[414]. Our images of Rtn4-rich appendages suggest that these bridges serve to foster interactions between nearby tubules generating an organized macrostructure of densely packed ER tubules stacked in parallel to one another around the LCV. A similar structure has been observed with the sarcoplasmic reticulum, a special type of smooth ER that serves to store and release calcium ions, present in both smooth and striated muscle fibers[69,422]. Electron microscopy images of SR longitudinal slices resulted in images of closely packed parallel SR tubules, while cross sections produced images of clustered circular structures. These circular structures, which could easily be misidentified as trafficking vesicles, actually represent cross-sections of SR tubules organized around the myofibrils inside a muscle cell. Moreover, this ultrastructure was shown, at least in part, to be mediated by Ca^{2+} ATPase molecules running diagonally around the tubule walls producing a well-defined helicoid organization of the ATPases [69]. Reticulon protein properties, such as their propensity to hetero- or homo-oligomerize and their ability to induce membrane curvature[459,570], suggest these proteins could facilitate an ER structure analogous to those observed in the SR. Although the preponderance of Rtn4 in the 'pseudovesicle' membranes suggests these structures are cross-sections of closely packed ER tubules rather than clusters of ER vesicles, additional high-resolution and 3-dimensional studies of the ER framework during *L. pneumophila* are needed to fully differentiate these curious structures.

Interestingly, these 'pseudovesicles' and their associated Rtn4-appendages were linked to Sde function, as the structures are rarely observed during infections when the

Sde family is absent (Figure 3.6). Even more curious, was the aberrant premature association of rough ER proximal to the LCV during mammalian infection studies with *L. pneumophila* lacking the Sde proteins (Figure 3.8). This suggested to us that *L. pneumophila* utilizes an alternative mechanism to rapidly associate ER membranes with the LCV during mammalian infection, albeit unconventional rough ER structures (Figure 3.8). This could potentially explain why *L. pneumophila* can robustly replicate within permissive macrophages in the absence of the Sde pathway, whereas during amoeba infection the absence of the Sde family abrogates any observable ER association with the LCV (Figure 3.3) and is ultimately detrimental to intracellular replication within this host (Figure 5.2.A).

Although the LCV association with rough ER has been documented numerous times, a scan of 54 manuscripts from the literature indicates that this event typically occurs 6 hrs post-infection of cells (Table 3.1) In fact, the overwhelming consensus among these studies is that one of the earliest morphological events observed at the LCV is the formation of these large round compartments. This observation is consistent across *L. pneumophila* studies, as 'pseudovesicle' structures rapidly arise at the LCV regardless of host (amoebae or macrophage), while the occurrence of rough ER at these early time points was a highly atypical event (Table 3.1)[180,270]. Since the two subtypes of ER observed at the LCV typically serve distinct functions for a homeostatic cell[77,539], it is not entirely surprising that *Legionella* would develop a mechanism to amend ER structure at the vacuole to adapt to the bacterium's evolving needs over the course of infection.

The early manifestation of 'pseudovesicles' at the LCV suggests the bacterium uses these smooth ER components as building blocks for the LCV conversion into a

rough ER-like compartment. Our results support a model in which *Legionella* immediately interacts with peripheral ER after phagocytosis and begins the process of ER acquisition to avoid endocytic maturation and initiate vacuole conversion into a rough ER-like compartment that can harbor bacterial replication. We propose that early ER-LCV association is a prerequisite for successful infection as it 1) supplies the LCV and proximal region with unknown membrane and protein components from the ER for vacuole biogenesis and expansion into an ER-like replication compartment; 2) provides the LCV with a rapidly acquired host-derived membranous disguise to avoid recognition by host degradation pathways by coating the vacuole surface with ER 'pseudovesicles'.

Additional evidence of *Legionella's* tight temporal regulation of an ER-LCV maturation process originates from previous studies examining the relationship between the 'metaeffector' SidJ and its target, the SidE enzyme family[184,232,397]. First, SidJ serves as an important SidE family regulator by releasing the enzymes from the LCV membrane [232]. This is critical during infection, as the absence of SidJ during amoeba challenge prolonged SidE family association with the LCV, which induced more than half of the vacuoles to mature along the endocytic-lysosomal pathway by 1 HPI and nearly 80% of vacuoles by 3 HPI (Figure 1.17.G)[232]. Furthermore, SidJ directly antagonizes SidE family enzymatic activity functioning as a SidE-specific DUB targeting the novel Ub-linkage catalyzed by SidE proteins[184,397]. These two regulatory properties of SidJ indicate *Legionella* has designed a system to tightly control the SidE activity, as improperly localized or improperly timed SidE function directs the LCV down an inescapable degradation pathway.

This model is further supported by comparisons of LCV-ER associations at early

time points (≥ 2 hrs) and intracellular replication outcomes in different hosts. In *D. discoideum* cells stably expressing the ER retention fusion HDEL::GFP, LCVs did not colocalize with the ER marker during challenge with either a *sidE* family deletion or a *ΔsidJ* mutant and both had significant intracellular growth defects[260,294,396]. On the contrary, challenge of permissive macrophages with a *sidE* family deletion mutant did not have a discernable defect on *L. pneumophila* intracellular replication or ER marker colocalization with the LCV (calnexin, not shown, V. Ramabhadran), except for Rtn4, which remained dependent on Sde protein expression for LCV colocalization[28,260,396]. Alternatively, a macrophage challenged with *ΔsidJ* delayed LCV-ER colocalization relative to WT infection and resulted in reduced intracellular replication, but was still able to subvert trafficking to lysosomes. These phenotypic and growth profile patterns imply a compensatory *L. pneumophila* ER-recruitment pathway functions in mammalian saving the bacterium from replication defects observed in an amoebal host.

The targeting of Rtn4 during early infection intimates that *L. pneumophila* may employ a host mechanism of ER structure conversion during the course of vacuole biogenesis. By manipulating the ratios of ER sheet to ER tubule-defining proteins at organelle sites proximal to the incoming LCV, the bacterium could dictate its preferred ER structure locally and adjust it as needed over the course of infection. The work presented here also indicates that the coordinated transition of the LCV into a rough ER-associated compartment likely begins much earlier than previously described, specifically through Sde-mediated accumulation and manipulation of tubular ER upon entry. We argue that this ER-maturation process initiates through the formation of 'pseudovesicle' structures that are derived from tubular ER as a consequence of a biochemical

ubiquitination pathway catalyzed by Sde family members (Figure 6.9.B and 8.2). The structural or oligomerization changes that Rtn4 undergoes upon Sde ubiquitination remains elusive, but beautiful *in vitro* tubular ER systems present a unique tool to explore these macrostructure changes in a simplified visual system through EM or IF microscopy. These studies break open the classic *Legionella* paradigm, where hijacked ER-Golgi vesicles are the vesicular structures surrounding the LCV and the source of ER donor material to the LCV. Our studies of the host-pathogen interface between *L. pneumophila* and host ER strongly argue for a new phase in the *L. pneumophila* life cycle where peripheral ER tubules are transformed by the bacterium and interfaces directly with the vacuole through the described 'pseudovesicle' structures.

8.2. Novel multi-step ubiquitination pathway catalyzed by Sde proteins.

PTM of proteins with ubiquitin is a highly conserved eukaryotic process used to dictate the trafficking, localization, stability, protein-protein interactions, and ultimately the fate of the proteome[257,380,473]. To coordinate ubiquitin signaling across an entire proteome, signaling must be regulated with considerable finesse, and the first step in the process is controlled by E2/E3 enzyme substrate specificity (Figure 1.8). Once the substrate has been chosen, a variety of other variations generate further diversity in the nature of the modified protein. These include variations in: 1) ubiquitin conjugation patterns (mono-, multi mono-, poly-Ub); 2) types of chain linkages (K63 vs. K48); 3) heterogeneity of chain linkages (branched vs. linear); 4) ubiquitin chain lengths; and 5) PTM to ubiquitin itself (phosphorylation)[217,247,257,432,433]. The conservation of Ub from yeast to humans, combined with the ability to target any protein substrate for an

assortment of phenotypic effects makes this PTM system an ideal target for pathogens [10,22,199,376,389,431,478,567].

Bacterial and viral pathogens directly subvert this host system through mimicry of ubiquitin editing proteins, such as *Legionella's* SidE family deubiquitinases or the E3 ligases LubX and SidC [206,265,398]. Pathogens also manipulate ubiquitin signaling by directly modifying eukaryotic ubiquitin conjugation/editing proteins, for example the OspG kinase from *Shigella* that targets host E2 enzymes to suppress innate immune responses[33,290,567]. We discovered that the *L. pneumophila* Sde proteins combine these two tactics, using both mimicry and direct modification of ubiquitin through a combination of three enzymatic activities, including deubiquitinase, mono ADP-ribosyltransferase, and a nucleotidase/phosphohydrolase activities. These three activities function in collaboration to act as a master regulator of ubiquitin at the LCV, controlling both ubiquitin conjugation and deconjugation. Direct control of both ubiquitin addition (Figure 6.7) and removal (Figure 4.6) through a single polypeptide is a highly unusual tactic. The eukaryotic protein A20 (TNFIA3P), which finely tunes NF-Kβ responses, is the only other protein described to date, besides the Sde family, that can both cleave and conjugate ubiquitin via the same polypeptide[196,307,516,537].

Our work shows that a single bacterial protein catalyzes a unique multi-step biochemical pathway that in the absence of host Ub enzymes, leads to Rtn4 ubiquitination and structural rearrangements of the ER. Bacterial and viral pathogens are known to directly subvert the Ub system through mimicry of eukaryotic Ub editing proteins, such as the *Legionella* SidE family deubiquitinases or the E3 ligases LubX and SidC [203,206,265,398,452]. The work presented here along with several other recent

publications describes the unique process of Sde ubiquitination, which occurs completely independently of the host Ub conjugation system (Figure 6.7)[40,260,396]. Initiation of this ubiquitination pathway requires the Sde proteins ART and NP domain[396]. We show that ADP-ribosylation of the R42 residue on ubiquitin is merely the first step in a pathway that leads to direct conjugation of Ub to recipient host proteins (Figure 6.10). To conjugate ubiquitin, the Sde proteins first ADP-ribosylate the ubiquitin R42 residue, generating a relatively stable reaction intermediate. Next, Sde proteins further process the ADP-ribose modification into ribose-monophosphate through the Sde nucleotidase activity (Figure 8.2). In our model, the Sde pathway is initiated by highly efficient ADP-ribosylation of Ub R42, which occurs catalytically at 0°C using a ratio of 1:50 SdeC:Ub, arguing for ADPr modification of Ub almost immediately after Sde, dependent on NAD concentrations. The ADPr-Ub is then used as a substrate by the NP domain that can either trim the ADPr to ribose-monophosphate *or* promote trimming of adenosine monophosphate (AMP) and transfer of Ub to Rtn4 or other ER associated Rabs[40,260] (Figure 6.9.B, Figure 8.2).

Consistent with this model, we have shown that in a purified system using only Rtn4, Ub, and nanomolar concentrations of SdeC, there is rapid conjugation of Ub dependent on both ART and NP activities, arguing that the observed ADPr-Ub is a brief intermediate that is acted on by the NP domain to promote ubiquitination of substrates (Figure 6.7). This model is supported by the fact that when an NP-deficient mutant protein is mixed with an ART- deficient mutant, ubiquitination of Rtn4 is extraordinarily efficient (Figure 6.7). Our work, in agreement with Bhogaraju and colleagues[41] demonstrates the sequential nature of Sde ubiquitination pathway through successive *in*

vitro reactions. We showed that the reaction would only proceed if Ub was first ADP-ribosylated and then exposed to an active NP domain while in the presence of a target protein, like Rtn4 (Figure 6.7). Every successful Ub ligation reaction required concurrent incubation with an active NP domain and target protein. Native, unmodified Ub or ADP-ribosylated Ub could serve as substrates for Ub ligation, but phosphoribosylated Ub was not a viable intermediate for ligation to target proteins and served to inhibit Sde activity. It is unclear if ADP-ribosylated or phosphoribosylated ubiquitin could serve as unique signaling molecules during infection or serve as a substrate for other eukaryotic proteins, such as NUDIX hydrolases, which target pyrophosphate links in ADP-ribose or nucleosides[100,367].

Our *in vitro* studies also exposed Sde proteins ability to self-cannibalize ubiquitin attachments on both target proteins and Sde mediated auto-ubiquitination events (Figure 6.8). Although we have not explored the domain responsible for the reversal, we hypothesize that the NP domain, which already recognizes phosphate linkages and cleaves them in ADP-ribose, could serve as to reverse the reaction activity upon prolonged incubation or increased Sde concentrations. This rapid hydrolysis of freshly conceived Ub linkages, both mediated by Sde proteins, along with the highly selective list of Sde Ub targets has serious implications for the role of the 'metaeffector' SidJ in Sde regulation. The target selectivity suggests SidJ is designed to limit Sde mediated phospho-ribosylation of resident monoubiquitin and polyubiquitin conjugates not reverse Sde specific ligation. This concept is supported by increasing levels of Rtn4 ubiquitination at 3 HPI relative to 10 MPI during infection with Sde and SidJ expressing *L. pneumophila* strains (Figure 3.10) and by the continued association of Rtn4 with the

LCV at 8 HPI (Figure 2.1.A). Both of these time points represent infection time points well past the described dissociation of Sde from the LCV membrane, effectively allowing SidJ access to remove Sde modifications without continual Sde ubiquitin additions. Furthermore, SidJ could serve to prevent Sde cannibalization of its own ubiquitination by allowing Sde brief access to the LCV membrane to target preferred substrates and then SidJ promotes rapid release to other undefined cellular compartment to prevent prolonged targeting of the same substrate population[232].

In contrast to the specific transfer reaction described here, phosphoribosylated Ub has the potential to serve as a nonspecific reactive intermediate able to undergo a non-enzymatic Maillard reaction that would conjugate Ub to recipient proteins through an irreversible sugar crosslink. In Maillard reactions, the electrophilic carbonyl of a reactive sugar, such as glucose or ribose, reacts with a free amino group of recipient proteins, generating advanced end products (AGEs) [345]. The kinetics of AGE formation is typically quite slow, so a Maillard mechanism would require some accessary factors that could allow a biologically relevant reaction. Non-enzymatic ubiquitin ligation through a glycation reactions represents a possible mechanism for generating a phosphoribose linkage between ubiquitin a substrate protein. Furthermore, protein glycation is frequently associated with stable, cross-linked, high molecular weight complexes, similar to the Rtn4 transformation induced by Sde ubiquitination of the membrane protein[157,345]. Rather than non-enzymatic glycation as a ubiquitin ligation mechanism, our evidence argues for a model in which Sde proteins combine enzymatic ART and NP activities to ubiquitinate high specificity. This ligation process is dependent on an enzymatically active NP domain to complete the reaction. Therefore, it is more likely that the formation

of phosphoribose-Ub terminal reaction product serves to down modulates Sde-mediated Ub conjugation, rather than facilitate non-enzymatic ligation. We propose that the phosphoribose ubiquitin modification reduces the concentration of both native and ADPr-Ub that can act as substrates for Sde-mediated transfer to host protein targets.

The substrate specificity and the level of ubiquitination amongst Sde members display different activity patterns between *in vitro* experiments and infection, revealing key insight to the bacterial proteins' regulation. Each Sde protein, SdeA, SdeB, and SdeC, produced robust Rtn4 ubiquitination after transient expression in mammalian cells (Figure 3.2.A), but during infection only SdeA and to a lesser extend SdeB were found to induce detectable levels of Rtn4 ubiquitination (Figure 3.10). Since these bacterial proteins use the same ubiquitin conjugation mechanism, this additional layer of specificity during infection likely results from Sde interactions with other T4SS substrates that direct Sde activity, rather than minor affinity differences or a eukaryotic regulator. Another explanation of Ub ligation differences in targets is that during infection SdeC is physically limited having access only to a small Rtn4 subpopulation immediately surrounding the LCV. Whereas SdeA expression, which produced excessive Rtn4 ubiquitination, occasionally generated aberrant pockets of Rtn4 far from the LCV, suggesting the protein may target a vastly larger Rtn4 pools relative to other Sde proteins. A final possibility is that Sde ubiquitination patterns are governed by DUB activity or substrate preference. The Sde DUB domain specificity for K63-polyubiquitin chains could serve to preferentially localize the Sde Ub ligase activity to a unique subset of ubiquitination substrates. Consistent with this idea, expression of SdeA in a *Δsde* mutant background consistently reduced LCV polyubiquitination more efficiently than other Sde

proteins during the first 15-20 MPI, which could then serve as new Ub monomer for Sde Ub ligation. Yet Rtn4 reorganization was associated with far fewer bacterial vacuoles when compared with singular expression of SdeB or SdeC in a *Δsde* background (Figure 4.2). The enhanced SdeA DUB capacity may represent the enzyme targeting a broader substrate pool, which also potentially broadens the pool of Ub ligation substrates, decreasing specificity for Rtn4 and ultimately lowering the number of LCV's associated with structurally transformed Rtn4. Further examination of DUB and Ub ligation target preferences and the variation amongst different Sde proteins is needed to parse out these .

This work provides a new direct link between ubiquitination and modulation of ER structure. This research describes the discovery of a novel single-enzyme catalyzed ubiquitination mechanism that ignores all the classic ubiquitination paradigms, including the requirement for ATP and a cascade of enzymes. This challenges not only the most conserved ubiquitin field archetypes, but offers a first hand example of how bacterial proteins using classic eukaryotic mimicry can devise wholly new signaling pathways from otherwise conventional protein functions in order to manipulate host systems, often in a more efficient manner than the system they mimic. Numerous questions linger on this completely novel mechanism of ubiquitination and will likely remain the focus of intense study. In particular, we are still working to identify the Rtn4 and HA-Ub residues targeted for Sde ubiquitination. These questions are critical as Rtn4 ubiquitination at specific functional regions, such as oligomerization domains or protein interaction sites, would have strong implications for the modification intent or purpose. Our evidence supports a model where Sde ubiquitination is mono- or multi-monoubiquitination, but the studies presented here are unable to decipher between multi-mono- and

polyubiquitination at this time. To understand the ubiquitin 'tit-for-tat' battle between the host and *Legionella*, kinetic immunofluorescence studies in macrophages versus amoeba, with specific respect to distinct Sde enzymatic combinations through single and double point mutants, would provide a more complete systemic view of ubiquitin manipulation through single cell analysis.

8.3. Sde family DUB domain

We believe that during intracellular growth, the amino terminal DUB domain[452] also plays an important role during infection, even though the domain was not essential for intracellular replication in *Dictyostelium discoideum,* in contrast to the ART and NP domains[260,396]. We propose that the DUB domain serves two beneficial functions during infection: 1) preventing the accumulation of K63-linked polyUb conjugates on the LCV membrane; and 2) producing a localized pool of mono-Ub that can then serve as a substrate for Sde ubiquitination. In this model, immediately upon Sde protein translocation the DUB domain cleaves away developing K63-polyubiquitin chains, preventing both lysosomal trafficking of the LCV and additional innate immune signaling mediated by this type of Ub linkage [87,185,276,295]. Trimming away ubiquitin chains could also allow Sde proteins unobstructed access to underlying ER membrane proteins, including Rtn4 and ER associated Rabs. Sde-mediated cleavage of polyubiquitin chains would increase the pool of free ubiquitin in the LCV vicinity, augmenting Sde proteins access to ubiquitin for conjugation to newly accessible ER proteins. Both of those activities would rapidly down-regulate DUB activity either by elimination of a polyUb substrate pool and or modification of Ub with ADP-ribose or phosphoribose to produce DUB-resistant chains. Consistent with this model, preliminary evidence indicates the Sde

family functions in parallel with other *L. pneumophila* IDTS, like RavZ, to limit autophagy within the first hours of infection (Figure 7.4), but it is unclear whether this effect is mediated by the DUB domain or in all likelihood, facilitated by Sde ubiquitination and ubiquitin modification through the ART and NP domain.

Strong support for the importance of DUB domain in generating a free pool of localized Ub monomer comes from examining Rtn4 ubiquitination changes during infection with DUB defective Sde proteins. Expression of either SdeA or SdeB DUB mutants failed to produce detectable levels of Rtn4 ubiquitination (Figure 6.4), while transient expression of these mutant Sde proteins in mammalian cells was sufficient to induce robust Rtn4 ubiquitination and HMW Rtn4 species. Furthermore, evidence of the importance of the DUB domain to Rtn4 ubiquitination can be observed downstream in the effects on Rtn4 structure around the LCV as examined by IF microscopy. The percentage of LCVs associated with Rtn4 dropped by 50% or more when comparing Δsde family expressing single WT Sde proteins with their DUB deficient counterparts. These experiments argue that without the DUB domain there is a minimal pool of unconjugated Ub monomer accessible for Sde ubiquitination, but this reduced supply is sufficient in some individual cells to initiate ubiquitin-mediated ER reorganization. It remains to be determined if the DUB domain also plays other regulatory roles such as targeting Sde ubiquitination targets. Our research shows that a 200 amino acid N-terminal domain, conserved across the SidE family, functions as a K63-polyubiquitin specific DUB that serves to limit polyUb accumulation within the first 30-60 min of infection and provide a free pool of monoubiquitin for Sde ligase activity. The DUB domain serves to enhance ART and NP activities, while the DUB domain is negatively regulated by ART

and NP modification of Ub chains and its own DUB activity eliminating available UB chains.

8.4. Sde mediated effects on autophagy and host Ub system.

With the discovery of Sde catalyzed ADP-ribosylation or phospho-ribosylation of Ub, some researchers postulated that the bacterial enzymes' purpose was to systemically halt the host Ub system. Consistent with this model, Sde overexpression in either mammalian or yeast cells was highly toxic or lethal[184,232,396], respectively, and results in inhibition of the host Ub system[41,394]. Furthermore, *in vitro* studies showed that treatment of Ub with SdeA resulted in failed interactions with E1, E2, and E3 components. Similarly we and others demonstrated Sde modified polyUb chains became cleavage resistant species, impervious to eukaryotic or bacterial DUB activities and this inhibition occurred independent of chain linkage (Figure 7.2)[260,394].

The model that Sde proteins shut down ubiquitination by phosphoribose addition during *Legionella* infection is entirely unsupported by extensive work from many labs, and we consider it highly unlikely. Our results argue for an alternative model, whereby any inhibitory role on polyubiquitination by Sde proteins during intracellular growth may be of secondary importance. Inhibition of polyubiquitination by SdeA requires merely ART modification of Ub and is independent of the NP domain [40]. Both phosphoribose and ADP-ribose Ub effectively limit interactions with Ub related enzymes and Ub binding proteins, such as the autophagic cargo receptor p62 during *in vitro* or artificial expression systems (Figure 7.3)[40,394]. We have shown, however, that a *L. pneumophila* NP mutant, which can still effectively ADP-ribosylate Ub and is therefore competent to interfere with the Ub system [40] is defective for intracellular amoebal growth relative to

WT or a *Δsde* mutant expressing WT SdeC (Figure 6.2). This indicates that Sde-promoted ubiquitination, which requires both ART and NP activity, is necessary for robust intracellular growth in *Dictyostelium discoideum*. The one caveat is that a *Δsde* mutant expressing a SdeC NP point mutant does grow slightly better than the *Δsde* parent, indicating that terminal ART modification of Ub can serve a beneficial role in the absence of Sde ubiquitination (Figure 6.2). The importance of the NP activity is further exemplified by IF microscopy of LCV ubiquitination during the first hour. Expression of a SdeC NP mutant that could ADP-ribosylate resident Ub, but not ligate any Ub itself, resulted in profuse polyUb at the LCV as indicated by the both the percentage of vacuoles staining positive and the overall intensity. This is compelling evidence that the primary role of terminal Ub modification resulting from either ADP-ribose or phosphoribose addition is to *stabilize* polyubiquitin, and not prevent polyubiquitination as argued by Bhogaraju, *et al*[41].

These results support an infection model in which Sde proteins function locally at the vacuole membrane during the first hour(s) of infection, rather than inducing a complete Ub system halt. There is evidence indicating a complete Ub system halt would actually be counterproductive to a successful infection. First, it would be unlikely a cell would survive the entirety of a *L. pneumophila* life cycle if the Ub system were completely halted as the PTM regulates many pro-survival pathways and would be needed for normal cellular homeostasis. Secondly, with a widespread Ub system freeze, proteasome function would also be blocked and reports have shown *L. pneumophila* specifically utilizes this host degradation pathway to increase amino acid pools[8,388]. The final argument stems from the numerous reports of *L. pneumophila* IDTS that mimic

eukaryotic Ub enzymes and therefore would likely be subject to the same Sde mediated inhibitory effects, if the inhibition was widespread or prolonged[10,21,265,387,389,543].

We propose that Sde modification of LCV resident polyUb serves to block autophagy induction by preventing cargo receptors from interacting with the heavily polyubiquitinated vacuole. Our *in vitro* experiments demonstrate the capacity for phosphoribose and ADP-ribose additions to almost completely eliminate p62 binding to either K63 or K48 polyUb chains (Figure 7.3). The ability to block autophagy was further supported by an increase in LC3 lipidation (LC3-II) during mammalian cell challenge with minimalized genome background (*Δpentuple*) that lacked the that lacked the *sde* operon relative to the *Δpentuple* strain that maintained the operon. The pentuple background offers an impressive genetic tool for deciphering genetic redundancy. This background lacks at least two IDTS that inhibit autophagy, including the well described LC3-II protease RavZ[202,271] and recently reported syntaxin 17 protease Lpg1137[15]. To further investigate the Sde proteins role as autophagy inhibitors, a thorough genetic analysis of the Sde family relative to other established IDTS that target the autophagic pathway is needed.

The novelty of Sde-mediated cellular effects combined with its unusual mechanism of action indicates that the functions of these proteins likely have a broad range of consequences during infection. It has already been shown that a subset of Rab proteins can be ubiquitinated by SdeA[396] in addition to the structural ER membrane protein demonstrated in this study (Figure 6.4; Figure 6.7)[260]. These results argue for multiple pools of specific targets that could serve to function in several host signaling pathways.

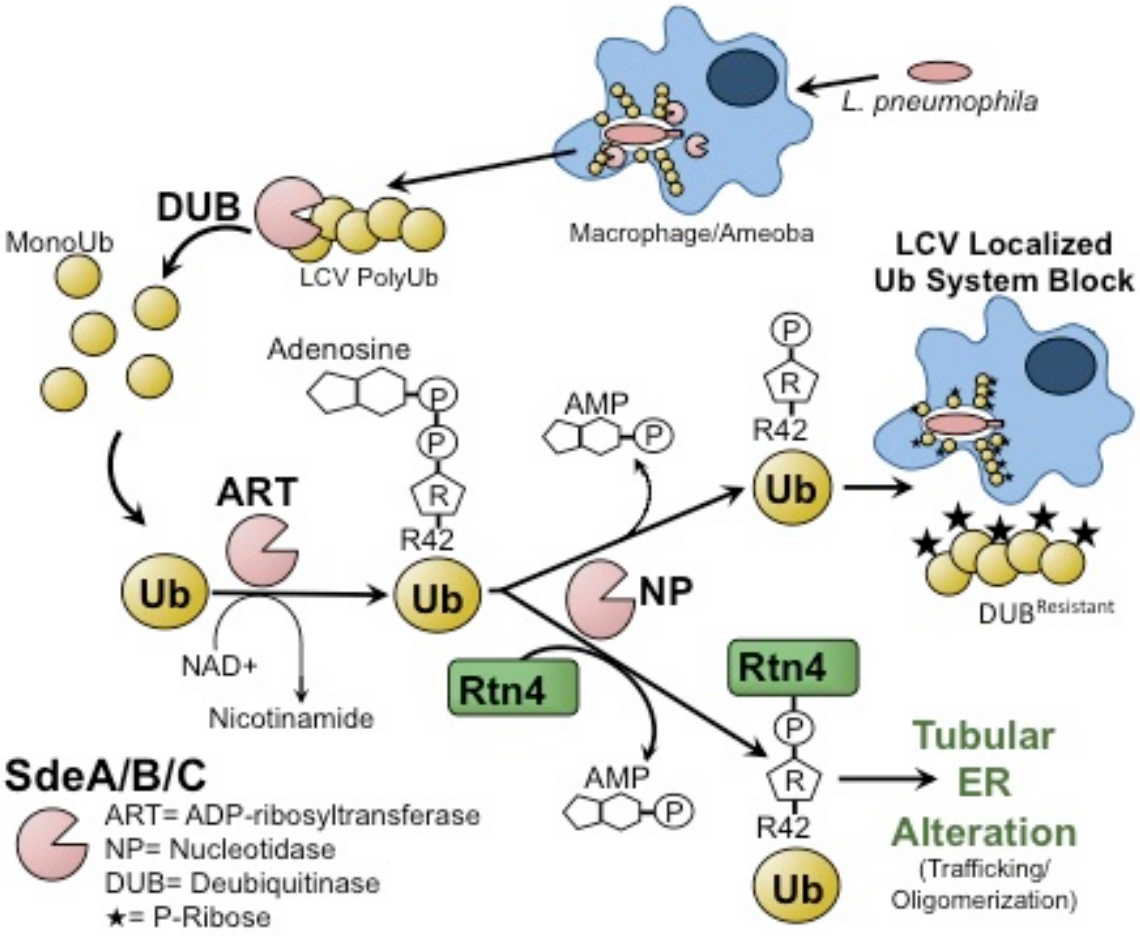

Figure 8.2. Model for Sde family processing of Ub during infection.
Diagram of Sde functions in the context of infection. *L. pneumophila* is phagocytized by a host cell, macrophage or amoeba, and virulent *Legionella* containing vacuoles are rapidly polyubiquitinated, predicted to be host mediated. The LCV polyubiquitination then serves as fuel for Sde DUB activity that generates a pool of localized free monoubiquitin. Free monoubiquitin then feeds into the Sde Ub ligation pathway, where Sde ART activity ADP-ribosylates monoubiquitin at R42, then the NP domain further processes Ub-ADP-ribose into Ub-phosphoribose in the absence of a Ub target proteins (top branch) or if Ub ligation targets are readily accessible, like Rtn4, the NP domain facilitates ADP-ribose Ub processing and conjugation to the target. Sde ubiquitination of Rtn4 leads to structural changes in Rtn4, potentially due to altered trafficking or oligomerization. Adapted with permission from Kotewicz *et al*, 2017. Biochemical reaction modified from a graphical abstract to include additional infection steps and diagram description.

8.5. Conclusion

In the study presented here, we demonstrate direct manipulation of a host organelle structure, specifically tubular endoplasmic reticulum, for the production of a pathogen replication compartment. We utilized the intravacuolar bacterial pathogen *L. pneumophila*, which resides within an ER-derived compartment during infection, to examine how pathogens interact with the ER during infection. In the *Legionella* field, the accepted paradigm, prior to this study, was that the ER-like composition of LCVs results from hijacking trafficking ER-Golgi vesicles. Our research argues instead that direct interactions with the peripheral ER play a critical role during LCV biogenesis into an ER-derived compartment. By investigating *L. pneumophila* interactions with the tubular ER protein Rtn4, we demonstrated that the replication compartment undergoes a highly temporal, organized restructuring of the vacuole through a preliminary association with peripheral ER tubules within minutes of phagocytosis followed by a delayed transition into a ribosome studded rough ER-like compartment hours later. We identified the bacterial Sde proteins as the IDTS responsible for tubular ER manipulation and the accumulation of vesicle-like structures around LCVs as seen by electron micrograph. Our work supports a new *Legionella* paradigm, where the LCV 'pseudovesicles' represent cross-sections of enlarged stacked ER tubules.

Through further analysis of the Sde proteins' distinct protein domains we deciphered the molecular mechanism underlying the observed ER rearrangement. We found that Sde proteins contain three distinct enzymatic domains, including a K63-specific deubiquitinase domain, an arginine mono-ADP-ribosyltransferase (mART), and a nucleotidase/phosphohydrolase (NP) domain. We showed that the mART and NP

domain collaborate to consecutively to modify ubiquitin with ADP-ribose and ribose phosphate, respectively, while in the absence of a Ub recipient or alternatively the domains collaborate to function as an E1/E2 independent Ub ligase when specific substrates, like Rtn4, are present. Furthermore, we demonstrate that either Sde modification to ubiquitin (ADP-ribose or phosphoribose) inhibits interactions Ub enzymes or signaling cascades, like DUB cleavage and autophagy cargo receptor recognition. Although, some research groups have proposed the Sde proteins serve to shutdown the host Ub system in its entirety by Ub PTM based on overexpression studies outside the context of infection, our results indicate that the Sde system represents a far more stringent localized response at the LCV, rather than a universal attack on the host Ub system. In the context of *L. pneumophila* infection, we observed that Ub ADP-ribosylation produced hyper-polyubiquitination at the LCV and was insufficient to fully restore *L. pneumophila* replication in amoeba, indicating the beautifully nuanced nature of Sde activity associated with complete processing of the Ub PTM. The spectrum of cellular functions controlled by this protein family is likely to be quite large, with tubular ER rearrangement being the most rapid and visually spectacular response, controlling a morphological change that had previously been a mystery for much of the past two decades. This study goes further and illustrates the molecular mechanism underlying this dramatic ER rearrangement, whereby a single polypeptide utilizes a multi-step biochemical pathway involving sequential ART and NP activities to ubiquitinate recipient proteins with only NAD+ for a cofactor.

Chapter 9: Bibliography

1. Abbas AK, Sen R. Intracellular Pathogens and Antigen Presentation — New Challenges with Legionella Pneumophila. *Immunity*. 2003;18(6):722–724.
2. Abdullaev IF, Bisaillon JM, Potier M, Gonzalez JC, Motiani RK, Trebak M. Stim1 and orai1 mediate crac currents and store-operated calcium entry important for endothelial cell proliferation. *Circ Res*. 2008;103(11):1289–1299. doi:10.1161/01.RES.0000338496.95579.56.
3. Abeywardana T, Lin YH, Rott R, Engelender S, Pratt MR. Site-Specific Differences in Proteasome-Dependent Degradation of Monoubiquitinated a -Synuclein. *Cell Chem Biol*. 2013;20:1207–1213.
4. Abu Kwaik Y. The phagosome containing legionella-pneumophila within the protozoan hartmannella-vermiformis is surrounded by the rough endoplasmic-reticulum. *Appl Environ Microbiol*. 1996;62(6):2022–2028.
5. Achleitner G, Gaigg B, Krasser A, et al. Association between the endoplasmic reticulum and mitochondria of yeast facilitates interorganelle transport of phospholipids through membrane contact. *Eur J Biochem*. 1999;264(2):545–553. doi:10.1046/j.1432-1327.1999.00658.x.
6. Agrawal G, Joshi S, Subramani S. Cell-free sorting of peroxisomal membrane proteins from the endoplasmic reticulum. *Proc Natl Acad Sci*. 2011;108(22):9113–9118. doi:10.1073/pnas.1018749108.
7. Aktories K, Wilde C, Vogelsgesang M. Rho-modifying C3-like ADP-ribosyltransferases. *Rev Physiol Biochem Pharmacol*. 2004;152(September):1–22. doi:10.1007/s10254-004-0034-4.
8. Al-quadan T, Price CT, Kwaik YA, Abu Kwaik Y. Exploitation of evolutionarily conserved amoeba and mammalian processes by Legionella. *Trends Microbiol*. 2012;20(6):299–306. doi:10.1016/j.tim.2012.03.005.
9. Alli O a T, Gao L, Pedersen LL, et al. Temporal Pore Formation-Mediated Egress from Macrophages and Alveolar Epithelial Cells by Legionella pneumophila Temporal Pore Formation-Mediated Egress from Macrophages and Alveolar Epithelial Cells by Legionella pneumophila. *Infect Immun*. 2000;68(11):6431. doi:10.1128/IAI.68.11.6431-6440.2000.Updated.
10. Allombert J, Fuche F, Michard C, Doublet P. Molecular mimicry and original biochemical strategies for the biogenesis of a Legionella pneumophila replicative niche in phagocytic cells. *Microbes Infect*. 2013;15:981–988. doi:10.1016/j.micinf.2013.09.007.
11. Amer AO, Swanson MS. Autophagy is an immediate macrophage response to Legionella pneumophila. *Cell Microbiol*. 2005;7(6):765–778. doi:10.1111/j.1462-5822.2005.00509.x.
12. Anderson DM, Frank DW. Five mechanisms of manipulation by bacterial effectors: a ubiquitous theme. *PLoS Pathog*. 2012;8(8):e1002823. doi:10.1371/journal.ppat.1002823.
13. Ao X, Zou L, Wu Y. Regulation of autophagy by the Rab GTPase network. *Cell Death Differ*. 2014;21(3):348–358. doi:10.1038/cdd.2013.187.
14. Araki N, Johnson MT, Swanson JA. A role for phosphoinositide 3-kinase in the completion of macropinocytosis and phagocytosis by macrophages. *J Cell Biol*.

1996;135(5):1249–1260. doi:10.1083/jcb.135.5.1249.
15. Arasaki K, Mikami Y, Shames SR, Inoue H, Wakana Y, Tagaya M. Legionella effector Lpg1137 shuts down ER-mitochondria communication through cleavage of syntaxin 17. *Nat Commun*. 2017;8(May):15406. doi:10.1038/ncomms15406.
16. Arasaki K, Roy CR. Legionella pneumophila promotes functional interactions between plasma membrane syntaxins and Sec22b. *Traffic*. 2010;11(5):587–600. doi:10.1111/j.1600-0854.2010.01050.x.
17. Arasaki K, Toomre DK, Roy CR. The legionella pneumophila effector DrrA is sufficient to stimulate SNARE-dependent membrane fusion. *Cell Host Microbe*. 2012;11(1):46–57. doi:10.1016/j.chom.2011.11.009.
18. Arg RJ, Reverendo M, Reverendo M, Gatti E. Regulation of protein synthesis and autophagy in activated dendritic cells : implications for antigen processing and presentation. *Immunol Rev*. 2016;272:28–38.
19. Arias E, Cuervo AM. Chaperone-mediated autophagy in protein quality control. *Curr Opin Cell Biol*. 2011;23(2):184–189. doi:10.1016/j.ceb.2010.10.009.
20. Arroyo DS, Gaviglio EA, Peralta Ramos JM, Bussi C, Rodriguez-Galan MC, Iribarren P. Autophagy in inflammation, infection, neurodegeneration and cancer. *Int Immunopharmacol*. 2014;18(1):55–65. doi:10.1016/j.intimp.2013.11.001.
21. Ashida H, Kim M, Sasakawa C. Exploitation of the host ubiquitin system by human bacterial pathogens. *Nat Rev Microbiol*. 2014;12(6):399–413. doi:10.1038/nrmicro3259.
22. Ashida H, Kim M, Sasakawa C. Exploitation of the host ubiquitinsystem by human bacterial pathogens. *Nat Rev Microbiol*. 2014;12(6):399–413. doi:10.1038/nrmicro3259.
23. Asrat S, de Jesús DA, Hempstead AD, Ramabhadran V, Isberg RR. Bacterial Pathogen Manipulation of Host Membrane Trafficking. *Annu Rev Cell Dev Biol*. 2014;30(1):79–109. doi:10.1146/annurev-cellbio-100913-013439.
24. Auerbuch V, Brockstedt DG, Meyer-Morse N, O'Riordan M, Portnoy DA. Mice lacking the type I interferon receptor are resistant to Listeria monocytogenes. *J Exp Med*. 2004;200(4):527–33. doi:10.1084/jem.20040976.
25. Auerbuch V, Golenbock DT, Isberg RR. Innate immune recognition of Yersinia pseudotuberculosis type III secretion. *PLoS Pathog*. 2009;5(12). doi:10.1371/journal.ppat.1000686.
26. Axe EL, Walker SA, Manifava M, et al. Autophagosome formation from membrane compartments enriched in phosphatidylinositol 3-phosphate and dynamically connected to the endoplasmic reticulum. *J Cell Biol*. 2008;182(4):685–701. doi:10.1083/jcb.200803137.
27. Balducci E, Bonucci A, Picchianti M, Pogni R, Talluri E. Structural and Functional Consequences Induced by Post-Translational Modifications in α -Defensins. *Int J Pept*. 2011;2011:1–7. doi:10.1155/2011/594723.
28. Bardill JP, Miller JL, Vogel JP. IcmS-dependent translocation of SdeA into macrophages by the Legionella pneumophila type IV secretion system. *Mol Microbiol*. 2005;56(1):90–103. doi:10.1111/j.1365-2958.2005.04539.x.
29. Barth H, Preiss JC, Hofmann F, Aktories K. Characterization of the Catalytic Site of the ADP-Ribosyltransferase Clostridium botulinum C2 Toxin by Site-directed Mutagenesis *. *J Biol Chem*. 1998;273(45):29506–29511.

30. Barth S, Glick D, Macleod KF. Autophagy: Assays and artifacts. *J Pathol*. 2010;221(2):117–124. doi:10.1002/path.2694.
31. Baughman JM, Perocchi F, Girgis HS, et al. Integrative genomics identifies MCU as an essential component of the mitochondrial calcium uniporter. *Nature*. 2011;476(7360):341–5. doi:10.1038/nature10234.
32. Baumann NA, Sullivan DP, Ohvo-Rekilä H, et al. Transport of newly synthesized sterol to the sterol-enriched plasma membrane occurs via nonvesicular equilibration. *Biochemistry*. 2005;44(15):5816–5826. doi:10.1021/bi048296z.
33. Baxt LA, Garza-Mayers AC, Goldberg MB. Bacterial Subversion of Host Innate Immune Pathways. *Science (80-)*. 2013;340(6133):697–701. doi:10.1126/science.1235771.
34. Bejarano E, Cuervo AM. Chaperone-Mediated Autophagy. *Proc Am Thorac Soc*. 2010;7(1):29–39. doi:10.1513/pats.200909-102JS.
35. Bennett TL, Kraft SM, Reaves BJ, Mima J, Brien KMO, Starai VJ. LegC3 , an Effector Protein from Legionella pneumophila , Inhibits Homotypic Yeast Vacuole Fusion In Vivo and In Vitro. *PLoS One*. 2013;8(2). doi:10.1371/journal.pone.0056798.
36. Bento CF, Renna M, Ghislat G, et al. Mammalian Autophagy: How Does It Work? *Annu Rev Biochem*. 2016;85(1):685–713. doi:10.1146/annurev-biochem-060815-014556.
37. Berger KH, Merriam JJ, Isberg RR. Altered intraceilular targeting properties associated with mutations in the Legionella pneumophila dotA gene. *Mol Microbiol*. 1994;14(4):809–822.
38. Berger KH, Ralph R. Two distinct defects in intracellular growth complemented by a single genetic locus in Legionelia pneumophila. *Mol Microbiol*. 1993;7(1):7–19.
39. Berke SJS, Paulson HL. Protein aggregation and the ubiquitin proteasome pathway: gaining the UPPer hand on neurodegeneration. *Curr Opin Genet Dev*. 2003;13(3):253–261. doi:10.1016/S0959-437X(03)00053-4.
40. Bhogaraju S, Kalayil S, Liu Y, et al. Phosphoribosylation of Ubiquitin Promotes Serine Ubiquitination and Impairs Conventional Article Phosphoribosylation of Ubiquitin Promotes Serine Ubiquitination and Impairs Conventional Ubiquitination. *Cell*. 2016;167:1636–1649.
41. Bhogaraju S, Kalayil S, Liu Y, et al. Phosphoribosylation of Ubiquitin Promotes Serine Ubiquitination and Impairs Conventional Ubiquitination. *Cell*. 2016;167(6):1636–1649.e13. doi:10.1016/j.cell.2016.11.019.
42. Bian X, Klemm RW, Liu TY, et al. Structures of the atlastin GTPase provide insight into homotypic fusion of endoplasmic reticulum membranes. *Proc Natl Acad Sci*. 2011;108(10):3976–3981. doi:10.1073/pnas.1101643108.
43. Biazik J, Vihinen H, Anwar T, Jokitalo E, Eskelinen EL. The versatile electron microscope: An ultrastructural overview of autophagy. *Methods*. 2015;75:44–53. doi:10.1016/j.ymeth.2014.11.013.
44. Biology C, Lebiedzinska M, Szabadkai G, Jones AWE, Duszynski J, Wieckowski MR. Interactions between the endoplasmic reticulum, mitochondria, plasma membrane and other subcellular organelles. *Int J Biochem Cell Biol*. 2009;41:1805–1816. doi:10.1016/j.biocel.2009.02.017.

45. Bitar DM, Han L, Kwaik YA. Disruption of the Phagosomal Membrane and Egress of Legionella pneumophila into the Cytoplasm during the Last Stages of Intracellular Infection of Macrophages and Acanthamoeba polyphaga. *Infect Immun*. 2004;72(7):4040–4051. doi:10.1128/IAI.72.7.4040.
46. Bjørkøy G, Lamark T, Brech A, et al. p62/SQSTM1 forms protein aggregates degraded by autophagy and has a protective effect on huntingtin-induced cell death. *J Cell Biol*. 2005;171(4):603–614. doi:10.1083/jcb.200507002.
47. Black MW, Boothroyd JC. Lytic cycle of Toxoplasma gondii. *Microbiol Mol Biol Rev*. 2000;64(3):607–623. doi:10.1128/MMBR.64.3.607-623.2000.
48. Blumental-perry A, Haney CJ, Weixel KM, Watkins SC, Weisz OA, Aridor M. Phosphatidylinositol 4-Phosphate Formation at ER Exit Sites Regulates ER Export. *Dev Cell*. 2006;11:671–682. doi:10.1016/j.devcel.2006.09.001.
49. Bola B, Allan V. How and why does the endoplasmic reticulum move? *Biochem Soc Trans*. 2009;37:961–965. doi:10.1042/BST0370961.
50. de Bolle X, Letesson J-J, Gorvel J-P. Small GTPases and Brucella entry into the endoplasmic reticulum. *Biochem Soc Trans*. 2012;40(6):1348–52. doi:10.1042/BST20120156.
51. Bondalapati S, Mansour W, Nakasone MA, Maity SK, Glickman MH, Brik A. Chemical synthesis of phosphorylated ubiquitin and diubiquitin exposes positional sensitivities of E1-E2 enzymes and deubiquitinases. *Chem - A Eur J*. 2015;21(20):7360–7364. doi:10.1002/chem.201500540.
52. Bongiorno D, Petratos S. Molecular regulation of Nogo-A in neural cells: Novel insights into structure and function. *Int J Biochem Cell Biol*. 2010;42(7):1072–1075. doi:10.1016/j.biocel.2010.02.007.
53. Bononi A, Missiroli S, Poletti F, et al. Mitochondria-Associated Membranes (MAMs) as Hotspot Ca2+ Signaling Units BT - Calcium Signaling. In: Islam MS, ed. Dordrecht: Springer Netherlands; 2012:411–437. doi:10.1007/978-94-007-2888-2_17.
54. Borgese N, Francolini M, Snapp E. Endoplasmic reticulum architecture: structures in flux. *Curr Opin Cell Biol*. 2006;18(4):358–364. doi:10.1016/j.ceb.2006.06.008.
55. Boya P, Reggiori F, Codogno P. Emerging regulation and functions of autophagy. *Nat Cell Biol*. 2013;15(7):713–720. doi:10.1038/ncb2788.
56. Boyle KB, Randow F. The role of " eat-me " signals and autophagy cargo receptors in innate immunity. *Curr Opin Microbiol*. 2013;16(3):339–348. doi:10.1016/j.mib.2013.03.010.
57. Brady JP, Claridge JK, Smith PG, Schnell JR. A conserved amphipathic helix is required for membrane tubule formation by Yop1p. *Proc Natl Acad Sci*. 2014;112(5):E639–E648 PNAS. doi:10.1073/pnas.1415882112.
58. de Brito OM, Scorrano L. An intimate liaison: spatial organization of the endoplasmic reticulum-mitochondria relationship. *EMBO J*. 2010;29(16):2715–23. doi:10.1038/emboj.2010.177.
59. Brüggemann H, Cazalet C, Buchrieser C. Adaptation of Legionella pneumophila to the host environment: role of protein secretion, effectors and eukaryotic-like proteins. *Curr Opin Microbiol*. 2006;9(1):86–94. doi:10.1016/j.mib.2005.12.009.
60. Budnik A, Stephens DJ. ER exit sites – Localization and control of COPII vesicle formation. *FEBS Lett*. 2009;583(23):3796–3803.

doi:10.1016/j.febslet.2009.10.038.
61. Burstein D, Zusman T, Degtyar E, Viner R, Segal G, Pupko T. Genome-scale identification of Legionella pneumophila effectors using a machine learning approach. *PLoS Pathog*. 2009;5(7):e1000508. doi:10.1371/journal.ppat.1000508.
62. Cadwell K. Crosstalk between autophagy and inflammatory signalling pathways: balancing defence and homeostasis. *Nat Rev Immunol*. 2016;16(11):661–675. doi:10.1038/nri.2016.100.
63. Cain NE, Starr DA. SUN proteins and nuclear envelope spacing SUN proteins and nuclear envelope spacing. *Nucleus*. 2015;6(1):2–7. doi:10.4161/19491034.2014.990857.
64. Cajee UF, Hull R, Ntwasa M. Modification by ubiquitin-like proteins: Significance in apoptosis and autophagy pathways. *Int J Mol Sci*. 2012;13(9):11804–11831. doi:10.3390/ijms130911804.
65. Campodonico EM, Roy CR, Ninio S. Legionella pneumophila Type IV Effectors YlfA and YlfB Are SNARE-Like Proteins that Form Homo- and Heteromeric Complexes and Enhance the Efficiency of Vacuole Remodeling. *PLoS One*. 2016;11(17):1–20. doi:10.1371/journal.pone.0159698.
66. Canadien V, Tan T, Zilber R, Szeto J, Perrin AJ, Brumell JH. Cutting Edge: Microbial Products Elicit Formation of Dendritic Cell Aggresome-Like Induced Structures in Macrophages. *J Immunol*. 2005;174:2471–2475. doi:10.4049/jimmunol.174.5.2471.
67. Carrasco S, Meyer T. STIM proteins and the endoplasmic reticulum-plasma membrane junctions. *Annu Rev Biochem*. 2011;80:973–1000. doi:10.1146/annurev-biochem-061609-165311.
68. Castellani L, Hardwicke PMD, Franzini-Armstrong C. Effect of Ca 2+ on the Dimeric Structure of Scallop Sarcoplasmic Reticulum. *J Cell Biol*. 1989;108(4):511–520.
69. Castellani L, Hardwicke PMD, Vibert P. Dimer Ribbons in the Three-dimensional Structure of Sarcoplasmic Reticulum. *J Mol Biol*. 1985;185:579–594.
70. Celli J. Surviving inside a macrophage: The many ways of Brucella. *Res Microbiol*. 2006;157(2):93–98. doi:10.1016/j.resmic.2005.10.002.
71. Celli J, Salcedo SP, Gorvel J-P. Brucella coopts the small GTPase Sar1 for intracellular replication. *Proc Natl Acad Sci U S A*. 2005;102(5):1673–8. doi:10.1073/pnas.0406873102.
72. Celli J, Tsolis RM. Bacteria, the endoplasmic reticulum and the unfolded protein response: friends or foes ? *Nat Rev Microbiol*. 2014;(December). doi:10.1038/nrmicro3393.
73. Chambers JE, Petrova K, Tomba G, Vendruscolo M, Ron D. ADP ribosylation adapts an ER chaperone response to short-term fluctuations in unfolded protein load. *J Cell Biol*. 2012;198(3):371–85. doi:10.1083/jcb.201202005.
74. Chandra M, Saran R, Datta S. Deciphering the role of Atg5 in nucleotide dependent interaction of Rab33B with the dimeric complex, Atg5-Atg16L1. *Biochem Biophys Res Commun*. 2016;473(1):8–16. doi:10.1016/j.bbrc.2016.03.043.
75. Chen R, Jin R, Wu L, et al. Reticulon 3 attenuates the clearance of cytosolic prion aggregates via inhibiting autophagy. *Autophagy*. 2011;7(2):205–216.

doi:10.4161/auto.7.2.14197.
76. Chen S, Novick P, Ferro-novick S. ER network formation requires a balance of the dynamin-like GTPase Sey1p and the Lunapark family member Lnp1p. *Nat Cell Biol*. 2012;14(7):707–716. doi:10.1038/ncb2523.
77. Chen S, Novick P, Ferro-Novick S. ER structure and function. *Curr Opin Cell Biol*. 2013;25(4):428–433. doi:10.1016/j.ceb.2013.02.006.
78. Chen Y, Tascón I, Neunuebel MR, et al. Structural Basis for Rab1 De-AMPylation by the Legionella pneumophila Effector SidD. *PLoS Pathog*. 2013;9(5). doi:10.1371/journal.ppat.1003382.
79. Cherfils J. Arf GTPases and their effectors: assembling multivalent membrane-binding platforms. *Curr Opin Struct Biol*. 2014;29:67–76. doi:10.1016/j.sbi.2014.09.007.
80. Chiurchiu V, Maccarrone M, Orlacchio A. The Role of Reticulons in Neurodegenerative Diseases. *Neuromolecular Med*. 2014;16:3–15. doi:10.1007/s12017-013-8271-9.
81. Cho I-T, Adelmant G, Lim Y, Marto JA, Cho G, Golden JA. Ascorbate peroxidase proximity labeling coupled with biochemical fractionation identifies promoters of endoplasmic reticulum–mitochondrial contacts. *J Biol Chem*. 2017. doi:10.1074/jbc.M117.795286.
82. Choi J, Park S, Biering SB, et al. The Parasitophorous Vacuole Membrane of Toxoplasma gondii Is Targeted for Disruption by Ubiquitin-like Conjugation Systems of Autophagy. *Immunity*. 2014;40(6):924–935. doi:10.1016/j.immuni.2014.05.006.
83. Choy A, Dancourt J, Mugo B, et al. The Legionella Effector RavZ Inhibits Host Autophagy Through Irreversible Atg8 Deconjugation. *Science (80-)*. 2012;338(November):1072–1077. doi:10.1126/science.1227026.
84. Christodoulou A, Santarella-mellwig R, Santama N, Mattaj IW. Transmembrane protein TMEM170A is a newly discovered regulator of ER and nuclear envelope morphogenesis in human cells. *J Cell Sci*. 2016;129:1552–1565. doi:10.1242/jcs.175273.
85. Ciani B, Layfield R, Cavey JR, Sheppard PW, Searle MS. Structure of the ubiquitin-associated domain of p62 (SQSTM1) and implications for mutations that cause Paget's disease of bone. *J Biol Chem*. 2003;278(39):37409–37412. doi:10.1074/jbc.M307416200.
86. Ciechanover A, Brundin P. The ubiquitin proteasome system in neurodegenerative diseases: sometimes the chicken, sometimes the egg. *Neuron*. 2003;40(2):427–46. Available at: http://www.ncbi.nlm.nih.gov/pubmed/14556719.
87. Clough B, Wright JD, Pereira PM, et al. K63-Linked Ubiquitination Targets Toxoplasma gondii for Endo-lysosomal Destruction in IFN-Stimulated Human Cells. *PLoS Pathog*. 2016;12(11). doi:10.1371/journal.ppat.1006027.
88. Cluett EB, Brown WJ. Adhesion of Golgi cisternae by proteinaceous interactions : intercisternal bridges as putative adhesive structures. *J Cell Sci*. 1992;784:773–784.
89. Coers J, Vance RE, Fontana MF, Dietrich WF. Restriction of Legionella pneumophila growth in macrophages requires the concerted action of cytokine and Naip5/Ipaf signalling pathways. *Cell Microbiol*. 2007;9(10):2344–2357.

doi:10.1111/j.1462-5822.2007.00963.x.
90. Collins CA, Brown EJ. Cytosol as battleground: Ubiquitin as a weapon for both host and pathogen. *Trends Cell Biol*. 2010;20(4):205–213. doi:10.1016/j.tcb.2010.01.002.
91. Connor HFO, Huibregtse JM. Enzyme – substrate relationships in the ubiquitin system : approaches for identifying substrates of ubiquitin ligases. *Cell Mol Life Sci*. 2017;74(18):3363–3375. doi:10.1007/s00018-017-2529-6.
92. Conover GM, Derré I, Vogel JP, Isberg RR. The Legionella pneumophila LidA protein: a translocated substrate of the Dot/Icm system associated with maintenance of bacterial integrity. *Mol Microbiol*. 2003;48(2):305–21. Available at: http://www.ncbi.nlm.nih.gov/pubmed/12675793.
93. Corda D, Girolamo M Di. Functional aspects of protein mono-ADP- ribosylation. *EMBO J*. 2003;22(9):1953–1958.
94. Cozier GE, Carlton J, McGregor AH, et al. The phox homology (PX) domain-dependent, 3-phosphoinositide-mediated association of sorting nexin-1 with an early sorting endosomal compartment is required for its ability to regulate epidermal growth factor receptor degradation. *J Biol Chem*. 2002;277(50):48730–48736. doi:10.1074/jbc.M206986200.
95. Csordás G, Renken C, Várnai P, et al. Structural and functional features and significance of the physical linkage between ER and mitochondria. *J Cell Biol*. 2006;174(7):915–921. doi:10.1083/jcb.200604016.
96. Cuervo AM. Chaperone-mediated autophagy: Selectivity pays off. *Trends Endocrinol Metab*. 2010;21(3):142–150. doi:10.1016/j.tem.2009.10.003.
97. van Cuijk L, Vermeulen W, Marteijn JA. Ubiquitin at work: The ubiquitous regulation of the damage recognition step of NER. *Exp Cell Res*. 2014;329(1):101–109. doi:10.1016/j.yexcr.2014.07.018.
98. Cunningham CN, Corn JE. Decoding a chain letter for degradation. *Structure*. 2013;21(7):1068–1070. doi:10.1016/j.str.2013.06.009.
99. Dabora SL, Sheetz MF. The microtubule-dependent formation of a tubulovesicular network with characteristics of the ER from cultured cell extracts. *Cell*. 1988;54(1):27–35. doi:10.1016/0092-8674(88)90176-6.
100. Daniels CM, Thirawatananond P, Ong S-E, Gabelli SB, Leung AKL. Nudix hydrolases degrade protein-conjugated ADP-ribose. *Sci Rep*. 2015;5(1):18271. doi:10.1038/srep18271.
101. Dawson TR, Lazarus MD, Hetzer MW, Wente SR. ER membrane – bending proteins are necessary for de novo nuclear pore formation. *J Cell Biol*. 2009;184(5):659–675. doi:10.1083/jcb.200806174.
102. Degenhardt K, Mathew R, Beaudoin B, et al. Autophagy promotes tumor cell survival and restricts necrosis, inflammation, and tumorigenesis. *Cancer Cell*. 2006;10(1):51–64. doi:10.1016/j.ccr.2006.06.001.
103. Deng M, He W, Tan Y, et al. Increased expression of reticulon 3 in neurons leads to reduced axonal transport of β site amyloid precursor protein-cleaving enzyme 1. *J Biol Chem*. 2013;288(42):30236–45. doi:10.1074/jbc.M113.480079.
104. Denton D, Nicolson S, Kumar S. Cell death by autophagy: facts and apparent artefacts. *Cell Death Differ*. 2012;19(1):87–95. doi:10.1038/cdd.2011.146.
105. Deretic V, Saitoh T, Akira S. *Autophagy in infection, inflammation and immunity*.;

2013. doi:10.1038/nri3532.
106. Deshaies RJ, Joazeiro CAP. RING Domain E3 Ubiquitin Ligases. *Annu Rev Biochem*. 2009;78:399–434. doi:10.1146/annurev.biochem.78.101807.093809.
107. Diao J, Liu R, Rong Y, et al. ATG14 promotes membrane tethering and fusion of autophagosomes to endolysosomes. *Nature*. 2015;520(7548):563–566. doi:10.1038/nature14147.
108. Diaz A, Ahlquist P. Role of host reticulon proteins in rearranging membranes for positive-strand RNA virus replication. *Curr Opin Microbiol*. 2012;15:519–524.
109. Dice JF, Chiang HL. Peptide signals for protein degradation within lysosomes. *Biochem Soc Symp*. 1989;55:45–55.
110. Dodd DA, Niederoest B, Bloechlinger S, Dupuis L, Loeffler JP, Schwab ME. Nogo-A, -B, and -C are found on the cell surface and interact together in many different cell types. *J Biol Chem*. 2005;280(13):12494–12502. doi:10.1074/jbc.M411827200.
111. Dolinsky S, Haneburger I, Cichy A, Hannemann M, Itzen A. The Legionella longbeachae Icm/Dot Substrate SidC Selectively Binds Phosphatidylinositol 4-Phosphate with Nanomolar Affinity and Promotes Pathogen Vacuole-Endoplasmic Reticulum Interactions. *Infect Immun*. 2014;82(10):4021–4033. doi:10.1128/IAI.01685-14.
112. Dong N, Niu M, Hu L, Yao Q, Zhou R, Shao F. Modulation of membrane phosphoinositide dynamics by the phosphatidylinositide 4-kinase activity of the Legionella LepB effector. *Nat Microbiol*. 2016;2(0):16236. doi:10.1038/nmicrobiol.2016.236.
113. Dooley HC, Razi M, Polson HEJ, Girardin SE, Wilson MI, Tooze SA. WIPI2 Links LC3 Conjugation with PI3P, Autophagosome Formation, and Pathogen Clearance by Recruiting Atg12–5-16L1. *Mol Cell*. 2014;55(2):238–252. doi:10.1016/j.molcel.2014.05.021.
114. Dowling JJ, Moore SA, Kalimo H, Minassian BA. X-linked myopathy with excessive autophagy: a failure of self-eating. *Acta Neuropathol*. 2015;129(3):383–390. doi:10.1007/s00401-015-1393-4.
115. Dume G. The Legionella pneumophila IcmR protein exhibits chaperone activity for IcmQ by preventing its participation in high-molecular-weight complexes. *Mol Microbiol*. 2001;40(5):1113–1127.
116. Ekkebus R, Flierman D, Geurink PP, Ovaa H. Catching a DUB in the act: Novel ubiquitin-based active site directed probes. *Curr Opin Chem Biol*. 2014;23:63–70. doi:10.1016/j.cbpa.2014.10.005.
117. Ekkebus R, van Kasteren SI, Kulathu Y, et al. On terminal alkynes that can react with active-site cysteine nucleophiles in proteases. *J Am Chem Soc*. 2013;135(8):2867–70. doi:10.1021/ja309802n.
118. Eng JK, Mccormack AL, Yates JR. An Approach to Correlate Tandem Mass Spectral Data of Peptides with Amino Acid Sequences in a Protein Database. *Am Soc Mass Spectrom*. 1994;5:976–989. doi:10.1016/1044-0305(94)80016-2.
119. Engelender S. Ubiquitination of A-synuclein and autophagy in Parkinson ' s disease. *Autophagy*. 2008;(April):372–374.
120. English AR, Voeltz GK. Endoplasmic reticulum structure and interconnections with other organelles. *Cold Spring Harb Perspect Biol*. 2013;5(4):a013227.

doi:10.1101/cshperspect.a013227.
121. English AR, Zurek N, Voeltz GK. Peripheral ER structure and function. *Curr Opin Cell Biol*. 2009;21(4):596–602. doi:10.1016/j.ceb.2009.04.004.
122. English AR, Zurek N, Voeltz GK. Peripheral ER Structure to Function. *Curr Opin Cell Biol*. 2010;21(4):596–602. doi:10.1016/j.ceb.2009.04.004.Peripheral.
123. Ensminger AW, Isberg RR. E3 Ubiquitin Ligase Activity and Targeting of BAT3 by Multiple Legionella pneumophila Translocated Substrates. *Infect Immun*. 2010;78(9):3905–3919. doi:10.1128/IAI.00344-10.
124. Ensminger AW, Isberg RR. Legionella pneumophila Dot/Icm Translocated Substrates: A Sum of Parts. *Curr Opin Microbiol*. 2009;12(1):67–73. doi:10.1016/j.mib.2008.12.004.Legionella.
125. Ensminger AW, Yassin Y, Miron A, Isberg RR. Experimental evolution of Legionella pneumophila in mouse macrophages leads to strains with altered determinants of environmental survival. *PLoS Pathog*. 2012;8(5):e1002731. doi:10.1371/journal.ppat.1002731.
126. Escoll P, Rolando M, Buchrieser C. Modulation of host autophagy during bacterial infection: Sabotaging host munitions for pathogen nutrition. *Front Immunol*. 2016;7(MAR):1–5. doi:10.3389/fimmu.2016.00081.
127. Eskelinen E-L, Saftig P. Autophagy: a lysosomal degradation pathway with a central role in health and disease. *Biochim Biophys Acta*. 2009;1793(4):664–673. doi:10.1016/j.bbamcr.2008.07.014.
128. Fan W, Nassiri A, Zhong Q. Autophagosome targeting and membrane curvature sensing by Barkor/Atg14(L). *Proc Natl Acad Sci*. 2011;108(19):7769–7774. doi:10.1073/pnas.1016472108.
129. Fang Y, Fu D, Shen X-Z. The potential role of ubiquitin c-terminal hydrolases in oncogenesis. *Biochim Biophys Acta*. 2010;1806(1):1–6. doi:10.1016/j.bbcan.2010.03.001.
130. Fass E, Shvets E, Degani I, Hirschberg K, Elazar Z. Microtubules Support Production of Starvation-induced Autophagosomes but Not Their Targeting and Fusion. *J Biol Chem*. 2006;281(47):36303–36316. doi:10.1074/jbc.M607031200.
131. Faßbender M, Herter S, Holtappels R, Schild H. Correlation of dendritic cell maturation and the formation of aggregates of poly-ubiquitinated proteins in the cytosol. *Med Microbiol Immunol*. 2008;197:185–189. doi:10.1007/s00430-008-0091-4.
132. Feldman M, van der Goot FG. Novel ubiquitin-dependent quality control in the endoplasmic reticulum. *Trends Cell Biol*. 2009;19(8):357–63. doi:10.1016/j.tcb.2009.05.005.
133. de Felipe KS, Glover RT, Charpentier X, et al. Legionella eukaryotic-like type IV substrates interfere with organelle trafficking. *PLoS Pathog*. 2008;4(8):e1000117. doi:10.1371/journal.ppat.1000117.
134. Fergani A, Dupuis L, Jokic N, et al. Reticulons as markers of neurological diseases: Focus on amyotrophic lateral sclerosis. *Neurodegener Dis*. 2006;2(3–4):185–194. doi:10.1159/000089624.
135. Finan TM, Kunkel B, Vos GFDE, Signer ER. Second Symbiotic Megaplasmid in Rhizobium meliloti Carrying Exopolysaccharide and Thiamine Synthesis Genes. 1986;167(1):66–72.

136. Fitzwalter BE, Thorburn A. Recent insights into cell death and autophagy. *FEBS J*. 2015;282(22):4279–4288. doi:10.1111/febs.13515.
137. Fournier AE, GrandPre T, Strittmatter SM. Identification of a receptor mediating Nogo-66 inhibition of axonal regeneration. *Nature*. 2001;409(6818):341–346. doi:10.1038/35053072.
138. Fredlund J, Enninga J. Cytoplasmic access by intracellular bacterial pathogens. *Trends Microbiol*. 2014;22(3):128–137. doi:10.1016/j.tim.2014.01.003.
139. Friedman JR, Dibenedetto JR, West M, Rowland AA, Voeltz GK. Endoplasmic reticulum – endosome contact increases as endosomes traffic and mature. *Mol Biol Cell*. 2013;7:1030–1040. doi:10.1091/mbc.E12-10-0733.
140. Friedman JR, Lackner LL, West M, DiBenedetto JR, Nunnari J, Voeltz GK. ER tubules mark sites of mitochondrial division. *Science (80-)*. 2011;334(6054):358–62. doi:10.1126/science.1207385.
141. Friedman JR, Voeltz GK. The ER in 3D: a multifunctional dynamic membrane network. *Trends Cell Biol*. 2011;21(12):709–17. doi:10.1016/j.tcb.2011.07.004.
142. Friedman JR, Webster BM, Mastronarde DN, Verhey KJ, Voeltz GK. ER sliding dynamics and ER-mitochondrial contacts occur on acetylated microtubules. *J Cell Biol*. 2010;190(3):363–75. doi:10.1083/jcb.200911024.
143. Fujita N, Morita E, Itoh T, et al. Recruitment of the autophagic machinery to endosomes during infection is mediated by ubiquitin. *J Cell Biol*. 2013;203(1):115–128. doi:10.1083/jcb.201304188.
144. Fushman D, Walker O. Exploring the Linkage Dependence of Polyubiquitin Conformations Using Molecular Modeling. *J Mol Biol*. 2010;395(4):803–814. doi:10.1016/j.jmb.2009.10.039.
145. Gagnon E, Duclos S, Rondeau C, et al. Endoplasmic reticulum-mediated phagocytosis is a mechanism of entry into macrophages. *Cell*. 2002;110(1):119–131. doi:10.1016/S0092-8674(02)00797-3.
146. Galardy P, Ploegh HL, Ovaa H. Mechanism-based proteomics tools based on ubiquitin and ubiquitin-like proteins: Crystallography, activity profiling, and protease identification. *Methods Enzymol*. 2005;399(5):120–131. doi:10.1016/S0076-6879(05)99008-3.
147. Galluzzi L, Baehrecke EH, Ballabio A, et al. Molecular definitions of autophagy and related processes. *EMBO J*. 2017;36(13):1811–1836. doi:10.15252/embj.201796697.
148. Ganesan AK, Mende-Mueller L, Selzer J, Barbieri JT. Pseudomonas aeruginosa exoenzyme S, a double ADP-ribosyltransferase, resembles vertebrate mono-ADP-ribosyltransferases. *J Biol Chem*. 1999;274(14):9503–9508. doi:10.1074/jbc.274.14.9503.
149. Garofalo T, Matarrese P, Manganelli V, et al. Evidence for the involvement of lipid rafts localized at the ER-mitochondria associated membranes in autophagosome formation. *Autophagy*. 2016;12(6):917–935. doi:10.1080/15548627.2016.1160971.
150. Gazdag EM, Schöbel S, Shkumatov A V., Goody RS, Itzen A. The structure of the N-terminal domain of the Legionella protein SidC. *J Struct Biol*. 2014;186(1):188–194. doi:10.1016/j.jsb.2014.02.003.
151. Ge J, Shao F. Manipulation of host vesicular trafficking and innate immune

defence by Legionella Dot/Icm effectors. *Cell Microbiol*. 2011;13(12):1870–80. doi:10.1111/j.1462-5822.2011.01710.x.
152. Ge L, Melville D, Zhang M, Schekman R. The ER-Golgi intermediate compartment is a key membrane source for the LC3 lipidation step of autophagosome biogenesis. *Elife*. 2013;2013(2):1–23. doi:10.7554/eLife.00947.001.
153. Geng J, Klionsky DJ. The Atg8 and Atg12 ubiquitin-like conjugation systems in macroautophagy. "Protein Modifications: Beyond the Usual Suspects" Review Series. *EMBO Rep*. 2008;9(9):859–864. doi:10.1038/embor.2008.163.
154. Gibbs K a, Urbanowski ML, Greenberg EP. Genetic determinants of self identity and social recognition in bacteria. *Science (80-)*. 2008;321(5886):256–9. doi:10.1126/science.1160033.
155. Giordano F, Saheki Y, Idevall-hagren O, et al. PI(4,5)P2-Dependent and Ca2+-Regulated ER-PM Interactions Mediated by the Extended Synaptotagmins. *Cell*. 2013;153:1494–1509.
156. Giovane A, Balestrieri C, Servillo L. 1-N6-Etheno-ADP-ribosylation of elongation factor-2 by diphtheria toxin. *FEBS*. 1985;191(2):191–194.
157. Gkogkolou P, Böhm M. Advanced glycation end products: Key players in skin aging? *Dermatoendocrinol*. 2012;4(3):259–70. doi:10.4161/derm.22028.
158. Glick D, Barth S, Macleod KF. Autophagy : cellular and molecular mechanisms. *J Pathol*. 2010;221(1):3–12. doi:10.1002/path.2697.Autophagy.
159. Glowacki G, Braren R, Firner K, et al. The family of toxin-related ecto-ADP-ribosyltransferases in humans and the mouse. *Protein Sci*. 2002;11:1657–1670. doi:10.1110/ps.0200602.The.
160. Goder V. Roles of Ubiquitin Degradation (ERAD) in Endoplasmic Reticulum-Associated Protein. *Curr Protein Pept Sci*. 2012;13:1–12.
161. Goetz JG, Genty H, St-Pierre P, et al. Reversible interactions between smooth domains of the endoplasmic reticulum and mitochondria are regulated by physiological cytosolic Ca2+ levels. *J Cell Sci*. 2007;120(Pt 20):3553–64. doi:10.1242/jcs.03486.
162. Goldszmid RS, Coppens I, Lev A, Caspar P, Mellman I, Sher A. Host ER-parasitophorous vacuole interaction provides a route of entry for antigen cross-presentation in Toxoplasma gondii-infected dendritic cells. *J Exp Med*. 2009;206(2):399–410. doi:10.1084/jem.20082108.
163. Gorvel JP, Moreno E. Brucella intracellular life: From invasion to intracellular replication. *Vet Microbiol*. 2002;90(1–4):281–297. doi:10.1016/S0378-1135(02)00214-6.
164. Goyal U, Blackstone C. Untangling the web: Mechanisms underlying ER network formation. *Biochim Biophys Acta*. 2013;1833:2492–2498.
165. Graef M, Friedman JR, Graham C, Babu M, Nunnari J. ER exit sites are physical and functional core autophagosome biogenesis components. *Mol Biol Cell*. 2013;24(18):2918–31. doi:10.1091/mbc.E13-07-0381.
166. GrandPré T, Nakamura F, Vartanian T, Strittmatter SM. Identification of the Nogo inhibitor of axon regeneration as a Reticulon protein. *Nature*. 2000;403(6768):439–444. doi:10.1038/35000226.
167. Griffing LR, Gao HT, Sparkes I. ER network dynamics are differentially

controlled by myosins XI-K, XI-C, XI-E, XI-I, XI-1 and XI-2. *Front Plant Sci*. 2014;5(May):1–12. doi:10.3389/fpls.2014.00218.
168. Grose C, Buckingham E, Carpenter J, Kunkel J. Varicella-Zoster Virus Infectious Cycle: ER Stress, Autophagic Flux, and Amphisome-Mediated Trafficking. *Pathogens*. 2016;5(4):67. doi:10.3390/pathogens5040067.
169. Grumati P, Morozzi G, Hölper S, et al. Full length RTN3 regulates turnover of tubular endoplasmic reticulum via selective autophagy. *Elife*. 2017;6:1–32. doi:10.7554/eLife.25555.
170. Guimaraes RS, Delorme-Axford E, Klionsky DJ, Reggiori F. Assays for the biochemical and ultrastructural measurement of selective and nonselective types of autophagy in the yeast Saccharomyces cerevisiae. *Methods*. 2015;75:141–150. doi:10.1016/j.ymeth.2014.11.023.
171. Guo Y, Chang C, Huang R, Liu B, Bao L, Liu W. AP1 is essential for generation of autophagosomes from the trans-Golgi network. *J Cell Sci*. 2012;125(7):1706–1715. doi:10.1242/jcs.093203.
172. Haenssler E, Ramabhadran V, Murphy CS, Heidtman MI, Isberg RR. Endoplasmic Reticulum Tubule Protein Reticulon 4 Associates with the Legionella pneumophila Vacuole and with Translocated Substrate Ceg9. *Infect Immun*. 2015;83(9):3479–3489. doi:10.1128/IAI.00507-15.
173. Haglund K, Sigismund S, Polo S, Szymkiewicz I, Di Fiore PP, Dikic I. Multiple monoubiquitination of RTKs is sufficient for their endocytosis and degradation. *Nat Cell Biol*. 2003;5(5):461–466. doi:10.1038/ncb983.
174. Hailey DW, Rambold AS, Satpute-Krishnan P, et al. Mitochondria Supply Membranes for Autophagosome Biogenesis during Starvation. *Cell*. 2010;141(4):656–667. doi:10.1016/j.cell.2010.04.009.
175. Hajnoczky G, Csordas G, Das S, et al. Mitochondrial calcium signalling and cell death: Approaches for assessing the role of mitochondrial Ca2+ uptake in apoptosis. *Cell Calcium*. 2006;40(5–6):553–560. doi:10.1016/j.ceca.2006.08.016.
176. Ham H, Sreelatha A, Orth K. Manipulation of host membranes by bacterial effectors. *Nat Rev Microbiol*. 2011;9(9):635–646. doi:10.1038/nrmicro2602.
177. Hamasaki M, Furuta N, Matsuda A, et al. Autophagosomes form at ER-mitochondria contact sites. *Nature*. 2013;495(7441):389–393. doi:10.1038/nature11910\rnature11910 [pii].
178. Hamasaki M, Shibutani ST, Yoshimori T. Up-to-date membrane biogenesis in the autophagosome formation. *Curr Opin Cell Biol*. 2013;25:455–460.
179. Han S, Arvai AS, Clancy SB, Tainer J a. Crystal structure and novel recognition motif of rho ADP-ribosylating C3 exoenzyme from Clostridium botulinum: structural insights for recognition specificity and catalysis. *J Mol Biol*. 2001;305:95–107. doi:10.1006/jmbi.2000.4292.
180. Harb OS, Venkataraman C, Haack BJ, Gao LY, Abu Kwaik Y. Heterogeneity in the attachment and uptake mechanisms of the Legionnaires' disease bacterium, Legionella pneumophila, by protozoan hosts. *Appl Environ Microbiol*. 1998;64(1):126–132.
181. Hardiman CA, Roy CR. AMPylation is critical for Rab1 localization to vacuoles containing Legionella pneumophila. *MBio*. 2014;5(1):1–11. doi:10.1128/mBio.01035-13.

182. Harrison KD, Miao RQ, Fernandez-Hernándo C, Suárez Y, Dávalos A, Sessa WC. Nogo-B Receptor Stabilizes Niemann-Pick Type C2 Protein and Regulates Intracellular Cholesterol Trafficking. *Cell Metab*. 2009;10(3):208–218. doi:10.1016/j.cmet.2009.07.003.
183. Hatakeyama S, Yada M, Matsumoto M, Ishida N, Nakayama KI. U Box Proteins as a New Family of Ubiquitin-Protein Ligases. *J Biol Chem*. 2001;276(35):33111–33120. doi:10.1074/jbc.M102755200.
184. Havey JC, Roy CR. Toxicity and SidJ-Mediated Suppression of Toxicity Require Distinct Regions in the SidE Family of Legionella pneumophila Effectors. *Infect Immun*. 2015;83(9):3506–3514. doi:10.1128/IAI.00497-15.
185. Hayakawa M. Role of K63-linked polyubiquitination in NF-KB signalling: Which ligase catalyzes and what molecule is targeted? *J Biochem*. 2012;151(2):115–118. doi:10.1093/jb/mvr139.
186. Hayashi-Nishino M, Fujita N, Noda T, Yamaguchi A, Yoshimori T, Yamamoto A. A subdomain of the endoplasmic reticulum forms a cradle for autophagosome formation. *Nat Cell Biol*. 2009;11(12):1433–1437. doi:10.1038/ncb1991.
187. Hayashi T, Rizzuto R, Hajnoczky G, Su TP. MAM: more than just a housekeeper. *Trends Cell Biol*. 2009;19(2):81–88. doi:10.1016/j.tcb.2008.12.002.
188. He W, Hu X, Shi Q, et al. Mapping of Interaction Domains Mediating Binding between BACE1 and RTN/Nogo Proteins. *J Mol Biol*. 2006;363(3):625–634. doi:10.1016/j.jmb.2006.07.094.
189. He W, Lu Y, Qahwash I, Hu XY, Chang A, Yan R. Reticulon family members modulate BACE1 activity and amyloid-beta peptide generation. *Nat Med*. 2004;10(9):959–965. doi:10.1038/nm1088.
190. He W, Shi Q, Hu X, Yan R. The membrane topology of RTN3 and its effect on binding of RTN3 to BACE1. *J Biol Chem*. 2007;282(40):29144–29151. doi:10.1074/jbc.M704181200.
191. Heidtman M, Chen EJ, Moy M, Isberg RR. Large-scale identification of Legionella pneumophila Dot/Icm substrates that modulate host cell vesicle trafficking pathways. *Cell Microbiol*. 2009;11(2):230–48. doi:10.1111/j.1462-5822.2008.01249.x.
192. Heinzer S, Wörz S, Kalla C, Rohr K, Weiss M. A model for the self-organization of exit sites in the endoplasmic reticulum. *J Cell Sci*. 2008;12(1):55–64. doi:10.1242/jcs.013383.
193. Hempstead AD, Isberg RR. Inhibition of host cell translation elongation by Legionella pneumophila blocks the host cell unfolded protein response. *Proc Natl Acad Sci*. 2015;112(49):E6790-7. doi:10.1073/pnas.1508716112.
194. Herhaus L, Dikic I. Expanding the ubiquitin code through post-translational modification. *EMBO Rep*. 2015;16(9):1071–83. doi:10.15252/embr.201540891.
195. Hetzer MW, Walther TC, Mattaj IW. Pushing the Envelope: Structure, Function, and Dynamics of the Nuclear Periphery. *Annu Rev Cell Dev Biol*. 2005;21:347–380. doi:10.1146/annurev.cellbio.21.090704.151152.
196. Heyninck K, Beyaert R. A20 inhibits NF- kB activation by dual ubiquitin-editing functions. *Trends Biochem Sci*. 2005;30(1).
197. Hicke L. Protein Regulation By Monoubiquitin. *Nat Rev Mol Cell Biol*. 2001;2(March):195–201. doi:10.1038/35056583.

198. Hicke L, Dunn R. Regulation of membrane protein transport by ubiquitin and ubiquitin-binding proteins. *Annu Rev Cell Dev Biol*. 2003;19:141–172. doi:10.1146/annurev.nutr.23.011702.073408.
199. Hicks SW, Galán JE. Hijacking the host ubiquitin pathway: structural strategies of bacterial E3 ubiquitin ligases. *Curr Opin Microbiol*. 2010;13(1):1–12. doi:10.1016/j.mib.2009.11.008.
200. Hirota Y, Tanaka Y. A small GTPase, human Rab32, is required for the formation of autophagic vacuoles under basal conditions. *Cell Mol Life Sci*. 2009;66(17):2913–2932. doi:10.1007/s00018-009-0080-9.
201. Holthuis JCM, Levine TP. Lipid traffic: floppy drives and a superhighway. *Nat Rev Mol Cell Biol*. 2005;6(3):209–20. doi:10.1038/nrm1591.
202. Horenkamp FA, Kauffman KJ, Kohler LJ, et al. The Legionella Anti-autophagy Effector RavZ Targets the Autophagosome via PI3P- and Curvature-Sensing Motifs. *Dev Cell*. 2015;34(5):569–576. doi:10.1016/j.devcel.2015.08.010.
203. Horenkamp FA, Mukherjee S, Alix E, et al. Legionella pneumophila subversion of host vesicular transport by SidC effector proteins. *Traffic*. 2014;15(5):488–499. doi:10.1111/tra.12158.
204. Horwitz MA. Formation of a Novel Phagosome by the Legionnaires' disease bacterium (Legionella pneumophila) in Human Monocytes. *J Exp Med*. 1983;158(October):1319–1331.
205. Horwitz MA, Maxfield FR. Legionella pneumophila inhibits acidification of its phagosome in human monocytes. *J Cell Biol*. 1984;99(6):1936–1943. doi:10.1083/jcb.99.6.1936.
206. Hsu F, Luo XX, Qiu J, et al. The Legionella effector SidC defines a unique family of ubiquitin ligases important for bacterial phagosomal remodeling. *Proc Natl Acad Sci*. 2014;111(29):10538–10543. doi:10.1073/pnas.1402605111.
207. Hu J, Shibata Y, Voss C, et al. Membrane Proteins of the Endoplasmic Reticulum Induce High-Curvature Tubules. *Science (80-)*. 2008;319:1247–1250.
208. Hu J, Shibata Y, Zhu PP, et al. A Class of Dynamin-like GTPases Involved in the Generation of the Tubular ER Network. *Cell*. 2009;138(3):549–561. doi:10.1016/j.cell.2009.05.025.
209. Huang F, Zeng X, Kim W, et al. Lysine 63-linked polyubiquitination is required for EGF receptor degradation. *Proc Natl Acad Sci*. 2013;110(39):15722–15727. doi:10.1073/pnas.1308014110.
210. Huang J, Birmingham CL, Shahnazari S, et al. Antibacterial autophagy occurs at PtdIns(3)P-enriched domains of the endoplasmic reticulum and requires Rab1 GTPase. *Autophagy*. 2011;7(1):17–26. doi:10.4161/auto.7.1.13840.
211. Huang J, Brumell JH. Bacteria – autophagy interplay : a battle for survival. *Nat Rev Microbiol*. 2014;12(2):101–114. doi:10.1038/nrmicro3160.
212. Huang L, Marvin JM, Tatsis N, Eisenlohr LC. Cutting Edge: Selective role of ubiquitin in MHC class I antigen presentation. *J Immunol*. 2011;186(4):1904–1908. doi:10.4049/jimmunol.1003411.
213. Hubber A, Roy CR. Modulation of host cell function by Legionella pneumophila type IV effectors. *Annu Rev Cell Dev Biol*. 2010;26:261–83. doi:10.1146/annurev-cellbio-100109-104034.
214. Hubert V, Peschel A, Langer B, Gröger M, Rees A, Kain R. LAMP-2 is required

for incorporating syntaxin-17 into autophagosomes and for their fusion with lysosomes. *Biol Open*. 2016;5(10):1516–1529. doi:10.1242/bio.018648.
215. Hughes H, Budnik A, Schmidt K, et al. Organisation of human ER-exit sites: requirements for the localisation of Sec16 to transitional ER. *J Cell Sci*. 2009;122(16):2924–2934. doi:10.1242/jcs.044032.
216. Huibregtse J, Rohde JR. Hell ' s BELs : Bacterial E3 Ligases That Exploit the Eukaryotic Ubiquitin Machinery. *PLoS Pathog*. 2014;10(8):8–11. doi:10.1371/journal.ppat.1004255.
217. Husnjak K, Dikic I. Ubiquitin-Binding Proteins: Decoders of Ubiquitin-Mediated Cellular Functions. *Annu Rev Biochem*. 2012;81(May):291–332. doi:10.1146/annurev-biochem-051810-094654.
218. Ingmundson A, Delprato A, Lambright DG, Roy CR. Legionella pneumophila proteins that regulate Rab1 membrane cycling. *Nature*. 2007;450(7168):365–9. doi:10.1038/nature06336.
219. Ingmundson A, Roy CR. Analyzing Association of the Endoplasmic Reticulum with Legionella pnumophila-Containing Vacuoles by Fluorescence Microscopy. In: Deretic V, ed. *Methods in Molecular Biology*.Vol 445. Totowa: Humana Press; 2008:379–387.
220. Isberg RR, O'Connor TJ, Heidtman M. The Legionella pneumophila replication vacuole: making a cosy niche inside host cells. *Nat Rev Microbiol*. 2009;7(1):13–24. doi:10.1038/nrmicro1967.
221. Islam S. Calcium Signaling. *Adv Exp Med Biol*. 740. doi:10.1007/978-94-007-2888-2.
222. Itakura E, Kishi-itakura C, Mizushima N. The Hairpin-type Tail-Anchored SNARE Syntaxin 17 Targets to Autophagosomes for Fusion with Endosomes/Lysosomes. *Cell*. 2012;151(6):1256–1269. doi:10.1016/j.cell.2012.11.001.
223. Itakura E, Kishi C, Inoue K, Mizushimi N. Beclin 1 Forms Two Distinct Phosphatidylinositol 3-Kinase Complexes with Mammalian Atg14 and UVRAG. *Mol Biol Cell*. 2008;19:5360–5372. doi:10.1091/mbc.E08.
224. Itakura E, Mizushima N. Syntaxin 17: The autophagosomal SNARE. *Autophagy*. 2013;9(6):917–919. doi:10.4161/auto.24109.
225. Itoh T, Fujita N, Kanno E, Yamamoto A, Yoshimori T, Fukuda M. Golgi-resident Small GTPase Rab33B Interacts with Atg16L and Modulates Autophagosome Formation. *Mol Biol Cell*. 2008;19:2916–2925. doi:10.1091/mbc.E07.
226. Ivanov SS, Roy CR. Modulation of ubiquitin dynamics and suppression of DALIS formation by the Legionella pneumophila Dot/Icm system. *Cell Microbiol*. 2009;11(2):261–78. doi:10.1111/j.1462-5822.2008.01251.x.
227. Jackson CL. GEF-effector interactions. *Cell Logist*. 2014;4(2). doi:10.4161/21592780.2014.943616.
228. Jackson LP. Structure and mechanism of COPI vesicle biogenesis. *Curr Opin Cell Biol*. 2014;29:67–73. doi:10.1016/j.ceb.2014.04.009.
229. Jahreiss L, Menzies FM, Rubinsztein DC. The itinerary of autophagosomes: From peripheral formation to kiss-and-run fusion with lysosomes. *Traffic*. 2008;9(4):574–587. doi:10.1111/j.1600-0854.2008.00701.x.
230. Janssens S, Pulendran B, Lambrecht BN. Emerging functions of the unfolded

protein response in immunity. *Nat Immunol*. 2014;15(10):910–919. doi:10.1038/ni.2991.
231. Jeong KC, Ghosal D, Chang Y, Jensen GJ, Vogel JP. Polar delivery of Legionella type IV secretion system substrates is essential for virulence. *Proc Natl Acad Sci*. 2017;114(30):8077–8082. doi:10.1073/pnas.1621438114.
232. Jeong KC, Sexton JA, Vogel JP. Spatiotemporal Regulation of a Legionella pneumophila T4SS Substrate by the Metaeffector SidJ. *PLoS Pathog*. 2015:1–22. doi:10.1371/journal.ppat.1004695.
233. Jiang P, Mizushima N. LC3- and p62-based biochemical methods for the analysis of autophagy progression in mammalian cells. *Methods*. 2015;75:13–18. doi:10.1016/j.ymeth.2014.11.021.
234. Jin L, Pahuja KB, Wickliffe KE, et al. Ubiquitin-dependent regulation of COPII coat size and function. *Nature*. 2012;482(7386):495–500. doi:10.1038/nature10822.
235. Jo EK, Yuk JM, Shin DM, Sasakawa C. Roles of autophagy in elimination of intracellular bacterial pathogens. *Front Immunol*. 2013;4(May):1–9. doi:10.3389/fimmu.2013.00097.
236. de Jong MF, Starr T, Winter MG, den Hartigh AB, Child R, Knodler LA, van Dijl JM, Celli J TR. Sensing of Bacterial Type IV Secretion via the Unfolded Protein. *MBio*. 2013;4(1):1–10. doi:10.1128/mBio.00418-12.Invited.
237. Jongsma MLLM, Berlin I, Wijdeven RHHM, et al. An ER-Associated Pathway Defines Endosomal Architecture for Controlled Cargo Transport. *Cell*. 2016;166(1):152–166. doi:10.1016/j.cell.2016.05.078.
238. Joshi AD, Swanson MS. Secrets of a successful pathogen: Legionella resistance to progression along the autophagic pathway. *Front Microbiol*. 2011;2(JUNE):1–9. doi:10.3389/fmicb.2011.00138.
239. Jozsef L, Tashiro K, Kuo A, et al. Reticluon 4 is necessary for ER tubulation, STIM1-Orai1 coupling and store-operated calcium entry. *J Biol Chem*. 2014;289:9380–9395. doi:10.1074/jbc.M114.548602.
240. Kagan JC, Roy CR. Legionella phagosomes intercept vesicular traffic from endoplasmic reticulum exit sites. *Nat Cell Biol*. 2002;4(12):945–954. doi:10.1038/ncb883.
241. Kagan JC, Stein M-P, Pypaert M, Roy CR. Legionella subvert the functions of Rab1 and Sec22b to create a replicative organelle. *J Exp Med*. 2004;199(9):1201–11. doi:10.1084/jem.20031706.
242. Kane LA, Lazarou M, Fogel AI, et al. PINK1 phosphorylates ubiquitin to activate parkin E3 ubiquitin ligase activity. *J Cell Biol*. 2014;205(2):143–153. doi:10.1083/jcb.201402104.
243. Kaushik S, Cuervo AM. Chaperone-mediated autophagy: A unique way to enter the lysosome world. *Trends Cell Biol*. 2012;22(8):407–417. doi:10.1016/j.tcb.2012.05.006.
244. Kazlauskaite A, Kondapalli C, Gourlay R, et al. Parkin is activated by PINK1-dependent phosphorylation of ubiquitin at Ser ^{65}. *Biochem J*. 2014;460(1):127–141. doi:10.1042/BJ20140334.
245. Kelly L, Sternberg M. Protein structure prediction on the web: a case study using the Phyre server. *Nat Protoc*. 2009;4:363–371.

246. Kempf A, Schwab ME. Nogo-A Represses Anatomical and Synaptic Plasticity in the Central Nervous System. *Physiology*. 2013;28:151–163. doi:10.1152/physiol.00052.2012.
247. Kerscher O, Felberbaum R, Hochstrasser M. Modification of proteins by ubiquitin and ubiquitin-like proteins. *Annu Rev Cell Dev Biol*. 2006;22:159–80. doi:10.1146/annurev.cellbio.22.010605.093503.
248. Khweek AA, Caution K, Akhter A, et al. A bacterial protein promotes the recognition of the Legionella pneumophila vacuole by autophagy. *Eur J Immunol*. 2013;43(5):1333–1344. doi:10.1002/eji.201242835.
249. Kim HC, Huibregtse JM. Polyubiquitination by HECT E3s and the determinants of chain type specificity. *Mol Cell Biol*. 2009;29(12):3307–18. doi:10.1128/MCB.00240-09.
250. Kim W, Bennett EJ, Huttlin EL, et al. Systematic and quantitative assessment of the ubiquitin-modified proteome. *Mol Cell*. 2011;44(2):325–40. doi:10.1016/j.molcel.2011.08.025.
251. King NP, Newton P, Schuelein R, et al. Soluble NSF attachment protein receptor molecular mimicry by a Legionella pneumophilaDot/Icm effector. *Cell Microbiol*. 2015;17(6):767–784. doi:10.1111/cmi.12405.
252. Kingry LC, Petersen JM. Comparative review of Francisella tularensis and Francisella novicida. *Front Cell Infect Microbiol*. 2014;4(March):35. doi:10.3389/fcimb.2014.00035.
253. Kirichok Y, Krapivinsky G, Clapham DE. The mitochondrial calcium uniporter is a highly selective ion channel. *Nature*. 2010;427(January 2004):1874–1878.
254. Klebl BM, Pette D. A Fluorometric Assay for Measurement of Mono-ADP-Ribosyltransferase Activity. *Anal Biochem*. 1996;239:145–152.
255. Kohler LJ, Roy CR. Biogenesis of the lysosome-derived vacuole containing Coxiella burnetii. *Microbes Infect*. 2015;17(11–12):766–771. doi:10.1016/j.micinf.2015.08.006.
256. Kolter R, Inuzuka M, Helinski DR. Trans-complementation-dependent replication of a low molecular weight origin fragment from plasmid R6K. *Cell*. 1978;15(4):1199–1208. doi:10.1016/0092-8674(78)90046-6.
257. Komander D, Rape M. The ubiquitin code. *Annu Rev Biochem*. 2012;81:203–29. doi:10.1146/annurev-biochem-060310-170328.
258. Kon M, Cuervo AM. Chaperone-mediated autophagy in health and disease. *FEBS Lett*. 2010;584(7):1399–1404. doi:10.1016/j.febslet.2009.12.025.
259. Kornmann B, Currie E, Collins SR, et al. An ER-Mitochondria Tethering Biology Screen. *Science (80-)*. 2009;325(July):477–481.
260. Kotewicz KM, Ramabhadran V, Sjoblom N, Behringer J, Scheck RA, Isberg RR. A Single Legionella Effector Catalyzes a Multistep Ubiquitination Pathway to Rearrange Tubular Endoplasmic Reticulum for Replication. *Cell Host Microbe*. 2017;21(Febuary):169–181.
261. Koyano F, Okatsu K, Kosako H, et al. Ubiquitin is phosphorylated by PINK1 to activate parkin. *Nature*. 2014;510(7503):162–166. doi:10.1038/nature13392.
262. Krebs C, Koestner W, Nissen M, et al. Flow cytometric and immunoblot assays for cell surface ADP-ribosylation using a monoclonal antibody specific for ethenoadenosine. *Anal Biochem*. 2003;314(1):108–115. doi:10.1016/S0003-

2697(02)00640-1.
263. Krska D, Ravulapalli R, Fieldhouse RJ, Lugo MR, Merrill AR. C3larvin Toxin, an ADP-ribosyltransferase from Paenibacillus larvae. *J Biol Chem*. 2015;290(3):1639–1653. doi:10.1074/jbc.M114.589846.
264. Kubisch J, Türei D, Földvári-Nagy L, et al. Complex regulation of autophagy in cancer - Integrated approaches to discover the networks that hold a double-edged sword. *Semin Cancer Biol*. 2013;23(4):252–261. doi:10.1016/j.semcancer.2013.06.009.
265. Kubori T, Hyakutake A, Nagai H. Legionella translocates an E3 ubiquitin ligase that has multiple U-boxes with distinct functions. *Mol Microbiol*. 2008;67(6):1307–1319. doi:10.1111/j.1365-2958.2008.06124.x.
266. Kubori T, Shinzawa N, Kanuka H, Nagai H. Legionella metaeffector exploits host proteasome to temporally regulate cognate effector. *PLoS Pathog*. 2010;6(12):1–8. doi:10.1371/journal.ppat.1001216.
267. Kumar Y, Valdivia RH. Leading a Sheltered Life: Intracellular Pathogens and Maintenance of Vacuolar Compartments. *Cell Host Microbe*. 2009;5(6):593–601. doi:10.1016/j.chom.2009.05.014.
268. Kume H, Murayama KS, Araki W. The two-hydrophobic domain tertiary structure of reticulon proteins is critical for modulation of beta-secretase BACE1. *J Neurosci Res*. 2009;87(13):2963–72. doi:10.1002/jnr.22112.
269. Kung C-P, Budina A, Balaburski G, Bergenstock MK, Murphy M. Autophagy in tumor suppression and cancer therapy. *Crit Rev Eukaryot Gene Expr*. 2011;21(1):71–100. Available at: http://www.pubmedcentral.nih.gov/articlerender.fcgi?artid=3187613&tool=pmcentrez&rendertype=abstract.
270. Kwaik YABU. The Phagosome Containing Legionella pneumophila within the Protozoan Hartmannella vermiformis Is Surrounded by the Rough Endoplasmic Reticulum. *Appl Environ Microbiol*. 1996;62(6):2022–2028.
271. Kwon DH, Kim S, Jung YO, et al. The 1:2 complex between RavZ and LC3 reveals a mechanism for deconjugation of LC3 on the phagophore membrane. *Autophagy*. 2017;13(1):70–81. doi:10.1080/15548627.2016.1243199.
272. Laing S, Unger M, Koch-Nolte F, Haag F. ADP-ribosylation of arginine. *Amino Acids*. 2011;41(2):257–69. doi:10.1007/s00726-010-0676-2.
273. Lam SS, Martell JD, Kamer KJ, et al. Directed evolution of APEX2 for electron microscopy and proximity labeling. *Nat Methods*. 2015;12(1):51–54. doi:10.1038/NMETH.3179.
274. Lamb CA, Yoshimori T, Tooze SA. The autophagosome: origins unknown, biogenesis complex. *Nat Rev Mol Cell Biol*. 2013;14(12):759–774. doi:10.1038/nrm3696.
275. Langhans M, Meckel T, Kress A, Lerich A, Robinson DG. ERES (ER exit sites) and the "Secretory Unit Concept." *J Microsc*. 2012;247(1):48–59. doi:10.1111/j.1365-2818.2011.03597.x.
276. Laplantine E, Fontan E, Chiaravalli J, et al. NEMO specifically recognizes K63-linked poly-ubiquitin chains through a new bipartite ubiquitin-binding domain. *EMBO J*. 2009;28(19):2885–2895. doi:10.1038/emboj.2009.241.
277. Lee C, Chen LB. Dynamic behavior of endoplasmic reticulum in living cells. *Cell*.

1988;54(1):37–46. doi:10.1016/0092-8674(88)90177-8.
278. Lee J-S, Shukla A, Schneider J, et al. Histone crosstalk between H2B monoubiquitination and H3 methylation mediated by COMPASS. *Cell*. 2007;131(6):1084–96. doi:10.1016/j.cell.2007.09.046.
279. Lee S, Kang M, Park J, et al. APEX Fingerprinting Reveals the Subcellular Localization of Proteins of Interest. *Cell Rep*. 2016;15(8):1837–1847. doi:10.1016/j.celrep.2016.04.064.
280. Lee Y-M, Babu CS, Chen YC, Milcic M, Qu Y, Lim C. Conserved structural motif for recognizing nicotinamide adenine dinucleotide in poly(ADP-ribose) polymerases and ADP-ribosylating toxins: implications for structure-based drug design. *J Med Chem*. 2010;53(10):4038–49. doi:10.1021/jm1001106.
281. Lelouard H, Ferrand V, Marguet D, et al. Dendritic cell aggresome-like induced structures are dedicated areas for ubiquitination and storage of newly synthesized defective proteins. *J Cell Biol*. 2004;164(5):667–675. doi:10.1083/jcb.200312073.
282. Levine B, Mizushima N, Virgin H. Autophagy in immunity and inflammation. *Nature*. 2011;469:1–5. doi:10.1038/nature09782.
283. Li W, Yang Q, Mao Z. Chaperone-mediated autophagy: Machinery, regulation and biological consequences. *Cell Mol Life Sci*. 2011;68(5):749–763. doi:10.1007/s00018-010-0565-6.
284. Li WW, Li J, Bao JK. Microautophagy: Lesser-known self-eating. *Cell Mol Life Sci*. 2012;69(7):1125–1136. doi:10.1007/s00018-011-0865-5.
285. Li Y, Prinz WA. ATP-binding cassette (ABC) transporters mediate nonvesicular, raft-modulated sterol movement from the plasma membrane to the endoplasmic reticulum. *J Biol Chem*. 2004;279(43):45226–45234. doi:10.1074/jbc.M407600200.
286. Liang X, Tang J, Liang Y, Jin R, Cai X. Suppression of autophagy by chloroquine sensitizes 5-fluorouracil-mediated cell death in gallbladder carcinoma cells. *Cell Biosci*. 2014;4(1):10. doi:10.1186/2045-3701-4-10.
287. Liang X, De Vera ME, Buchser WJ, et al. Inhibiting systemic autophagy during interleukin 2 immunotherapy promotes long-term tumor regression. *Cancer Res*. 2012;72(11):2791–2801. doi:10.1158/0008-5472.CAN-12-0320.
288. Lifshitz Z, Burstein D, Peeri M, et al. Computational modeling and experimental validation of the Legionella and Coxiella virulence-related type-IVB secretion signal. *Proc Natl Acad Sci*. 2013;110(8):E707-15. doi:10.1073/pnas.1215278110.
289. Lin S, Sun S, Hu J. Molecular basis for sculpting the endoplasmic reticulum membrane. *Int J Biochem Cell Biol*. 2012;44(9):1436–1443. doi:10.1016/j.biocel.2012.05.013.
290. Lin Y, Machner MP. Exploitation of the host cell ubiquitin machinery by microbial effector proteins. *J Cell Sci*. 2017;130:1985–1996. doi:10.1242/jcs.188482.
291. Linares JF, Duran A, Yajima T, Pasparakis M, Moscat J, Diaz-Meco MT. K63 polyubiquitination and activation of mTOR by the p62-TRAF6 complex in nutrient-activated cells. *Mol Cell*. 2013;51(3):283–296. doi:10.1016/j.molcel.2013.06.020.
292. Liou J, Kim ML, Won DH, et al. STIM is a Ca2+ sensor essential for Ca2+-store-depletion-triggered Ca2+ influx. *Curr Biol*. 2005;15(13):1235–1241.

doi:10.1016/j.cub.2005.05.055.
293. Liu R, Zhi X, Zhong Q. ATG14 controls SNARE-mediated autophagosome fusion with a lysosome. *Autophagy*. 2015;11(5):847–849. doi:10.1080/15548627.2015.1037549.
294. Liu Y, Luo Z-Q. The Legionella pneumophila effector SidJ is required for efficient recruitment of endoplasmic reticulum proteins to the bacterial phagosome. *Infect Immun*. 2007;75(2):592–603. doi:10.1128/IAI.01278-06.
295. Liu Z, Gong Z, Jiang WX, et al. Lys63-linked ubiquitin chain adopts multiple conformational states for specific target recognition. *Elife*. 2015;4(JUNE 2015):1–19. doi:10.7554/eLife.05767.001.
296. Lockshin RA, Zakeri Z. Apoptosis, autophagy, and more. *Int J Biochem Cell Biol*. 2004;36(12):2405–2419. doi:10.1016/j.biocel.2004.04.011.
297. Lohmann D, Spandl J, Stevanovic A, Schoene M, Philippou-Massier J, Thiele C. Monoubiquitination of ancient ubiquitous protein 1 promotes lipid droplet clustering. *PLoS One*. 2013;8(9):e72453. doi:10.1371/journal.pone.0072453.
298. Long J, Gallagher TRA, Cavey JR, et al. Ubiquitin Recognition by the Ubiquitin-associated Domain of p62 Involves a Novel Conformational Switch. *J Biol Chem*. 2008;283(9):5427–5440. doi:10.1074/jbc.M704973200.
299. Losick VP, Haenssler E, Moy M, Isberg RR. LnaB : a Legionella pneumophila activator of NF- k B. *Cell Microbiol*. 2010;12(March):1083–1097. doi:10.1111/j.1462-5822.2010.01452.x.
300. Lui HM, Chen J, Wang L, Naumovski L. ARMER, apoptotic regulator in the membrane of the endoplasmic reticulum, a novel inhibitor of apoptosis. *Mol Cancer Res*. 2003;1(7):508–518.
301. Luo Z-Q, Isberg RR. Multiple substrates of the Legionella pneumophila Dot/Icm system identified by interbacterial protein transfer. *Proc Natl Acad Sci*. 2004;101(3):841–6. doi:10.1073/pnas.0304916101.
302. Lynes EM, Simmen T. Urban planning of the endoplasmic reticulum (ER): How diverse mechanisms segregate the many functions of the ER. *Biochim Biophys Acta*. 2011;1813(10):1893–1905. doi:10.1016/j.bbamcr.2011.06.011.
303. Ma C, Agrawal G, Subramani S. Peroxisome assembly: Matrix and membrane protein biogenesis. *J Cell Biol*. 2011;193(1):7–16. doi:10.1083/jcb.201010022.
304. Machner MP, Isberg RR. A Bifunctional Bacterial Protein Links GDI Displacement to Rab1 Activation. *Science (80-)*. 2007;318(November):974–978.
305. Marchi S, Patergnani S, Pinton P. The endoplasmic reticulum – mitochondria connection: One touch, multiple functions. *Biochim Biophys Acta*. 2014;1837(4):461–469. doi:10.1016/j.bbabio.2013.10.015.
306. Martell JD, Deerinck TJ, Sancak Y, et al. Engineered ascorbate peroxidase as a genetically-encoded reporter for electron microscopy. *Nat Biotechnol*. 2013;30(11):1143–1148. doi:10.1038/nbt.2375.
307. Martin F, Dixit VM. A20 edits ubiquitin and autoimmune paradigms. *Nat Genet*. 2011;43(9):822–823. doi:10.1038/ng.916.
308. Martin PE De, Novick P, Ferro-novick S. The organization, structure, and inheritance of the ER in higher and lower eukaryotes. *Biochem Cell Biol*. 2005;83:752–761. doi:10.1139/O05-159.
309. Martinon F, Glimcher LH. Regulation of innate immunity by signaling pathways

emerging from the endoplasmic reticulum. *Curr Opin Immunol*. 2011;23(1):35–40. doi:10.1016/j.coi.2010.10.016.
310. Mashimo M, Kato J, Moss J. Structure and function of the ARH family of ADP-ribosyl-acceptor hydrolases. *DNA Repair (Amst)*. 2014;23:88–94. doi:10.1016/j.dnarep.2014.03.005.
311. Matsunaga K, Morita E, Saitoh T, et al. Autophagy requires endoplasmic reticulum targeting of the PI3-kinase complex via Atg14L. *J Cell Biol*. 2010;190(4):511–521. doi:10.1083/jcb.200911141.
312. McEwan DG, Dikic I. Not All Autophagy Membranes Are Created Equal. *Cell*. 2010;141(4):564–566. doi:10.1016/j.cell.2010.04.030.
313. van Meer G, Voelker DR, Feigenson GW. Membrane lipids: where they are and how they behave. *Nat Rev Mol Cell Biol*. 2008;9(2):112–124. doi:10.1038/nrm2330.
314. Merriam JJ, Mathur R, Maxfield-boumil R, Isberg RR. Analysis of the Legionella pneumophila fliI Gene: Intracellular Growth of a Defined Mutant Defective for Flagellum Biosynthesis. *Infect Immun*. 1997;65(6):2497–2501.
315. Miao RQ, Gao Y, Harrison KD, et al. Identification of a receptor necessary for Nogo-B stimulated chemotaxis and morphogenesis of endothelial cells. *Proc Natl Acad Sci U S A*. 2006;103(29):10997–1002. doi:10.1073/pnas.0602427103.
316. Mihai Gazdag E, Streller A, Haneburger I, et al. Mechanism of Rab1b deactivation by the Legionella pneumophila GAP LepB. *EMBO Rep*. 2013;14(2):199–205. doi:10.1038/embor.2012.211.
317. Miller C, Celli J. Avoidance and Subversion of Eukaryotic Homeostatic Autophagy Mechanisms by Bacterial Pathogens. *J Mol Biol*. 2016;428(17):3387–3398. doi:10.1016/j.jmb.2016.07.007.
318. Mitchell G, Isberg RR. Innate Immunity to Intracellular Pathogens: Balancing Microbial Elimination and Inflammation. *Cell Host Microbe*. 2017;22(2):166–175. doi:10.1016/j.chom.2017.07.005.
319. Mizushima N. Methods for monitoring autophagy. *Int J Biochem Cell Biol*. 2004;36(12):2491–2502. doi:10.1016/j.biocel.2004.02.005.
320. Mizushima N, Komatsu M. Autophagy : Renovation of Cells and Tissues. *Cell*. 2011;147(4):728–741. doi:10.1016/j.cell.2011.10.026.
321. Mizushima N, Noda T, Yoshimori T, et al. A protein conjugation system essential for autophagy. *Nature*. 1998;395(6700):395–398. doi:10.1038/26506.
322. Mizushima N, Yoshimori T. How to interpret LC3 immunoblotting. *Autophagy*. 2007;3(6):542–545. doi:10.4161/auto.4600.
323. Mizushima N, Yoshimori T, Levine B. Methods in Mammalian Autophagy Research. *Cell*. 2010;140(3):313–326. doi:10.1016/j.cell.2010.01.028.
324. Molmeret M, Alli OAT, Zink S, Flieger A, Cianciotto NP, Abu Kwaik Y. icmT is essential for pore formation-mediated egress of Legionella pneumophila from mammalian and protozoan cells. *Infect Immun*. 2002;70(1):69–78. doi:10.1128/IAI.70.1.69-78.2002.
325. Molmeret M, Bitar DM, Han L, Kwaik YA. Cell biology of the intracellular infection by Legionella pneumophila. *Microbes Infect*. 2004;6(1):129–139. doi:10.1016/j.micinf.2003.11.004.
326. Molmeret M, Kwaik YA. How does Legionella pneumophila exit the host cell?

Trends Microbiol. 2002;10(6):258–260.
327. Morar M, Evdokimova E, Chang C, Ensminger AW, Savchenko A. Crystal structure of the Legionella pneumophila lem10 effector reveals a new member of the HD protein superfamily. *Proteins*. 2015;(August):2319–2325. doi:10.1002/prot.24933.
328. Morimoto A, Shibuya H, Zhu X, et al. A conserved KASH domain protein associates with telomeres, SUN1, and dynactin during mammalian meiosis. *J Cell Biol*. 2012;198(2):165–172. doi:10.1083/jcb.201204085.
329. Mostowy S, Cossart P. Bacterial autophagy : restriction or promotion of bacterial replication ? *Trends Cell Biol*. 2012;22(6):283–291. doi:10.1016/j.tcb.2012.03.006.
330. Mousnier A, Schroeder GN, Stoneham CA, et al. A New Method To Determine In Vivo Interactomes Reveals Binding of the Legionella pneumophila Effector PieE to Multiple Rab GTPases. *MBio*. 2014;5(4):1–10. doi:10.1128/mBio.01148-14.Editor.
331. Mukherjee A, Patel B, Koga H, Cuervo AM, Jenny A. Selective endosomal microautophagy is starvation-inducible in Drosophila. *Autophagy*. 2016;12(11):1984–1999. doi:10.1080/15548627.2016.1208887.
332. Mukherjee S, Liu X, Arasaki K, McDonough J, Galan JE, Roy CR. Modulation of Rab GTPase function by a protein phosphocholine transferase. *Nature*. 2011;477(7362):103–106. doi:10.1038/nature10335.
333. Munch D, Rodriguez E, Bressendorff S, Park OK, Hofius D, Petersen M. Autophagy deficiency leads to accumulation of ubiquitinated proteins, ER stress, and cell death in Arabidopsis. *Autophagy*. 2014;10(9):1579–1587. doi:10.4161/auto.29406.
334. Muppirala M, Gupta V, Swarup G. Syntaxin 17 cycles between the ER and ERGIC and is required to maintain the architecture of ERGIC and Golgi. *Biol Cell*. 2011;103:333–350. doi:10.1042/BC20110006.
335. Murata T, Delprato A, Ingmundson A, Toomre DK, Lambright DG, Roy CR. The Legionella pneumophila effector protein DrrA is a Rab1 guanine nucleotide-exchange factor. *Nat Cell Biol*. 2006;8(9):971–977. doi:10.1038/ncb1463.
336. Murayama KS, Kametani F, Saito S, Kume H, Akiyama H, Araki W. Reticulons RTN3 and RTN4-B/C interact with BACE1 and inhibit its ability to produce amyloid β-protein. *Eur J Neurosci*. 2006;24(5):1237–1244. doi:10.1111/j.1460-9568.2006.05005.x.
337. Nagai H, Kagan JC, Zhu X, Kahn RA, Roy CR. A Bacterial Guanine Nucleotide Exchange Factor Activates ARF on Legionella Phagosomes. *Science (80-)*. 2002;295(January):679–683.
338. Nascimbeni AC, Codogno P, Morel E. Phosphatidylinositol-3-phosphate in the regulation of autophagy membrane dynamics. *FEBS J*. 2017;284(9):1267–1278. doi:10.1111/febs.13987.
339. Neumeister B, Faigle M, Spitznagel D, et al. Legionella pneumophila down-regulates MHC class I expression of human monocytic host cells and thereby inhibits T cell activation. *Cell Mol Life Sci*. 2005;62:578–588. doi:10.1007/s00018-005-4518-4.
340. Neunuebel MR, Chen Y, Gaspar AH, et al. De-AMPylation of the Small GTPase

Rab1 by the Pathogen Legionella pneumophila. *Science (80-)*. 2011;333(6041):453–6. doi:10.1126/science.1207193.
341. Neunuebel MR, Machner MP. The taming of a Rab GTPase by Legionella pneumophila. *Small GTPases*. 2012;3(1):28–33.
342. Neunuebel MR, Mohammadi S, Jarnik M, Machner MP. Legionella pneumophila lida affects nucleotide binding and activity of the host GTPase Rab1. *J Bacteriol*. 2012;194(6):1389–1400. doi:10.1128/JB.06306-11.
343. Newton HJ, Ang DKY, Driel IR Van, Hartland EL, van Driel IR, Hartland EL. Molecular pathogenesis of infections caused by Legionella pneumophila. *Clin Microbiol Rev*. 2010;23(2):274–98. doi:10.1128/CMR.00052-09.
344. Newton HJ, Kohler LJ, McDonough JA, et al. A Screen of Coxiella burnetii Mutants Reveals Important Roles for Dot/Icm Effectors and Host Autophagy in Vacuole Biogenesis. *PLoS Pathog*. 2014;10(7). doi:10.1371/journal.ppat.1004286.
345. Van Nguyen C. Toxicity of the AGEs generated from the Maillard reaction: On the relationship of food-AGEs and biological-AGEs. *Mol Nutr Food Res*. 2006;50(12):1140–1149. doi:10.1002/mnfr.200600144.
346. Nikoletopoulou V, Markaki M, Palikaras K, Tavernarakis N. Crosstalk between apoptosis, necrosis and autophagy. *Biochim Biophys Acta - Mol Cell Res*. 2013;1833(12):3448–3459. doi:10.1016/j.bbamcr.2013.06.001.
347. Ninio S, Zuckman-cholon DM, Cambronne ED, Roy CR. The Legionella IcmS – IcmW protein complex is important for Dot/Icm-mediated protein translocation. *Mol Microbiol*. 2005;55(3):912–926. doi:10.1111/j.1365-2958.2004.04435.x.
348. Nixon-abell J, Obara CJ, Weigel A V, et al. Increased spatiotemporal resolution reveals highly dynamic dense tubular matrices in the peripheral ER. *Science (80-)*. 2016;354(6311). doi:10.1126/science.aaf3928.
349. Nixon-abell J, Obara CJ, Weigel A V, et al. Supplementary Materials for matrices in the peripheral ER. 2016. doi:10.1126/science.aaf3928.
350. Nunes-Hasler P, Demaurex N. The ER phagosome connection in the era of membrane contact sites. *Biochim Biophys Acta*. 2017;(January). doi:10.1016/j.bbamcr.2017.04.007.
351. Nunes P, Cornut D, Bochet V, et al. Article STIM1 Juxtaposes ER to Phagosomes , Generating Ca 2+ Hotspots that Boost Phagocytosis. *Curr Biol*. 2012;22(21):1990–1997. doi:10.1016/j.cub.2012.08.049.
352. Nziengui H, Bouhidel K, Pillon D, Der C, Marty F, Schoefs B. Reticulon-like proteins in Arabidopsis thaliana : Structural organization and ER localization. *FEBS Lett*. 2007;581:3356–3362. doi:10.1016/j.febslet.2007.06.032.
353. Nziengui H, Schoefs B. Functions of reticulons in plants: What we can learn from animals and yeasts. *Cell Mol Life Sci*. 2009;66(4):584–595. doi:10.1007/s00018-008-8373-y.
354. O'Connor TJ, Adepoju Y, Boyd D, Isberg RR. Minimization of the Legionella pneumophila genome reveals chromosomal regions involved in host range expansion. *Proc Natl Acad Sci*. 2011;108(36):14733–40. doi:10.1073/pnas.1111678108.
355. O'Connor TJ, Boyd D, Dorer MS, Isberg RR. Aggravating genetic interactions allow a solution to redundancy in a bacterial pathogen. *Science (80-)*. 2012;338(6113):1440–4. doi:10.1126/science.1229556.

356. Ogawa M, Nakagawa I, Yoshikawa Y, Hain T, Chakraborty T, Sasakawa C. Chapter 22 Streptococcus-, Shigella-, and Listeria-Induced Autophagy. *Methods Enzymol*. 2009;451(C):363–381. doi:10.1016/S0076-6879(08)03622-7.
357. Oh S hee, Choi Y bok, Kim J hyun, Weihl CC, Ju J sun. Quantification of autophagy flux using LC3 ELISA. *Anal Biochem*. 2017;530:57–67. doi:10.1016/j.ab.2017.05.003.
358. Ohtake F, Saeki Y, Sakamoto K, et al. Ubiquitin acetylation inhibits polyubiquitin chain elongation. *EMBO Rep*. 2015;16(2):192–201. doi:10.15252/embr.201439152.
359. Okamoto M, Kurokawa K, Matsuura-tokita K, Saito C, Hirata R. High-curvature domains of the ER are important for the organization of ER exit sites in Saccharomyces cerevisiae. *J Cell Sci*. 2012;125(14):3412–3420. doi:10.1242/jcs.100065.
360. Oligomers PF, Perieteanu A a, Visschedyk DD, Merrill a R, Dawson JF. ADP-Ribosylation of Cross-Linked Actin Generates Barbed-End Polymerization-Deficient F-Actin Oligomers. *Biochemistry*. 2010;49(41):8944–54. doi:10.1021/bi1008062.
361. Ordureau A, Heo J, Duda DM, et al. Defining roles of PARKIN and ubiquitin phosphorylation by PINK1 in mitochondrial quality control using a ubiquitin replacement strategy. *Proc Natl Acad Sci*. 2015;112(21):6637–6642. doi:10.1073/pnas.1506593112.
362. Orenstein SJ, Cuervo AM. Chaperone-mediated autophagy: Molecular mechanisms and physiological relevance. *Semin Cell Dev Biol*. 2010;21(7):719–726. doi:10.1016/j.semcdb.2010.02.005.
363. Orso G, Pendin D, Liu S, et al. Homotypic fusion of ER membranes requires the dynamin-like GTPase Atlastin. *Nature*. 2009;460(20):978–983. doi:10.1038/nature08280.
364. Ott DE, Coren L V, Copeland TD, et al. Ubiquitin is covalently attached to the p6Gag proteins of human immunodeficiency virus type 1 and simian immunodeficiency virus and to the p12Gag protein of Moloney murine leukemia virus. *J Virol*. 1998;72(4):2962–2968.
365. Otto GP, Wu MY, Clarke M, et al. Macroautophagy is dispensable for intracellular replication of Legionella pneumophila in Dictyostelium discoideum. *Mol Microbiol*. 2004;51(1):63–72. doi:10.1046/j.1365-2958.2003.03826.x.
366. Padmakumar VC, Libotte T, Lu W, et al. The inner nuclear membrane protein Sun1 mediates the anchorage of Nesprin-2 to the nuclear envelope. *J Cell Sci*. 2005;118(15):3419–3430. doi:10.1242/jcs.02471.
367. Palazzo L, Thomas B, Jemth A, et al. Processing of protein ADP-ribosylation by Nudix hydrolases. *Biochem J*. 2015;468:293–301. doi:10.1042/BJ20141554.
368. Pankiv S, Clausen TH, Lamark T, et al. p62/SQSTM1 binds directly to Atg8/LC3 to facilitate degradation of ubiquitinated protein aggregates by autophagy*[S]. *J Biol Chem*. 2007;282(33):24131–24145. doi:10.1074/jbc.M702824200.
369. Pantoom S, Yang A, Wu Y. Lift and cut: Anti-host autophagy mechanism of Legionella pneumophila. *Autophagy*. 2017;9:1–3.
370. Park JS, Kim DH, Yoon SY. Regulation of amyloid precursor protein processing by its KFERQ motif. *BMB Rep*. 2016;49(6):337–342.

doi:10.5483/BMBRep.2016.49.6.212.
371. Parzych KR, Klionsky DJ. An Overview of Autophagy: Morphology, Mechanism, and Regulation. *Antioxid Redox Signal*. 2014;20(3):460–473. doi:10.1089/ars.2013.5371.
372. Patel KJ, Joenje H. Fanconi anemia and DNA replication repair. *DNA Repair (Amst)*. 2007;6(7):885–90. doi:10.1016/j.dnarep.2007.02.002.
373. Patnaik A, Chau V, Wills JW. Ubiquitin is part of the retrovirus budding machinery. *Proc Natl Acad Sci U S A*. 2000;97(24):13069–13074. doi:10.1073/pnas.97.24.13069.
374. Peng J, Gygi SP. Proteomics: The move to mixtures. *J Mass Spectrom*. 2001;36(10):1083–1091. doi:10.1002/jms.229.
375. Perkins G, Renken C. Electron Tomography of Neuronal Mitochondria : Three-Dimensional Structure and Organization of Cristae and Membrane Contacts. *J Struct Biol*. 1997;119:260–272.
376. Perrett CA, Lin DY-W, Zhou D. Interactions of bacterial proteins with host eukaryotic ubiquitin pathways. *Front Microbiol*. 2011;2(July):143. doi:10.3389/fmicb.2011.00143.
377. Petroski MD, Deshaies RJ. Function and regulation of cullin–RING ubiquitin ligases. *Nat Rev Mol Cell Biol*. 2005;6(1):9–20. doi:10.1038/nrm1547.
378. Phillips MJ, Voeltz GK. Structure and function of ER membrane contact sites with other organelles. *Nat Rev Mol cell Biol*. 2015;17(2):69–82. doi:10.1038/nrm.2015.8.
379. Pichler H, Gaigg B, Hrastnik C, et al. A subfraction of the yeast endoplasmic reticulum associates with the plasma membrane and has a high capacity to synthesize lipids. *Eur J Biochem*. 2001;268(8):2351–2361. doi:10.1046/j.1432-1327.2001.02116.x.
380. Pickart CM, Eddins MJ. Ubiquitin : structures , functions , mechanisms. *Biochim Biophys Acta*. 2004;1695:55–72. doi:10.1016/j.bbamcr.2004.09.019.
381. Pickart CM, Fushman D. Polyubiquitin chains: Polymeric protein signals. *Curr Opin Chem Biol*. 2004;8(6):610–616. doi:10.1016/j.cbpa.2004.09.009.
382. Pierre P. Dendritic cells , DRiPs , and DALIS in the control of antigen processing. *Immunol Rev*. 2005;207:184–190.
383. Pizarro-Cerdá J, Méresse S, Parton RG, et al. Brucella abortus transits through the autophagic pathway and replicates in the endoplasmic reticulum of nonprofessional phagocytes. *Infect Immun*. 1998;66(12):5711–5724.
384. Pizarro-Cerdá J, Moreno E, Sanguedolce V, Mege JL, Gorvel JP. Virulent Brucella abortus prevents lysosome fusion and is distributed within autophagosome-like compartments. *Infect Immun*. 1998;66(5):2387–2392.
385. Plutner H, Cox AD, Pind S, et al. Rab1b regulates vesicular transport between the endoplasmic reticulum and successive Golgi compartments. *J Cell Biol*. 1991;115(1):31–43. doi:10.1083/jcb.115.1.31.
386. Popovic D, Akutsu M, Novak I, Harper JW, Behrends C, Dikic I. Rab GTPase-Activating Proteins in Autophagy: Regulation of Endocytic and Autophagy Pathways by Direct Binding to Human ATG8 Modifiers. *Mol Cell Biol*. 2012;32(9):1733–1744. doi:10.1128/MCB.06717-11.
387. Price CT, Al-Khodor S, Al-Quadan T, et al. Molecular mimicry by an F-box

effector of Legionella pneumophila hijacks a conserved polyubiquitination machinery within macrophages and protozoa. *PLoS Pathog*. 2009;5(12):e1000704. doi:10.1371/journal.ppat.1000704.
388. Price CT, Richards AM, Abu Kwaik Y. Nutrient generation and retrieval from the host cell cytosol by intra-vacuolar Legionella pneumophila. *Front Cell Infect Microbiol*. 2014;4(August):111. doi:10.3389/fcimb.2014.00111.
389. Price CTD, Abu Kwaik Y. Exploitation of host polyubiquitination machinery through molecular mimicry by eukaryotic-like bacterial F-box effectors. *Front Microbiol*. 2010;1(NOV):1–12. doi:10.3389/fmicb.2010.00122.
390. Prior M, Shi Q, Hu X, He W, Levey A, Yan R. RTN/Nogo in forming Alzheimer's neuritic plaques. *Neurosci Biobehav Rev*. 2010;34(8):1201–1206. doi:10.1016/j.neubiorev.2010.01.017.
391. Pugsley HR. Quantifying autophagy: Measuring LC3 puncta and autolysosome formation in cells using multispectral imaging flow cytometry. *Methods*. 2017;112:147–156. doi:10.1016/j.ymeth.2016.05.022.
392. Puhka M, Joensuu M, Vihinen H, Belevich I, Jokitalo E. Progressive sheet-to-tubule transformation is a general mechanism for endoplasmic reticulum partitioning in dividing mammalian cells. *Mol Biol Cell*. 2012;23(13):2424–32. doi:10.1091/mbc.E10-12-0950.
393. Puhka M, Vihinen H, Joensuu M, Jokitalo E. Endoplasmic reticulum remains continuous and undergoes sheet-to-tubule transformation during cell division in mammalian cells. *J Cell Biol*. 2007;179(5):895–909. doi:10.1083/jcb.200705112.
394. Puvar K, Zhou Y, Qiu J, Luo Z-Q, Wirth MJ, Das C. Ubiquitin Chains Modified by the Bacterial Ligase SdeA Are Protected from Deubiquitinase Hydrolysis. *Biochemistry*. 2017:acs.biochem.7b00664. doi:10.1021/acs.biochem.7b00664.
395. Qin QM, Pei J, Ancona V, Shaw BD, Ficht TA, De Figueiredo P. RNAi screen of endoplasmic reticulum-associated host factors reveals a role for IRE1α in supporting Brucella replication. *PLoS Pathog*. 2008;4(7). doi:10.1371/journal.ppat.1000110.
396. Qiu J, Sheedlo MJ, Yu K, et al. Ubiquitination independent of E1 and E2 enzymes by bacterial effectors. *Nature*. 2016;533(7601):1–17. doi:10.1038/nature17657.
397. Qiu J, Yu K, Fei X, et al. A unique deubiquitinase that deconjugates phosphoribosyl-linked protein ubiquitination. *Cell Res*. 2017;(December 2016):865–881. doi:10.1038/cr.2017.66.
398. Quaile AT, Urbanus ML, Stogios PJ, et al. Molecular Characterization of LubX: Functional Divergence of the U-Box Fold by Legionella pneumophila. *Structure*. 2015;23(8):1459–1469. doi:10.1016/j.str.2015.05.020.
399. Ragaz C, Pietsch H, Urwyler S, Tiaden A, Weber SS, Hilbi H. The Legionella pneumophila phosphatidylinositol-4 phosphate-binding type IV substrate SidC recruits endoplasmic reticulum vesicles to a replication-permissive vacuole. *Cell Microbiol*. 2008;10(12):2416–33. doi:10.1111/j.1462-5822.2008.01219.x.
400. Raices M, Angelo MAD. Nuclear pore complex composition : developmental functions. *Nat Rev Mol Cell Biol*. 2012;13(November):687–699. doi:10.1038/nrm3461.
401. Rajan R, Karbowniczek M, Pugsley HR, Sabnani MK, Astrinidis A, La-Beck NM. Quantifying autophagosomes and autolysosomes in cells using imaging flow

cytometry. *Cytom Part A*. 2015;87(5):451–458. doi:10.1002/cyto.a.22652.
402. Ramanathan HN, Ye Y. Cellular strategies for making monoubiquitin signals. *Crit Rev Biochem Mol Biol*. 2012;47(1):17–28. doi:10.3109/10409238.2011.620943.
403. Ramo O, Kumar D, Gucciardo E, et al. NOGO-A/RTN4A and NOGO-B are simultaneously expressed in epithelial, fibroblast, and neuronal cells and maintain ER morphology. *Sci Rep*. 2016;6(35969):1–14. doi:10.1038/srep35969.
404. Raturi A, Simmen T. Where the endoplasmic reticulum and the mitochondrion tie the knot: The mitochondria-associated membrane (MAM). *Biochim Biophys Acta - Mol Cell Res*. 2013;1833(1):213–224. doi:10.1016/j.bbamcr.2012.04.013.
405. Ravikumar B, Moreau K, Jahreiss L, Puri C, Rubinsztein DC. Plasma membrane contributes to the formation of pre-autophagosomal structures. *Nat Cell Biol*. 2010;12(8):747–757. doi:10.1038/ncb2078.
406. Razafsky D, Hodzic D. Bringing KASH under the SUN : the many faces of nucleo-cytoskeletal connections. *J Cell Biol*. 2009;186(4):461–472. doi:10.1083/jcb.200906068.
407. Reggiori F, Komatsu M, Finley K, Simonsen A. Selective types of autophagy. *Int J Cell Biol*. 2012;2012:2012–2014. doi:10.1155/2012/156272.
408. Richter B, Sliter DA, Herhaus L, Stolz A, Wang C, Beli P. Phosphorylation of OPTN by TBK1 enhances its binding to Ub chains and promotes selective autophagy of damaged mitochondria. *Proc Natl Acad Sci*. 2016;113(15). doi:10.1073/pnas.1523926113.
409. Rigden DJ. Identification and modelling of a PPM protein phosphatase fold in the Legionella pneumophila deAMPylase SidD. *FEBS Lett*. 2011;585(17):2749–2754. doi:10.1016/j.febslet.2011.08.006.
410. Rismanchi N, Soderblom C, Stadler J, Zhu PP, Blackstone C. Atlastin GTPases are required for Golgi apparatus and ER morphogenesis. *Hum Mol Genet*. 2008;17(11):1591–1604. doi:10.1093/hmg/ddn046.
411. Rizzuto R, Pinton P, Carrington WA, et al. Close contacts with the endoplasmic reticulum as determinants of mitochondrial Ca2+ responses. *Science*. 1998;280(5370):1763–6. doi:10.1126/science.280.5370.1763.
412. Rizzuto R, De Stefani D, Raffaello A, Mammucari C. Mitochondria as sensors and regulators of calcium signalling. *Nat Rev Mol Cell Biol*. 2012;13(9):566–578. doi:10.1038/nrm3412.
413. Roberts P, Moshitch-Moshkovitz S, Erik K, O'Toole E, Winey M, Goldfarb D. Piecemeal Microautophagy of Nucleus in Saccharomyces cerevisiae. *Mol Biol Cell*. 2003;14:2372–2384. doi:10.1091/mbc.E02.
414. Robinson CG, Roy CR. Attachment and fusion of endoplasmic reticulum with vacuoles containing Legionella pneumophila. *Cell Microbiol*. 2006;8(5):793–805. doi:10.1111/j.1462-5822.2005.00666.x.
415. Rocha N, Kuijl C, Van Der Kant R, et al. Cholesterol sensor ORP1L contacts the ER protein VAP to control Rab7-RILP-p150Glued and late endosome positioning. *J Cell Biol*. 2009;185(7):1209–1225. doi:10.1083/jcb.200811005.
416. Rodríguez-feo JA, Gallego-delgado J, Puerto M, Wandosell F, Osende J. Reticulon-4B / Nogo-B acts as a molecular linker between microtubules and actin cytoskeleton in vascular smooth muscle cells. *Biochim Biophys Acta*. 2016;1863:1985–1995.

417. Rolando M, Escoll P, Buchrieser C. Legionella pneumophila restrains autophagy by modulating the host's sphingolipid metabolism. *Autophagy*. 2016;12(6):1053–1054. doi:10.1080/15548627.2016.1166325.
418. Rolando M, Escoll P, Nora T, et al. Legionella pneumophila S1P-lyase targets host sphingolipid metabolism and restrains autophagy. *Proc Natl Acad Sci U S A*. 2016;113(7):1901–6. doi:10.1073/pnas.1522067113.
419. Rolland T, Taşan M, Charloteaux B, et al. A proteome-scale map of the human interactome network. *Cell*. 2014;159(5):1212–1226. doi:10.1016/j.cell.2014.10.050.
420. Roos J, DiGregorio PJ, Yeromin A V., et al. STIM1, an essential and conserved component of store-operated Ca 2+ channel function. *J Cell Biol*. 2005;169(3):435–445. doi:10.1083/jcb.200502019.
421. Ross C a, Pickart CM. The ubiquitin-proteasome pathway in Parkinson's disease and other neurodegenerative diseases. *Trends Cell Biol*. 2004;14(12):703–11. doi:10.1016/j.tcb.2004.10.006.
422. Rossi D, Barone V, Giacomello E, Cusimano V, Sorrentino V. The sarcoplasmic reticulum: An organized patchwork of specialized domains. *Traffic*. 2008;9(7):1044–1049. doi:10.1111/j.1600-0854.2008.00717.x.
423. Rott R, Szargel R, Haskin J, Bandopadhyay R, Lees AJ. α -Synuclein fate is determined by USP9X-regulated monoubiquitination. *Proc Natl Acad Sci*. 2011;108(46):1–6. doi:10.1073/pnas.1105725108/-/DCSupplemental.www.pnas.org/cgi/doi/10.1073/pnas.1105725108.
424. Rowland A a., Voeltz GK. Endoplasmic reticulum–mitochondria contacts: function of the junction. *Nat Rev Mol Cell Biol*. 2012;13(10):607–625. doi:10.1038/nrm3440.
425. Roy CR. Exploitation of the endoplasmic reticulum by bacterial pathogens. *Trends Microbiol*. 2002;10(9):418–424. Available at: http://www.ncbi.nlm.nih.gov/pubmed/12217507.
426. Roy CR. The Dot/Icm transporter of Legionella pneumophila : A bacterial conductor of vesicle trafficking that orchestrates the establishment of a replicative organelle in eukaryotic hosts. *Int J Med Microbiol*. 2002;467:463–467.
427. Roy CR, Salcedo SP, Gorvel JP. Pathogen-endoplasmic-reticulum interactions: in through the out door. *NatRevImmunol*. 2006;6(1474–1733 (Print)):136–147. doi:10.1038/nri1775.
428. Rubinsztein DC, Shpilka T, Elazar Z. Mechanisms of Autophagosome Biogenesis. *Curr Biol*. 2012;22:29–34. doi:10.1016/j.cub.2011.11.034.
429. Rusiñol AE, Cui Z, Chen MH, Vance JE. A unique mitochondria-associated membrane fraction from rat liver has a high capacity for lipid synthesis and contains pre-Golgi secretory proteins including nascent lipoproteins. *J Biol Chem*. 1994;269(44):27494–27502.
430. Ryter SW, Cloonan SM, Choi AMK. Autophagy: A critical regulator of cellular metabolism and homeostasis. *Mol Cells*. 2013;36(1):7–16. doi:10.1007/s10059-013-0140-8.
431. Rytkönen A, Holden DW, Rytko A, Holden DW. Bacterial interference of ubiquitination and deubiquitination. *Cell Host Microbe*. 2007;1(1):13–22. doi:10.1016/j.chom.2007.02.003.

432. Sadowski M, Sarcevic B. Mechanisms of mono- and poly-ubiquitination: Ubiquitination specificity depends on compatibility between the E2 catalytic core and amino acid residues proximal to the lysine. *Cell Div*. 2010;5:19. doi:10.1186/1747-1028-5-19.
433. Sadowski M, Suryadinata R, Tan AR, Roesley SNA, Sarcevic B. Protein monoubiquitination and polyubiquitination generate structural diversity to control distinct biological processes. *Life*. 2012;64(2):136–142. doi:10.1002/iub.589.
434. Sahu R, Kaushik S, Clement CC, et al. Microautophagy of Cytosolic Proteins by Late Endosomes. *Dev Cell*. 2011;20(1):131–139. doi:10.1016/j.devcel.2010.12.003.
435. Sakai Y, Koller A, Rangell LK, Keller G a, Subramani S. Peroxisome Degradation by Microautophagy in Pichia pastoris: Identification of Specific Steps and Morphological Intermediates. *J Cell Biol*. 1998;141(3):625–636.
436. Salminen A, Kaarniranta K, Kauppinen A, et al. Progress in Neurobiology Impaired autophagy and APP processing in Alzheimer's disease: The potential role of Beclin 1 interactome. *Prog Neurobiol*. 2013;106–107:33–54. doi:10.1016/j.pneurobio.2013.06.002.
437. Sanchez-wandelmer J, Ktistakis NT, Reggiori F. ERES: sites for autophagosome biogenesis and maturation? *J Cell Sci*. 2015;128:185–192. doi:10.1242/jcs.158758.
438. Sandri M, Coletto L, Grumati P, Bonaldo P. Misregulation of autophagy and protein degradation systems in myopathies and muscular dystrophies. *J Cell Sci*. 2013;126(23):5325–5333. doi:10.1242/jcs.114041.
439. Di Sano F, Bernardoni P, Piacentini M. The reticulons: Guardians of the structure and function of the endoplasmic reticulum. *Exp Cell Res*. 2012;318(11):1201–1207. doi:10.1016/j.yexcr.2012.03.002.
440. Santos JC, Enninga J. At the crossroads: Communication of bacteria-containing vacuoles with host organelles. *Cell Microbiol*. 2016;18(3):330–339. doi:10.1111/cmi.12567.
441. Di Scala F, Dupuis L, Gaiddon C, et al. Tissue specificity and regulation of the N-terminal diversity of reticulon 3. *Biochem J*. 2005;385:125–134. doi:10.1042/BJ20040458.
442. Schanda K, Hermann M, Stefanova N, Gredler V, Bandtlow C, Reindl M. Nogo-B is associated with cytoskeletal structures in human monocyte-derived macrophages. *BMC Res Notes*. 2011;4(6):6. doi:10.1186/1756-0500-4-6.
443. Schmandke A, Schmandke A, Schwab ME. Nogo-A: Multiple Roles in CNS Development, Maintenance, and Disease. *Neuroscientist*. 2014;(January). doi:10.1177/1073858413516800.
444. Schoebel S, Oesterlin LK, Blankenfeldt W, Goody RS, Itzen A. RabGDI Displacement by DrrA from Legionella Is a Consequence of Its Guanine Nucleotide Exchange Activity. *Mol Cell*. 2009;36(6):1060–1072. doi:10.1016/j.molcel.2009.11.014.
445. Schuck S, Prinz WA, Thorn KS, Voss C, Walter P. Membrane expansion alleviates endoplasmic reticulum stress independently of the unfolded protein response. *J Cell Biol*. 2009;187(4):525–536. doi:10.1083/jcb.200907074.
446. Schulze JM, Jackson J, Nakanishi S, et al. Linking cell cycle to histone modifications: SBF and H2B monoubiquitination machinery and cell-cycle

regulation of H3K79 dimethylation. *Mol Cell*. 2009;35(5):626–41. doi:10.1016/j.molcel.2009.07.017.
447. Scott CC, Botelho RJ, Grinstein S. Phagosome Maturation: A Few Bugs in the System. *J Membr Biol*. 2008;193(2003):137–152. doi:10.1007/s00232-002-2008-2.
448. Seibenhener M, Babu J. Sequestosome 1 / p62 Is a Polyubiquitin Chain Binding Protein Involved in Ubiquitin Proteasome Degradation. *Mol Cell Biol*. 2004;24(18):8055–8068. doi:10.1128/MCB.24.18.8055.
449. Senden N, van de Velde H, Broers J, et al. Subcellular localization and supramolecular organization of neuroendocrine-specific protein B (NSP-B) in small cell lung cancer. *Eur J Cell Biol*. 1994;65(2):341–353.
450. Sexton JA, Pinkner JS, Roth R, Heuser JE, Hultgren SJ, Vogel JP. The Legionella pneumophila PilT Homologue DotB Exhibits ATPase Activity That Is Critical for Intracellular Growth. *J Bacteriol*. 2004;186(6):1658–1666. doi:10.1128/JB.186.6.1658.
451. Sharifi MN, Mowers EE, Drake LE, Macleod KF. Measuring Autophagy in Stressed Cells. *Methods Mol Biol*. 2015;1292:129–150. doi:10.1007/978-1-4939-2522-3.
452. Sheedlo MJ, Qiu J, Tan Y, Paul LN, Luo Z, Das C. Structural basis of substrate recognition by a bacterial deubiquitinase important for dynamics of phagosome ubiquitination. *Proc Natl Acad Sci*. 2015:3–8. doi:10.1073/pnas.1514568112.
453. Shen L, Liu H, Dong C, Xirodimas D, Naismith JH, Hay RT. Structural basis of NEDD8 ubiquitin discrimination by the deNEDDylating enzyme NEDP1. *EMBO J*. 2005;24(7):1341–1351. doi:10.1038/sj.emboj.7600628.
454. Shen WC, Li HY, Chen GC, Chern Y, Tu PH. Mutations in the ubiquitin-binding domain of OPTN/optineurin interfere with autophagy- mediated degradation of misfolded proteins by a dominant-negative mechanism. *Autophagy*. 2015;11(4):685–700. doi:10.4161/auto.36098.
455. Shevchenko A, Wilm M, Vorm O, Mann M. Mass spectrometric sequencing of proteins silver-stained polyacrylamide gels. *Anal Chem*. 1996;68(5):850–8.
456. Shi X, Halder P, Yavuz H, Jahn R, Shuman HA. Direct targeting of membrane fusion by SNARE mimicry : Convergent evolution of Legionella effectors. *Proc Natl Acad Sci*. 2016;113(31):8807–8812. doi:10.1073/pnas.1608755113.
457. Shibata Y, Shemesh T, Prinz WA, Palazzo AF, Kozlov MM, Rapoport TA. Mechanisms determining the morphology of the peripheral ER. *Cell*. 2010;143(5):774–788. doi:10.1016/j.cell.2010.11.007.
458. Shibata Y, Voeltz GK, Rapoport T a. Rough sheets and smooth tubules. *Cell*. 2006;126(3):435–9. doi:10.1016/j.cell.2006.07.019.
459. Shibata Y, Voss C, Rist JM, et al. The reticulon and DP1/Yop1p proteins form immobile oligomers in the tubular endoplasmic reticulum. *J Biol Chem*. 2008;283(27):18892–904. doi:10.1074/jbc.M800986200.
460. Shibutani ST, Yoshimori T. A current perspective of autophagosome biogenesis. *Cell Res*. 2014;24(1):58–68. doi:10.1038/cr.2013.159.
461. Shin S, Roy CR. Microreview Host cell processes that influence the intracellular survival of Legionella pneumophila. *Cell Microbiol*. 2008;10(6):1209–1220. doi:10.1111/j.1462-5822.2008.01145.x.

462. Shintani T, Klionsky DJ. Autophagy in Health and Disease: A Double-Edged Sword. *Science (80-)*. 2004;306(November):990–996.
463. Shpilka T, Elazar Z. Shedding Light on Mammalian Microautophagy. *Dev Cell*. 2011;20(1):1–2. doi:10.1016/j.devcel.2010.12.010.
464. Sidm ED, Campo CM Del, Mishra AK, et al. Article Structural Basis for PI (4) P-Specific Membrane Recruitment of the Legionella pneumophila. *Structure*. 2014;22(3):397–408. doi:10.1016/j.str.2013.12.018.
465. Sigismund S, Polo S, Di Fiore PP. Signaling through monoubiquitination. *Curr Top Microbiol Immunol*. 2004;286:149–85. doi:10.1007/978-3-540-69494-6_6.
466. Simon NC, Aktories K, Barbieri JT. Novel bacterial ADP-ribosylating toxins: structure and function. *Nat Rev Microbiol*. 2014;12(9):599–611. doi:10.1038/nrmicro3310.
467. Sinai AP, Webster P, Joiner KA. Association of host cell endoplasmic reticulum and mitochondria with the Toxoplasma gondii parasitophorous vacuole membrane: a high affinity interaction. *J Cell Sci*. 1997;110(17):2117–2128. Available at: http://jcs.biologists.org/content/110/17/2117.abstract%5Cnhttp://www.ncbi.nlm.nih.gov/pubmed/9378762.
468. Smyth JT, Hwang SY, Tomita T, DeHaven WI, Mercer JC, Putney JW. Activation and regulation of store-operated calcium entry. *J Cell Mol Med*. 2010;14(10):2337–2349. doi:10.1111/j.1582-4934.2010.01168.x.
469. So EC, Mattheis C, Tate EW, Frankel G, Schroeder GN. Creating a customized intracellular niche : subversion of host cell signaling by Legionella type IV secretion system effectors 1. *Can J Microbiol*. 2015;61:617–635.
470. Sohn Y, Shin H, Park WS, et al. Lpg0393 of Legionella pneumophila Is a Guanine-Nucleotide Exchange Factor for. *PLoS One*. 2015;3:1–16. doi:10.1371/journal.pone.0118683.
471. Solomon JM, Rupper a, Cardelli J a, Isberg RR. Intracellular growth of Legionella pneumophila in Dictyostelium discoideum, a system for genetic analysis of host-pathogen interactions. *Infect Immun*. 2000;68(5):2939–2947. doi:10.1128/IAI.68.5.2939-2947.2000.
472. Sosa BA, Rothballer A, Kutay U, Schwartz TU. LINC Complexes Form by Binding of Three KASH Peptides to Domain Interfaces of Trimeric SUN Proteins. *Cell*. 2012;149(5):1035–1047. doi:10.1016/j.cell.2012.03.046.
473. Spasser L, Brik A. Chemistry and Biology of the Ubiquitin Signal A. *Angew Rev*. 2012;51:6840–6862. doi:10.1002/anie.201200020.
474. Starr DA, Fridolfsson HN. Interactions Between Nuclei and the Cytoskeleton Are Mediated by SUN-KASH. *Annu Rev Cell Dev Biol*. 2010;26:421–444. doi:10.1146/annurev-cellbio-100109-104037.
475. Starr T, Child R, Wehrly TD, et al. Selective Subversion of Autophagy Complexes Facilitates Completion of the Brucella Intracellular Cycle. *Cell Host Microbe*. 2012;11:33–45. doi:10.1016/j.chom.2011.12.002.
476. Starr T, Ng TW, Wehrly TD, Knodler LA, Celli J. Brucella intracellular replication requires trafficking through the late endosomal/lysosomal compartment. *Traffic*. 2008;9(5):678–694. doi:10.1111/j.1600-0854.2008.00718.x.
477. Stathopulos PB, Ikura M. *Structure and Function of Endoplasmic Reticulum STIM Calcium Sensors*. 1st ed. Elsevier Inc.; 2013. doi:10.1016/B978-0-12-407870-

3.00003-2.
478. Steele-Mortimer O. Exploitation of the ubiquitin system by invading bacteria. *Traffic*. 2011;12(2):162–9. doi:10.1111/j.1600-0854.2010.01137.x.
479. Stefan CJ, Manford AG, Baird D, Yamada-Hanff J, Mao Y, Emr SD. Osh proteins regulate phosphoinositide metabolism at ER-plasma membrane contact sites. *Cell*. 2011;144(3):389–401. doi:10.1016/j.cell.2010.12.034.
480. Stefan CJ, Manford AG, Emr SD. ER – PM connections : sites of information transfer and inter-organelle communication. *Curr Opin Cell Biol*. 2013;25(4):434–442. doi:10.1016/j.ceb.2013.02.020.
481. Stefano G, Hawes C, Brandizzi F. ER – the key to the highway. *Curr Opin Plant Biol*. 2014;22:30–38.
482. Steiner AB, Weber S, Hilbi H. Formation of the Legionella-containing vacuole: phosphoinositide conversion, GTPase modulation and ER dynamics. *Int J Med Microbiol*. 2017. doi:http://dx.doi.org/10.1016/j.ijmm.2017.08.004.
483. Steiner B, Weber S, Hilbi H. Formation of the Legionella -containing vacuole: phosphoinositide conversion, GTPase modulation and ER dynamics. *Int J Med Microbiol*. 2017. doi:10.1016/j.ijmm.2017.08.004.
484. Stolz A, Ernst A, Dikic I. Cargo recognition and trafficking in selective autophagy. *Nat Cell Biol*. 2014;16(6):495–501.
485. Stone SJ, Vance JE. Phosphatidylserine synthase-1 and -2 are localized to mitochondria-associated membranes. *J Biol Chem*. 2000;275(44):34534–34540. doi:10.1074/jbc.M002865200.
486. Strack B, Calistri A, Accola MA, Palu G, Gottlinger HG. A role for ubiquitin ligase recruitment in retrovirus release. *Proc Natl Acad Sci U S A*. 2000;97(24):13063–8. doi:10.1073/pnas.97.24.13063.
487. Sturgill-Koszycki S, Swanson MS. Legionella pneumophila Replication Vacuoles Mature into Acidic, Endocytic Organelles. *J Exp Med*. 2000;192(9):1261–1272. doi:10.1084/jem.192.9.1261.
488. Sugai M, Chen C, Wu HC. Bacterial ADP-ribosyltransferase with a substrate specificity of the rho protein disassembles the Golgi apparatus in Vero cells and mimics the action of brefeldin A. *Proc Natl Acad Sci*. 1992;89(October):8903–8907.
489. Sun Q, Fan W, Chen K, Ding X, Chen S, Zhong Q. Identification of Barkor as a mammalian autophagy-specific factor for Beclin 1 and class III phosphatidylinositol 3-kinase. *Proc Natl Acad Sci U S A*. 2008;105(49):19211–6. doi:10.1073/pnas.0810452105.
490. Suzuki K, Kubota Y, Sekito T, Ohsumi Y. Hierarchy of Atg proteins in pre-autophagosomal structure organization. *Genes to Cells*. 2007;12(2):209–218. doi:10.1111/j.1365-2443.2007.01050.x.
491. Swaney DL, Rodriguez-Mias RA, Villen J. Phosphorylation of ubiquitin at Ser65 affects its polymerization, targets, and proteome-wide turnover. *EMBO Rep*. 2015;16(9):1131–1144. doi:10.15252/embr.201540298.
492. Swanson MS, Isberg RR. Association of Legionella pneumophila with the Macrophage Endoplasmic Reticulum. *Infect Immun*. 1995;63(9):3609–3620.
493. Tagami S, Eguchi Y, Kinoshita M, Takeda M, Tsujimoto Y. A novel protein, RTN-XS, interacts with both Bcl-XL and Bcl-2 on endoplasmic reticulum and

reduces their anti-apoptotic activity. *Oncogene*. 2000;19(50):5736–5746. doi:10.1038/sj.onc.1203948.
494. Taghavi F, Habibi-rezaei M, Amani M, Akbar A, Moosavi-movahedi AA. The status of glycation in protein aggregation. *Int J Biol Macromol*. 2017;100:67–74.
495. Tan Q, Wang M, Yu M, et al. Role of Autophagy as a Survival Mechanism for Hypoxic Cells in Tumors. *Neoplasia (United States)*. 2016;18(6):347–355. doi:10.1016/j.neo.2016.04.003.
496. Tan Y, Luo Z-Q. Legionella pneumophila SidD is a deAMPylase that modifies Rab1. *Nature*. 2011;475(7357):506–9. doi:10.1038/nature10307.
497. Tanida I. Autophagosome formation and molecular mechanism of autophagy. *Antioxid Redox Signal*. 2011;14(11):2201–2214. doi:10.1089/ars.2010.3482.
498. Tanida I. Autophagy basics. *Microbiol Immunol*. 2011;55:1–11. doi:10.1111/j.1348-0421.2010.00271.x.
499. Teng FYH, Bor LT, Tang BL, Yu F, Teng H. Cell autonomous function of Nogo and reticulons: The emerging story at the endoplasmic reticulum. *J Cell Physiol*. 2008;216(2):303–8. doi:10.1002/jcp.21434.
500. Terasaki M, Chen LB. Microtubules and the Endoplasmic Reticulum Are Highly Interdependent Structures. *J Cell Biol*. 1986;103(October):1557–1568.
501. Terasaki M, Reese TS. Interactions Among Endoplasmic Reticulum, Microtubules, and Retrograde Movements of the Cell Surface. *Cell Motil Cytoskeleton*. 1994;29:291–300.
502. Terasaki M, Shemesh T, Kasthuri N, et al. Stacked Endoplasmic Reticulum Sheets Are Connected by Helicoidal Membrane Motifs. *Cell*. 2013;154(2):285–296. doi:10.1016/j.cell.2013.06.031.
503. Tezcan-Merdol D, Engstrand L, Rhen M. Salmonella enterica SpvB-mediated ADP-ribosylation as an activator for host cell actin degradation. *Int J Med Microbiol*. 2005;295(4):201–12. doi:10.1016/j.ijmm.2005.04.008.
504. Tilney LG, Harb OS, Connelly PS, Robinson CG, Roy CR. How the parasitic bacterium Legionella pneumophila modifies its phagosome and transforms it into rough ER: implications for conversion of plasma membrane to the ER membrane. *J Cell Sci*. 2001;114(24):4637–4650. doi:10.1111/j.1365-2958.1994.tb01317.x.
505. Todde V, Veenhuis M, van der Klei IJ. Autophagy: Principles and significance in health and disease. *Biochim Biophys Acta*. 2009;1792(1):3–13. doi:10.1016/j.bbadis.2008.10.016.
506. Tolley N, Sparkes IA, Hunter PR, et al. Overexpression of a Plant Reticulon Remodels the Lumen of the Cortical Endoplasmic Reticulum but Does not Perturb Protein Transport. *Traffic*. 2008;9:94–102. doi:10.1111/j.1600-0854.2007.00670.x.
507. Toman R, Heinzen RA, Samuel JE, Mege J-L. Coxiella burnetii: Recent Advances and New Perspectives in Research of the Q Fever Bacterium. *Adv Exp Med Biol*. 2012;984.
508. Treier M, Staszewski LM, Bohmann D. Ubiquitin-dependent c-Jun degradation in vivo is mediated by the delta domain. *Cell*. 1994;78(5):787–798. doi:10.1016/S0092-8674(94)90502-9.
509. Trotter PJ, Voelker DR. Lipid transport processes in eukaryotic cells. *Biochim Biophys Acta*. 1994;1213(3):241–262.
510. Uchiki T, Weikel K a., Jiao W, et al. Glycation-altered proteolysis as a

pathobiologic mechanism that links dietary glycemic index, aging, and age-related disease (in nondiabetics). *Aging Cell*. 2012;11(1):1–13. doi:10.1111/j.1474-9726.2011.00752.x.
511. Udeshi ND, Svinkina T, Mertins P, et al. Refined preparation and use of anti-diglycine remnant (K-ε-GG) antibody enables routine quantification of 10,000s of ubiquitination sites in single proteomics experiments. *Mol Cell proteomics*. 2013;12(3):825–31. doi:10.1074/mcp.O112.027094.
512. Uemura T, Yamamoto M, Kametaka A, et al. A Cluster of Thin Tubular Structures Mediates Transformation of the Endoplasmic Reticulum to Autophagic Isolation Membrane. *Mol Cell Biol*. 2014;34(9):1695–1706. doi:10.1128/MCB.01327-13.
513. Vance JE. Phospholipid Mitochondria * Synthesis in a Membrane Fraction Associated identified. *J Biol Chem*. 1990;265(13):7248–7257.
514. Vance JE, Shiao YJ. Intracellular trafficking of phospholipids: import of phosphatidylserine into mitochondria. *Anticancer Res*. 1996;16(3B):1333–1339.
515. Veiga E, Cossart P. Listeria hijacks the clathrin-dependent endocytic machinery to invade mammalian cells. *Nat Cell Biol*. 2005;7(9):894–900. doi:10.1038/ncb1292.
516. Vereecke L, Beyaert R, Loo G Van, van Loo G, Loo G Van. The ubiquitin-editing enzyme A20 (TNFAIP3) is a central regulator of immunopathology. *Trends Immunol*. 2009;30(8):383–391. doi:10.1016/j.it.2009.05.007.
517. Verlhac P, Gre IP, Viret C, Faure M, Azocar O, Petkova DS. Autophagy Receptor NDP52 Regulates Pathogen- Containing Autophagosome Maturation Short Article Autophagy Receptor NDP52 Regulates Pathogen-Containing Autophagosome Maturation. *Cell Host Microbe*. 2015;17:515–525.
518. Voelker DR. Interorganelle transport of aminoglycerophospholipids. *Biochim Biophys Acta - Mol Cell Biol Lipids*. 2000;1486(1):97–107. doi:10.1016/S1388-1981(00)00051-2.
519. Voeltz GK, Prinz WA. Sheets, ribbons and tubules — how organelles get their shape. *Nat Rev Mol Cell Biol*. 2007;8(3):258–264. doi:10.1038/nrm2119.
520. Voeltz GK, Prinz WA, Shibata Y, Rist JM, Rapoport TA. A class of membrane proteins shaping the tubular endoplasmic reticulum. *Cell*. 2006;124(3):573–86. doi:10.1016/j.cell.2005.11.047.
521. Vogel JP, Isberg RR. Cell biology of Legionella pneumophila. *Curr Opin Microbiol*. 1999;2(1):30–4. Available at: http://www.ncbi.nlm.nih.gov/pubmed/10047559.
522. Voss C, Lahiri S, Young BP, Loewen CJ, Prinz WA. ER-shaping proteins facilitate lipid exchange between the ER and mitochondria in S . cerevisiae. *J Cell Sci*. 2012;125(20):4791–4799. doi:10.1242/jcs.105635.
523. Wagner S a., Beli P, Weinert BT, et al. A proteome-wide, quantitative survey of in vivo ubiquitylation sites reveals widespread regulatory roles. *Mol Cell proteomics*. 2011;10(10):M111.013284. doi:10.1074/mcp.M111.013284.
524. Walters AD, Bommakanti A, Cohen-Fix O. Shaping the Nucleus : Factors and Forces. *J Cell Biochem*. 2012;113:2813–2821. doi:10.1002/jcb.24178.
525. Wan Q, Kuang E, Dong W, et al. Reticulon 3 mediates Bcl-2 accumulation in mitochondria in response to endoplasmic reticulum stress. *Apoptosis*. 2007;12(2):319–328. doi:10.1007/s10495-006-0574-y.
526. Wang P, Hawkins TJ, Hussey PJ. Connecting membranes to the actin

cytoskeleton. *Curr Opin Plant Biol*. 2017;40:71–76. doi:10.1016/j.pbi.2017.07.008.
527. Wang S, Tukachinsky H, Romano FB, Rapoport TA. Cooperation of the ER-shaping proteins atlastin , lunapark , and reticulons to generate a tubular membrane network. *Elife*. 2016;5:1–29. doi:10.7554/eLife.18605.
528. Wang Y, Li Y, Wei F, Duan Y. Optical Imaging Paves the Way for Autophagy Research. *Trends Biotechnol*. 2017;xx:1–13. doi:10.1016/j.tibtech.2017.08.006.
529. Warnes G. Flow cytometric assays for the study of autophagy. *Methods*. 2015;82:21–28. doi:10.1016/j.ymeth.2015.03.027.
530. Wasilko DJ, Mao Y. Exploiting the ubiquitin and phosphoinositide pathways by the Legionella pneumophila effector, SidC. *Curr Genet*. 2016;62(1):105–108. doi:10.1007/s00294-015-0521-y.
531. Waterman-Storer CM, Salmon ED. Endoplasmic reticulum membrane tubules are distributed by microtubules in living cells using three distinct mechanisms. *Curr Biol*. 1998;8(14):798–807.
532. Watson P, Forster R, Palmer KJ, Pepperkok R, Stephens DJ. Coupling of ER exit to microtubules through direct interaction of COPII with dynactin. *Nat Cell Biol*. 2005;7(1):48–55. doi:10.1038/ncb1206.
533. Watts C. Phagocytosis: How the phagosome became the phag-ER-some. *Curr Biol*. 2002;12(19):666–668. doi:10.1016/S0960-9822(02)01163-6.
534. Wauer T, Swatek KN, Wagstaff JL, et al. Ubiquitin Ser65 phosphorylation affects ubiquitin structure, chain assembly and hydrolysis. *EMBO J*. 2015;34(3):307–25. doi:10.15252/embj.201489847.
535. Weber SS, Ragaz C, Reus K, Nyfeler Y, Hilbi H. Legionella pneumophila exploits PI(4)P to anchor secreted effector proteins to the replicative vacuole. *PLoS Pathog*. 2006;2(5):e46. doi:10.1371/journal.ppat.0020046.
536. van Weering JRT, Sessions RB, Traer CJ, et al. Molecular basis for SNX-BAR-mediated assembly of distinct endosomal sorting tubules. *EMBO J*. 2012;31(23):4466–4480. doi:10.1038/emboj.2012.283.
537. Wertz IE, Rourke KMO, Zhou H, et al. De-ubiquitination and ubiquitin ligase domains of A20 downregulate NF-kB signalling. *Nature*. 2004;430(7000):694–699. doi:10.1038/nature02794.
538. West M, Zurek N, Hoenger A, Voeltz GK. A 3D analysis of yeast ER structure reveals how ER domains are organized by membrane curvature. *J Cell Biol*. 2011;193(2):333–346. doi:10.1083/jcb.201011039.
539. Westrate LM, Lee JE, Prinz WA, Voeltz GK. Form Follows Function: The Importance of Endoplasmic Reticulum Shape. *Annu Rev Biochem*. 2015;84(1):791–811. doi:10.1146/annurev-biochem-072711-163501.
540. Wild P, McEwan DG, Dikic I. The LC3 interactome at a glance. *J Cell Sci*. 2014;127(1):3–9. doi:10.1242/jcs.140426.
541. Wo MJ, Bola B, Brownhill K, Yang Y, Levakova V, Allan VJ. Role of kinesin-1 and cytoplasmic dynein in endoplasmic reticulum movement in VERO cells. *J Cell Sci*. 2009;122(12):1979–1989. doi:10.1242/jcs.041962.
542. Wong K, Kozlov G, Zhang Y, Gehring K. Structure of the Legionella effector, lpg1496, suggests a role in nucleotide metabolism. *J Biol Chem*. 2015;290(41):24727–24737. doi:10.1074/jbc.M115.671263.

543. Wong K, Perpich JD, Kozlov G, Cygler M, Abu Kwaik Y, Gehring K. Structural Mimicry by a Bacterial F Box Effector Hijacks the Host Ubiquitin-Proteasome System. *Structure*. 2017;25(2):376–383. doi:10.1016/j.str.2016.12.015.
544. Wooten MW, Geetha T, Seibenhener ML, Babu JR, Diaz-Meco MT, Moscat J. The p62 scaffold regulates nerve growth factor-induced NF-κB activation by influencing TRAF6 polyubiquitination. *J Biol Chem*. 2005;280(42):35625–35629. doi:10.1074/jbc.C500237200.
545. Wu M, Ke P, Hsu JT, Yeh C, Horng J. Reticulon 3 interacts with NS4B of the hepatitis C virus and negatively regulates viral replication by disrupting NS4B self-interaction. *Cell Microbiol*. 2014;16(11):1603–1618. doi:10.1111/cmi.12318.
546. Xu L, Luo Z-QQ. Cell biology of infection by Legionella pneumophila. *Microbes Infect*. 2012;15(November):1–11. doi:10.1016/j.micinf.2012.11.001.
547. Xu P, Duong DM, Seyfried NT, et al. Quantitative Proteomics Reveals the Function of Unconventional Ubiquitin Chains in Proteasomal Degradation. *Cell*. 2009;137(1):133–145. doi:10.1016/j.cell.2009.01.041.
548. Yamamoto Y, Yamamoto H. Controlling the receptor for advanced glycation end-products to conquer diabetic vascular complications. *J Diabetes Investig*. 2012;3(2):107–114. doi:10.1111/j.2040-1124.2011.00191.x.
549. Yan R, Shi Q, Hu X, Zhou X. Review Reticulon proteins : emerging players in neurodegenerative diseases. *Cell Mol Life Sci*. 2006;63:877–889. doi:10.1007/s00018-005-5338-2.
550. Yang A, Pantoom S, Wu YW. Elucidation of the anti-autophagy mechanism of the Legionella effector RavZ using semisynthetic LC3 proteins. *Elife*. 2017;6:1–23. doi:10.7554/eLife.23905.
551. Yang YS, Strittmatter SM. The reticulons: a family of proteins with diverse functions. *Genome Biol*. 2007;8(12):234. doi:10.1186/gb-2007-8-12-234.
552. Yang Z, Klionsky DJ. Eaten alive: a history of macroautophagy. *Nat Cell Biol*. 2010;12(9):814–822. doi:10.1038/ncb0910-814.
553. Yla-Anttila P, Vihinen H, Jokitalo E, Eskelinen E-L. 3D tomography reveals connections between the phagophore and endoplasmic reticulum. *Autophagy*. 2009;5(8):1180–1185.
554. Ylä-Anttila P, Vihinen H, Jokitalo E, Eskelinen EL. *Chapter 10 Monitoring Autophagy by Electron Microscopy in Mammalian Cells*. 1st ed. Elsevier Inc.; 2009. doi:10.1016/S0076-6879(08)03610-0.
555. Yokota T, Mishra M, Akatsu H, et al. Brain site-specific gene expression analysis in Alzheimer's disease patients. *Eur J Clin Invest*. 2006;36(11):820–830. doi:10.1111/j.1365-2362.2006.01722.x.
556. Yoshii SR, Mizushima N. Monitoring and Measuring Autophagy. *Int J Mol Sci*. 2017;18(9):1865. doi:10.3390/ijms18091865.
557. Yu Q, Hu L, Yao Q, et al. Structural analyses of Legionella LepB reveal a new GAP fold that catalytically mimics eukaryotic RasGAP. *Cell Res*. 2013;23(6):775–787. doi:10.1038/cr.2013.54.
558. Yuan P, Dong L, Cheng Q, et al. Prototype foamy virus elicits complete autophagy involving the ER stress-related UPR pathway. *Retrovirology*. 2017;14:1–11. doi:10.1186/s12977-017-0341-x.
559. Yutsudo M. RTN4 (reticulon 4). *Atlas Genet Cytogenet Oncol Haematol*.

2011;11(2):128–130. doi:10.4267/2042/38416.
560. Van Der Zand A, Gent J, Braakman I, Tabak HF. Biochemically distinct vesicles from the endoplasmic reticulum fuse to form peroxisomes. *Cell*. 2012;149(2):397–409. doi:10.1016/j.cell.2012.01.054.
561. Zhang D, Vjestica A, Oliferenko S. Plasma membrane tethering of the cortical ER necessitates its finely reticulated architecture. *Curr Biol*. 2012;22(21):2048–2052. doi:10.1016/j.cub.2012.08.047.
562. Zhang L, Xu M, Scotti E, Chen ZJ, Tontonoz P. Both K63 and K48 ubiquitin linkages signal lysosomal degradation of the LDL receptor. *J Lipid Res*. 2013;54:1410–1420. doi:10.1194/jlr.M035774.
563. Zhang Y, Zhou X, Huang P. Fanconi anemia and ubiquitination. *J Genet Genomics*. 2007;34(7):573–80. doi:10.1016/S1673-8527(07)60065-4.
564. Zhang Y, Zhou X, Zhao L, et al. UBE2W Interacts with FANCL and Regulates the Monoubiquitination of Fanconi Anemia Protein FANCD2. *Mol Cells*. 2011;31:113–122.
565. Zhao G, Zhu PP, Renvoisé B, Maldonado-Báez L, Park SH, Blackstone C. Mammalian knock out cells reveal prominent roles for atlastin GTPases in ER network morphology. *Exp Cell Res*. 2016;349(1):32–44. doi:10.1016/j.yexcr.2016.09.015.
566. Zheng JY, Koda T, Fujiwara T, Kishi M, Ikehara Y, Kakinuma M. A novel Rab GTPase, Rab33B, is ubiquitously expressed and localized to the medial Golgi cisternae. *J Cell Sci*. 1998;111 (Pt 8:1061–1069.
567. Zhou Y, Zhu Y. Diversity of bacterial manipulation of the host ubiquitin pathways. *Cell Microbiol*. 2015;17(1):26–34. doi:10.1111/cmi.12384.
568. Zhu L, Xiang R, Dong W, Liu Y, Qi Y. Anti-apoptotic activity of Bcl-2 is enhanced by its interaction with RTN3. *Cell Biol Int*. 2007;31(8):825–830. doi:10.1016/j.cellbi.2007.01.032.
569. Zhu Y, Hu L, Zhou Y, Yao Q, Liu L, Shao F. Structural mechanism of host Rab1 activation by the bifunctional Legionella type IV effector SidM/DrrA. *Proc Natl Acad Sci*. 2010;107(10):4699–4704. doi:10.1073/pnas.0914231107.
570. Zurek N, Sparks L, Voeltz G. Reticulon short hairpin transmembrane domains are used to shape ER tubules. *Traffic*. 2011;12(1):28–41. doi:10.1111/j.1600-0854.2010.01134.x.